University of Nottingham
UK | CHINA | MALAYSIA

T cell activation and function investigated using fully-defined 3D culture

By Ilona Sica, MSc

Thesis submitted to the University of Nottingham
For the degree of
Doctor of Philosophy
December 2022

University of Nottingham
Faculty of Medicine and Health Sciences
School of Medicine
Translational Medical Sciences

Abstract

3D culture is gaining recognition as the advanced *in vitro* culture system to study cells. It bridges planar culture (2D culture) and *in vivo* studies, which could overcome oversimplified environment settings and genetic/physical differences to humans by animal models. For example, planar culture plates lack the architecture of tissues with extracellular matrix (ECM), whereas mouse tumours are poor representations of human ones. T cells are part of the immune system, and various studies have been conducted to understand their role in healthy or diseased tissues and the efficacy of therapies targeting these cells. To get more constructive *in vitro* results, by avoiding oversimplified culture (or in some cases animal models), 3D culture could be used by selecting appropriate biomaterial to study cells. Various biomaterials were tested for 3D T cell culture, enabling observation of cell-cell interaction, migration, effector function, and the effect of the microenvironment (i.e. oxygen gradient, stiffness) on cells. However, some of them have limitations such as modified environment (e.g. collagen hydrogel), tumour origins (e.g. Matrigel), poor stiffness level control or even immunogenic properties which could activate an unwanted immune response. In this case, self-assembling peptide gel offers solutions to those common biomaterial problems and makes it a great candidate for T cell 3D culture.

Self-assembling peptide gel is composed of FEFEFKFK octapeptide (F, phenylalanine, K, lysine, E, glutamic acid); under correct temperature, pH and

salt concentration makes the hydrogel. The whole gelation process relies on electrostatic interactions between amino acids, avoiding complex and toxic crosslinking methods for gel formation. Primary human T cells were encapsulated in the peptide gel to analyse the biomaterial's biocompatibility and suitability as the 3D culture system for cells.

T cells were encapsulated in the peptide gel; their viability and effector functions over 7 days were observed. T cells were encapsulated with antigen presenting cells (APCs) to simulate their activation process as found in the peripheral tissues. APCs were either artificial (antibody CD3 and CD28 coated polystyrene beads) or actual cells such as dendritic cells (DC) isolated from the healthy human donors. The purpose of these experiments was to test their ability to respond to stimuli and deliver an appropriate response in the hydrogel. The material itself was modified to test the microenvironment effect on T cell response from the soft to the harder material, representing lymph node to tumour-like properties, respectively. In addition, the hydrogel was functionalized with extracellular matrix (ECM) proteins, fibronectin and collagen type I, by adsorption process to indicate whether proteins influence T cell behaviour (i.e. co-stimulation effect) as described in the literature. All of these distinctive experiments were set up to test the peptide gel's ability to support these complex immune cells, and whether future immune studies could benefit from this novel *in vitro* platform. Cells were monitored by proliferation assays (3H Thymidine, Cell-Trace CFSE), IFNγ and IL-10 cytokine secretion (ELISA) and phenotype marker expression (flow cytometry).

T cells showed better growth in the softer gels (average 283 Pa) than the rigid ones, which restrained expanding proliferating clusters of cells. They responded to various stimuli provided by artificial and actual pro-inflammatory APC the peptide gel. Furthermore, functionalized gels with matrix proteins demonstrated a co-stimulatory effect on cells, which reflected inflammatory tissue scenarios experienced by cells. The peptide gel was also used to test the immunomodulatory effect of p38 inhibitor (BIRB196 drug) treated CD1c cells, which under 2D culture settings enhance T cells' immune response. T cells under 3D culture demonstrated similar results to the published 2D culture studies, indicating peptide gel compatibility as the novel *in vitro* culture. However, in the presence of fibronectin, the p38-treated CD1c effect was diminished on T cells, and this could represent a possible scenario of glioblastoma tumour.

In conclusion, peptide gel demonstrated its ability to support basic T cell function. Adding additional parameters to the gel that reflect tissue microenvironments - demonstrated different cell behaviour, which is most of the time misrepresented by 2D cultures. The material itself is inert and showed no immunogenic properties that could mislead immune-related studies. This conducted research demonstrates the need for 3D culture-like studies to build a better understanding of immune cells, and self-assembling peptide gel is a good start to advance these *in vitro* studies.

Abbreviations

2D culture	2-dimensional culture
3D culture	3-dimensional culture
Ab	Antibody
ACT	Adoptive cell therapy
AICD	Activation-induced cell death
AP1	Activation protein 1
APC	Antigen presenting cell
ARG1	Arginase 1
ATP	Adenosine triphosphate
Bcl	B-cell lymphoma (e.g. Bcl-2, Bcl-xL)
CAF	Cancer-associated fibroblast
CAR T cell	Chimeric antigen receptor T cell
CCR	CC chemokine receptor (e.g. CCR7)
CD	Cluster of differentiation (e.g. CD4+)
CFSE	Carboxyfluorescein succinimidyl ester
CGC	Critical gelation concentration
CLP	Common lymphoid progenitor
cTECs	Cortical thymic epithelial cells
CTL	Cytotoxic T lymphocytes
CTLA-4	Cytotoxic T lymphocytes associated protein 4
CXCL	Chemokine (C-X-C motif) ligand (e.g. CXCL12)
DAMP	Damage-associated molecular patterns
DC	Dendritic cell
Dex	Dexamethasone
DI	Division index
DN	Double negative
DNA	Deoxyribonucleic acid
DP	Double positive
DTH	Delayed-type hypersensitivity
ECM	Extracellular matrix
Eomes	Eomesodermin
FCS	Fetal calf serum
Foxp3	Forkhead box protein 3
FRC	Fibroblastic reticular cells
GAG	Glycosaminoglycans
GATA-3	GATA binding protein 3
GelMa	Gelatin methacrylate
GITR	Glucocorticoid-induced TNFR-related protein
GM-CSF	Granulocyte macrophage-colony stimulating factor
HA	Hyaluronic acid
HEV	High endothelial venules
HLA	Human leukocyte antigens
HSC	Hematopoietic stem cells
ICAM-1	Intercellular adhesion molecule 1
ICOS	Inducible costimulator

iDC	Immature dendritic cell
IFN	Interferon
IL-	Interleukin (e.g. IL-2)
Ki67	Kiel 67
LFA-1	Lymphocyte function-associated antigen-1
LINC	Linker of nucleoskeleton and cytoskeleton
LPS	Lipopolysaccharide
LOX	Lipoxygenases
MAIT	Mucosal-associated invariant T cells
MAPK	Mitogen-activated protein kinase
mDC	Mature dendritic cell
MFI	Median fluorescence intensity
MHC	Major histocompatibility complex
MLR	Multiple leukocyte reaction
MMP	Matrix metalloproteinase
moDC	Monocyte-derived DC
MR1	MHC class I related molecule 1
mTEC	Medullary thymic epithelial cells
mTORC1	Mammalian target of rapamycin complex 1
NaOH	Sodium hydroxide
NFAT	Nuclear factor of activated T cells
NF-κB	Nuclear factor kappa-light-chain-enhancer of activated B cells
NK	Natural killer cells
NO	Nitric oxide
NSCLC	Non–small cell lung cancer
nTreg	Natural T regulatory cell
Pa	Pascal
PAMP	Pathogen-associated molecular pattern
PBL	Peripheral blood lymphocytes
PBMC	Peripheral blood mononuclear cells
PD	Programmed death (e.g. PD-1L)
PEG	Poly(ethylene glycol)
PEG2	Prostaglandin E2
PLGA	Poly D,L-lactic-co-glycolic acid
PLLA	Poly-l-Lactic acid
PMA	Phorbol 12-myristate 13-acetate
Poly:I:C	Polyinosinic-polycytidylic acid
PRR	Pattern recognition receptors
R848	Resiquimod
RAG 1/2	Recombination-activating gene 1 and gene 2
RNA	Ribonucleic acid
ROR-γt	Retinoic acid-related orphan receptor
ROS	Reactive oxygen species
Runx-3	RUNX family transcription factor 3
SLO	Secondary lymphoid organ
TAM	Tumour-associated macrophage

T-bet	T-box transcription factor TBX21
Tcm	Central memory T cells
TCM	T cell media
TCR	T cell receptor
TdT	Terminal deoxynucleotidyl transferase
Tem	Effector memory T cells
TF	Transcription factor
TGF	Transforming growth factor
Th	Helper T cell
TIM-1	T-cell immunoglobulin and mucin domain1
TLR	Toll-like receptor
TME	Tumour microenvironment
TNF	Tumour necrosis factor
Tr1	Type 1 regulatory T cell
Trm	Tissue-resident memory T cell
VEGF	Vascular endothelial growth factor
YAP	Yes-associated protein

Acknowledgements

I want to take the first opportunity to thank many people who were involved through my PhD journey. Without anyone's contribution, help, support, and encouragement this journey would have been very difficult. This work reflects on many people who have advised and helped me to conceptualise the experiments, ask the right questions, take the right approaches to make this research possible.

First, I want to thank all of my healthy donors who have donated their blood voluntarily and contributed to my research. Without their generosity and willingness, this research would not have been impossible.

Second, I want to thank people from different research groups who have shared their expertise and knowledge to conduct my research. Stem cell glycobiology group, especially Dr. Jennifer Ashworth, Dr. Jenna James, Dr. Jonathan Curd, Dr. Jamie Thompson and Katarzyna-Lis Slimak for all their expertise and assistance on the peptide gels. Cancer immunology and Host tumour interaction groups Dr. Tajka Mussarat, Dr. Charles Iniobong, Dr. Aanchal Kaur, Dr. Salaheddin Mohammad, Dr. Anna Malecka, Dr. Hester Franks, Prof. Poulam Patel, Dr. Judith Ramage, Christopher Chisanga and Bryony-Heath for all their expertise on immuno-oncology research.

Finally, I want to thank my supervisors Prof. Cathy L. Merry, Dr. Andrew M. Jackson and Dr. Ian Spendlove, for the immense amount of support and guidance I received during my PhD. These people taught me the qualities of becoming a good scientist on both professional and research level. I also want to thank Prof. Felicity Rose for giving me an opportunity to be part of 'Bioinstructive biomaterials for healthcare applications' project and funding by EPSRC and University of Nottingham.

I also want to thank my family members for being here for me through this PhD journey. And most important to my husband, to whom I cannot thank enough for his constant support and belief in me through this entire journey and furthermore in life.

Table of Contents

Abstract **1**

Abbreviations **4**

Acknowledgments **7**

Chapter 1 Introduction **11**

1.1. Immune system 11

1.1.1. Innate immune system 12
1.1.2. Adaptive immune system 14
1.1.3. T cells 19
1.1.3.1. T cell development 19
1.1.3.2. TCR arrangement 21
1.1.3.3. T cell activation by antigen presenting cells (APC) 22
1.1.3.4. Antigen presenting cells (APC) 29
1.1.3.5. Memory T cells 32
1.1.3.6. T cell plasticity 35

1.2. 3D culture 37

1.2.1. Distinction between 2D and 3D cell cultures 39
1.2.2. T cells and 3D cell culture 43
1.2.3. Lymph node microenvironment 44
1.2.4. Inflammatory tissue microenvironment 48
1.2.5. Tumour microenvironment 54
1.2.6. Mechanobiology of T cells 58
1.2.7. Animal models versus 3D culture 61

1.3. Biomaterials 64

1.3.1. Type of biomaterials 65
1.3.2. Biomaterial characteristics 71
1.3.2.1. Porosity 71
1.3.2.2. Biodegradability 72
1.3.2.3. Biomaterial functionalisation 72
1.3.2.4. Immunogenicity 73

1.4. Self-assembling peptide hydrogel 75

1.4.1. FEFEFKFK peptide hydrogel 77

1.5. Hypotheses and aim 81

Chapter 2 Materials and methods **82**

2.1. Ethical approval 82
2.2. Peripheral blood mononuclear cells (PBMCs) isolation 82
2.3. Cell counting with Trypan blue 84
2.4. Human CD4+ T cell isolation 85
2.5. CD14+ monocyte isolation and differentiation into dendritic cells (DC) 86
2.6. CD1c+ DC isolation 87
2.7. Preparation of immature and mature DC, and treatment with dexamethasone and p38 inhibitor (BIRB196) 88
2.8. Coating polystyrene particles with antibodies – preparation of artificial APC 89
2.9. Precursor FEFEFKFK peptide hydrogel preparation 90
2.10. Peptide hydrogel formation and cells (and co-culture) encapsulation 91

2.11. 3-Thymidine incorporation assay……92
2.12. CFSE staining CD4+ T cells……93
2.13. Bulk Oscillatory rheology……95
2.14. ELISA for IFNγ……95
2.15. ELISA for IL-10……97
2.16. ELISA for IL-12p40……97
2.17. Flow cytometry……98
2.18. Peptide hydrogel degradation and cell release for flow cytometry……99
2.19. Dead cell detection by propidium iodide (flow cytometry)……100
2.20. Live/Dead staining of cells in the peptide hydrogel, and cell viability % calculations……101
2.21. DC staining with PKH26……103
2.22. T cell stimulation with mitogens (positive control)……103
2.23. Multiple lymphocyte reaction (MLR) with artificial and actual APC……104
2.24. Confocal microscopy, 3D imaging and immunocytochemistry……104
2.25. Coating plates with fibronectin and collagen type I……106
2.26. Functionalising peptide hydrogel with collagen type I and plasma fibronectin……107
2.27. Statistical analyses……107

Chapter 3 Proof-of-principle: peptide hydrogel use for T cell culture ……**111**

3.1. Introduction……111

3.2. Results……115
3.2.1. Determining purity of CD4+ T cells post-isolation……115
3.2.2. The effect of alkaline pH on the viability of resting T cells……117
3.2.3 The impact of the mechanical properties of peptide hydrogel on T cells……120
3.2.4 Optimising peptide hydrogel density for T cell culture……124
3.2.5 Optimisation of resting T cell density in peptide hydrogel……132
3.2.6 Coating polystyrene particles with stimulating T cell antibodies (artificial APC) and testing against alkaline conditions……136
3.2.7. Modifying T cell response with different co-stimulation signals on artificial APC……142
3.2.8. Modifying T cell function with different co-stimulating signals in the peptide hydrogels……151
3.2.9. Stimulation of T cells in the peptide hydrogel with artificial APC……158
3.2.10. The optimal time point to analyse T cell response to artificial APC and ratio in the hydrogel……162
3.2.11. T cells express activation and proliferation markers in the peptide hydrogel..170
3.3. Discussion……176

Chapter 4 T cell stimulation by dendritic cells in the peptide hydrogel……**189**

4.1. Introduction……189
4.2. Results……191
4.2.1 Dendritic cells' viability in the peptide hydrogel……191
4.2.2 Assessing peptide gel ability to induce non-specific immune response……196
4.2.3 Optimal time point for T cell stimulation in response to DC cells in the peptide hydrogel……201
4.2.4 Optimal ratio between DCs and T cells in the peptide hydrogel……207
4.2.5 Distribution of DC and T cell culture across the peptide hydrogel……211

4.2.6 Modulating T cells response with dexamethasone and viral analogs conditioned DC in the peptide hydrogel……217
4.3. Discussion……223

Chapter 5 T cell function in matrix protein functionalised peptide hydrogel (and 3D in vitro therapy analyses)……**231**

5.1. Introduction……231
5.2. Results……234
5.2.1 The effect of matrix proteins on T cell stimulation……234
5.2.2 The impact of matrix protein on the physical properties of peptide gel……239
5.2.3 Matrix protein effect on T cells in the peptide hydrogel……244
5.2.4 T cell stimulation by Dendritic cells in fibronectin functionalised peptide hydrogel……252
5.2.5 T cell stimulation by primary DC (CD1c+) in functionalised peptide hydrogel……255
5.3. Discussion……261

Chapter 6 Discussion……**271**

Appendix 1……**285**

References……**292**

Chapter 1 Introduction

1.1. Immune system

The immune system is a complex network composed of cells, proteins, and organs that altogether protect and maintain a healthy tissue environment [13]. Humans and other mammals are constantly exposed to the pathogenic microbes and their toxins, which require a constant immune surveillance against possible infections or inflicted damages [13]. This also includes cancer, where immune cells exclude the abnormally dividing and differentiated normal cells [14]. The immune system's responsibility is enormous in scope, which is why it is composed from different defence layers to protect the body.

The immune system is composed from two lines of defence: innate and adaptive immunity [15]. Innate immunity is the first line of defence; it induces a rapid but non-specific response. As it is reviewed in Marshall et al. (2018) it is composed of several barriers, which originate from different physiological systems [15]. For example, skin provides an anatomical barrier, temperature increases to reduce the microbial growth and leukocytes (immune cells) clear the evading pathogens [15]. Alongside of this, the innate system activates the adaptive immune system, for a more efficient and targeted response. This primes the specific immune cells (i.e. lymphocytes) which are responsible for antibody secretion and cytotoxic effect [16]. At the end of adaptive response, immunological memory is established, resulting in subsequent pathogen exposure - a rapid and specific immune response.

The immune system is mainly composed of specialised cells, which are activated through the controlled processes. As the defence system, it is extensive through the entire body and its malfunction could result in detrimental diseases or disorders such as: immunodeficiency, chronic inflammation, cancer, hypersensitivity, and autoimmunity [17-21]. The importance of studying and understanding this system is essential to creating effective treatments and maintaining healthy tissue environments [13, 15].

1.1.1. Innate immune system

Innate immunity is composed from several defence layers defined as physical, biochemical and cellular barriers [15, 22]. Physical barriers contain specific anatomical and morphological features that specialise in restricting the pathogen entrance [13]. One of the examples is skin, where keratinocytes of the epidermal layer create an impermeable barrier due to tight junctions between the cells [23]. In addition, it is also covered with microflora which limits the pathogens growth [24]. From the chemical barrier perspective, this involves chemicals/proteins released by cells to inhibit microbial growth [22]. For example, the stomach releases hydrochloric acid, which lowers the pH to prevent bacterial outgrowth, whereas blood's plasma contains 'complement' proteins that induce the bacterial lysis [22, 25]. However, the innate immune system is mainly driven by cells identifying foreign organisms, also known as 'non-self', from the healthy 'self' cells [13, 15].

The innate immune system is equipped with cells which are able to respond to the extracellular (i.e. bacteria) and intracellular (i.e. virus) pathogens [22]. They contain pattern recognition receptors (PRR) which recognise conserved features of the microbes [22]. The conserved features are known as pathogen-associated molecular patterns (PAMPs) which can either be complex polysaccharides, glycolipids, lipoproteins or nucleotides [22]. For example, *Candida albicans* cell wall contains mannosyl residues which are recognised by mannose receptors found on the phagocytes [26].Whereas intracellular pathogens such as viruses release their DNA/RNA content and interact with phagocyte's Toll-like receptors (TLRs) [22]. For example, TLR3 recognise double-stranded RNA which is released by the rotavirus during the viral replication stage within cells [27]. Furthermore, PRRs can recognise damage-associated molecular patterns (DAMPs) released during the sterile inflammation (absence of pathogens) [28]. As reviewed by Zindel and Kubes (2020) DAMPs could be a ruptured cell's content (e.g. heat shock proteins, DNA) or fragments of extracellular matrix (ECM, e.g. collagen, biglycan) [28]. Altogether these components can initiate the innate response.

During the inflammation, pathogens or damage related particles activate the local cells, such as epithelial cells, to secrete the pro-inflammatory cytokines and chemokines to recruit the immune cells [16, 28-30]. In addition, local phagocytes (i.e. neutrophils, macrophages, dendritic cells (DC)) release the soluble factors in response to engulfed microbes to increase the vascular permeability [28, 31-34]. This enhances the recruitment and migration of the immune cells to the inflammation site [16, 28]. Antigen presenting cells (APCs), such as macrophages

and dendritic cells, process the pathogen and present its relevant antigen to initiate the adaptive immune response [13, 16]. This occurs once APCs migrate to the local draining lymph nodes and activate T and B cells response [13, 16].

1.1.2. Adaptive immune system

Adaptive immunity is the final response specifically activated by APCs to target the source of inflammation. This part of the immune system is mainly initiated and controlled by the lymphocytes, known as T and B cells [13, 16]. Cells originate in the thymus and bone marrow, respectively, but mainly get activated in the lymph nodes. These lymphocytes induce their response specific to the antigen - a substance derived from foreign organism or damage associated particles [13, 35].

B cells are responsible for the humoral immune response, which is driven by secreted antibodies against the specific antigens [15]. Antibodies have multiple roles, for example: to neutralise pathogens and toxins, opsonise and assist a phagocytic response by macrophages, and aid Natural Killer (NK) cells (part of the innate immunity) to induce cytotoxic effect [36-38]. Antibody secreting B cells are known as plasma cells, which reside in the lymph nodes for a short-term until immune response is resolved against the pathogen [39].

T cells' responses are defined as a cell-mediated response, which either support the nearby immune cells functions or induce cytotoxic effects [15]. There are CD4+ T cells, also known as helper T cells (Th) and CD8+ T cells identified as

cytotoxic T cells (CTL) [15]. Th aid the work of other immune cells such as B cells, whereupon activation they secrete cytokines (e.g. IL-4, IL-5) and express co-stimulatory molecules (e.g. CD40L) to induce the antibody type response [40, 41]. Where CTL mediate cytotoxic effect against virally infected or cancerous cells [42, 43]. However, depending on the source of antigen, T cells can differentiate into several phenotypes with different types of functions (Table 1.1). This ensures the correct set of T cells are activated to deliver an immune response according to the source of antigen [13, 35].

Once the pathogen has been cleared, T and B cell population reduce to a fraction of cells, known as memory cells [44, 45]. This is also termed as immunological memory, which is essential for subsequent pathogen exposure. Primary stimulation of cells to the antigen could take more than a week, whereas secondary 'memory' response will occur over a few days. One example is chickenpox, caused by varicella-zoster virus, whereupon primary infection T cells number and response increases within 1-2 weeks of infection, but upon secondary exposure memory T cells appear within 3-4 days [46, 47]. People with acquired immunity to the varicella-zoster virus felt well after the virus re-exposure, and showed no clinical symptoms [48]. In addition, there are reports on innate immune memory, which are reviewed in depth by Sherwood et al. (2022) [49]. The sequence of innate, adaptive and memory response is summarised in Figure 1.1.

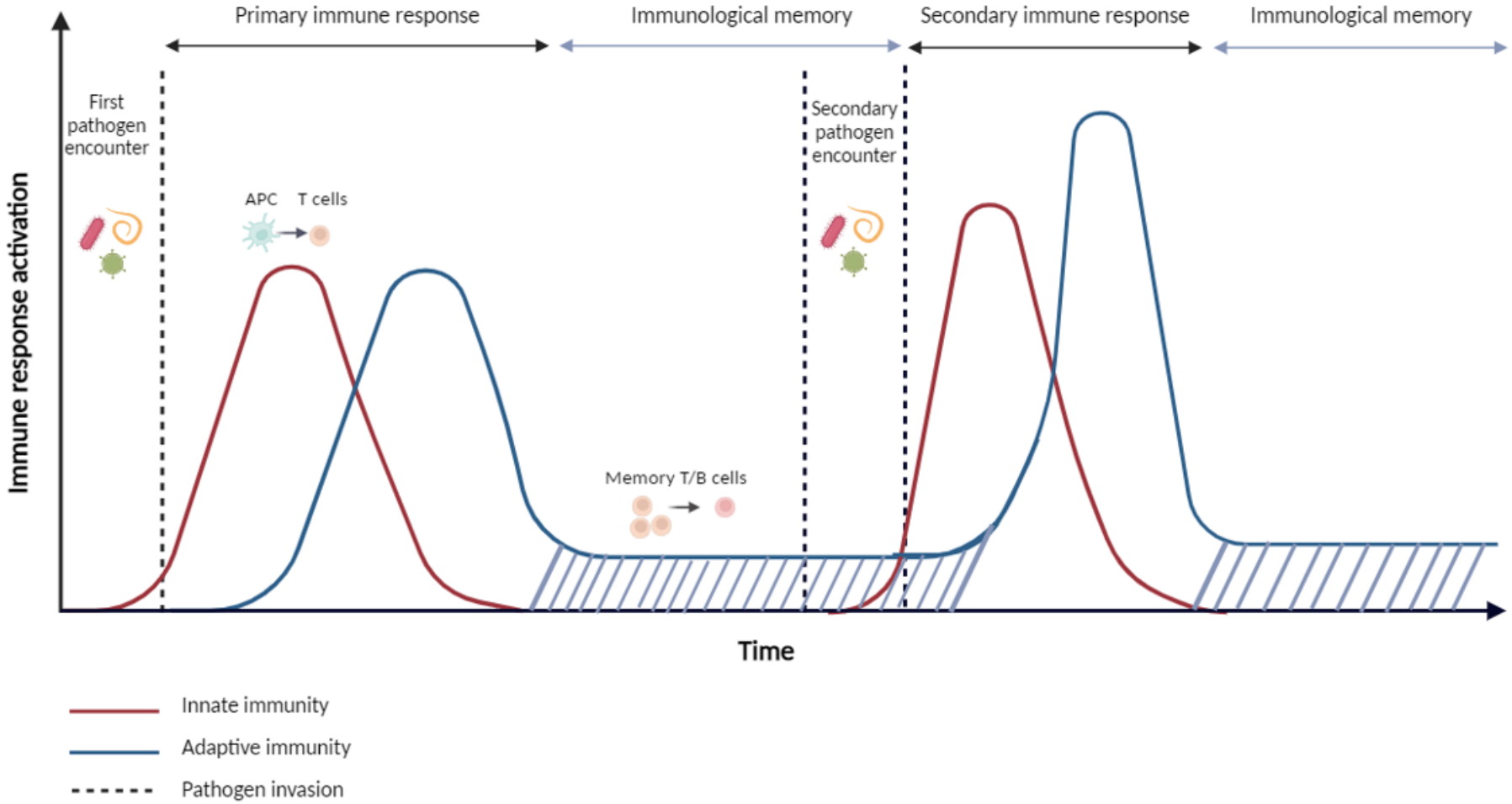

Figure 1.1 Sequence of the immune response. The innate immune system is the first responder to the pathogen invasion, which limits the pathogen outgrowth whilst activated APC migrate to the lymph nodes. APC initiate adaptive immunity by interacting with T cells to induce a more targeted immune response. Upon T cell activation, these cells differentiate into CTL or Th, which either kill or aid B cell differentiation into plasma cells, respectively. Activated B and T cells drive the adaptive immune response until the pathogen clearance, which also ends the innate and adaptive responses. A fraction of B and T cells become memory cells and establish immunological memory. Upon secondary pathogen exposure, memory cells induce a more effective and rapid immune response (defined by narrow and higher peaks). Figure created with BioRender.com

Table 1.1 T cell phenotypes and function

T-cell subtypes (phenotype markers)	Mechanisms	Functions	Ref.
Cytotoxic T cells (CTL)			
Cytotoxic T cells (CTL) (CD8+, Eomes*)	Secrete perforin, granzymes, INF-γ, TNF Express CD95L (FasL) interacting with CD95 (Fas) on target cells Cytokines: INF-γ, TNF	Activated CTL induce apoptosis of the target cells such us virally infected or malignant cells. The apoptosis is initiated by released cytotoxic molecules such as granzymes and perforin, and direct cell-to-cell contact by FasL to Fas expressed on target cells. Secreted INF-γ polarises Th into Th1 type cells, activates macrophages and promotes B cell differentiation. Whereas TNF aids the apoptosis and activate nearby cells to support inflammation process.	[50, 51] [52]
Helper T cells (Th)			
Th1 (CD4+, T-bet*, Runx-3*)	Secrete: IL-2, INF-γ, TNF-α, lymphotoxin	Responsible for pro-inflammatory response by secreting cytokines to support macrophage and CTL activity. By secreting INF-γ it also polarises other nearby Th cells and maintains their phenotype. Th1 role is important in anti-viral, anti-tumour and delayed type hypersensitivity (DTH) responses.	[50, 53-55]
Th2 (CD4+, GATA-3*)	Secrete: IL-4, IL-5, IL-13	Dedicated to humoral response, driven by B cells. Th2 secretes a mixture of cytokines which promote B-cell activation and differentiation into plasma cells. This subtype of cells causes non-inflammatory response, driven against extracellular infections such as parasitic (i.e. helminths). Also, Th2 partake in allergic response such as asthma.	[50, 53, 56, 57]
Th17 (CD4+, ROR-γt*)	Secrete: IL-17, IL-22	Induce pro-inflammatory responses in the peripheral tissues, mainly against extracellular pathogens (e.g. bacteria or fungi). Responsible for macrophages recruitment and neutrophil activation by secreted IL-17 cytokine. IL-22 induce antimicrobial	[50, 56, 58]

Table 1.1 T cell phenotypes and function (continue)

		peptide secretion from local epithelial cells.	
Th9 (CD4+)	Secrete: IL-9	Known for their anti-tumour response, by their enhanced cytotoxic molecule secretion, recruitment of other immune cells and promoting survival of activated T cells and DC. In addition, cells are responsible for anti-parasitic response, where secreted IL-9 recruits mast cells (part of innate immunity).	[50, 59, 60]
Follicular helper T cell (Tfh) (CD4+)	Secrete: IL-4, IL-21	Mainly found in lymph nodes, where upon activation T cells release cytokines important for B cell differentiation into antibody secreting cells – plasma cells.	[51, 56]
Natural T regulatory cells (nTreg) (CD4+, $CD25^{high}$, $CD127^{low}$, Foxp3*)	Secrete: TGF-β, IL-10, IL-35 Expresses CTLA-4, GITR	Cells are activated in response to 'self' antigens derived from healthy/normal cells. This prevents an autoimmune response, by suppressing activated effector T and B cells and maintains peripheral tolerance. This occurs after pathogen clearance or presence of autoreactive cells. nTregs express CTLA-4 which interacts with DC. This reduces the pro-inflammatory cytokine release and depletion of tryptophan – a metabolite important for effector T cells' activity. Also, secrete anti-inflammatory cytokines (IL-10, TGF- β).	[50, 53, 61, 62]
Th3 (CD4+)	Secrete: TGF-β	Regulatory type T cells. They are responsible for oral tissues' tolerance by suppressing Th1 and Th2 type cells. Secreted TGF- β induces B cells to secrete IgA antibody for mucosal area protection.	[50, 63, 64]
Tr1 (CD4+)	Secrete: IL-10 Co-expresses CD39 and CD73 markers, which hydrolyse extracellular ATP to adenosines	Regulatory type T cells, responsible for intestines' tolerance. Anti-inflammatory IL-10 and adenosine depletion (metabolic disruption) suppress effector T cell activity.	[50, 61, 62, 65]

* Transcription factors

1.1.3. T cells

T cells, also known as T lymphocytes, are critical for the immune system as they mediate a specific and more targeted response [13]. They exist in several phenotypes, depending on their location (e.g. tumour, mucosal surfaces), source of antigen (i.e. extracellular or intracellular pathogen), memory status and effector function (e.g. immunosuppressive, pro-inflammatory) (Table 1.1.) [44]. These factors create a diverse T cell pool, which altogether maintain a healthy tissue environment and prevents re-occurring threats [13, 44]. This section explores the cell's ontogeny, activation and function as part of the immune system.

1.1.3.1 T cell development

The T cell development process occurs between two organs: bone marrow and thymus [66]. The first step occurs in the bone marrow, where hematopoietic stem cells (HSCs) give rise to the common lymphoid progenitors (CLPs) cells [66, 67]. T cells' lineage from CLPs are induced by the Notch signalling, which is initiated by the surrounding osteoblasts, endothelial and immune cells [68, 69]. This results in cells' migration to the thymus, where entering cells are named as 'thymocytes' (Fig. 1.2) [13, 68]. Thymocytes enter the thymus as the 'double negative' (DN) cells, due to the lack of CD4 and CD8 markers expression [66, 70, 71]. At this stage, cells rearrange their T cell receptor's (TCR) chains and upon completion they become 'double positive' (DP) cells, expressing CD4 and CD8 markers on their surface.

In the thymus cortex, DP cells undergo a selection process for CD4+ or CD8+ marker expression [70, 71]. It is also known as 'positive selection' which is led by the cortical thymic epithelial cells (cTECs) (Fig. 1.2). cTECs express major

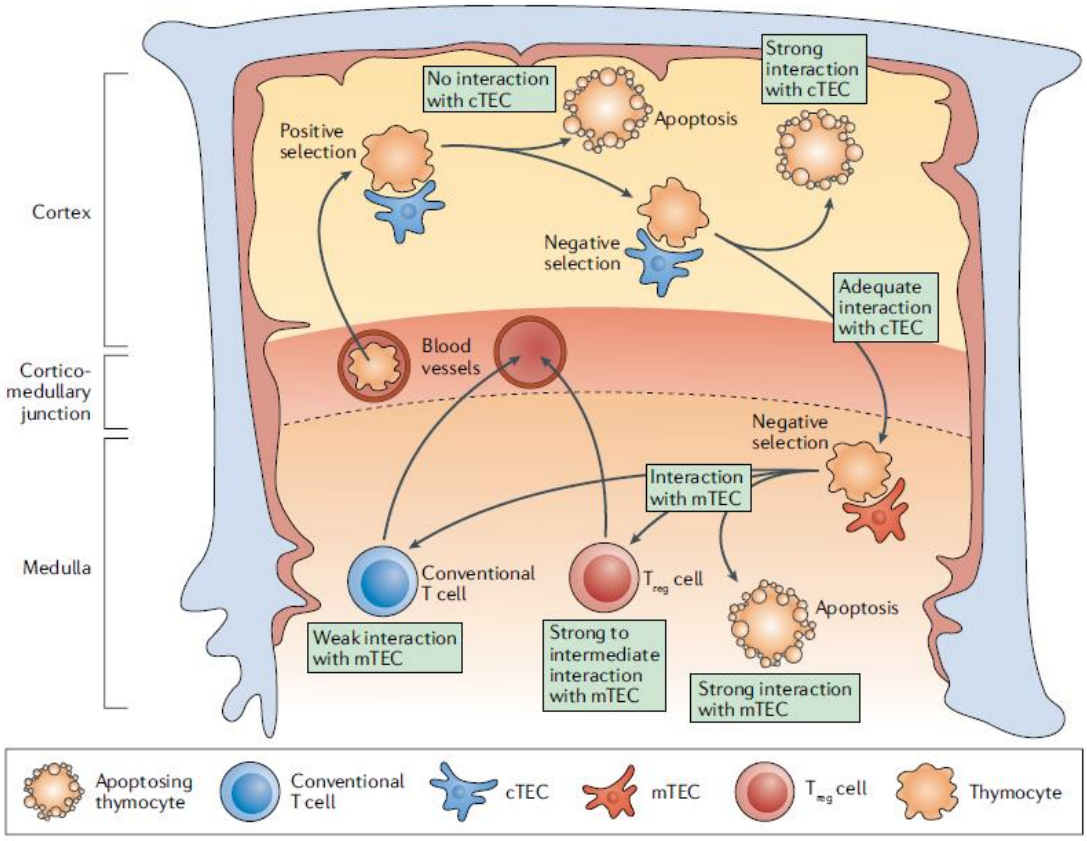

Figure 1.2 T cell development in thymus. Thymocytes enter thymus through the cortico-medullary junction and migrate towards the cortex region for 'negative selection'. cTECs maintain this process by presenting self-antigens on MHC molecules. This determines T cell subset: CD4+ or CD8+ type. Subsequent process is 'positive selection' which eliminates self-reacting T cells, produces Treg and conventional cells which are released to the peripheral tissues. Image obtained from Handel et al. (2018) [8].

histocompatibility complex (MHC) class I and II, where they present self-antigens (peptides) to interact with TCRs of thymocytes. Depending on their affinity to the presented antigen, thymocytes become either CD8 or CD4 positive T cells [71, 72]. Newly selected cells continue to migrate to the thymus medulla, for a 'negative selection' process, which ensures the production of tolerant and non-

autoreactive cells. Medullary thymic epithelial cells (mTECs) present self-antigens for T cells, which excludes self-reactive cells via the apoptosis process. Whereas T cells with low affinity to the antigen are preserved and released to the peripheral tissues. Some self-reactive T cells, which express the transcription factor Foxp3, become nTregs [70-72]. This depends on the strong TCR stimulation by high affinity to antigens and presence of IL-15, IL-2 and TGF-β thymus cytokines leading to the Foxp3 expression [73]. Overall, at the end of the T cell development process only 5% of total cells leave the thymus and enter the peripheral tissues [13]. CD8+ T cells (CTL) in the periphery will recognise antigens presented on MHC Class I, whereas helper CD4+ T cells depend on MHC Class II [13].

1.1.3.2. TCR arrangement

The diversity of T cells relies on the TCR, where they recognise a unique set of antigens originating from the microbes or damage related particles [13, 74]. TCR is composed off α and β chains, which create a unique set of receptors to each T cell in the immune system [13, 74]. TCRs are formed by the gene rearrangement process mediated by RAG1/2 proteins and terminal deoxynucleotidyl transferase (TdT) at TCR loci [11, 75]. These enzymes initiate double strand DNA break, removal of gene segments and ligation process of adding/existing nucleotides. This random process creates a unique DNA sequence coding for TCRα and β chains (Fig. 1.3). The combination of two

different chains (αβ) increases the diversity of TCR recognising various antigens [11, 75].

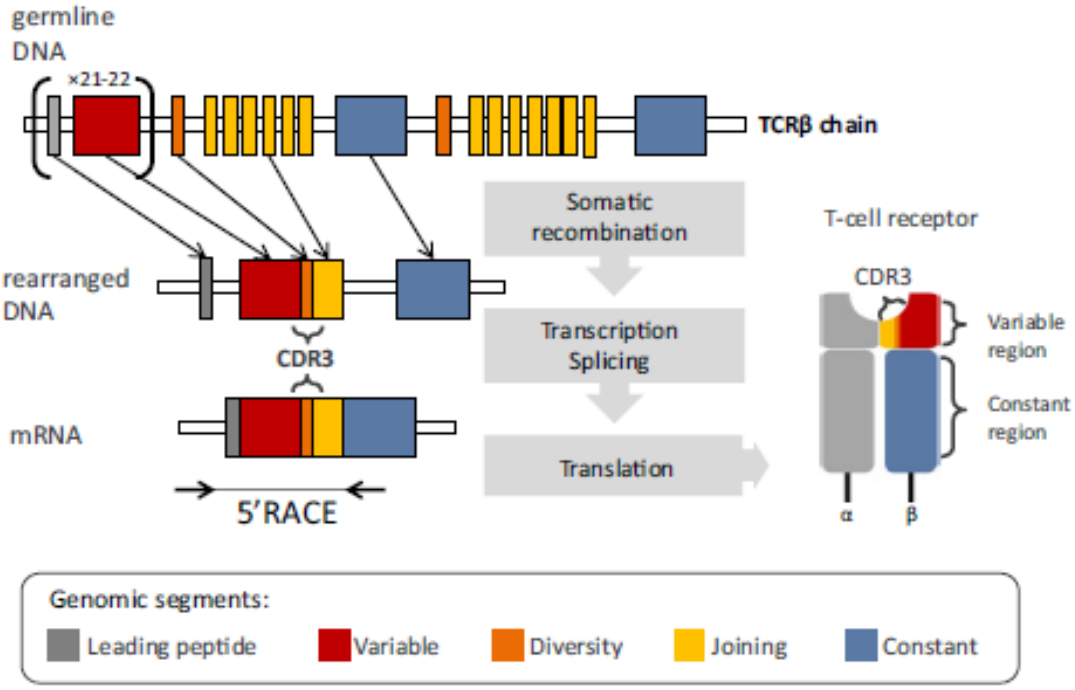

Figure 1.3 TCR arrangement. TCR loci are composed of Variable (V), diversity (D) and joining (J) gene segments which are rearranged by RAG1/2 proteins and modified by TdT enzymes. The process in graph presents TCR β chain which results with variable region, translated from the rearranged DNA. The similar process occurs for the TCRα chain as well, overall creating a unique set of TCR expressed by the T cell. This process increases the diversity of T cells able to recognize various antigens derived from pathogens. Image taken from Migalska et al. (2018) [11].

1.1.3.3. T cell activation by antigen presenting cells (APCs)

T cells circulate through the blood and lymphatic system searching for the APC presenting cognate antigen [76]. At this stage, T cells are in 'naïve' or antigen-inexperienced, state due to the absence of an invading pathogen [74]. T cells with unique TCR also exist in a minimal number, not enough to stop the infection and disease progression [77]. This relays on the proliferation process, also known as clonal expansion, which only occurs upon T cell activation during

microbial infection (e.g. COVID-19), cancer (e.g. melanoma) or autoimmune disease progression (e.g. psoriatic arthirtis) [78-80].

T cells' interaction with APCs occurs in the T-cell zones found in the spleen, lymph nodes and Peyer's patches [81]. Altogether, these organs are defined as secondary lymphoid organs (SLOs), which are positioned to induce immediate immune response upon microbial or damage-related particle exposure. The routes of exposure vary between organs, as lymph nodes 'filtrate' the interstitial fluid from the nearby tissues, the spleen checks the blood and Payer's patches survey the intestine's mucosal surfaces [81-85]. The similar process occurs in the peripheral tissues, where APCs constantly sample the environment by phagocytosis or pinocytosis processes [86-88]. APC could be monocytes, B cells, macrophages and DC, but DC are the most common cells responsible for T cell activation [1, 81, 82].

Upon pathogen exposure and interaction with one of the PRRs, DC undergo an activation process to become mature cells [89]. They process the pathogen or microbial patterns into linear peptide fragments and present them on MHC Class I/II for lymphocytes. This takes two different pathways, as it depends on the intracellular or extracellular microbial fragments [90]. As mature cells, they express co-stimulatory molecules to enhance T cell activation, and upregulate CCR7, a chemokine receptor, to facilitate their migration towards the lymph node where T cells commonly reside [12, 82, 89]. Lymph nodes contain a denser

cellular environment, where a compact area ensures increased T cells and DCs encounters [81].

In the absence of pathogen, T cells interaction with DCs in the lymph nodes only lasts a few minutes [91]. This short-lived interaction ensures a continuous T cell search through the lymph nodes, until they encounter a cognate antigen presented by DCs. Once a T cell recognises the cognate antigen, the interaction with DC lasts for 12-24 hours, which is allocated for a full T cell activation and proliferation process [82, 91].

T cell activation depends on TCRs' interactions with antigen presented on the MHC molecule, which is also known as Signal 1 [92, 93] (Fig. 1.4). The number of

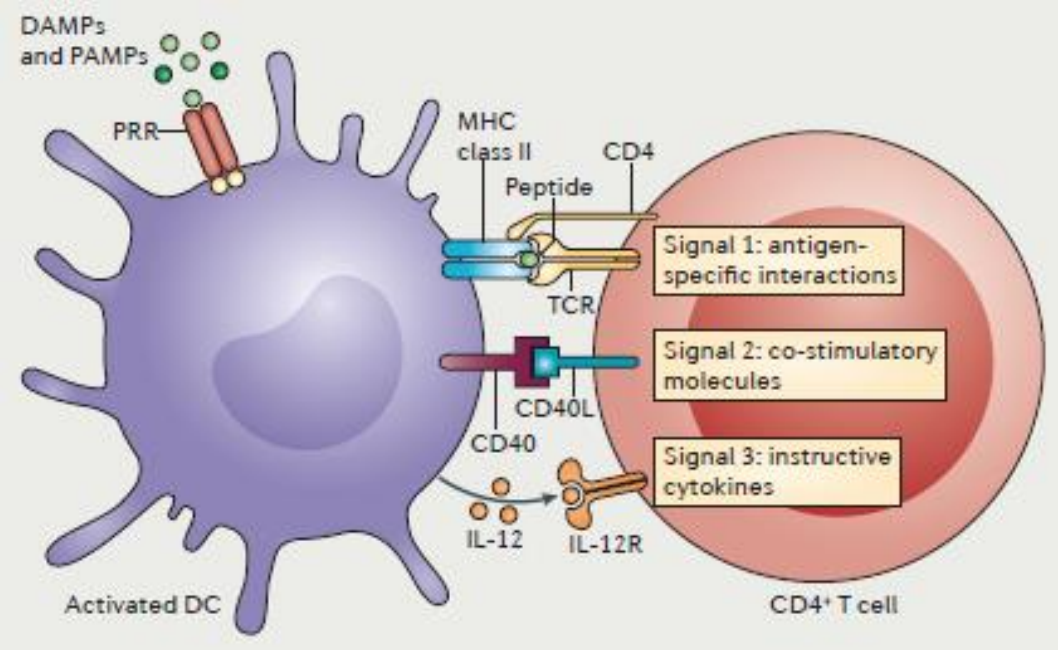

Figure 1.4 T cell activation by DC. T cell activation depends on the antigen presented on MHC by DC. This provides Signal 1, which induces T cell activation. Next, co-stimulatory molecules such as CD40L mediates Signal 2, which amplifies Signal 1 response in T cells. Released cytokines from DC also cause the Signal 3 response, which results in T cell differentiation and effector function. Image obtained from Kambayashi et al. (2014) [1].

interacting TCRs with antigen-MHC (i.e. avidity) and the level of binding between TCR and peptide (i.e. affinity) directs T cell activation [94, 95]. If a presented antigen on MHC has a high affinity to TCR, it will require a low number of TCRs to interact with MHC for T cell activation [95]. Whereas avidity helps T cells to respond to the antigens with low affinity or density, and increase cells' activation response [94]. The signal from TCRs is further passed by the CD3 complex, which induces further signal transduction in cells [96]. This initiates the cytoskeletal structure (actin and microtubules) organisation, forming an immunological synapse between cells [97] (Fig. 1.5). The Signal 1 activates nuclear TFs such as AP1, NFAT and NF-κB, that initiate the gene expression for IL-2 cytokine production to support T cells' survival and proliferation [97, 98]. In addition, lymphocyte function-associated antigen-1 (LFA-1), an adhesion ligand of T cells, undergoes a conformational change to increase their avidity and affinity to the intracellular adhesion molecule-1 (ICAM-1) expressed on other immune cells [98-100]. LFA-1 is usually expressed on non-activated T cells' surfaces but at a low affinity state [100]. Upon cells' activation, LFA-1 provides a stop signal for T cell migration, which also enhances cell-cell interaction and further maintains TCR stimulation response [98, 101] After Signal 1, T cells require co-stimulation (Signal 2) to sustain and enhance activation signalling within the cell [93, 97] (Fig. 1.4). This also prevents T cells from hyporesponsive 'anergy' state or cell apoptosis [82, 102]. During Signal 1, CD28 is upregulated on the T cell's surface and interacts with CD80 and CD86 expressed on DCs. Signal 2 is driven by CD28 function, which mainly amplifies the Signal 1 by upregulating already activated transcription factors. This sustains IL-2 secretion and induces

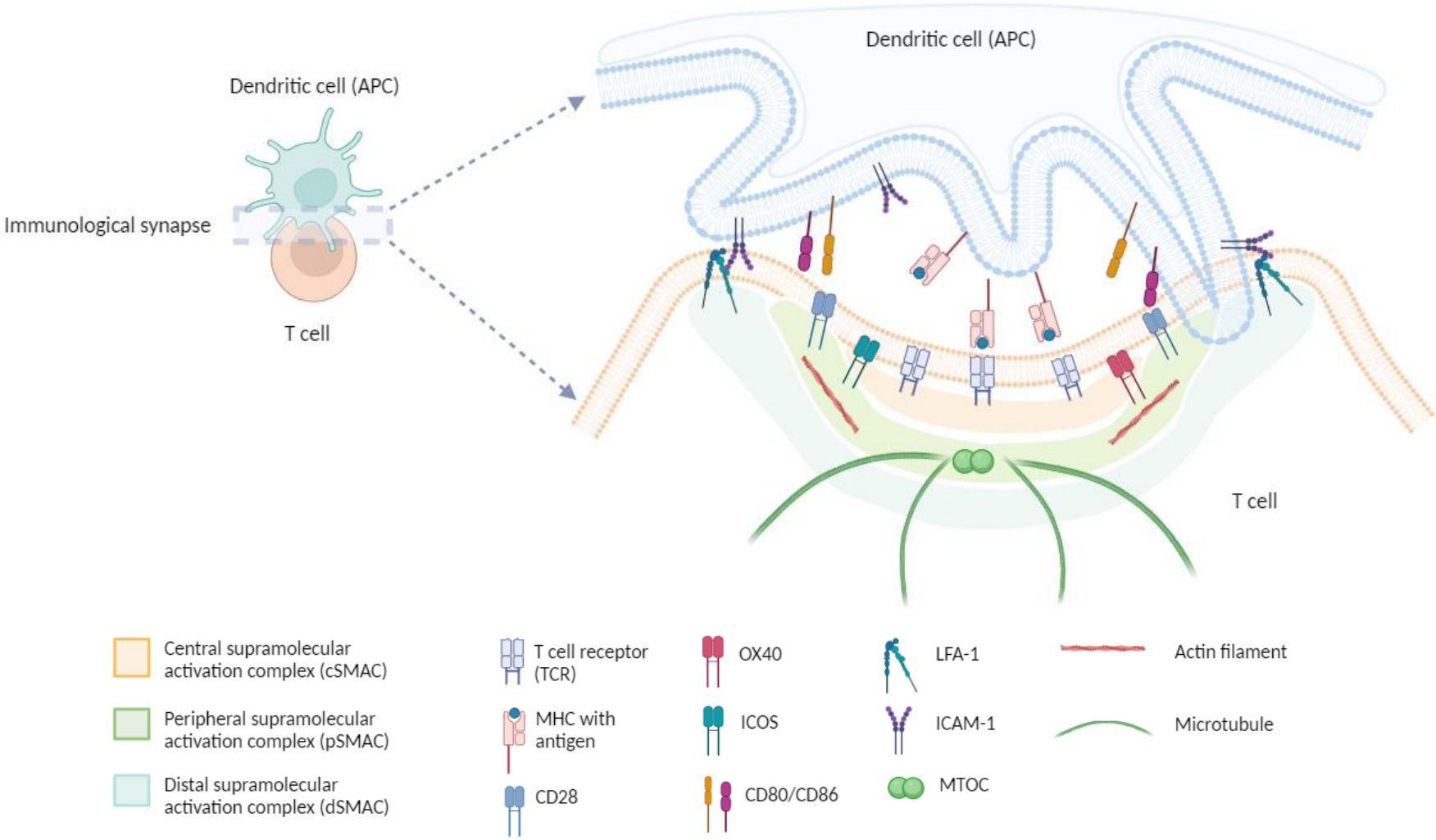

Figure 1.5 Immunological synapse between T cells and APC. During T cell activation, immunological synapse forms between cells to sustain T cell's signaling process. This process involves numerous molecules, which are clustered into three regions found on T cell's membrane: central supramolecular activation complex (cSMAC), peripheral (pSMAC) and distal (dSMAC) regions. cSMAC region initiates TCR activation by MHC molecules found on APC (induce Signal 1), whereas co-stimulatory molecules such as CD28 and ICOS (part of Signal 2) amplify the Signal 1 and mediate the cytoskeleton arrangement (i.e. actin filaments and microtubules) to shape T cell's synapse. pSMAC contain adhesion molecules (e.g. LFA-1) which secures and endures the interaction between cells [5]. Keyword: MTOC – microtubule organizing center. Figure created with Biorender.com.

the proliferation response [102, 103]. At this stage, T cells support their own survival and proliferation via autocrine manner by producing IL-2. CD28 co-stimulation also prevents cells from apoptosis by accumulating anti-apoptotic Bcl-Xl and increasing metabolic activity such as glucose uptake for T cells [104]. Other co-stimulatory molecules such as CD40L, ICOS and OX40 promote T cell activation by priming, enhancing cell's survival and tolerance in cells, respectively [105]. If co-stimulation occurs without a TCR signal, the expressed inhibitory signals such as CTLA-4 (cytotoxic T-lymphocyte associated protein 4) stops T cell activation by binding to CD80/CD86 [102].

Antigen-experienced (memory) T cells are co-stimulation independent, as reactivation by antigen only (i.e. Signal 1) is sufficient enough to induce T cells' activation response [105]. In some cases, the adaptive immune response driven by T cells becomes the first responder even before the innate immune system, generally known to be a vice versa response [44]. One study reported where tissues residential memory T cells induced DCs maturation, activated NK cells and recruited more T cells to the site upon viral re-infection [106]. Clearly, it was another way by the immune system to induce an immediate response.

T cells activation require a cytokine based Signal 3, that determines cells' phenotype and effector functions [92, 93] (Fig. 1.4). After the phagocytosed extracellular or intracellular pathogen, APCs secrete a specific set of cytokines instructing naïve T cells on the required response [92] (Fig. 1.6). For example,

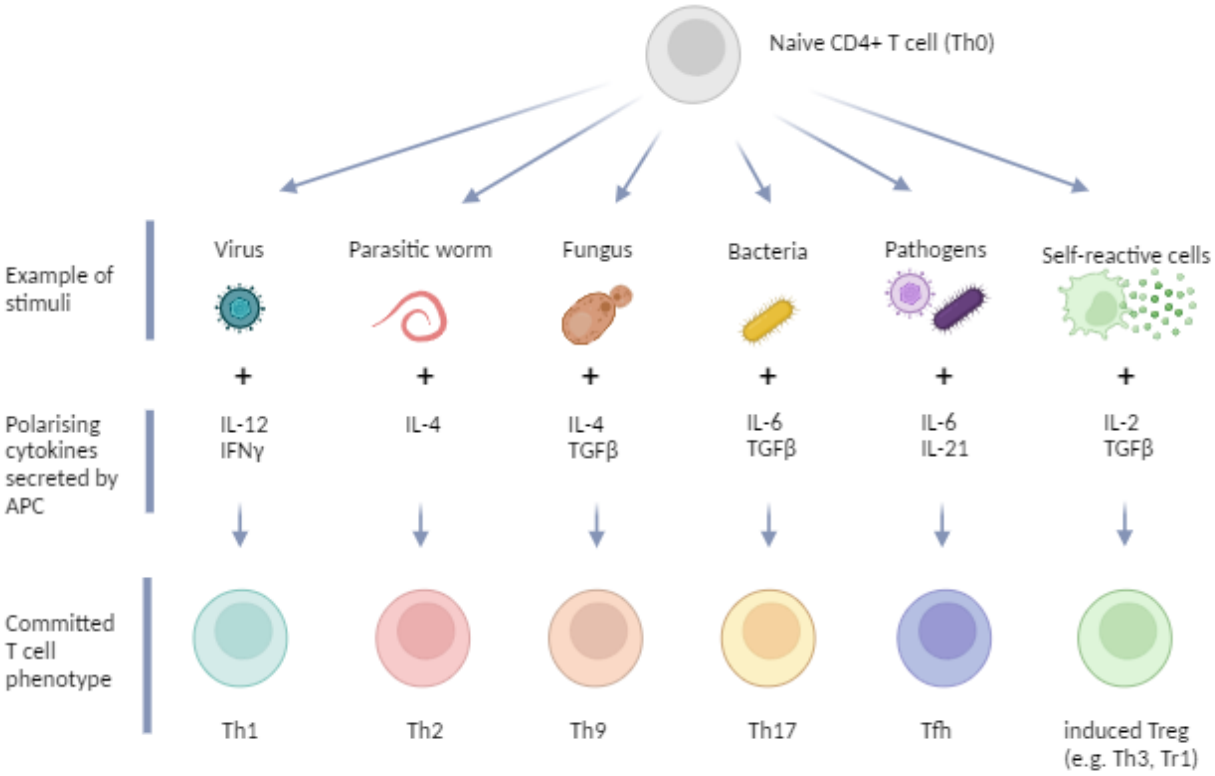

Figure 1.6 Cytokine pool effect CD4+ T cell phenotype. Stimulus, which could be any pathogen or self-reactive cell, induces APC activation. This causes the release of specific set of cytokines which instructs the activated, naïve T cells (already received Signal 1 and 2) on the required cell's phenotype to mediate an appropriate immune response. Figure created with BioRender.com

bacteria and parasites cause the IL-4 secretion which cause Th2 type response [107, 108]. This leads to B cell activation by Th2 cells and the generation of antibodies [108, 109]. Whereas viral infection causes IL-12 secretion, thus inducing Th1 and CTL function [110]. Th1 cells will support CTL activity whilst CTL are clearing the virally infected cells [6, 111, 112]. In addition, the combination of cytokines and the signal strength from TCRs activate specific TFs responsible for defining the T cell's phenotype [54, 113]. For example, IL-12 and INFγ cytokines with a strong TCR signal activate T-bet TFs to induce Th1; whereas IL-2, TGFβ and a strong TCR signal activate Foxp3 TFs for Treg [6, 114-116]. Signal

3 is defined as the final signal received by T cells over the course of activation process [117].

T cell responses can also be induced by non-peptide derived antigens presented by CD1 and MHC class I-related protein (MR1) [118, 119]. CD1 can present lipids, a small synthetic molecules or skin oil for T cell activation, whereas MR1 presents Vitamin B metabolites produced by a broad range of bacteria, activating mucosal associated invariant T cells (MAIT) [118-120]. This helps to set the immune response against various antigens, not just peptide-derived ones.

1.1.3.4. Antigen presenting cells (APC)

DCs take a great role in inducing T cells' activation [89, 121]. In absence of pathogen, DC retain an immature state, where they reside in the peripheral tissues and 'sample' the surroundings for potential stimulus [122]. At this stage, they also present the self-antigens and ICOSL (inducible co-stimulator-ligand) for T cells to maintain the immunotolerance response [105]. DC's ICOSL binds to the presented ICOS on T cells, which induces DC to maintain the low levels of co-stimulatory molecules and cytokine secretion [89, 105]. In some tissue areas, where microbial growth is normal (e.g. lungs, skin, intestine), DC receive tolerogenic mediators (i.e. IL-10, TGF-b) to prevent their own activation [105, 122]. But it is a different situation for blood or other sterile tissue areas, where DC undergo a maturation process upon pathogen encounter [105].

Upon pathogen exposure, DC undergo activation and become 'mature' cells [89, 123]. On their surface, they increase MHC molecules presenting antigen, express co-stimulatory molecules and secrete pro-inflammatory cytokines to induce T cells' response [89, 105]. DC morphology also changes into a 'stellate' shape, which increases its surface area for interaction with T cells', simultaneously increasing the number of interacting TCRs with MHC molecules (Fig. 1.7). This makes DC a favourable APC cell for the T cell activation, as B-cells lack the dynamic membrane needed for effective stimulation response [121]. Mature DCs express high levels of CCR7 chemokine receptor that enhances their

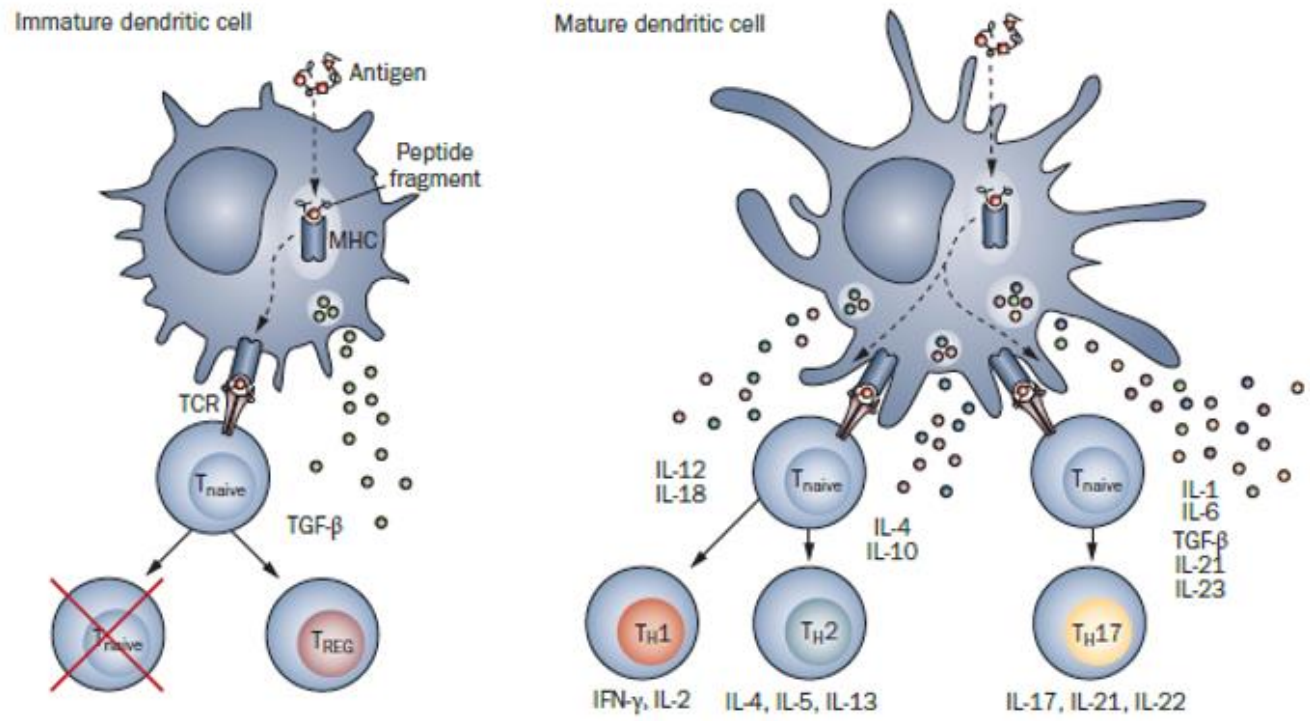

Figure 1.7 Immature and mature DC phenotypes, and T cell activation. Immature DCs search the surrounding environment by phagocytosis for pathogen or damage-related stimuli. They express autoantigens or environmental cues on the MHC molecules to maintain the immune tolerance and Treg activity. Upon pathogen encounter, DCs upregulate MHC and co-stimulatory molecules on their surface, and secrete the specific set of cytokines to activate T cells. Mature DCs morphology also change into the stellate shape, which enhances the immunological synapses formation between cells. Image is collected from Comabella et al. (2010) [9].

migration to the nearest lymph node from the peripheral tissues [105, 124]. In this state, DCs also stop further antigen uptake and processing, mainly to present the current antigen related to the pathogen found in the nearby tissues [105].

T cell activation could be induced by any other cells that express MHC on their surface. All nucleated cells express MHC Class I, which at all times present self-antigens as an indication of 'healthy cells' [90]. During intracellular infection, the same cell will present non-self antigens derived from pathogens on MHC Class I, and will signal for cytotoxic CTL response [44, 90, 105]. This is useful if the re-infection occurs and residential memory T cells (antigen-experienced) induce a localised immune response [10]. This delays local pathogens from spreading until newly activated T cells from the local lymph nodes arrive to enhance the immune response [10].

Upon extracellular pathogen encounter, DCs will present the antigens on MHC Class II molecules [90]. MHC Class II is mainly associated with 'professional' APCs, such as B cells and macrophages, but it can also be expressed by other cells such as neutrophils, monocytes, epithelial and endothelial cells under the influence of IFNγ cytokine [1, 90, 125, 126]. However, these types of APCs under IFNγ influence are only able to activate memory T cells.

In summary, DCs take the large part of presenting the antigen and activating T cells. Together with other types of APCs, frequent and multiple encounters of

antigen for T cells are needed to support their function until complete pathogen clearance. In absence of pathogen or danger associated stimuli, APCs with self-antigens maintain the tolerogenic response and support homeostatic survival of naïve T cells via MHC Class I [127].

1.1.3.5. Memory T cells

The adaptive immune system forms immunological memory after the first antigen encounter [44, 128, 129]. It occurs at the end of infection, where the large population of effector T cells (90-95%) commit apoptosis and leave a fraction of cells, known as memory cells [129]. Memory cells will respond to the subsequent antigen exposure with an increased proliferation rate and effector function capacity which cause a secondary response quicker than the primary one [128, 131]. They also have access to the peripheral tissues, and restrict for naïve cells [44]. There are three types of memory T cells that are functionally and locally distinctive amongst themselves. CD4+ and CD8+ T cell subsets can become memory T cells, classed as effector (Tem), central (Tcm) or residential cells (Trm) [129, 130].

Tem mainly circulate through the spleen, blood, lymph nodes and peripheral tissues, such as lung and intestines [76, 129, 130, 132]. After antigen encounter, they induce a rapid effector response with low proliferation rate, making them 'first responders' to the infection until more effector cells arrive (Fig. 1.8) [10, 129, 130]. Tcm have the same role as Tem, but they circulate through the blood and lymphoid tissues rather than residing in non-lymphoid tissues [76]. A key

characteristic of Tcm is increased proliferation capacity, whereupon antigen encounter produce a larger number of effector cells [44]. Whilst Tem in the periphery deliver the first response, this gives time for Tcm to proliferate and form a large number of effector cells (Fig. 1.8) [44]. In the absence of infection, Tcm together with naïve T cells circulate through the lymphatic and blood system and dedicate 6-18 hours per lymph node to detect the cognate antigen [130].

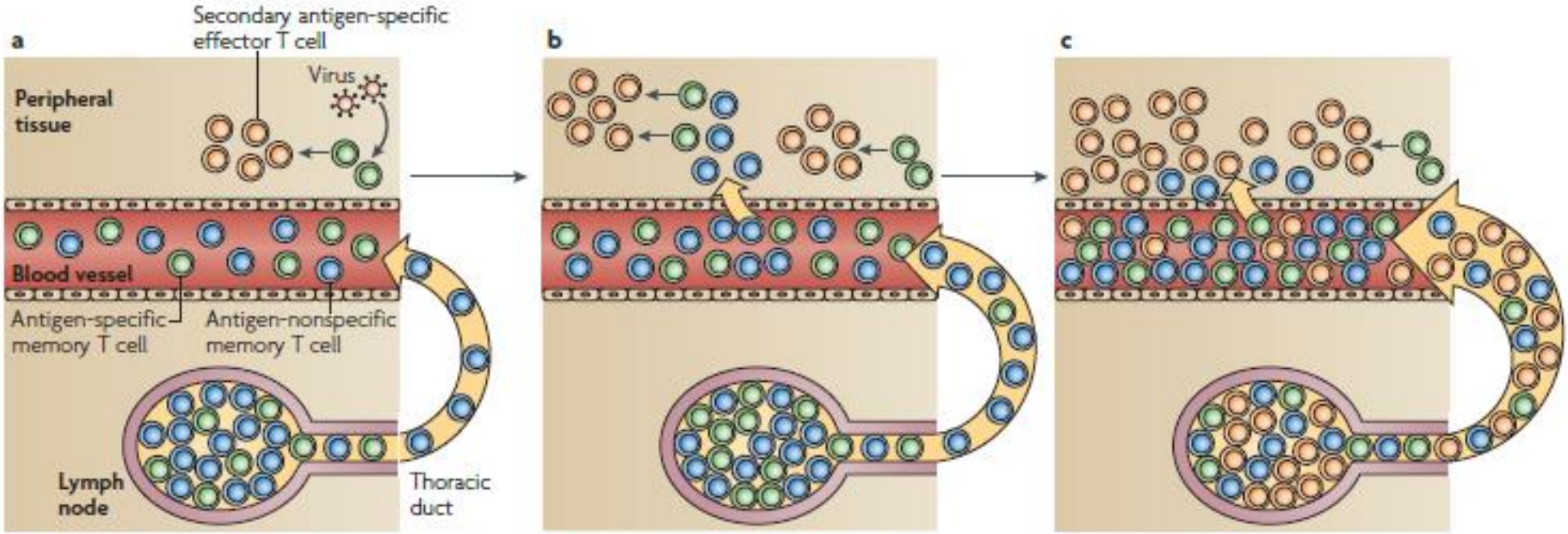

Figure 1.8 Memory T cell response in the peripheral tissues. a) During secondary antigen exposure, local memory T cells (i.e.Tem, Trm) are the first to respond to the pathogen (i.e. virus). In the meantime, antigen specific Tcm circulates through the system until they encounter the cognate antigen in lymph nodes. Activated antigen-specific memory cells migrate to the infected site, proliferate and initiate the immune response. **b**) At the infection site, only antigen-specific memory T cells will deliver the effector response. **c**) The increasing number of antigen-specific effector T cells at tissue and lymph node sites, ensures the effective pathogen clearance. Image obtained from Woodland et al. (2009) [10].

Memory T cells entering non-lymphoid tissue areas can become residential T cells (Trm) [76]. They are mainly found in mucosal tissues (intestine, lungs, skin), where frequent antigen exposure occurs [76]. These cells reside permanently in tissues by expressing high levels of adhesion markers and do not circulate through the system as other memory cells [129]. In tissues, cells maintain their own expansion and induce immediate response until Tcm produce active effector cells [76, 129].

Immunological memory develops throughout childhood upon constant exposure to the environmental microbes and danger-related particles [129]. At an early age, the T cell pool is mainly composed of naïve T and Treg cells, which become memory cells upon antigen exposure. During the aging process, memory T cells pool increases whilst naïve T cells population declines over time [129]. This is due to thymus 'shrinkage', also known as thymic involution, where at an elderly age the output of naïve T cells is reduced [74, 133]. In contrast, memory T cells pool is maintained throughout aging by homeostatic proliferation mediated by IL-7 and IL-15 cytokines [76, 129, 134].

1.1.3.6. T cell plasticity

During T cell activation, a naïve cell differentiates into the mature effector cell with a defined function and lineage subset (Table 1.1). CD4+ T cells subtype is defined by the antigen type, TCR signal strength and cytokine milieu (Fig. 1.6) [135]. Whereas CD8+ T cells mainly get activated into 'killer' cells to mediate their cytotoxic effect [136]. However, the committed effector cells can still alter

their phenotype and function under the changing tissue environment. This is known as T cell 'plasticity', wherein a committed cells change its characteristics to a different T cell lineage (Fig. 1.10) [6, 137]. One example is Th17, which normally expresses RORγt transcription factor and IL-17, where found to be secreting IL-17 and IFNγ during bacterial infection [138]. Th17 also expressed T-bet transcription factor, that are mainly found in Th1 cells. It is speculated that the reason for Th17 plasticity and acquired Th1 function is to prevent the bacterial systematic spread [138]. It is clear that under the right circumstances, T cells adapt to deliver an appropriate response.

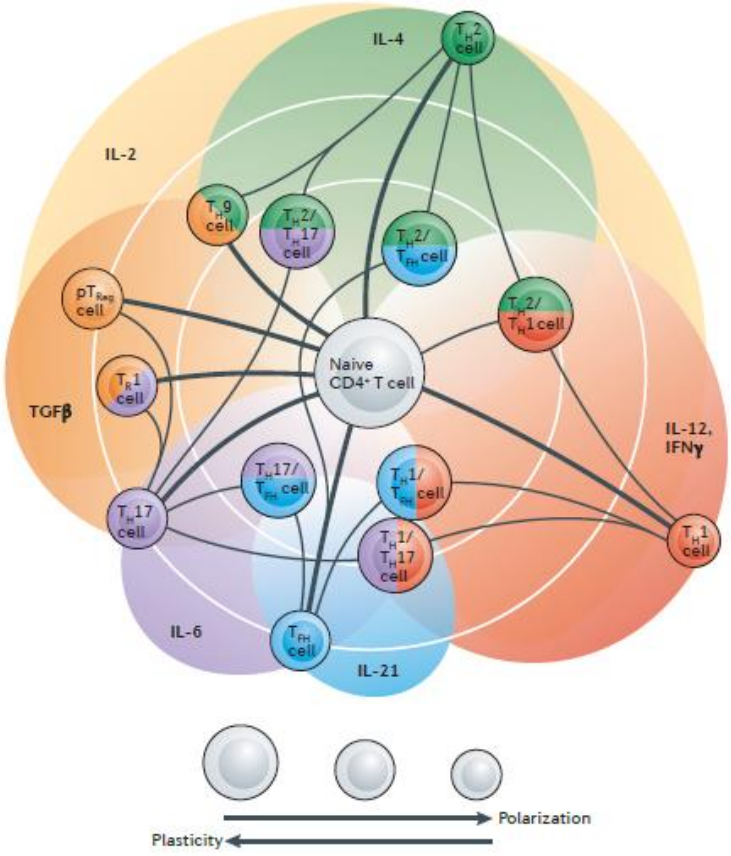

Figure 1.10 CD4+ T cell plasticity. Naive T cells have the greater capacity of plasticity (hence the cell size) under the influence of cytokine milieu. During naïve T cell differentiation towards fully-committed phenotype (i.e. polarised cell, small cell size), at midpoint of the process it still has the capacity to commit to several phenotypes. This produces T cells with distinctive effector functions, which are not normally found in fully polarised cell. Image obtained from Du Page et al. (2016) [6]

1.2 3D culture

The majority of the biological experiments contain *in vitro* (outside of living organisms) and *in vivo* (within living organisms) studies. *In vitro* studies are carried out in plastic or glass containers (defined as 2 dimensional i.e. 2D cultures), which lack the multicellular organism analyses commonly found in animal models [139]. However, 3D (3-dimensional) culture is getting more attention as the 'bridge' between these two types of studies because it can overcome the simplistic culture experimental set ups and avoid genetic and physical differences to human-related studies [139, 140].

The demand for the 3D culture system could be reflected in article publishing, which peaked in 1990 (Fig. 1.11). This could be attributed to the available novel methods and materials and the demand for tissue-specific experiments. However, there was a clear decline in publishing in 2022 that may have been affected by the COVID-19 pandemic - causing research facilities' closures, delayed data acquisitions and reduced research funding [141].

3D culture is part of *in vitro* studies and can be set up with scaffold or scaffold-free techniques [139]. Scaffold-based cultures require a biomaterial that allows a structural platform for cells to grow. This could be hydrogels, hard polymer scaffolds, micropatterned materials (e.g. electrospinning), decellularized tissues and microfluidic devices [142, 143]. Conversely, scaffold-free techniques are mainly based on the cellular aggregates (i.e. spheroids and hanging drop

cultures) [140, 142]. Depending on the research question, there is an array of methods and biomaterials to study a specific cell response. For example, spheroids made from the cancer cells represent compact tumour tissues ideal for drug-screening studies [144]. Microfluidic devices can be used to study the valve formation by controlling the effect of lymph flow and wall shear stress on the lymphatic endothelial cells [145]. However, hydrogels are ideal for 3D culture studies due to their ability to recapitulate cell-ECM interaction commonly found *in vivo* studies [140, 146]. Notably, they can retain >95% of water in their structure, which recreates fluid-filled like tissues [142, 146].

The rest of this section will explore key aspects of 3D culture and discuss its relevance for T cell studies.

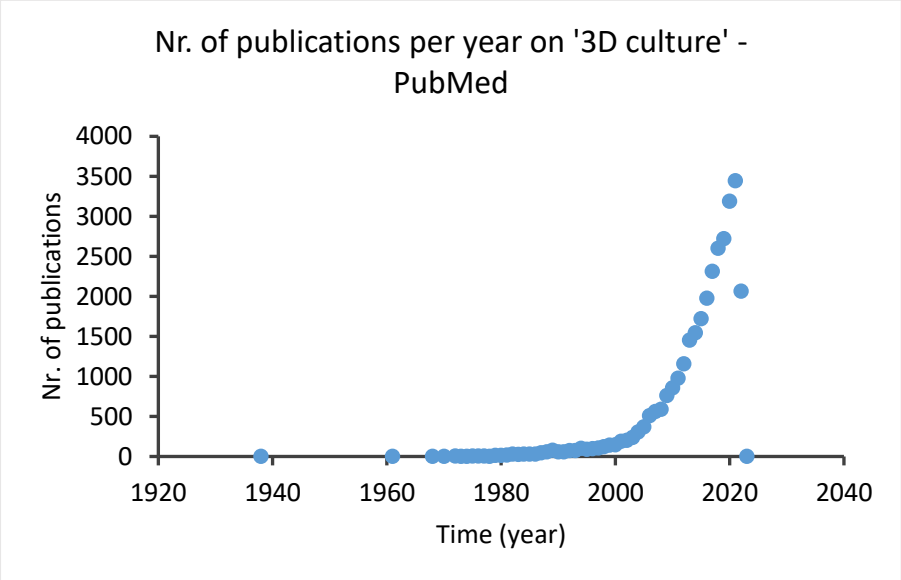

Figure 1.11 Number of publications per year on the '3D culture' system. The graph is generated from PubMed based on the '3D culture' keyword. The publication number is reported by year from 1938 – 2023. The decline of publications in 2022 are attributed to COVID-19 pandemic effect on research [141].

1.2.1. Distinction between 2D and 3D cell cultures

2D culture is a commonly used method in various research studies. Due to its simplistic method and low costs, it makes the studies more affordable and achievable [142]. However, cells still lack the natural tissue environment that could effect their natural response. For example, one study explored HIV-1 infected macrophage migration, where the virus-related protein Nef enhanced migration response in 3D culture but not in 2D culture [147]. 3D culture observations supported *in vivo* studies in mice, where HIV infected macrophages became migrating cells [147]. The distinctions between two culture systems are highlighted in Table 1.2, which summarises the overall effect on cells and technical aspects of the *in vitro* experiments.

The clear differences between two *in vitro* cultures highlights the importance of improving 2D culture settings. However, in some scenarios 2D culture studies can provide constructive results reflecting some of the features found in the tissue environment. For example, studies on the immune cell-cell interaction like in lymph nodes could be studied in 2D culture. This is because the lymph node contains more of a cellular compartments of immune cells, which lack the interstitial ECM environment for the purpose to maintain cell-cell interactions to elicit an immune response (Fig. 1.12) [148, 149]. ECM of the lymph nodes appear in a reticular network form, which sheathed by the fibroblastic reticular cells (FRC), leaving a small patches of ECM exposed to the immune cells for adhesion and antigen sampling processes [150, 151]. However, 2D culture could be

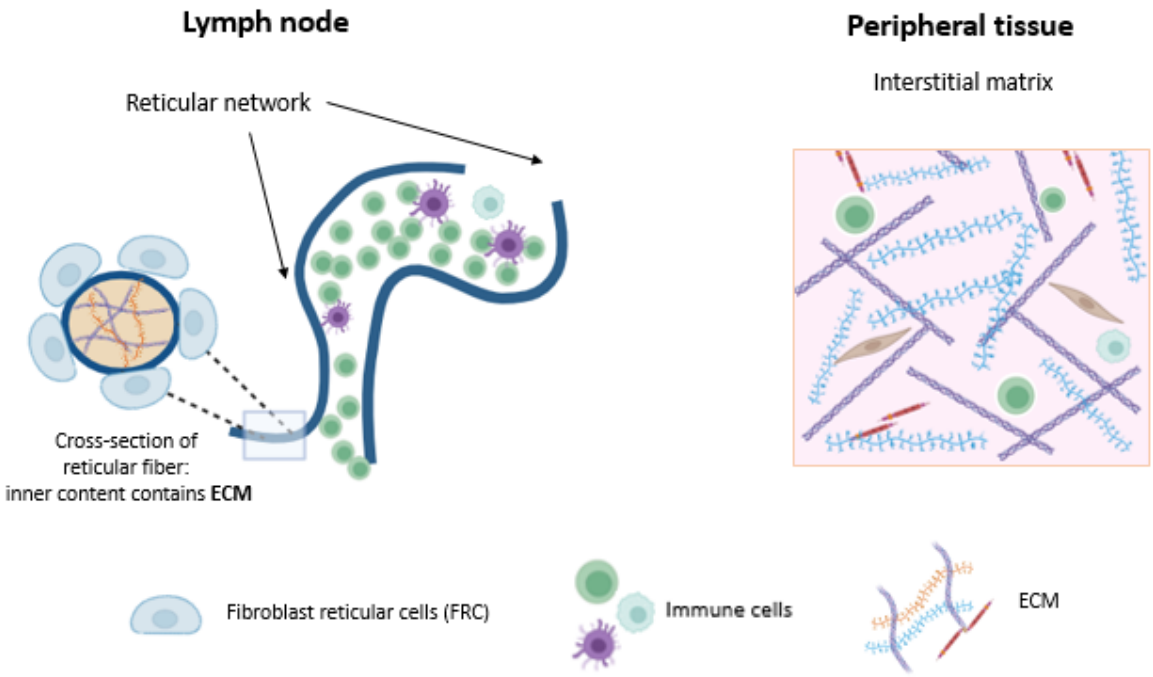

Figure 1.12. ECM interaction with immune cells in lymph nodes and peripheral tissues. Lymph nodes contain the reticular networks, which create a 'cellular compartments' for immune cells to interact with each other. Reticular fibers are surrounded by FRC which deposit ECM content within inner structure of the fiber. A small gaps between FRC allows immune cells to interact with ECM content. Whereas immune cells in the peripheral tissues are surrounded by the ECM network. Figure created by BioRender.

replaced by large-porous scaffolds to replicate lymph nodes' 3D structure, which still support the cell-cell interactions [67]. The decision on culture type depends on the research question as to what extent 2D or 3D culture is required and feasible for the research; however, examples in Table 1.2 indicate clear advantages of using the 3D culture system.

Table 1.2. Differences between 2D and 3D cultures

Cell/material related characteristics	2D culture	3D culture	Example	Ref.
Cell morphology	Cell morphology is different to cells found in tissues	Retain the morphology like in tissue areas	Dendritic cells (DC) in 2D culture formed long dendrites, whereas in collagen hydrogel cells appeared rounder with short protrusions.	[139, 152, 153]
Cell polarity	Forced polarity and elongated cell shapes	Cell polarity and shape maintained	Macrophage with IL-4 in GelMa hydrogels polarised into more to M2 type (induce wound healing) than cultured on 2D culture.*	[153-155]
Cell differentiation	Poor marker expression, limited differentiation	Support cell differentiation	Bone marrow cells in the collagen hydrogel differentiated to DC, expressing specific DC markers (e.g. CD11b, CD40, CD80) than in 2D culture.	[139, 155, 156]
Cell to cell interaction	Direct cell-cell contact; unrealistic/enhanced cell response	Cell have controlled and limited response to other cells; set up the related complexity of cell-cell interactions	CAR T cells (engineered cancer specific T cells) were cultured with ovarian cancer cells. Under 2D culture superb cytotoxic effects were detected; gelatin methacryloyl hydrogel in the microfluidic device showed poor cytotoxic effect.	[155, 157, 158]
Cell to matrix interaction	Plates can be coated with ECM components but cell-ECM interaction is one sided	Cells exposed to ECM components from all directions; mitigate cell realistic behaviour (i.e. migration, adhesion)	T cells' stimulation by DC in the 2D culture caused large proliferating clusters of T cells, due to prolonged interaction with one DC. In the 3D collagen matrix, T cells formed smaller proliferating aggregates and maintained short interactions with DC due to induced cell migration by collagen. T cells under 3D interact with multiple DC.	[140, 142, 155, 159]
Gradient exposure to nutrients, oxygen, drugs, stimulus	Cells are equally exposed to nutrients, oxygen, drugs; no molecular gradient	Molecular gradient is present, unevenly affect cells	Regions of hydrogel which had hypoxia (low oxygen) induced a higher T cell cytotoxic effect against ovarian cancer cells than normoxia (normal oxygen level) regions.	[139, 155, 157]
Adhesion and migration	Cell migration is limited to *xy* directions; due to adhesion cells retained in one position; gravitational setting	Migration induced to *xyz* directions	Tumour specific T cells migrated across collagen and induced 25% killing of tumour cells. Whereas in 2D culture, T cells settled down to the bottom of plate due to gravity and induced complete killing of cancer cells.	[140, 155, 160]

Table 1.2. Differences between 2D and 3D cultures (continue)

Cell proliferation	Due to high cell-cell contact and encounter cell proliferation is rapid and enhanced	Cell proliferation is lower due to reduced cell-cell to encounter	T cells proliferated less in alginate hydrogel than in 2D culture once they encountered APC. This is due to low cell encounter frequency; T cell proliferation was lower to DC in the collagen hydrogel than in 2D, as T cell migration on collagen caused short lived interaction with DC.	[139, 155, 159, 161]
Costs	Inexpensive	Expensive, but in some scenarios could replace expensive animal models		[139, 142, 162]
Availability of equipment and assays	Wide range of assays and equipment available to analyse cell response	Limited availability of kits and equipment to analyse 3D cell cultures		[162]
Experiment set up and data analyses	Less complicated experiment set up and data analyses	Experiment readouts could be complicated, especially when study involves various factors (i.e. type of material and its properties influencing cells)		[158]
Reproduction of *in vivo* environment	Limited	Tissue specific features could be included in studies, closer resemblance of *in vivo*	Collagen scaffold-based3D cancer model increased cancer cell growth (tumour mass), invasion across the basement membrane (migration) and structure's packed lumens with cancer cells. Altogether replicated cancer architecture found in tissues. The model was used to study anti-tumour CAR T cell function.**	[139, 140, 142, 155, 163]
Stiffness	Limited; commonly used tissue culture plates are rigid, reaching stiffness level to GPa	Wide array of biomaterials are available to represent soft to hard/solid tissue environments	T cell proliferation to APC was improved in porous alginate hydrogel with high stiffness level as opposed to soft; high collagen hydrogel density limits T cell proliferation response morethan low density.	[142, 155, 161, 164, 165]

*M2 – macrophage type 2 (induce anti-inflammatory response); ** CAR T cell – chimeric antigen receptor (CAR) T cells, genetically engineered patient's T cells to deliver anti-tumour response.

1.2.2. T cells and 3D cell culture

The 3D T cell culture research area gained its popularity from late 2000, evident by an increased number of publications per year (Fig. 1.13). There is a clear interest from material science and T cell biology on improving current *in vitro* studies, but the number of publications is still low in comparison to other research areas (e.g. Fig. 1.11). A limited number of published studies challenges current researchers to understand T cell requirements in a 3D culture system.

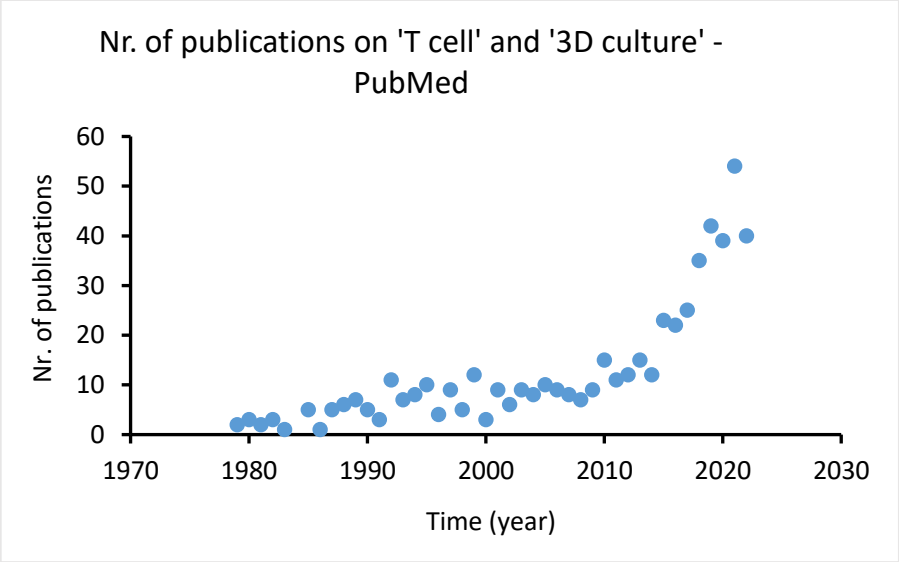

Figure 1.13 Number of publications per year on '3D culture' and ' T cells' system. The graph is generated from PubMed based on '3D culture' and 'T cells' keywords. The publication number is reported by year from 1938 – 2022. The decline of publications in 2022 is attributed to the COVID-19 pandemic's effect on research [141].

The majority of 3D culture studies begin by reflecting first to the tissue surroundings where T cells are commonly found [157, 160, 161, 164, 166-169]. For example, Mollica et al. (2021) studied the impact on T cell infiltration via the endothelial cell wall to target the pancreatic cancer cells [170]. The pancreatic tumour microenvironment contains stromal and fibroblast cells, which cause excessive ECM deposition, a tumour-associated

endothelial cells that create an anergic vasculature to limit T cell infiltration to the tumour site. In the microfluidic device, pancreatic cancer cells were encapsulated in the collagen hydrogels (abundant protein in ECM), surrounded by pancreatic stellate cells and endothelial cell wall. The data has shown T cells had greater migration towards cancer cells and stellate cells only in the absence of endothelial cell wall, rather than in presence of it [170]. It is clear that 3D pancreatic cancer models would be unfeasible under 2D culture settings because it could not provide 3D architecture, different cell compartments and might misrepresent cell morphology/polarity. The majority of T cell work occurs in the tissue surroundings, thus 2D culture studies underrepresent T cells and their functions. Specific tissue areas are reviewed in the following sections that explain how different environments affect T cell functions.

1.2.3. Lymph node microenvironment

Lymph nodes are known as 'biological filters', as they mainly contain immune cells checking the draining lymph fluid from the adjacent peripheral tissues for the incoming pathogens [171]. Lymph enters via afferent lymphatic vessel and goes through the conduit system crossing the superficial cortex, paracortex and medulla regions (Fig. 1.14) [150]. Each region contains distinctive populations of immune cells that increase the chance of detecting any incoming pathogen. [7, 12, 171]. The paracortex region is the main site for T cells, where iDC or peripheral migrated mDC initiate the adaptive immune response. Lymph fluid is also screened by the iDC in the paracortex region, and if DC are activated, the mature DC will initiate T cell response [171].

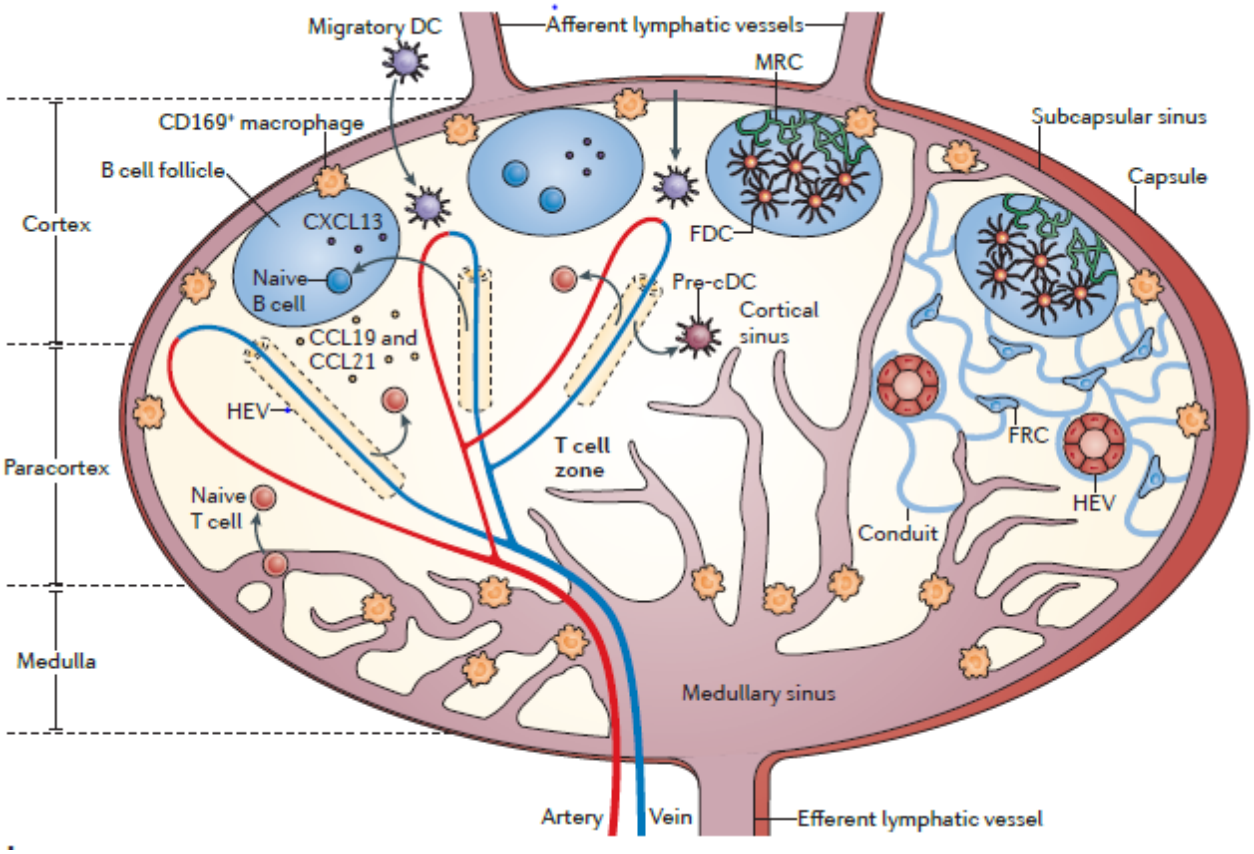

Figure 1.14 Structure of the lymph node. Each different lymph node region is dedicated to the specific population of immune cells, which are attracted by the 'homing' chemokines. Cortex region is dedicated for B cell activation with assistance of FDC and MRC, paracortex for T cells and medullary sinus is mainly populated by macrophages. T cells enter lymph nodes via HEV to the paracortex region, and search for the cognate antigen presented by DCs. Upon antigen encounter, T cells undergo activation and remain in the lymph node for several days. In the absence of antigen, T cells re-enter the HEV system and circulate to the subsequent lymph node for the continuous antigen search. Keywords: HEV – high endothelial venule; FDS – follicular dendritic cells; MRC – marginal reticular cells. Image obtained from Girard et al. (2012) [12]

The paracortex region contains reticular meshwork and FRC [150, 151]. As reviewed by Willard-Mack (2006), the entire lymph node is made from the reticular meshwork, a sponge-like tissue composed off ECM (collagen type I, III and IV, elastin, entactin, fibronectin, laminin-1, tenascin, vitronectin, heparan sulphate) [171]. The ECM itself is 'wrapped' by the FRC that maintain the ECM structure (Fig. 1.15) [150, 151]. FRCs show the features of the epithelial cells as well, as they elongate across the reticular fibres and

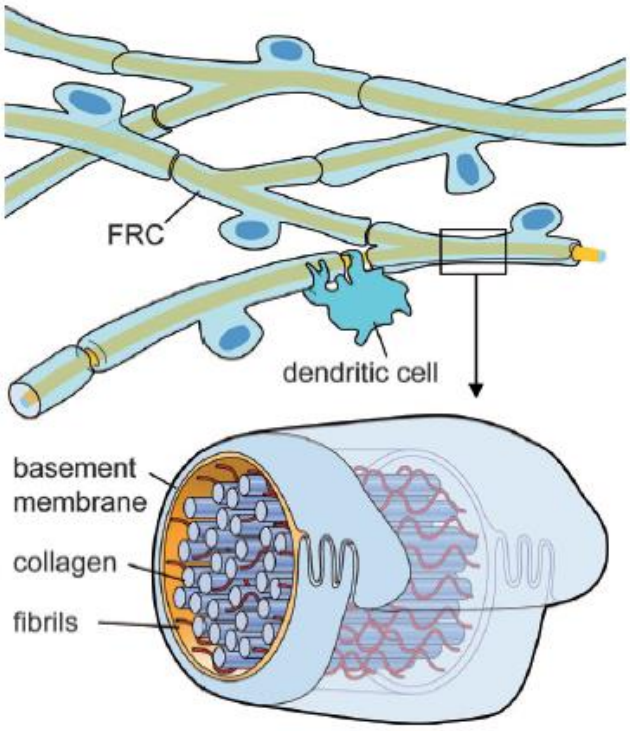

Figure 1.15 Reticular meshwork and conduit system. Reticular meshwork is wrapped by the FRC, which maintain the ECM structure. Small gaps are mainly occupied by APC cells, such as DC, as they sample the running lymph through the conduit system and search for the antigen. Image obtained from Roozendaal et al. (2008) [7].

form tight junctions between the cells. 90% of reticular meshwork is wrapped by FRC, leaving a small regions exposed to the immune cells [171]. The small regions are mainly occupied by APCs, sampling the lymph running through the conduit system (within reticular meshwork) for pathogens [150].

T cell migration is mainly mediated via fibronectin and collagen IV expressed on the FRC cell membrane [7, 148, 171]. The same studies emphasise that T cells do not interact with ECM found in reticular network. One study have showed that activated T cells have increased expression of integrins on their surface, which mediate cell attachment to the ECM in tissues [172]. If ECM in lymph nodes are exposed to the activated T cells, this could

cause the prolonged localisation of cells and delayed immune response. T cell motility via paracortex area is also controlled by FRC secreted homing chemokines such as CCL19, CCL21, CXCL12 and lysophosphatidic acid (LPA) [173]. This cause naïve T cells (antigen-inexperienced) to remain in the lymph node for nearly 8-12 hours only, until they migrate to the subsequent lymph node for the continuous antigen search [173, 174]. Once they encounter the antigen, T cells remain for 3-4 days for the stimulation and differentiation processes in the lymph node [175].

In addition, T cells enter and exit lymph nodes via high endothelial venules (HEVs), specialised blood vessels formed by high cuboidal shape endothelial cells, permitting lymphocyte transmigration across the vessel [171]. HEVs are only found in lymphoid tissues (except the spleen) where they express heparan sulphate which immobilise secreted chemokines (e.g. CCL21) to induce transmigration of T cells to lymph nodes [12, 176]. Distinctive blood vessels and immobilised chemokines targeting only immune cells ensures T cell homing to the lymph nodes for the continuous search process.

The lymph nodes are elastic organs, whereupon increased lymphocyte proliferation they increase their size to maintain the expanding cell population [148]. During a healthy state, lymph nodes are classified as soft tissues where the stiffness level ranges from 120 Pa - 1kPa [177, 178]. But during the disease state, lymph node stiffness increases, for example: metastatic breast cancer causes lymph nodes to reach 45.4 kPa, Kawasaki disease 12.2 kPa, and bacterial infection 16.37kPa [178, 179]. This also affects T cell metabolic activity, as they express Yes-associated protein (YAP), a mechanosensor which feeds back to cells about the changing mechanical forces in the surroundings [180]. During inflammation,

lymph nodes' stiffness level increases whilst T cells undergo an activation process. But in the resolution process, the stiffness level decreases in the lymph node area which results in reduced mechanical forces on cells. Upon reduced mechanical force, YAP reduces NFAT activity, a TF responsible for activation and proliferation response in T cells [180]. This eventually brings the T cells to the senescence stage, as their response is not needed.

One more specific feature of the lymph node for T cells is the narrow passages for cells to migrate in between the reticular meshwork. Kaldjian et al. (2001) indicates the reticular meshwork interspaces ranges between 5-20μm wide, which is enough for 2-3 T cells to pass [148]. It is possible that narrow passage of cells is structured to increase the cell-cell interaction, especially with APCs bearing the cognate antigen. One study mentioned that one APC will interact with 500-5000 T cells per 1 hour in the lymph node, which ensures that upon frequent cell-cell interactions an immediate immune response is induced when it is needed [175].

Overall, lymph node structure provides T cells with a cellular rather than matrix microenvironment. The organ itself is organised to provide an immediate and efficient T cell response by limiting contact with ECM and induce frequent encounters amongst the local cells.

1.2.4. Inflammatory tissue microenvironment

T cells enter the peripheral tissue site once there is inflammation caused by pathogen or danger-related stimuli. These cells, as mentioned before, have to be activated first to change their naïve phenotype to enter the peripheral tissues

[44]. Naïve T cells are not equipped to deal with peripheral tissues due to the lack of active adhesion molecules suitable for ECM [172]. They express adhesion molecules (e.g. CD62L) to maintain their circulation through the lymphoid system and search for the cognate antigen [76]. This means that inflammatory tissue areas are mainly dealt with by antigen-activated or memory T cells, since they are equipped with adhesion receptors to maintain their location and function in the peripheral tissues.

Peripheral tissues contain two types of ECM, known as the interstitial matrix and basement membrane [181] . Basement membrane is a compact matrix mainly made off the collagen IV, laminins, heparan sulphate proteoglycan, perlecan and small proteins like nidogen and entactin [181-183]. The ECM itself is highly crosslinked with glycoproteins and densely packed with protein fibres, which altogether serve as the boundary between different types of tissues [182, 184]. The interstitial matrix is a more loose, fibrous network composed from collagen I, III and V and fibronectin, which provides scaffold and strength for the peripheral tissues [182]. It also contains the chondroitin-, dermatan, keratan sulphates and hyaluronic acid (HA), all together identified as glycosaminoglycans (GAGs). The basement membrane controls extravasation of the immune cells from the blood vessel to the tissues' matrix, whereas the interstitial matrix permits cell migration across the tissues' areas [182]. Chemokines and cytokines released by endothelial and inflammatory cells direct T cell adhesion to the endothelium and intraluminal crawling until they find the permeable site to mediate transendothelial migration [185].

During the inflammation process, one of the key transitional moments in the interstitial matrix is ECM degradation (Fig. 1.16) [3, 182, 184]. It is induced by released proteases such as metalloproteinases (MMPs) that degrade all ECM proteins [181]. This facilitates leukocyte infiltration, especially for T cells, to the inflamed tissue areas where loose ECM networks provide wider gaps for incoming cells [182]. However, T cells can migrate through the matrix in the absence of proteolytic enzymes by using amoeboid-type movement, known for its low-affinity migration, independence of β1 integrins and induced cell's actin cytoskeleton reorganisation [186]. Nevertheless, this movement can be restricted by dense tissue matrices, limiting T cell migration because of the smaller matrix gaps [182, 186]. This could be attributed to the expressed lamin-A protein, responsible for the nucleus's structural protection in cells [187]. Only activated T cells express this protein, thus limiting cells' migration through the dense ECM to prevent nucleus deformability and rupture [148, 164, 187]. In this circumstance, ECM degradation is compulsory for T cell infiltration to the inflammation site.

Upon ECM degradation, there are various ECM derivatives released to promote pro-inflammatory response [182]. Damaged interstitial matrix by pathogens or mechanical trauma, causes the release of molecules such as tenascin C (mainly occurring in synovial fluid and cartilage), biglycan, heparan sulphate and low-molecular weight hyaluronan –

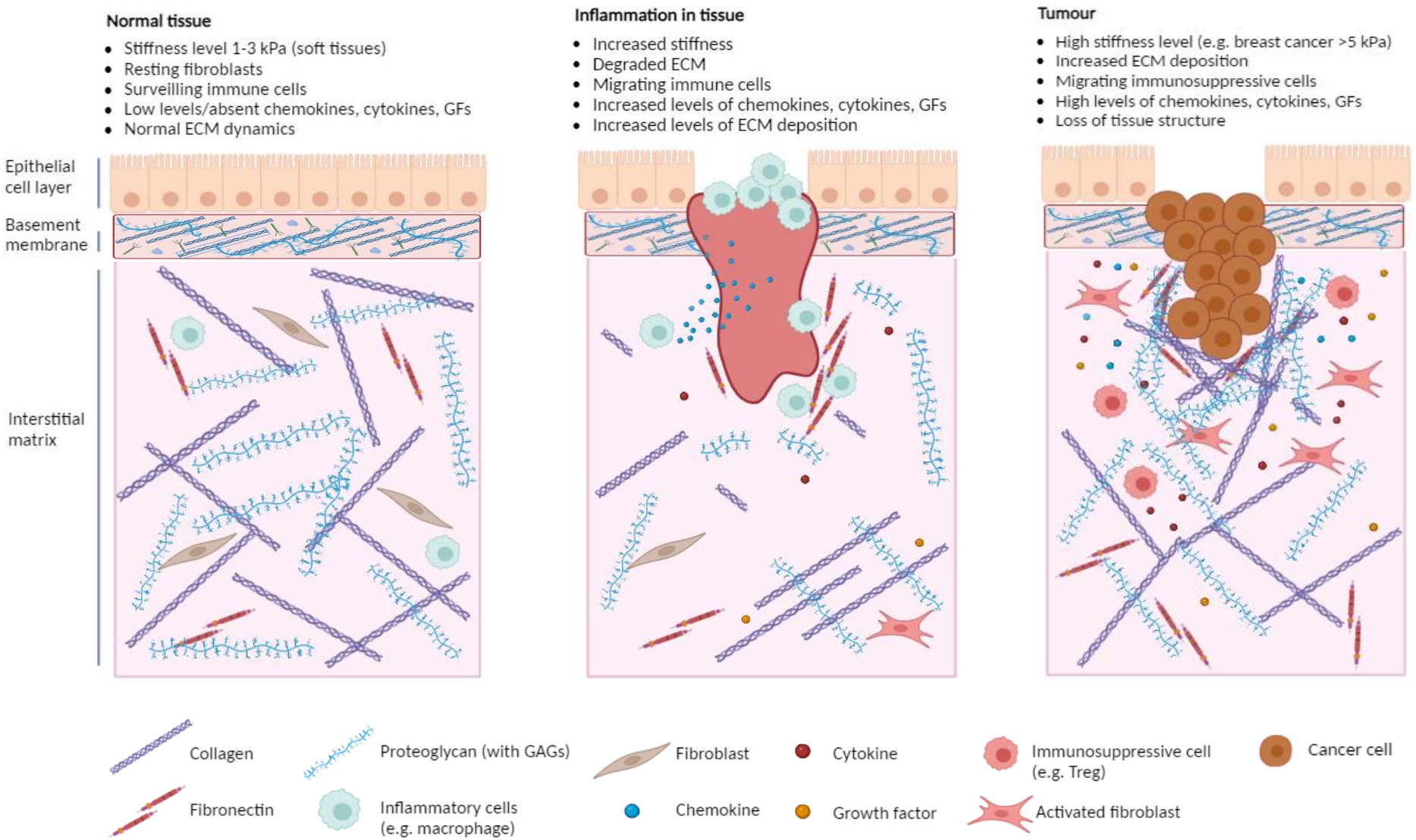

Figure 1.16 Cellular and matrix composition in normal, inflamed and tumour tissues. In the normal tissue, there is a healthy balance between cells and matrix components which produce a microenvironment with less mechanical tension and stress. During inflammation, damaged tissue area release the ECM fragments which act as 'danger' signals for the inflammatory cells. This also causes the local cells to secrete the chemokines, cytokines and growth factors which mediate the immune response and tissue repair processes. Towards resolution, activated fibroblasts deposit ECM to restore tissue's structure. In the tumour microenvironment, there is high disorganization of matrix and cellular components which result in excessive ECM deposition and amount of secreted molecules. The abnormal cancer cells growth, recruitment of immunosuppressive cells and activation of fibroblasts leads to more rigid and stiff tissue structures [3, 4]. Figure created with BioRender.com.

all known as extracellular DAMPs [28, 182]. Hyaluronan is a great example of how T cells' activity is mediated by this abundant GAG molecule found in all tissues [188]. It interacts with T cells via CD44 adhesion receptor, and depending on its molecular weight, it can induce pro- or anti-inflammatory responses [182, 188]. For example, high molecular weight hyaluronan is found in the healthy tissues, mainly promoting T regulatory cell activity to maintain local immunotolerance response [189]. But upon tissue damage, hyaluronan fragments (low molecular weight) will promote effector T cell activity by supporting their migration and survival during the inflammatoryresponse [182, 188, 190].

The ECM also manipulates the concentration gradient of molecules, which attract, localise and support T cells at the inflammation site [184]. One of the key players are heparan sulphate; another GAG molecule but with a strong negative charge that sequesters secreted chemokines, cytokines and growth factors in the matrix [191]. Heparan sulphate is known to sequester released IL-7 and IFNγ cytokines, which are important to maintain T cell survival and pro-inflammatory response, respectively [6, 192]. Without heparan sulphate cytokines would undergo proteolysis eventually limiting the effect on cells [191]. It also binds to the chemokines (e.g. CXCL12, CCL21, CCL19), which are present in the blood vessels and interstitial matrix, to mediate T cell chemotaxis [191]. The established chemokine gradient by heparan sulphate directs T cells to the specific site where an immune response is needed.

Another difference between inflamed and healthy tissue is an increased tissue's stiffness level (Fig. 1.16) [184]. Various healthy tissues retain specific stiffness levels - e.g. soft tissues such as brain (1-3 kPa) and liver (2kPa), and stiff tissues such as bone (10.4-20.7

GPa), and cartilage (5.7-6.2 MPa) [193]. But during the inflammatory response, the stiffness level increases due to increased ECM deposition such as collagen, elastin and hyaluronic acid [184, 194]. Collagen is one of the key modulators of the tissues' stiffness, whereupon increased secretion by fibroblasts and cross-linking by lysyl oxidase enzymes (LOX) alters the stiffness level [184, 195]. Enhanced collagen deposition and cross-linking also affects tissue porosity, which in some scenarios (i.e. fibrosis) can prevent cell migration. This was clearly demonstrated in research by Kuczek et al. (2019), where increased collagen density limited gradual T cell infiltration through the collagen hydrogel [164]. Upon enhanced ECM deposition it also shapes the ECM topography, where cell orientation and migration are diverted by the microenvironment [195]. For example, aligned collagen fibres induce faster, directional, and persistent T cell migration when compared to an unaligned collagen network [196].

Furthermore, ECM composition is different amongst tissues and T cells are exposed to various microenvironments during the immune response. Several examples of distinctive tissues are: synovial fluids which contain large hyaluronic acid contents to provide a lubricant effect; brain ECM is largely composed of GAGs to possibly mitigate neuron synapse plasticity; lungs contain large fibrous protein content (i.e. collagen and elastin) to maintain elasticity of tissue; liver lobule has no basement membrane to permit efficient macromolecule exchange between plasma and hepatocytes [197-201]. Since inflammation could occur anywhere due to physical trauma (i.e. 'sterile' inflammation) or infection, T cell function will be needed to restore a healthy tissue environment.

1.2.6. Tumour microenvironment (TME)

Tumour is defined as an abnormal tissue growth, where uncontrollable cells' division affects the normal tissues' structure and function [202]. T cells have shown ability to infiltrate the neoplastic tissues and selectively induce cytotoxic response to cancer cells [14, 203, 204]. In some scenarios T cell-based immunotherapy is deemed to be successful, especially against blood type cancers (i.e. leukaemia) [204, 205]. However, various developed therapies against solid tumours appeared to be challenging for T cells [205, 206]. The main reason for this challenge is the hostile TME; due to its unique mechanical, biochemical, and cellular environment it suppresses anti-tumour T cell response (Fig. 1.16) [207-209].

One of the challenges for T cells is increased stiffness level in the TME. It can begin from the persistent inflammation, where ongoing processes without resolution continuously synthesise ECM components in tumours [181, 210]. Cancer cells themselves could release stimulating factors to active fibroblasts (also known as cancer associated fibroblasts, CAFs) to induce ECM deposition [210, 211]. Northey et al. (2020) clearly showed that an increased stiffness level of breast cancer was a result from the excessive deposition of collagen type I protein [212]. Collagen fibrils were reported to be dense and linear in the tissues with elevated crosslinking, which eventually reduced tumour-suppressor miR-203 and increased oncogene *ZNF*217 expression in the epithelial cells [212]. Other studies reported similar results, where increased stroma stiffness promoted cancer, for example: colorectal cancer, pancreatic cancer, gastric

cancer, oral squamous cell carcinoma [213-216]. From a T cell perspective, high collagen crosslinking inhibits T cell migration to the tumour islets. One study inhibited collagen crosslinking, which reduced tumour stiffness level and permitted T cell infiltration [217]. It is clear that increased stiffness level of the tumour is a problem for effective T cell function.

Furthermore, a well-known cancer-related feature is hypoxia (low oxygen level); it negatively affects anti-tumour T cell function [209, 218]. Hypoxia occurs in nearly all solid tumours where poor oxygen supply by vasculature results in less than 2% of oxygen in TME [218]. Cancer cells adapt themselves with other pathways to sustain their energy e.g. increase glucose transporter expression, glycolysis process and/or promote angiogenesis [210]. Hypoxia related microenvironment downregulates MHC-Class I expression on cells, which limits T cell ability to recognise cancer cells [219]. In addition, Scharping et al. (2021) indicated poor T cells stimulation under hypoxic conditions left them as more exhausted and dysfunctional cells [220].

Another challenge for T cells is the recruited immunosuppressive cells in TME [207]. Tumour cells secrete various chemokines, cytokines and growth factors which recruit immune cells to promote tumour's tolerance and progression [207]. Various immunosuppressive cells have different roles and functions in TME (summarised in Table. 1.3), and they are commonly associated with poor prognosis in cancer patients. In addition, tumour associated macrophages (TAMs) promote CAFs activity, which could further remodel tumour's ECM [221,

222]. Overall, anti-tumour T cells are dealing with a dynamic tissue microenvironment, which are constantly challenged by various tumour associated factors.

Table 1.3. Function of immunosuppressive cells in TME

Immunosuppressive cell	Function	Cancer	Ref.
T regulatory cells	- Recruited by cancer cells secreting chemokine CCL22, CCL28 - Suppress tumour-antigen presentation for effector T cells - Secrete immunosuppressive cytokines IL-10, IL-35, TGF-β; - Increased consumption of IL-2, which is also important for activated effector T cell survival	Poor prognosis: head and neck, gastric, oesophageal, pancreatic, liver, breast, lung, renal, prostate, ovarian cancer Good prognosis: colorectal cancer	[207, 223]
Myeloid derived suppressor cells (MDSC)	- Recruited by cancer cells secreting chemokines (e.g. CCL2, CXCL12, CXCL5) - Produce ARG1 which depletes arginine in environment, important for T cell function - Induce nitric oxide (NO) synthesis and reactive oxygen species (ROS), which impair T cells function, induce apoptosis	Poor prognosis: melanoma, colorectal, breast, bladder, thyroid and non-small cell lung cancer (NSCLC)	[207, 224]
Tumour associated macrophages (TAMs)	- Recruited to tumour sites by cancer cells secreting chemokines (e.g. CCL2, CCL8), growth factors (VEGF, PDGF) and cytokines (TGF-β1, GM-CSF) - Pro-inflammatory TAMs promote angiogenesis by secreting VEGF-A and PDGF for tumour environment; enhance invasion and metastasis of cancer cells - Anti-inflammatory TAMs impair CD8+ cytotoxic T cell activity against cancer; secrete suppressive cytokines IL-10, TGF-β; express PD-L1 and PD-L2, negative co-stimulatory molecule inhibiting effector T cells function	Good prognosis: colorectal, stomach, skin cancer Poor prognosis: breast, prostate, ovarian, cervical cancer	[207]
Tolerogenic dendritic cells (Tol-DC, also known as regulatory DC)	- Cancer cells secreting IL-10, TGF-β, VEGF, PGE2 induce DC to transfer to tolerogenic state - Tolerogenic DC downregulates MHC, co-stimulatory molecules (i.e. CD86, CD80, LFA-1), cytokines (e.g. IL-12, TNF-α) which impairs further T cell activation;	Poor prognosis: lung, colorectal, breast, ovarian (murine) cancer	[225-227]
B regulatory cells (Breg)	- Promote CD4+ T cell differentiation to Tregs (express Foxp3+ transcription factor) by secreted TGF-β cytokine; secrete immunosuppressive cytokines IL-10, IL-35, IL-17, TGF-β and express negative co-stimulatory molecules (e.g. PD-L1) to inhibit t cell activity); release of Granzyme B, cytotoxic molecule to hampering down effector T cells work	Poor prognosis: lung, colorectal, breast, hepatocellular carcinoma, tongue squamous cell carcinoma, gastric cancer	[225, 228]

1.2.7. Mechanobiology of T cells

Previously given examples on changing tissue microenvironment gave an insight on how mechanical forces (i.e. tissue stiffness) influences T cell's function. The external forces of tissues such as tension, compression, shear stress, interstitial flow, stiffness (rigidity) influence the matrix architecture and modulate the specific cell response (Fig. 1.17) [229, 230]. The mechanical forces effect on cells is processed by their biochemical cues, known as mechanotransductors [2].

YAP is a mechanosensor that is important during the T cell activation process [2]. Meng et al. (2020) study looked into YAP activity in T cells during tissue's stiffness change [180]. Upon increased matrix stiffness (i.e. inflammation, tumour) YAP in the cytoplasm releases the NFAT transcription factor fromthe IQGAP1 binding complex found near the plasma membrane. NFAT translocates to the nucleus and induces T cell activation and metabolic programming. This activates mTORC1 pathway, glycolysis, mitochondrial respiration, and amino acid uptake to support T cell transition from the quiescent to active state [180]. In soft tissues (i.e. resolved inflammation) YAP will stabilise the interaction between NFAT1-IQGAP1 and attenuate T cell response [2].

T cells also sense the changing microenvironment by integrins, a transmembrane heterodimeric protein composed of α and β subunits [2]. Upon activation, integrins adhesion is enhanced to extracellular ligands found on cells or ECM environment [172]. On the intracellular side, integrin interaction with cytoskeleton is enhanced by talin and vinculin proteins, also known as 'clutch' proteins which translates mechanical cues from

the ECM-integrin binding to force-generating cytoskeleton [231, 232]. On the stiffer substrates, integrin binding to ECM ligands generates a higher force which exposes talin's regions for vinculin binding and recruits cytoskeleton components [231]. In contrast, on the softer substrate the low force fails the vinculin recruitment, and the formed bond between ligand and integrin breaks [231]. From a T cell perspective, this type of adhesion occurs to immobilise T cells on endothelial cells before mediating their extravasation from the blood vessel to the tissue matrix [232]. Also, this could explain enhanced T cell motility on the stiffer substrates (i.e. tumours) than soft ones, thus resulting in faster and more persistent migrations [196, 232].

There are limits on T cell migration through the stiffer tissue areas, especially those with a dense meshwork [232]. This is down to the lamin-A that composes nuclear membrane and LINC - a linker between nucleoskeleton and cytoskeleton [2]. Cytoskeleton arrangement via integrin affects nucleus shape and size to mediate cell migration and adhesion response. Lamin-A is upregulated during T cell activation and causes nuclei stability by preventing deformation during the migration process [233]. It also limits T cell migration through the dense matrix meshwork to prevent nuclear rupture, and allow cell migration through the tissue pores ranging from 5-40μm size [234]. Lamin-a and nuclear stability is important for long-lasting T memory cells [234].

Overall, this gives an insight on T cells' ability to sense the mechanical cues found in the tissue environments. It is also suggested that mechanical forces are recognised as 'danger' signals to elicit T cells response [2].

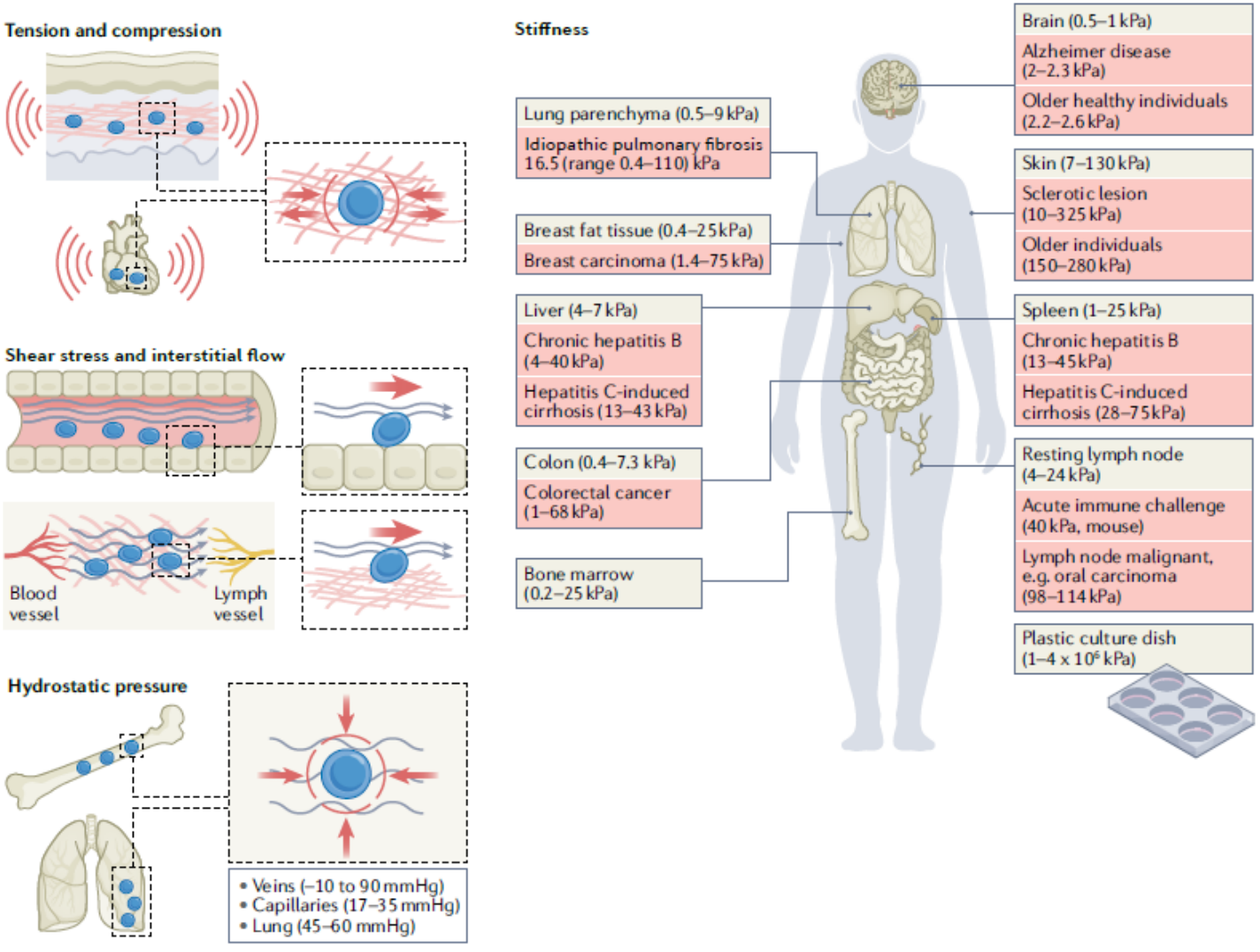

Figure 1.17 Mechanical properties and tissue stiffness level. Immune cells experience various mechanical forces found in tissues. They could arise from the blood/lymph flow (i.e. shear stress), cardiac tissue contractility or interstitial matrix (i.e. tension and compression). Immune cells are exposed to various stiffness levels (measured as storage modulus, kPa), which are different amongst the healthy tissue areas (white label). During the disease state (red label) the stiffness level changes significantly and differ from the normal tissue. Image is obtained from Du et al. (2022) [2].

1.2.8 Animal models versus 3D culture

In vivo studies are common in academic and industrial research where multicellular system and tissue microenvironment effects are accounted for in cells. However, translational studies (from animal to humans) have success rates below 50% which is problematic for clinical trial studies [235].

Mice are commonly used as animal models due their basic and translatable immunology to humans [236]. Nevertheless, they could also be genetically engineered to make humanised tissues that give a greater translation to the human studies (e.g. mice expressing human HLA type on cells) [237, 238]. However, as Mestas and Hughes (2004) reviewed, they indicated differences between mouse and human immunology, such as: 80% of human T cells express CD28 where in mouse is 100%; IL-10 is secreted by human Th1 and Th2, whereas Th2 only in mouse; and some chemokines (i.e. CXCL11) are absent in mice but not in humans [239]. The major disadvantage is the poor human disease presentation, where mice either demonstrate different disease characteristics or do not develop them at all [237, 240]. For example, *Mycobacterium tuberculosis* in mice do not show infection latency and highly organised granulomas as found in humans [236]. Even though mice and humans share >90 % of genes, the difference of pathogen exposure (greater in humans) and inbred mice (poor genetic heterogeneity compared to humans) limit translational studies [236, 237]. Other animal models can compensate for the limitations to mouse studies e.g. cows are a great model for human tuberculosis disease and non-human primates can help to study viral infections [241, 242]. Yet large animal models are associated

with increased costs and longer gestation periods, limiting the number of experimental studies [241].

Some research questions could be answered by a 3D culture system, without using animal models (summary of study examples in Table 1.4). However, 3D culture systems could not replicate all tissue complexities and whole organism interactions that makes animal models still valuable for research.

Table 1.4 3D culture studies replicating disease/healthy tissue models

Tissue model	3D culture	Aim and results	Ref.
Endothelial vessel and tumour model	Microfluidic device contains separate chambers recreating blood vessel with formed endothelial cell wall and adjacent chamber with Matrigel (ECM) embedding cancer cells	- Analyses of T cells transendothelial migration across the endothelial cell wall under the influence of CXCL12 chemokine gradient and melanoma cancer cells (A375) - Stimulated T cells migrated more across endothelial cell wall in presence of CXCL12 than unstimulated cells - Mimicked inflammatory conditions by using TNF-α which induced unstimulated T cell transendothelial migration (in presence of CXCL12) - In presence of A375 cancer cells it induced T cell migration no matter their stimulation status	[168]
Tumour models with different grades of invasiveness	Decellularized porcine jejunum (SISmuc scaffold) with tubing system circulating media through it	- Scaffold were seeded with non-small cell lung cancer (A549) and triple negative cancer cells (MDA-MB-231) and tested ROR1-specific CAR T cells antitumour effect - Both cancer cells produced tumour masses in scaffold and expressed ROR1 antigen - ROR1 CAR T cells infiltrated tumour masses and induced cytotoxic effects. Proving capability of genetically engineered T cell antitumour effect in comparison to control T cells	[163]
Brain ECM	Collagen I matrix were functionalised with poly(styrene-*alt*-maleic anhydride) and modified with hyaluronic acid and chondroitin sulphate	- Analyse T cell and microglia interaction in brain ECM environment - 3D model supported viability, cell-cell interaction (improved T cell viability in presence of microglia, rather than absence) and permit cell infiltration as found in actual brain ECM	[166]
Breast cancer model	Collagen type I hydrogel with different density	- Analyses of immunosuppressive activity on T cells (primary and Jurkats) by cancer associated fibroblasts (NIH/3T-3 and MRC-5) under influence of breast cancer cells (MDA-MB-231) - In the presence of breast cancer cell supernatant, fibroblast in collagen hydrogel induced ECM deposition and aligned collagen. This reduced T cell activity, evident by reduced IL-2 cytokine secretion.	[167]
Psoriatic skin model	Collagen type I hydrogel	- The hydrogel contains embedded fibroblasts with keratinocytes seeded on top and T cells were allocated to the bottom of the gel. Cells were isolated from human donors with psoriasis, and the established 3D model were used for drug screening - T cells were polarised into Th1/Th17 type or psoriasis patient derived T cells induced psoriatic epidermal phenotype in 3D model (caused thick epidermis formation). - Addition of psoriasis treatment (hydrocortisone or anti-IL-17a) reduced T cell infiltration and psoriasis development in 3D model	[169]

1.3. Biomaterials

The original definition of biomaterial is as described: the material used for the medical devices to repair or replace the damaged tissues caused by the disease or inflicted trauma [243]. However, over the decades the biomaterial field has significantly grown and changed to the point where its potential use is recognised in various fields, such as: diagnostic device, *in vitro* drug screening and toxicity studies, *in vitro* tissue models and clinical implants [244-247].

Biomaterials were tested to mediate specific T cell responses for the therapeutic, manufacturing or creating *in vitro* tissue models for the research purposes. Stephan et al. (2015) created a clinical implant from the alginate scaffold with collagen-mimicking peptides to deliver anti-tumour T cells to inoperable or tumour resected sites [248]. Research by Luo et al. (2017) created hydrogels from D-Tetra-peptide acting as a vaccine adjuvant [249]. Together with the relevant antigens, the peptide hydrogel induced cell-mediated (T cells) and humoral (B-cells) mediated anti-tumour responses. Griffin et al. (2021) used the microgel derived hydrogels, where upon *in vivo* degradation the material induced skin regeneration by recruiting Th1, Th2 and myeloid cells [250]. The biomaterial field also tackles another common problem in T cell-based therapies: poor scalability of tumour-reactive T cells for the adoptive cell therapy (ACT) [251]. ACT is used to enlarge tumour specific T cell population to obtain enough cells before injection to the cancer patients [252]. However, the methods suffer from the poor number and quality of therapeutic T cells [252]. Lin et al. (2018) designed a tubule system with alginate hydrogels to expand anti-

tumour T cells, and achieved a high yield of viable and functional cells [253]. The biomaterials' use and its significance is recognised in the T cell related fields, and the research will continue to grow due to their availability and novelty. The rest of this section will review currently used biomaterials, considering their specific characteristics and properties in research.

1.3.1. Type of biomaterials

The choice of the biomaterial depends on the research aim and purpose, as they have a distinctive properties enabling them to fulfil specific applications. In 3D culture, polymer biomaterials are commonly used due to their biocompatibility and ability to provide tissue specific features [254]. From a 3D culture perspective, different types of polymers are available with defined macroscale (size and shape), microscale (porosity, network density) and nanoscale (stiffness, ECM components) features for the cell culture [255].

Biomaterials could be composed from the synthetic or natural polymers, or even a mixture of both [254]. Nikolova and Chavali (2019) reviewed the advantages and disadvantages of natural and synthetic biomaterials in 3D culture [255]. In brief, the natural polymers are derived from living matter that provides good biocompatibility, low toxicity and suitable biochemical cues (i.e. adhesion motifs) to support basic cells' functions. Due to the material's origins, it is more biodegradable than synthetic polymers, where it can induce immunogenicity and vary batch to batch. Alternatively, synthetic polymers are more reproducible, due to the easier production process and more control on batch variability. As a material they are versatile, they have tunable properties and

good workability. Alas, they are less biocompatible, requiring a functionalisation process to provide cell supporting motifs [255]. Depending on the type of material, some crosslinking (a bond connecting one polymer to the other) could involve toxic methods and affect cell viability [254-256]. Crosslinking is the key process of the biomaterial formation, which provides the final 3D structure. From the hydrogel perspective, crosslinking is important to interconnect polymers, followed by a complete gel formation (gelation) [257]. Crosslinking could control material's density, where the number of crosslinking will regulate the material's swelling (e.g. high crosslinking results in low swelling) [255]. Hu et al. (2019) provide an in depth summary on two main forms of crosslinking, described as physical and chemical crosslinking [258]. In the review, they describe physical interactions which depend on ionic/electrostatic interaction, hydrogen bonds, hydrophobic/hydrophilic interaction, π-π stacking etc. which have no cytotoxic effect on cells; however, it is susceptible to the external factors that could break the polymer bonds and affect the material's stability [258]. In this case, chemical crosslinking (mainly relies on covalent bonding) could overcome these issues by forming polymer bonds with strong and permanent network, enhancing the material's stability and mechanical properties. Chemical crosslinking could involve enzymes, free radical polymerization, Diels-Alder "click" reaction or a Michael-type addition [258]. The only downside of chemical crosslinking is potential cytotoxicity due to unreacted crosslinking residues as mentioned above [258]. Overall Table 1.5 reviews different types of biomaterials, their associated properties and use for 3D culture studies.

Table 1.5 Natural and synthetic biomaterial polymers, crosslinking, and their properties

Material	Crosslinking	Material's properties	Use	Ref.
		Natural biomaterials		
Collagen	Physical: induced by amino and carboxyl telopeptides on collagen chains Covalent: induced by enzyme transglutaminase; UV photo-crosslinking	- Fibrous protein with a long, stiff, triple-stranded helical structure - *In vivo*: mechanical support for tissues, act as Template for cell distribution, capillary formation - Produce 'porous' scaffolds by freeze-drying method - Can be processed into various forms: cross-linked films, meshes, fibres, sponges - Biodegradable, biocompatible - Contains adhesion motifs promoting cell adhesion, spreading, migration	- Scaffold for tumour model e.g. breast cancer cells form tube-like structures as in tissues; enrich colorectal cancer stem-cells - Cultured cancer cells tested for drug resistance which was unnoticed in 2D culture - Scaffold used for cartilage, bone, drug delivery system, nerve regeneration - Analysed collagen type I density effect on T cell function	[164, 254, 259-262]
Chitosan	Physical: ionic bond Covalent: glutaraldehyde to increase material's strength	- Derived from chitin of exoskeleton from crustaceans and insects - Natural polysaccharide - Prone to enzymatic digestion e.g. chitosanase, lysozyme - Adjustable porosity and geometry for cell culture - Biocompatible - Low mechanical properties, which can be improved by covalent crosslinking	- Scaffold was used to analyse hepatocyte cells and analyse their metabolic activity - Tissue engineering field of orthopaedics - Hydrogel used as a delivery system of encapsulated T cells to promote anti-tumour response	[254, 261, 263]

Table 1.5 Natural and synthetic biomaterial polymers, crosslinking, and their properties (continue)

Hyaluronan (Hyaluronic acid)	Physical: hydrogen bonding, ionic, hydrophobic interactions Covalent: boronic ester and Schiff-base formation, click chemistry i.e. thiol chemistry, azide-alkyne, Diel Alder cycloaddition	- Glycosaminoglycan, produced from repeating disaccharide units of N-acetylglucosamine and glucuronic acid - Bind high amounts of water, form hydrogen bonds with solvent - Biocompatible - Physical hydrogels demonstrate self-healing properties, but low mechanical properties - Covalent hydrogel provides more stability for the material - Depending on the molecular weight in establishes pro- or anti-inflammatory response - Highly biodegradable by hydrolysis at ester linkages and hyaluronidinase enzyme - Interacts with cell receptors, but lacks cell adhesion motifs	- Scaffolds used for chondrocyte, bone, skin tissue regeneration - High molecular hyaluronic acid hydrogels promote infiltration of Tregs during dental extraction wound healing process	[146, 259, 261, 264, 265]
Agarose	Physical: hydrogen bonds Covalent: contains methacrylate side groups and induce crosslinking after UV-irradiation	- Polysaccharide produced from algae - Contains high amount of hydroxyl groups, soluble in water - Degradable by agarases enzymes - Strength and permeability of scaffold depends on agarose concentration - Share similar features as alginate	- Support chondrocytes, neural tissue regeneration, cardiac bioengineering, stem cell	[254, 258, 259, 266]

Table 1.5 Natural and synthetic biomaterial polymers, crosslinking, and their properties (continue)

Alginate	Gelation induced in presence of calcium ions	- Polysaccharide found in cell walls of brown algae - Highly soluble in water - Provide porous scaffold - Physical and mechanical properties depend on chain length and guluronate blocks, and crosslinking - Biocompatible, low toxicity - Produce microspheres, sponges, foams, fibres, hydrogels - No intrinsic cell binding motifs, requires functionalisation (e.g. RGD) to promote cell attachment - Poor degradability	- Cultured hepatocytes and analysed cell functionality (albumin secretion) - Supported growth of breast cancer cells and studies on drug resistance - Hydrogel with encapsulated T cells promote their memory phenotype, which prolong activity of anti-tumour specific cells	[254, 256, 259, 261, 267]
Matrigel	Physical: ionic interactions, Chemical: glutaraldehyde, enzymatic	- Derived from Engelbreth-Holm Swarm mouse tumour cell-derived basement membrane - Contains collagen IV, laminin, entactin, perlecan, multiple cytokines and growth factors - Provide adhesion motifs for cells - Limited mechanical properties (400-420 Pa) - Potential immunogenicity - Provide meshwork type network - Prone to degradations due to released MMP by cells	- Due to its low stiffness it represents more neural tissue – commonly used for neuron regeneration - Hydrogel suitable for embryonic stem cells - Tumour cell studies: culture and invasion models - Research on cancer stem-cells	[256, 261, 268, 269]
Gelatin	Chemical hydrogel: carbodiimides, formaldehyde, glutaraldehyde, genipin Physical hydrogel: hydrogen bonds	- Hydrolysed collagen - Biocompatible, biodegradable - More adjustable mechanical properties than collagen (depending on the crosslink) - Contains intrinsic RGD motifs – promote cell adhesion, spreading, migration - Degradable by released MMP	- Used for drug delivery system, wound healing, injectable fillers - Tissue engineering of cardiovascular, bone, skeletal muscle, hepatic tissue - Gelatin microgels used to induce T cell lineage form hematopoietic stem cells	[259, 261, 270-272]

Table 1.5 Natural and synthetic biomaterial polymers, crosslinking, and their properties (continue)

Fibrin	Chemical hydrogel: genipin Physical: gelation induces by Factor XVIII and thrombin	- Protein involved in blood coagulation - Formed from the thrombin-mediated cleavage of fibrinogen - High biodegradability (e.g. urokinase), requires mixture with other biomaterials to increase material's stability - Contains natural adhesion/binding motifs promoting cell adhesion, spreading, migration - Poor mechanical properties, requires combination with other hydrogels	- 3D scaffolds used for cell proliferation and migration studies - Supported stem cells, bone marrow stromal cells and promoted wound healing, muscle tissue engineering and organoid formation - Fibrin-collagen hydrogel reconstructing lymph node to analyse T cell and stromal cells' interaction	[261, 262, 273]
		Synthetic biomaterials		
Poly (glycolic acid, PGA), poly (lactic acid, PLA), and copolymers (PLGA)	Chemical crosslinking: esterification, photoinitiator (UV irradiation)	- Aliphatic polyesters degrade by hydrolysis, degradation rate depends on structure, molecular weight, crystallinity - Thermoplastic polymer – easily shaped - Pore size or meshwork can be controlled according to cell requirements - PLA degrades slower than PGA - Potential toxicity due to released acidic residues - Induce immunogenicity	- Drug delivery: transporting growth factors repairing cartilage tissue - Tumour models: PLGA-PEG-PLGA hydrogel for ovarian cancer cells; PLGA-sodium bicarbonate microparticles promoted lung cancer cells growth and detected drug resistance in comparison to 2D cultures	[254, 274-276]
Poly (ethylene glycol) (PEG)	Chemical hydrogel: 'click' chemistry; photo-initiated polymerization	- Hydrophilic polymer - Low cytotoxicity, no-immunogenicity - No adhesion mediating proteins – no cell adhesion and cause poor viability - Hydrogel pores adjusted according to chain length and crosslinker groups - Requires functionalisation to promote cell adhesion - Various crosslinkers available which control degradability, swelling, porosity, mechanical strength	- PEG-heparin hydrogel loaded with CCL21 chemokine induced greater T cell proliferation and differentiation to memory T cells - Scaffolds (functionalised with RGD) contain regular shape pores (5-15µm in diameter) and guide the growth of fibroblast cells	[258, 261, 262, 277, 278]

Key words: RGD - amino acid sequence (Arg-Gly-Asp) promoting cell binding in ECM matrix

1.3.2. Biomaterial characteristics

Several aspects of the biomaterial need to be considered for supporting cell culture. No matter their intended use (tissue engineering, regeneration, *in vitro* study models, and clinical implants) their initial design and capacity need to be adapted according to the given culture and wanted cell response.

1.3.2.1 Porosity

Pores within a material are described as 'cavities', which could have different roles depending on the material's purpose [279]. In 3D culture, pores provide space for cell growth, ECM deposition, exchange of molecules i.e. metabolism, cytokines and waste products within the structure [254]. The pores can vary in size and interconnectivity in the material, which could benefit the specific cell functions [255, 280]. For example: collagen-glycosaminoglycan scaffold with 325μm pore size promoted osteoblasts attachment, migration and mineralization; collagen-chitosan scaffold with 360 μm induced macrophage polarisation into anti-inflammatory type cells (i.e. M2) and promoted angiogenesis than scaffold with 160 μm pore size; poly-L-lactic acid (PLLA) scaffold with 100 μm pores induced chondrocyte differentiation into cartilage-specific cells than 200 μm pore size [281-283]. Any larger pores than 400 μm will lose 3D culture characteristics, as cell-cell organisation ends up like in 2D culture [255]. Hydrogels are known to form mesh-like structures, where fibrous networks form molecular/nanometer scale porosity [146, 279]. Mesh-works simulate mainly the intricate and organised nanoscale of ECM matrix, making

hydrogels more favourable compared to other synthetic biomaterials due to their ability to 'mimic' the tissue environment [284].

1.3.2.2. Biodegradability

Some biomaterials can undergo rapid degradation due to occurring hydrolysis, free radicals, temperature change or enzyme presence which eventually alters the material's structure [254]. Their stability could be adjusted by modifying their original properties (e.g. molecular weight, density, crosslinking) or mixing with other biomaterials (e.g. fibrin-collagen hydrogel) to reduce the degradation [255]. In some studies, the material's degradation is taken as an advantage to release the content gradually overtime. For example, Hamilton et al. (2021) used acrylated hyaluronic acid hydrogels to ensure a slow stem cell release over a 14-day period for the cell therapy [285]. Whereas Petterson et al. (2010) have used glycidyl methacrylate modified hyaluronic acid hydrogel; over 8 weeks of degradation they released growth factors for the bone regeneration [286]. Depending on the research question, biodegradability could be a challenge to retain a stable material or advantage to release the content of interest.

1.3.2.3. Biomaterial functionalisation

Synthetic and some natural polymers lack the active biomolecules, that are important for the specific cell's function (Table 1.5). Common biomolecule used in polymers is an adhesion motif that mediates cell spreading, adhesion, differentiation, and migration process [255]. Biomaterials like collagen, gelatin and Matrigel contain these natural motifs for the cell culture [261, 268]. Synthetic and some natural polymers (e.g. hyaluronan) require functionalisation

process, whilst adhesion motifs are added to the biomaterial to support cell culture [287]. This is also known as the conjugation process, which could involve chemical (e.g. thiol reactive), enzymatic (e.g. peroxidase mediated) or photo- (e.g. photo-acrylate crosslinking) approaches [287]. As reviewed by Spicer et al. (2018), there is no universal procedure in conjugating biomolecules to the materials, however a wide range of procedures are available to tether polypeptides, glycans and oligonucleotides [287]. In some cases, the biomaterials could be functionalised by a simple adsorption process, that depends on the physical interactions (e.g. ionic, hydrophobic interactions) [287, 288]. Due to its weak interaction desorption could occur where the attached biomolecules are eventually lost from the material. In contrast, covalent conjugation, which guarantees biomolecules presence, can affect its biological activity and become unusable for cells [287, 289]. Custodio et al. (2010) compared covalent immobilisation to the adsorption method of fibronectin in the chitosan hydrogel. The covalent conjugation resulted in a greater quantity of fibronectin present in the hydrogel, which also supported better osteoblast's adhesion and proliferation response [289]. Whereas adsorbed fibronectin quantity in hydrogel was much lower, resulting in poor osteoblasts' response. The functionalisation process of the biomaterial is subjective, as it depends on the type of biomaterial and biomolecule needed for the cells.

1.3.2.4. Immunogenicity

Biomaterials' use in the immunology related fields has to be carefully selected, as they could be recognised as 'danger' related signal and elicit immune

response [290, 291]. The biomaterial's particles could be classed as 'immunogenic' or 'antigenic', depending whether they triggered or not the immune response, respectively [291].

T cells cannot recognise proteins in native forms, but only once they are processed by APC into the peptides and presented on MHC class molecules [90]. APC are equipped with PRRs, where intact polymer chains of bacteria or virus, or especially biomaterials, could crosslink the PRR on APC and induce the immune response [292]. Park et al. (2012) demonstrated iDC activation into mDC once they were cultured on PLGA and chitosan biomaterials [293]. DC upregulated their MHC Class II molecules, CD86, CD83 and CD86 and secreted higher levels of pro-inflammatory TNF-α cytokine, that eventually caused T cell activation [293].

From a biomaterial perspective, natural polymers tend to have immunogenic properties rather than synthetic ones [291]. This could be caused by animal-derived content, recognised as foreign antigens by human immune cells. However, synthetic or natural biomaterials could have specific features that can cause the immunogenicity due to: hydrophobicity, molecular weight, surface charge, material's shape and size [292]. For example, one study showed induced DC activation by PLGA and chitosan biomaterials due to their hydrophobic nature and polysaccharide chains (*N*-acetyl-D-glucosamine), respectively [293]. Chitosan polysaccharides bind to the mannose receptor (i.e. PRR) and

hydrophobic surface of PLGA with adsorbed serum proteins – all together triggering DC response.

It is clear the specific features of biomaterial are responsible for inducing immune response, that could be problematic for 3D culture or clinical implant studies. However, in some scenarios induced immune response solely by biomaterials could improve vaccine, anti-tumour response or elimination of chronic inflammations in the clinical applications.

1.4. Self-assembling peptide hydrogels

Self-assembling peptide hydrogels are getting recognised in the clinical and academic fields [249, 294-297]. The materials are composed from the short amino acid chains, also known as peptides, which under the right conditions (e.g. pH, temperature, salt) self-assemble into the hydrogel [294]. Self-assembly is not a novel process, as it occurs in the ECM between proteins, GAGs and proteoglycan molecules [284]. Peptide hydrogels also contain a nanofibrous structure, which is more 'familiar' to the cells due to its similarity with ECM [298].

Different types of self-assembling peptide hydrogels are available for research [294, 299]. The difference relies on amino acids, which mitigate specific interactions between peptides to form the hydrogel. For example: small molecules such as di- and tri- peptides (e.g. Fmoc-D-Ala-D-Ala) interact by π-stacking; ionic complimentary peptides like EAK (glutamic acid, alanine, lysine) interact by hydrophilic, hydrophobic, and electrostatic amino acids' charges;

peptide amphiphiles (inspired by lipid molecule) form a hydrogel based on hydrophobic tails and hydrophilic heads [298, 299]. Even though the hydrogel is composed from the natural amino acids, it is still classed as a synthetic material [300]. Upon specific amino acids composition, peptides could form β-sheet or α-helical structures to form hydrogels [301]. β-sheet peptides are preferred for the hydrogels due to their ability to resist cellular processes (not like α-helical chains), easier design and chemical simplicity [302].

Peptide hydrogels have many advantages for culturing cells. As they retain a good biocompatibility, high water content, porosity (meshwork), modifiable stiffness level and functionalisation with biological motifs [298]. The main limitation of this type of material is to form high stiffness material representing hard tissues [294]. It could be achieved by increased peptide concentration, that could also affect cell viability and induce amyloid (i.e. abnormal protein structure) deposition [302, 303].

Currently, peptide hydrogels use are explored in the biomedical applications and 3D culture fields. From the biomedical applications perspective hydrogels were tested as: delivery system of antigens to induce a better anti-tumour response; promote better angiogenesis *in vivo* for spinal cord injuries; and deliver a haemostatic effect in the open wounds [249, 296, 304]. In 3D culture, RAD16-I scaffold functionalised with laminin I and collagen VI adhesion motifs - improved human aortic endothelial cells culture, which resulted in a better cell growth rate and protein deposition [305]. Another example is by Kopesky et al. (2010), where

KLD12 peptide hydrogel for bone marrow stem cells was used and promoted better chondrogenesis process than the same cells cultured in the agarose gel [297]. Due to peptide hydrogels' modifiable properties and similarity to ECM environment they are becoming a popular choice in the research areas [295].

1.4.1. FEFEFKFK peptide hydrogel

The FEFEFKFK octapeptide was created to simplify current complementary peptides used to make the gels [298]. It also has a rapid gelation process in comparison to other peptide gels (i.e. RAD16-1) [306].

FEFEFKFK is composed from phenylalanine (F, hydrophobic), lysine (K, positively charged) and glutamic acid (E, negatively charged) [295]. The peptide fibre contains the hydrophobic core formed by phenylalanine side groups, whereas the outside present hydrophilic groups from charged amino acids [307]. It is predicted that the phenylalanine will take the initiative of forming the fibres, whereas lysine and glutamic acid will interconnect them to make a nanofibrous network (Fig. 1.18 (a-c)). All these interactions to happen and ensure hydrogel formation, the optimal conditions of peptide's concentration, temperature, pH and salt concentration need to be met (Fig. 1.18 (d)) [307]. One study demonstrated hydrogel's formation with ~2.6 wt% of peptide concentration at pH 2.8, whereas ~1 wt% required pH 4-10 [302]. This indicates versatile hydrogel's properties, where under the right condition the hydrogel will solidify.

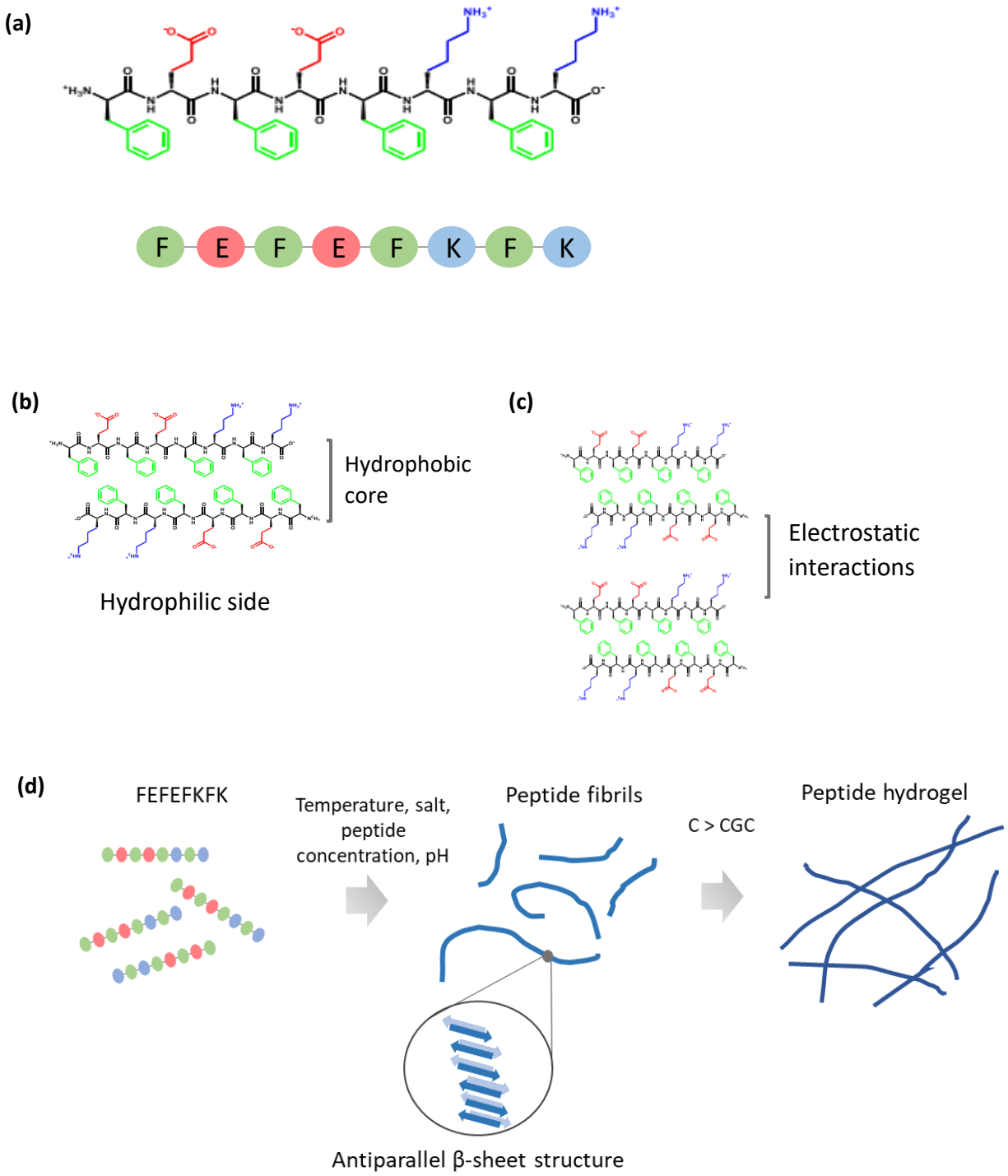

Figure 1.18 FEFEFKFK peptide hydrogel formation. **(a)** Chemical structure of the FEFEFKFK octapeptide. **(b)** Peptide fibre forms upon hydrophobic interactions caused by F, which creates a hydrophobic core, leaving a hydrophilic side created by E and K aa charged groups. **(c)** Fibres interact with each other via the hydrophilic side, creating a nanofibrous structure. **(d)** Peptide fibrils self-assemble into antiparallel β-sheet structure, and form above critical gelation concentration (CGC) the peptide hydrogel. Graphs were adapted from Burgess et al. (2021) and Gao et al. (2017) [307, 308].

Hydrogel's pH is adjusted by sodium hydroxide addition, which first leaves the material with an alkaline condition [306, 307]. At this state, the material is more liquid state which allows better mixing and distribution of added media and cells. At the same time, added media will reduce pH to 7 to induce the final gelation step. At neutral pH, lysine and glutamic acid interact with each other via electrostatic interactions, leaving the whole peptide to reduce its isoelectric point [306, 309, 310]. This causes the aggregation of fibres by tightening the fibrous network and encapsulating cells [306]. Added salt will sequester the excess charges of the peptides, allowing hydrophobic forces and hydrogen bond formation, leading to the nanofibrous network formation [309].

Mechanical stiffness of the peptide gel depends on the peptide concentration [307]. Increased peptide concentration forms a high density fibres, which also regulate the size of the meshwork [301]. For example, at neutral pH 10 mg/ml peptide gel have ~30nm meshwork size, whereas 40 mg/ml has ~15nm [301]. However, fibre diameter is not affected by increasing peptide concentrations and it seems to retain a similar diameter size between 3-4 nm [301, 307]. Castillo et al. (2014) studied the increasing peptide gel concentration on the osteoblasts cells, and upon an increase of mechanical stiffness and reduced porosity, cell viability was reduced as well [309]. It is suspected that the reduced porosity of the gel and limited diffusion of nutrients affected the cells. To this date no data has been published to confirm the possible restriction of molecule diffusion across the hydrogel.

FEFEFKFK peptide gel provides an unmodified environment for cells, which gives an opportunity for studies to incorporate adhesion motifs or ECM components for cell culture. Ashworth et al. (2019) via adsorption process (mixing the content into the gel) functionalised gel with collagen type I and hyaluronic acid [311]. Encapsulated fibroblast cells adhered to the funtcionalised peptide hydrogel and promoted cell spreading. In addition, cells themselves can modify the environment by depositing their own produced ECM content into the gel [309, 311, 312]. FEFEFKFK peptide gels can also be modified via conjugation process with adhesion motifs i.e. RGD sequence to promote cell adhesion and migration. Burgess et al. (2021) used functionalised peptide gel with RGD sequence for cardiac progenitor cells, which evidently promoted cell differentiation into cardiac cells and migration across the gel [308].

Overall, peptide gels have many adjustable properties which could be used to adapt the specific microenvironment for cells. They give more control than other hydrogels e.g. Matrigel, collagen, hyaluronic acid, that already have modified environment for cells. Nevertheless, the processing and production of peptide hydrogel is cost-effective, giving more opportunities for the research studies to adapt to the 3D cell culture system [311, 312].

1.5. Hypotheses and aim

T cells work mainly in tissue microenvironments, and the current *in vitro* models oversimplify the characteristics of tissues where cells are commonly found. In addition, improved *in vitro* studies could avoid animal models for the simpler research questions. There is a necessity of developing a realistic *in vitro* study to analyse functional T cell work under the influence of mechanical properties, 3D dimensions, cell-cell interactions and the presence of ECM components. The vast choice of biomaterials can improve *in vitro* cultures by providing tissue relevant features, but the lack of adjustable mechanical properties, modified environment (ECM presence), tumour origins, poor biocompatibility, immunogenicity, and expensive costs limits the 3D culture use. In this study, FEFEFKFK peptide hydrogel offers several advantages as a potential biomaterial to be used as the replacement for 2D culture. Due to their adjustable properties (from mechanical to biochemical) and related low costs, it could improve *in vitro* studies and deliver more realistic T cell response. Our hypotheses in this study are:

1. Self-assembling peptide hydrogel can support normal T cell activation and function process
2. Self-assembling peptide hydrogel can provide tissue related characteristics (e.g. stiffness, ECM components) and modulate T cell response
3. Biomaterial is inert (low immunogenicity) and support immune cell function, without background response
4. T cell response to the immunomodulators (i.e. DC modified by drugs) can be studied in 3D peptide hydrogel culture system

Chapter 2: Materials and methods

2.1 Ethical approval

Healthy volunteers were invited to donate blood under the study title 'Using human blood from normal donors for the study of immune response'. The study was conducted under the research ethics reference NB-161-1711, version 1.3: 02-12-2019, used at Biodiscovery Institute, University Park, University of Nottingham. Peripheral blood was obtained by venipuncture using a 19g needle and sodium heparin was used as anticoagulant.

2.2 Peripheral blood mononuclear cells (PBMCs) and peripheral blood lymphocyte (PBL) isolations

PBMCs were isolated from the human blood by the density gradient centrifugation process. Before the isolation process, all reagents (see Table 2.4 for manufacturer and catalogue number) were brought to room temperature. The collected donors' blood was first diluted by 1:1 ratio with DPBS to achieve a better purity of PBMCs. 35mL of blood was layered on top of the 15mL Histopaque 1077 aliquoted in the 50mL Falcon tube, and centrifuged at 800 x g, 21^{o}C, 9 ACC and 1 DCC for 25 minutes (min). After centrifugation, the 'buffy coat' (Graph 2.1) which contains the PBMCs, was collected without disturbing other layers in the tube. Harvested cells were transferred into separate tubes and diluted further with DPBS up to 50mL. The content was centrifuged at 1400 rpmi for 8 min, followed by supernatant removal, pellet dislodgement and further

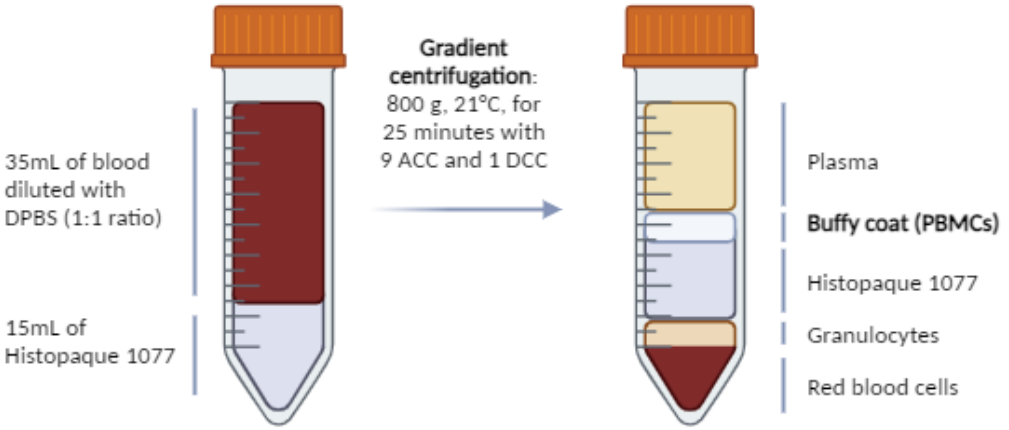

Graph 2.1: PBMC isolation by density gradient centrifugation. Diluted blood with DPBS was layered on Histopaque 1077 and processed by gradient centrifugation. Buffy coat (PBMCs) was collected carefully without disturbing other layers. Figure created with BioRender.com.

dilution with 25mL of DPBS. Cells were counted by hemocytometer (see section 2.3) and prepared for further isolation of the cells of interest e.g. CD4+ T cells).

For some experiments, PBL were isolated from the PBMCs population. In brief, PBMCs were removed from DPBS by a centrifugation at 300 x g for 10 min. The dislodged pellet of PBMCs was adjusted to $1x10^6$ cells/ml in T cell medium (see Table 2.5 for medium composition) and 20mL transferred to T75 flasks. Cells were incubated for 2 hours at 37°C in a 5% CO_2 incubator, which allowed adherent cells to attach to the flask whilst suspension cells (i.e. lymphocytes) remained unattached. Medium containing cells was collected and centrifuged at 300 x g for 10 min to obtain PBL.

.

2.3 Cell counting with Trypan blue

A small volume (10µL) of cell suspension was diluted with an equal volume of Trypan Blue. The dye itself helped to distinguish the dead cells, which are dye-permeable, from the viable cells [313]. 10 µL of diluted sample was loaded to the haemocytometer and cells in three regions counted under the light microscope (Graph 2.2).

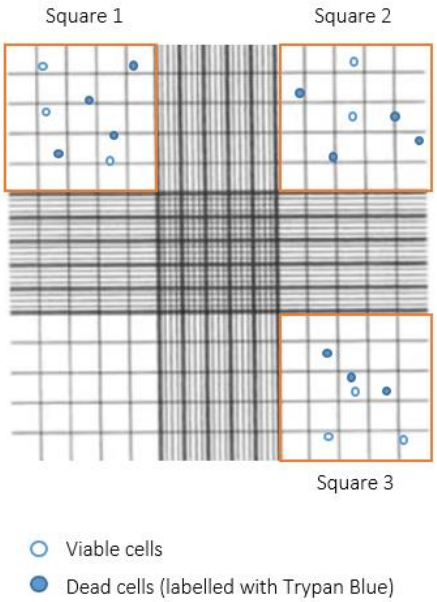

Graph 2.2: Haemocytometer's counting grid. Diluted cell suspension with Trypan Blue were loaded to the haemocytometer and only viable cells were counted from the total three squares.

The total number of viable cells in the prepared cell suspension was calculated as follows:

$$\frac{Total\ number\ of\ viable\ cells}{Total\ number\ of\ counted\ squares} \times Dilution\ factor\ by\ Trypan\ Blue \times Total\ volume\ of prepared\ cells\ suspension$$

$$= \boldsymbol{Total\ number\ of\ cells} \times \mathbf{10^4}$$

Based on the cell number, the calculated volume of reagent (such as cell culture medium) was added to obtained the required cell density.

2.4 Human CD4+ T cell isolation

CD4+ T cells were enriched from PBMC by positive selection with magnetic microbeads (Miltenyi Biotec) conjugated to the antibodies recognising human CD4+ marker [314]. The protocol was provided by the manufacturer and relevant reagents prepared according to the given instructions. All reagents were maintained at 4^{o}C degrees, which helped to prevent non-specific antibody binding [314]. The total number of PBMCs was defined before the procedure to select the appropriate column size. In brief, isolated PBMCs in DPBS were centrifuged at 300 x g for 10 min. According to the total cell number, the dislodged pellet of cells was resuspended in the cold MACS buffer (80µL per 1x10^{7} cells) and CD4+ microbeads (20µL of per 1x10^{7} cells) and incubated for 15 min at 4^{o}C. After incubation time, an additional 2mL of MACS buffer per 1x10^{7} cells was added to the tube and centrifuged at 300 x g for 10 min. In the meantime, the LS column was attached to the magnetic stand and washed once with 3mL of MACS buffer. Cells then were resuspended in 500µL of MACS buffer and loaded to the prepared LS column. The cell suspension was allowed to run first through the column, and then 3mL of MACS buffer was added to elute unbound cells (also known as negative selection). Three washing steps were completed and on the final one, the LS column was removed from the magnetic stand placed over the new tube. 5mL of MACS buffer was added to the column and the whole content was plunged down to elute CD4+ T cells. 5mL of cell suspension was diluted further with 25mL of T cell medium and the total number of cells determined. Cells were centrifuged (300x g, 10 min) and resuspended at 1x10^{6}/mL in T cell medium supplemented with IL-2 (30 U/mL). T cells were

cultured in 5mL per well in 6-well plates and rested overnight at 37°C in a 5% CO_2 incubator. The purity of isolated CD4+ T cells was determined by flow cytometry (MACSQuant Analyzer 10, Miltenyi Biotec), where 100µL of the cell sample was stained with anti-human CD4+ and CD3+ antibodies conjugated with respective fluorophores (see section 2.17).

2.5 Human CD14+ monocyte isolation and differentiation into dendritic cells (DCs)

CD14+ monocytes were isolated from the negative fraction collected during CD4+ T cell isolation (section 2.4). Monocytes were isolated by positive selection with CD14+ microbeads (Miltenyi Biotec) [315]. The procedure of isolation and required equipment was similar to section 2.4. In brief, cell number was determined, followed by a centrifuge step at 300 x g for 10 min. Based on the cell number, the dislodged pellet of cells was exposed to defined volumes of cold MACS buffer and CD14+ microbeads - i.e. $2x10^8$ cells required 400 µL of cold MACS buffer and 75 µL of CD14+ microbeads. Cells were incubated for 15 min at 4°C, followed by the addition of 20mL of MACS buffer and centrifugation step. The supernatant was discarded and the dislodged cells' pellet was resuspended in 1mL of MACS buffer before loading to the LS column. The rest of the procedure followed the exact steps as described in section 2.4. Collected CD14+ monocytes were further diluted in 10mL of DC medium and the total number of cells was counted. Cells were centrifuged, and diluted with DC medium (containing IL-4 1000 U/mL and GM-CSF 1000 U/mL) at $1x10^6$ cells/mL. Cells were transferred to appropriately sized flasks, i.e. $15x10^6$ cells in T75 flask or

$30x10^6$ cells in T175 flask, and incubated for 3-4 days at 37°C. On day 3 or 4 of incubation, additional DC medium (50% to the current volume) supplemented with cytokines was added to the cells and cultured until day 5. During days 5-7, iDCs were harvested.

2.6 Human CD1c+ DCs isolation

Whole PBMCs were processed for CD1c+ isolation with magnetic microbeads and cold reagents, as instructed by Miltenyi Biotec protocol [316]. In brief, PBMCs were reconstituted in cold MACS buffer (100µL per $1x10^8$ cells) with FcR blocking, CD14+ microbeads, CD19+ microbeads and CD1c (BDCA-1) Biotin reagents - all at 100µL / 10^8 cells. The content was mixed and incubated for 15 min at 4°C. After incubation, 10x of the MACS buffer volume was added to the current labelling solution and centrifuged (300 x g, 10 min). The supernatant was discarded and the dislodged cell pellet resuspended in 500µL of MACS buffer. The LD column was attached to the magnetic separator and equilibrated with 2mL of MACS buffer before addition of cells. Three washing steps were completed with 1mL of MACS buffer and the 'negative selection' was collected for the further process. Two times of MACS buffer volume was added to the current cell suspension's volume and centrifuged. Then 400µL of MACS buffer with 100µL (per $1x10^9$ cells) anti-biotin microbeads were added to the cells and incubated for 15 minutes at 4°C. At the end of incubation, ten times of MACS buffer volume was added to the cells, centrifuged and resuspended in 500µL of MACS buffer per $1x10^8$ cells. Further isolation required MS columns, which were pre-washed with 500µL of MACS buffer. The column with loaded cells was

washed three times with 500µL buffer and then flushed with 1mL of MACS buffer into the next MS column to increase the purity of cells. The same washing procedure was repeated with the final step of detaching the column from the magnet and flushing the cells into a separate collection tube. Isolated CD1c+ cells were immediately used for the experiment.

2.7 Preparation of immature and mature DC, and treatment with dexamethasone and p38 inhibitor (BIRB196)

DCs were activated into a 'mature' state prior to T cell activation process. Isolated CD14+ monocytes (section 2.5) were differentiated into iDC for 5 to 7 days, followed by exposure to the synthetic ligands to mDC. iDCs were centrifuged at 300 x g for 10 minutes and prepared at $1x10^6$ cells/ml in DC medium (section 2.5). 1ml of cells suspension was added to the 24-well plate, followed by an additional 1ml of medium containing 2x concentration of Poly:I:C (working concentration: 10 µg/ml), R848 (working concentration: 2.5 µg/ml) and GM-CSF (working concentration at 1000 U/mL) to initiate maturation. Additional wells with iDCs were supplemented with GM-CSF only. Cells were incubated at 37°C with a 5% CO_2 incubator for 24 hours.

iDCs were also exposed to the dexamethasone (Dex) before maturation. For Dex treatment, iDCs were cultured at $5x10^5$ cells per 100µL in a 96-well plate. Cells received an additional 50µL of DC medium prepared with 4x concentration of Dex (working concentration 10^{-6}M) and incubated for 1 hour at 37°C. Later on,

the same Dex-treated cell cultures received 50 µL of medium with 4x concentration of Poly:I:C and R848 and incubated for 24 hours.

CD1c cells (section 2.6) were treated with the same synthetic ligands, Dex and p38 inhibitor during differentiation process into mDC. At first, cells were resuspended at $1x10^5$ cells/ml in DC medium supplied with 1000 U/ml GM-CSF, then 100 µL of cells were aliquoted to a 96-well plate and rested for 1 hour before stimulus and drug treatment. After resting, cells were treated with p38 inhibitor (BIRB196), prepared at 5x concentration (final conc. 1µM) in the culture medium. The drug treatment lasted for 30 min, followed by an additional 50 µL of Dex (with 5x concentration) and then incubated for another hour. The final step of the process involved the addition of 50 µL of medium with 5x concentrations of Poly:I:C and R848, and further incubation by 24 hours. For conditions where stimulus/drug treatment was not added, cells received medium with GM-CSF only. Conditioned CD1c+ were summarised in Table 2.1.

Table 2.1 Treatment of CD1c+ with stimulus and immunomodulatory drugs

Conditioned CD1c	p38 inhibitor	Dexamethasone	Poly:I:C and R848
Immature			
Mature			50 µL
Mature-Dex		50 µL	50 µL
Mature-Dex-p38	50 µL	50 µL	50 µL

2.8 Coating polystyrene particles with functional antibodies – preparation of artificial APC

Polystyrene beads (size 10µm) were coated with functional antibodies capable of inducing T cell activation process. The selection of antibodies and their

concentrations were: anti-human CD3 at 30µg/mL or 1 µg /mL; anti-human CD28 30µg/mL or 3µg/mL; and anti-human CD55 at 3µg/mL. Antibodies were attached to the polystyrene particles by adsorption, a non-covalent coating method described by Bangs Laboratories, Inc [317]. In brief: 10mg/mL of beads were prepared in 1mL of PBS solution and centrifuged at 650 x g for 5min. In a separate tube, 1mL of PBS was prepared with the final working concentrations of antibodies. The supernatant from the beads was discarded, and the pellet was reconstituted in a total of 30µL PBS. All beads were collected and added to the prepared antibodies solution, achieving the final concentration at 1% (w/v). Adsorption was undertaken with constant rotation (15rpm for 2 hours at room temperature), followed by overnight rotation at 4°C. After absorption, beads were washed and reconstituted in 1mL of blocking buffer (PBS, 0.05% FBS) for 1hr. Beads were then washed, reconstituted in PBS and stored at 4^{o}C until further use. Every batch of produced beads was labelled with secondary rabbit anti-mouse polyclonal antibody FITC (protocol 2.17) and analysed by flow cytometry to detect the percentage of coated beads.

2.9 Precursor FEFEFKFK peptide hydrogel preparation

Peptide-based (sequence FEFEFKFK) powder was stored in the -20^{o}C freezer for long-term storage. Starting masses of the peptide powder (see Table 2.3) were dissolved in 800µL of sterile UltraPure distilled water and mixed in the

15mL Falcon tubes. Mixtures were vortexed for 3 min and centrifuged (1000 rpm, 3 min) followed by incubation (80°C, 2 hours). After incubation, 0.5M NaOH was gradually added into the hydrogel, followed by 10 seconds vortex and centrifugation. NaOH was added until hydrogels were visually transparent and self-supporting upon the tube inversion – see Table 2.3 for total NaOH volumes added to the given peptide.

Table 2.2 Amount of starting peptide powder and 0.5M NaOH required for peptide hydrogel production

Peptide Concentration (mg/mL)	Peptide powder (mg)	Volume of 0.5M NaOH (µL)
6	7.5	40
8	10.0	55
10	12.5	65

Once transparent, self-supporting hydrogel was achieved, 100µL of 10x PBS was added into the hydrogel's mix. The content was vortexed and centrifuged for 10 seconds and subsequently incubated overnight at 80°C. Hydrogels were stored at 4°C until further use.

2.10 Peptide hydrogel gelation and cells (and co-culture) encapsulation

Precursor hydrogels were liquefied at 80°C to achieve a homogenous mixture and cooled to 37°C in a water bath. A total of 250 µL cell suspension in T cell medium supplemented with IL-2 at 30U/mL was prepared for 1mL of hydrogel (final volume ratio 1:5). Cell density was prepared with extra cells to meet the desired cell concentration in the hydrogel, as the actual volume with cells and hydrogel totalled to 1.25mL. For example, to achieve $1x10^6$ cells/mL in hydrogel,

$1.25x10^6$ of cells were collected and resuspended in 250 µL medium. Added medium with cells was gently mixed into the precursor hydrogel by reverse pipetting until the content was evenly distributed. The hydrogel mixture was aliquoted into a 96-well plate (100µL / well) or hanging inserts in a 24-well plate (200µL / insert) followed by incubation at 37°C in a 5% CO_2 incubator for 10 min. For hydrogels in inserts, 1mL of complete T cell medium was added to the surrounding well and 200µL medium dropwise on top of the gel. For hydrogels in the 96-well plates, 200µL of medium was added dropwise to the gel. Medium was changed twice within the first hour to induce the gelation process, and the third wash was done 3-4 hours after the second wash or the following day.

The co-culture between T cells and artificial/actual APCs was set up in the hydrogels. Cell suspension of each cell type was prepared in a total of 125µL of T cell medium. Once both cell suspensions were combined it met the required volume for 1mL of hydrogel. For example, a co-culture between T cells and DC at ratio 10:1, respectively, requires $1.25x10^6$ T cells in 125 µL and $1.25x10^5$ DC in 125 µL for 1mL hydrogel.

2.11 3H-Thymidine incorporation assay

3H-Thymidine is a radioactive nucleotide, which gets incorporated into cell's DNA during DNA synthesis process [318]. From T cells perspective, activated and proliferating cells incorporate more the 3H-Thymidine in DNA due to actively synthesised DNA, than unstimulated/resting T cells. The assay cannot provide single cells readouts, as the produced results represent the whole cell

population in plate's well. T cells ($1x10^6$ cells/mL) and artificial APC ($1x10^5$ beads/mL) were resuspended in T cell medium and encapsulated in 1mL of peptide hydrogel. The experiment was set up in a 96-well plate and incubated for 6 days at 37°C with a 5% CO_2 incubator. On the final day of the experiment, 100µL of medium surrounding the hydrogel was collected and saved for ELISA assay to analyse the cytokines of interest. The removed medium was replaced with fresh culture medium containing 3H-Thymidine (0.5 µCi) and incubated for the final 18 hours of the experiment. The following day, medium was removed carefully without disturbing the hydrogel and 100µL of 2% of SDS (prepared in distilled water) was added to the wells. The content was gently mixed and incubated for 5 min to degrade the biomaterial and cells. The plate was washed with water six times to get rid of the culture debris and released DNA content was trapped in the UniFilter 96-well plate (see Table 2.6). The plate was left to dry overnight at room temperature in the fume hood. 30µL of β-scintillation liquid was added to each well and analysed for 3H-Thymidine incorporation (cpm) with TopCount NCT PerkinElmer radiometric counter.

2.12 CFSE staining of CD4+ T cells

T cells were labelled with carboxyfluorescein succinimidyl ester (CFSE) to trace down the cells during the microscopic imaging process and assessment of cell proliferation by flow cytometer. CFSE dye works once it crosses the cell's plasma membrane and gets processed by esterase enzymes which create a highly fluorescent dye [319]. CFSE binds covalently to the amine groups of the proteins, thus 'labelling' the entire cells with detectable fluorescent colour. Upon cell's

division the fluorescent content within cells gets halved into the daughter cells, making the dye popular as the surrogate for the proliferation studies (Graph 2.3).

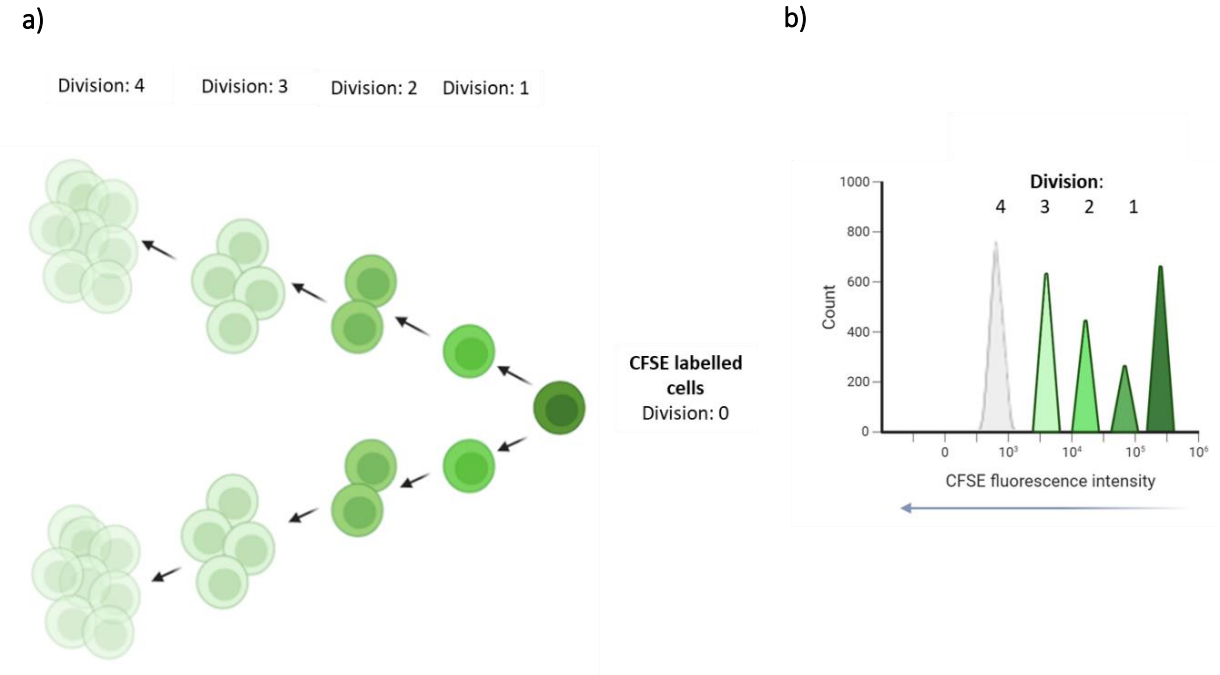

Graph 2.3. CFSE dye dilution by dividing cells and flow cytometry analyses. Cells labelled with CFSE dye have high fluorescence intensity. a) Upon T cell stimulation, dividing cells diluted the CFSE content into the daughter cells, and further cells' division allowed to monitor the proliferation process. b) CFSE dye dilution and proliferation can be monitored by the flow cytometry, where the decrease of CFSE fluorescence intensity reflects the dividing cells. Figure created with BioRender.com

Cells staining process began by dilution of CFSE stock with dimethyl sulfoxide (DMSO) to make a 5mM stock solution. Dye was further diluted to achieve 2µM final working concentration per 1mL of DPBS. Prior to staining, CD4+ T cells were resuspended ($1x10^6$ cells/mL in DPBS) and washed by centrifugation to remove the remaining serum content. The prepared CFSE staining solution was added to the dislodged cell pellet, mixed and incubated for 20 min at room temperature in the dark. The staining process was stopped by adding 5x times (v/v) complete T cell medium and incubated for 5 min to quench unbound CFSE. Cells were

washed and resuspended at $1x10^6$ cells/mL in complete T cell medium with IL-2 and rested overnight in 6-well plates (37^oC). The following day the uniformity and fluorescence intensity of CFSE-labelled cells were determined by flow cytometry prior to experimentation.

2.13 Bulk Oscillatory Rheology

Bulk Oscillatory Rheology was performed on a Physica MCR 301 rheometer (Anton Paar). Hydrogels were prepared in hanging inserts in a 24-well plate, and the gelation process was induced (by changing the medium in total three times) within one day. The following day, hydrogels were cut out from the inserts and mounted onto the rheometer plate set at 37°C and interrogated using PP08 (8mm) parallel plate. An amplitude sweep test was performed with the strain set between 0.1% and 100% to determine the linear viscoelastic region. After this test, the determined strain (i.e. 1%) was used for all samples at the frequency of 1 rad/s [311]. Storage modulus (Pa) of hydrogels was identified by the 'time sweeps' test, which was acquired with ten measurements over 5 min with constant strain and frequency settings. The peptide hydrogels' height ranged between 4-5mm.

2.14 ELISA for IFNγ

Cell culture supernatants were tested for the presence of cytokines. Supernatants were harvested from 2D and 3D cultures without disturbing cells

or hydrogels. Supernatant from the 2D culture were diluted 1:10 in reagent diluent, whereas 3D samples were diluted 1:2 reflecting the cellular response.

96-well high-binding plates were coated with capture antibody (1:100 in PBS), at 100 µL / well and incubated overnight at room temperature. The following day, the capture antibodies were removed and the plate was blocked with 300 µL reagent diluent (see table 2.5 for composition) for 1 hour at room temperature. After the removal of the reagent diluent, 100 µL of diluted samples and prepared standard (31-2000 pg/ml in reagent diluent) were added and incubated for 2 hours at room temperature. Plates were washed five times with washing buffer, before addition of 100 µL detection antibody (1:100 dilution in reagent diluent) and incubation (2 hr, room temperature). Plates were washed another five times, followed by the addition of 100 µL of poly-HRP-streptavidin-HS (1:1000 in reagent diluent) for 30 minutes. After further washing, 100µL of TMB substrate solution was added and incubated in the dark at room temperature. The plate was monitored for colour change in the standard samples. The process was stopped with 50 µL of stop solution (1M of $2NH_2SO_4$) once the gradient from the highest to the lowest concentration of the standard samples was visible. Optical densities were determined by absorbance at 450nm with Infinite F50 Tecan microplate reader.

2.15 ELISA for IL-10

The 96-well high-binding plate was coated with 100 µL of capture antibody diluted at 1:180 in DPBS, and incubated overnight at room temperature. The following day the plate was washed three times with washing buffer, and blocked with 300 µL reagent diluent for 1 hour. Plate was washed three times, and 100 µL of diluted samples (1:10 for 2D, non-diluted from 3D culture) and standards (31.2-2000 pg/ml in the reagent diluent) were added and incubated for 2 hours. The plates were washed three times with washing buffer, before addition of 100 µL detection antibody (diluted at 1:180 in the reagent diluent) and incubation for 2 hours at room temperature. Plates were washed for three times and 100 µL streptavidin-HRP (diluted at 1:200 in the reagent diluent) was added and incubated for 20min in the dark, followed by the washing step again. TMB substrate solution and plate development were finished in the same way as ELISA IFNγ plates. The entire assay was carried out at room temperature.

2.16 ELISA for IL-12p40

The 96-well high-binding plate was coated with 100 µL capture antibodies (diluted at 1:250 in the coating buffer) and incubated at 4°C overnight. Plate was washed three times with the washing buffer, followed by addition of 200 µL of assay diluent for the blocking step and incubation for 1 hour. Harvested 2D culture supernatants were diluted with an assay diluent by 1:50 dilution, whereas 3D culture sample was tested undiluted. Standards were prepared in the assay diluent with known concentrations ranging from 7.8-500 pg/ml. After

the washing step, 100 µL of samples and standards were aliquoted and incubated for 2 hours. The plate was washed five times and 100µL of detection antibody (1:500 dilution) with streptavidin-HRP (1:250 dilution) was added followed by 1 hour incubation. The plate was washed seven times with the washing buffer, followed by TMB substrate solution addition. The plate development process was finished in the same way as ELISA IFNγ and IL-10 plates. The described procedure (apart from the coating step) was carried out at room temperature.

2.17 Flow cytometry

For 2D culture, cells were collected from wells and washed with PBS (added at an equal volume as the sample) at 300 x g for 10 minutes. Cells were reconstituted in 200µL of MACS buffer and stained with a panel of antibodies (Table 2.3). Separate samples were prepared for isotype controls – antibodies matched the same class as the antibodies used for the marker detection. Isotype controls and antibodies against specific markers were also matched by fluorophores, concentrations and manufacturers. Stained samples were incubated (15 min at 4^{o}C, in the dark) followed by addition of an equal volume of PBS for the washing step. Cells were reconstituted in a total of 200µL MACS buffer prior to flow cytometry.

In order to stain cells from 3D cultures similar cells were first released from the hydrogel with an optimised method (section 2.18) and also stained with similar concentrations of antibodies to those from 2D culture. A further irrelevant

isotype (not matched to any antibody-detecting marker) was included to exclude hydrogel debris from the analyses. Flow cytometry data were analysed with FlowJo version VX and v10.8.

Table 2.3 Flow cytometry antibodies

Extracellular marker detecting antibodies (Catalogue number)	Isotype control (Catalogue number)	Used volume (µL) per 200µL sample	Manufacturer
CD4+ APC (130-113-772)	IgG2a (130-113-831)	2	Miltenyi Biotec
CD4+ PE (130-113-241)	IgG2a (130-113-834)	2	Miltenyi Biotec
CD3+ FITC (170-081-047)	IgG2a (130-113-833)	2	Miltenyi Biotec
CD8+ APC (130-113-154)	IgG2a (130-113-831)	2	Miltenyi Biotec
CD25+ APC eFluor 780 (47-0259-42)	IgG1 (47-4714-82)	5 (isotypes were used at 1.25µL)	eBioscience
HLA-DR PE Cy7 (25-9956-42)	IgG2b (25-4732-81)	5 (isotypes were used at 0.075µL)	eBioscience
HLA-DR VioBlue (130-133-968)	IgG2a (130-113-839)	2	Miltenyi Biotec
CD86+ FITC (130-114-097)	IgG2a (130-113-833)	2	Miltenyi Biotec
CD86 PE (130-114-098)	IgG1 ((130-123-746)	2	Miltenyi Biotec
Polyclonal Rabbit anti-mouse antibody FITC (F0232)	/	2	Dako
Hydrogel debris exclusion (isotype control only)	IgG1 VioBlue (130-093-197)	2	Miltenyi Biotec

2.18 Peptide hydrogel degradation and cell release for flow cytometry

Cells were released from the peptide hydrogel by using TrypLe 1x solution. TrypLE, a direct replacement of trypsin enzyme, was warmed to 37^{o}C before the

hydrogel degradation process. 100 µL of supernatant was removed from each well for subsequent ELISA, then 200 µL/well TrypLE was added. TrypLE solution aided gel degradation during pipetting which facilitated distribution of TrypLE throughout the sample. Plates were incubated (10 minutes, 37^{o}C) and content transfer to 50ml Falcon tubes. An additional 400 µL of normal T cell medium was added to degraded hydrogels prior to centrifuge (300 x g, 10 min). The resuspended pellet was exposed to a second round of degradation and 200µL of TrypLE added. After a further 10-minute incubation at 37^{o}C with weashing, the hydrogel was exposed for the third and final time to the TrypLE. Once washing steps were completed, 200µL of total cell content (adjusted with PBS) was stained with antibodies and irrelevant isotype to exclude hydrogel debris from the analyses. The procedure of this developmental and optimising method is discussed in Appendix 1.

2.19 Dead cell detection by propidium iodide (flow cytometry)

Propidium iodide (stock 1mg/mL) was used to detect the dead cells upon binding to the DNA content of cells and analysed by flow cytometry [320]. At the conclusion of experiments, 200µL of the test sample was stained with 5µL of propidium iodide stock and incubated for 5 min. Cells were analysed immediately by flow cytometry. Dead cells (positive control) were prepared by (10 minutes, 98^{o}C). After heating, cells were cooled to room temperature and stained with propidium iodide as above.

2.20 Live and dead staining of cells in the peptide hydrogel, and cell viability % calculation

Cell viability in hydrogels was determined by using a two-colour fluorescence Live/Dead staining kit. The staining solution was prepared in 1mL PBS with 1µL/mL calcein AM and 2µL/mL of ethidium homodimer to detect live and dead cells respectively. Hydrogels were removed from wells, placed on glass coverslips, covered with an excess of staining solution and incubated in the dark for 10 min. Live cells were detected at an excitation/emission of 494/517 nm, and dead cells at 526/617 nm using a 10x objective by Nikon Eclipse TS100 microscope (Nikon Instruments Europe) with a Nikon Digital Sight DS-Fi1 camera. Images were acquired from three different regions of interest (ROI) per hydrogel, then processed by ImageJ software to assess cell viability percentage. The procedure of image processing is described in Graph 2.4, where live and dead cell counts (distinguished by different fluorescent channels) were obtained to calculate the cell viability % as follows:

$$\%\ Cell\ Viability = \frac{l}{l+d} \times 100$$

where "l" is live, and "d" is dead cells [306]. Data were plotted with average % Cell Viability numbers calculated from the three ROIs of the hydrogel sample.

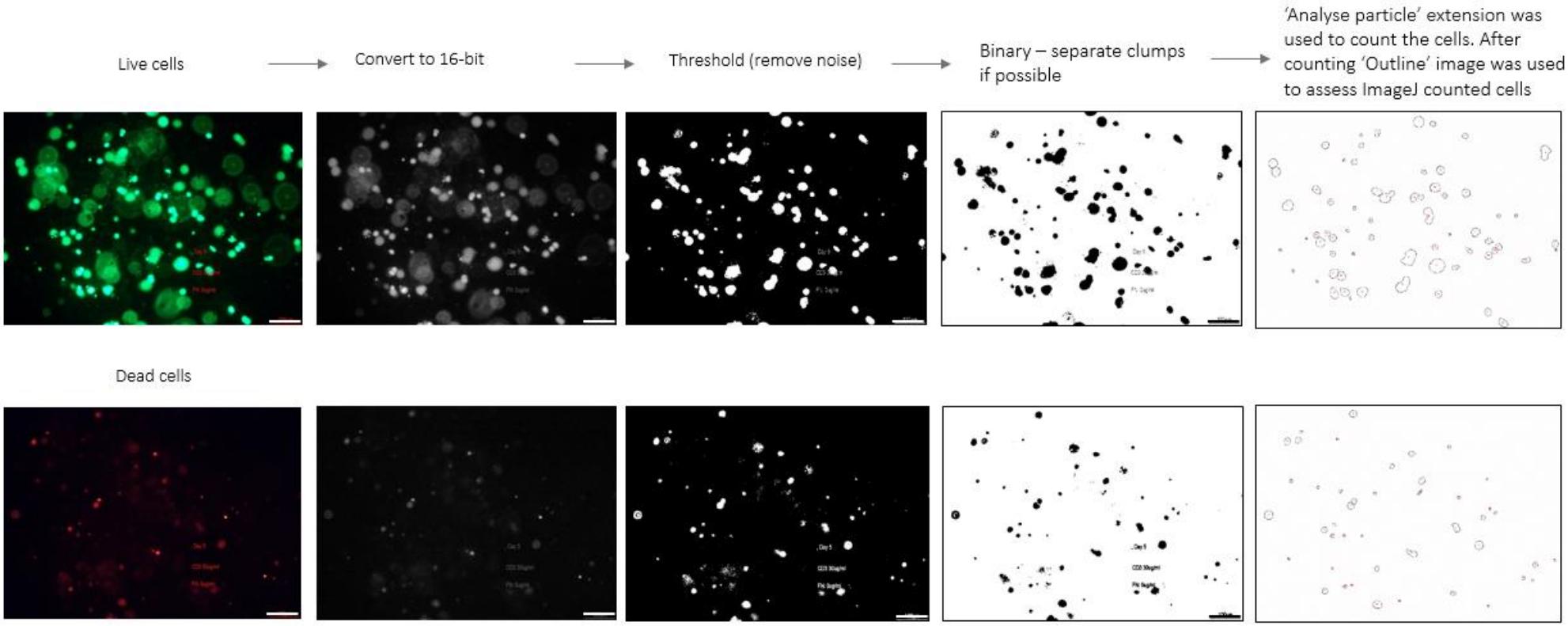

Graph 2.4: Live/Dead image processing steps to count cells within the peptide gel. From the same region of interest (ROI) the image was split into two channels representing live cells (stained by calcein AM) and dead cells (stained by ethidium homodimer). The image was processed to 16-bit, followed by a threshold to remove the noise background and distinguish individual cells. Next, the image was turned to the binary to make a two-colour image, which also reduced the background noise. ImageJ tool 'Analyse particles' was selected to define the size of cells (termed 'infinity') and the shape of cells (termed 'circularity') before the cell count. After the count, an 'Outline' image was produced, which indicated the software's counted spots. The 'Outline' image was compared to the binary image for any missing counts. If counts were missing, new adjustments (separating joined cells) or parameters (infinity and circularity) were defined again to produce a more accurate count. The values for 'infinity' and 'circularity' were constant per the conducted experiment. The scale bars presented here are 100µm. The method was adapted from Christine Labno (2020) [321].

2.21 DC staining with PKH26

PKH26 red fluorescent cell linker was used to label DC before hydrogel encapsulation. PKH26 interacts with long aliphatic tails of lipids and mainly stains the plasma membrane [322]. Before the assay, all reagents from the kit were warmed to room temperature. $2x10^7$ cells were collected into 15 Falcon tubes and washed in RPMI medium without serum (400 x g, 5 min). The supernatant was removed and the cell pellet gently reconstituted with 1mL of Diluent C. In a separate tube, 1mL of Diluent C was mixed with 4µL of PKH26 dye ($1x10^{-6}$M). 1mL of PKH26 was swiftly added to 1mL of cell suspension, wrapped with foil and rotated at 15rpm for 5 min. Staining was stopped by adding 10mL of serum-free RPMI prior to washing (400 x g, 10 min). Supernatants were carefully removed and cell pellets dislodged with an additional 10mL medium. The content was transferred to a new Falcon tube and washed twice (400 x g, 5 min). Only iDCs were stained with PKH26 which were later stimulated for mature DCs (mDCs) differentiation.

2.22 T cell stimulation with mitogens (positive control)

Prior to the encapsulation in the hydrogel, T cells were stimulated for 12 hours with PMA (25ng/ml) and Ionomycin (0.5µg/ml) in T cell medium supplemented with IL-2 (30 U/ml). A suspension of T cells ($1x10^6$ /mL) was aliquoted (1mL) into 12-well plates, followed by the addition of another 1mL of T cell medium containing 2x concentration of stimuli. Resting T cells were incubated for 12

hours in medium alone. Mitogen-stimulated T cells were used as a positive control in the peptide hydrogels.

2.23 Multiple lymphocyte reaction (MLR) with artificial and actual APC

Resting T cells stained with CFSE were encapsulated with DC (immature, mature, drug-treated) or artificial APC (antibody-coated polystyrene beads) in hydrogel. For encapsulation, T cells ($1.875x10^6$) were prepared in 125µL T cell medium and combined with APC. The quantity of APCs was adjusted according to the desired ratio to the T cells in the peptide hydrogel. For 2D culture, the cell density and ratio of cells were matched to those in 100 µL peptide hydrogel and set up in a 96-well plate. Both 2D and 3D cultures required medium replacement every 3-4 days during the experiment.

2.24 Confocal microscopy, 3D imaging and immunocytochemistry

Co-cultures of labelled CFSE-T cells and PKH26-DC in hydrogels were set up for 7 days in glass-bottomed 96-well plates. On the final day, 100 µL medium was removed and replaced with the same volume of PBS. This washing step was repeated twice. After the last wash, 100 µL of 4% paraformaldehyde solution was added and incubated for 1 hour at room temperature in the dark. The fixing solution was washed away with PBS before imaging. Samples were analysed by Leica SPE11 confocal microscope to determine the distribution of fluorescently labelled cells within the hydrogel. 500µm of Z-stack images were produced with

10x objective, starting from the top and moving towards the middle of the hydrogel. Z-stacks were processed with an optical section set at 12.85µm and z-step sizes at 4.28µm. Collected images were processed with ImageJ software.

Other experiments analysed Ki67 (proliferation marker) expression on T cells after stimulation by artificial APC in peptide hydrogels. The experiment was set up with T cells to artificial APC at ratio 1:2 (T cells:APC) in a 96-glass bottom plate and incubated for 7 days. On the final day, medium was removed from the peptide hydrogels and washed one time with 100 µL PBS. Next, 100µL of 4% paraformaldehyde was added to the wells and incubated for 1 hour at room temperature, in the dark. The excess of fixative solution was removed and washed once with 100 µL PBS. The hydrogel was transferred to small glass dish suitable for imaging and immersed in blocking buffer (see Table 2.5 for composition) for 1 hour at room temperature, in the dark. Blocking buffer was removed and 200µL of primary antibody targeting Ki67 (diluted 1:100 in blocking buffer) was added. The dish was covered with parafilm and aluminium foil and incubated overnight at 4^{o}C. Excess staining solution was removed and washed twice with 200 µL blocking buffer (5 minutes incubation for the final wash). Secondary antibody polyclonal anti-mouse Alexa Fluor 633 (1:400 dilution in blocking buffer, total 200µL) was added and incubated overnight at 4^{o}C. The next day, hydrogels were washed twice with 100 µL PBS and analysed using a Nikon AX confocal microscope, 10x objective.

2.25 Coating plates with fibronectin and collagen type I and analyses of co-stimulation effect on T cells

Fibronectin from bovine plasma and rat tail collagen type I was used to coat 96-well high-binding plates. First, working concentrations of collagen and fibronectin were prepared separately in non-high binding 96-well plates. During the coating procedure, all proteins and the 96-well plates were incubated on ice to prevent protein polymerisation. Plasma fibronectins were resuspended at 100µg/mL in PBS and 150µL aliquoted / well. Fibronectin stock was serially diluted with cold PBS as required. Collagen type I was prepared at 100µg/mL by mixing 33µL of collagen stock (3mg/mL) with 100µL of 10X PBS, 0.825µL of 1M NaOH and 866 µL of distilled sterile water. The preparation of various collagen concentrations followed the same steps as for the fibronectin. Dilutions of matrix proteins were transferred to 96-well high-binding plates, wrapped with parafilm and incubated overnight at 4^{o}C [323]. The following day, the plate was equilibrated for 2 hours at room temperature to complete coating and protein polymerisation. Before seeding T cells and artificial APC (coated with 1µg/mL anti-CD3), wells were washed three times with 200 µL PBS. CFSE labelled T cells were prepared at 1.5x10^{6}/ml in T cell medium and aliquoted to the protein-coated plate with APC (ratio 1:0.125) and incubated for 5 days at 37^{o}C, 5% CO_2. Anti-CD3 and anti-CD28 coated APC were used as a positive control, whereas resting T cells were used as a negative control. On day 5 cells were analysed by flow cytometry.

2.26 Functionalising peptide hydrogel with collagen type I and plasma fibronectin

Stock solutions (1mg/mL) of collagen type I and fibronectin were prepared and stored on ice. 250µL medium containing T cells, artificial APC (coated with 30µg/ml of CD3) and both matrix proteins were prepared for 1ml peptide hydrogel. For example, to make 33µg/ml of functionalised hydrogel with fibronectin and collagen type I, 1ml of peptide hydrogel received 41.24µL of fibronectin prepared stock, 41.24µL of collagen type 1, 80µL of T cell suspension and 80µL of artificial APC, making total 250µL. During the encapsulation process, first matrix proteins were mixed into the hydrogel followed by the addition of T cells and artificial APC on the top of the gel. The whole content was gently mixed and aliquoted 100µL per well into a 96-well plate. For this experiment, CFSE labelled T cells at $1.5x10^6$/ml were encapsulated with artificial APC at a ratio 1:0.25 and incubated for 7 days at 37^oC 5% CO_2. Medium was changed on days 3 and 4; on the final day, the supernatant was collected for IFNγ cytokine analyses. Hydrogel was further processed to analyse T cells' proliferation response in the presence of stimulus and matrix proteins by flow cytometer.

2.27 Statistical analyses

Statistical analyses were undertaken with GraphPad Prism version 9. Data normal distribution was tested by the Shapiro Wilk test and $p<0.05$ were classed as 'non-normally distributed', whereas $p>0.05$ determined normal distribution. If acquired data were non-normally distributed, the skewness test was run to

indicate the level of skewness. This is to determine the appropriate equation for data transformation so that parametric tests could be used to analyse the significance of data. Rheology data of the peptide gels were tested with an unpaired, two-tail t-test. The choice of statistical tests analysing cellular response data varied amongst experiments. Figure legends indicate the types of tests were used to analyse specific data. A normally paired, two-tail, t-test or repeated measures (RM) Two-way or One-way ANOVA tests were used. The significance was determined if p-value was less than 0.05. The approach of statistical analyses was discussed and advised by 'School Statistics Advice' based at University of Nottingham.

Table 2.4 List of reagents used for research

Reagent	Manufacturer and catalogue number
Histopaque 1077	Sigma-Aldrich, 10771
Dulbecco's phosphate buffered saline (DPBS)	Sigma-Aldrich, D8537
Trypan Blue	ThermoFisher, Gibco, 15250061
CD4+ human microbeads (CD4+ T cell isolation)	Miltenyi Biotec, 130-045-101
CD14+ human microbeads (CD14+ monocyte isolation)	Miltenyi Biotec, 130-050-201
LS columns	Miltenyi Biotec, 130-042-401
LD columns	Miltenyi Biotec, 130-042-901
MS columns	Miltenyi Biotec, 130-042-201
IL-2 cytokine	In house produced (stock $5x10^5$ U/mL, 2316198, JR338)
IL-4 cytokine	Immunotools 11340042
GM-CSF cytokine	Peprotech 300-03
Poly:I:C (TL3)	Invivogen
R848 (TLR 7/8)	Invivogen
Dexamethasone	4mg/ml Organon, UK (Clinical grade)
p38 inhibitor (BIRB196)	Selleck chemicals S1574
20µm polystyrene particles	Polysciences, Inc., 18329
Anti-human CD3	Clone: OKT3, Mouse IgG2a, in-house
Anti-human CD28	Clone: CD28.2, NA/LE, Mouse IgG1, BD Biosciences or Clone: YTH913.2, Rat IgG2b, in-house
Anti-human CD55	Clone:791T/36, Mouse IgG2b, in-house

Table 2.4 List of reagents used for research (continue)

FEFEFKFK peptide powder	Cambridge Research Biochemicals and Pepceuticals
UltraPure distilled water	Fischer scientific, Invitrogen, 11538646
1M Sodium hydroxide	Sigma-Aldrich, S2770
10X PBS	ThermoFisher, Gibco, 70011-036
3H-Thymidine	PerkinElmer, NET027001MC
Scintillating Fluid	Microscint PerkinElmer 86-15071
Sodium dodecyl sulfate (SDS)	Sigma-Aldrich, 436143
Cell Trace CFSE	ThermoFisher, Invitrogen, C34554
Dymethyl sulfoxide (DMSO)	Sigma-Aldrich, D2650
24-well inserts with 1µm pore	Greiner Bio-One, International, 662610
L-glutamine	Sigma-Aldrich, G7513
HEPES buffer	Sigma-Aldrich, H0887
Fetal bovine serum (FBS, for T cells)	ThermoFisher, Gibco, 10270-106
Fetal bovine serum (batch tested for DC)	Sigma-Aldrich, F6178
ELISA human IFNγ	Immunotools, 31673539
ELISA human IL-10	R&D systems, DY217B
ELISA human IL-12p40	BD Biosciences, 555171
Sulphuric acid 5M ($2NH_2SO4$)	Fisher chemical, 12963634
96-high binding well plates (EIA/RIA)	Costar, 3590
Bovine serum albumin (BSA)	Sigma-Aldrich, A/906-100G
Tween 20	Sigma-Aldrich, P1379
PBS tablets	Oxoid, BR0014G
TMB substrate solution	BD Bioscience, 555214
1M of 2NH2SO4 (ELISA stop solution)	Fischer scientific, 10666072
TrypLE 1x, phenol red	ThermoFisher, Gibco, 12605028
Propidium iodide	Sigma-Aldrich, P4864
Paraformaldehyde	Thermo Scientific, J19943.K2
LIVE/DEAD staining kit	ThermoFisher, L3224
PKH26 red fluorescent cell linker kit	Sigma-Aldrich, MINI26
PMA	Sigma Aldrich, P1585
Ionomycin	Sigma Aldrich, I0634
Glass-bottom 96-well plate for microscopic imaging	Fischer Scientific, 13539050
Anti-human Ki67 primary antibody	Abcam, ab279653
Anti-mouse Alexa-Fluor 633	ThermoFisher, Invitrogen, A-21052
Fibronectin bovine plasma	Sigma-Aldrich, F1141
Rat tail collagen type I	ThermoFisher, Gibco, A1048301
RPMI 1640	Sigma, R8758
EDTA 0.5M	ThermoFisher, Invitrogen, 15575-020
Sodium Pyruvate	Sigma-Aldrich, S8636
Penicillin/Streptomycin	Sigma-Aldrich, P4333

Table 2.5 List of medium and buffers

Medium and buffers	**Composition**
T cell medium	500mL RPMI, 1% L-Glutamine, 1% penicillin/streptomycin, 2% HEPES buffer, 1% sodium pyruvate, 10% FBS (T cells)

Table 2.5 List of medium and buffers

Dendritic cell (DC) medium	500ml RPMI, 10% FBS for DC, 1% sodium pyruvate
MACS buffer	500mL DPBS, 0.5% FBS, 2mM EDTA
0.5M NaOH	1:2 dilution of 1M NaOH with distilled sterile water (UltraPure)
Washing buffer (ELISA)	PBS with 0.05% Tween20
Blocking buffer (Immunocytochemistry)	PBS with 0.1% Triton, 0.5% BSA
Reagent diluent and blocking buffer (ELISA, IFNγ)	PBS, 2% BSA and 0.05% Tween20
Reagent diluent (ELISA, IL-10)	PBS with 1% BSA
Assay diluent (ELISA, IL-12p40)	PBS with 10% FBS
Coating buffer (ELISA, IL-12p40)	0.1M sodium carbonate (mixing 7.13g of sodium bicarbonate, 1.59g of sodium carbonate in 1L distilled water) and adjusting pH to 9.5 with 10N sodium hydroxide.

Table 2.6 List of experiment specific 96-well plates

Materials	**Supplier and catalogue number**
96-well UniFilter plate	PerkinElmer, 6055690 (for 3H-Thymidine)
96-well high binding plate	Corning, 3590 (for ELISA)
96-well glass bottom, optically clear plate	PerkinElmer, 6055302 (for fluorescence microscopy)

Chapter 3: Proof-of-principle: peptide hydrogel use for T cell culture

3.1 Introduction

Self-assembling peptide hydrogels were used to culture various cell lines, but there is a paucity of research studying immune cells, especially T cells [306, 308, 311, 312, 324-326]. Various biomaterials were investigated for their capacity to establish 3D T cell function; all of which permitted some or all of T cell responses (i.e. proliferation, migration, effector functions), which were heavily influenced by the type of the material [161, 164, 166, 277, 327-330]. Unmodified and adjustable hydrogel with mechanical stiffness would be ideal for 3D T cell culture studies, since these cells are commonly found to work their function in various tissue microenvironments. To this point, it is unknown whether peptide hydrogel is suitable for culturing primary human T cells, especially under 3-dimensional (3D) culture settings.

The majority of peptide hydrogel-related research with primary immune cells was done for the vaccine purposes. Different peptide units (i.e. RVQV, multipeptide from KRAD, poly-L-lysine with Fmoc-FF, PEG-b-poly(L-alanine) (polypeptide), Nap-GFFY D-peptides) bearing antigens were used to prime the immune responses [249, 331-335]. However, even if the peptide hydrogels do get recognition as the vaccine prototype to modulate immunity, no research has

explored the potential of FEFEFKFK peptide hydrogels on instructing the immune cells under 3D culture. Furthermore, only a limited number of studies explored the biocompatibility of encapsulated immune cells; they do not evidence enough data to predict the consequences of using peptide hydrogels, especially FEFEFKFK [332, 336, 337].

Due to marked differences in composition and gelation process between peptide hydrogels, the FEFEFKFK effect on primary immune cells remains to be determined [336]. One of the features of the peptide hydrogel that must be considered is high pH during the cell encapsulation process [310]. One study reported how T cell proliferation and CD25 (IL-2 receptor) expression were inhibited by small pH variations (from 7.0 to 7.4 pH) [338]. This should be taken into account when T cells are exposed to precursor FEFEFKFK hydrogel's pH since it could affect cells' viability and function. Another feature of the hydrogel to consider is the material's stiffness level, which could influence 'mechanosensing' T cells activity [164, 330, 339]. Few studies already showed opposing results on how T cells' activity was influenced by material's high stiffness level e.g. collagen type I hydrogel suppressed T cells proliferation, whereas alginate hydrogel enhanced it [161, 164]. Besides hydrogel's stiffness, biomaterial's architecture could effect cells as well, as collagen type I provided a fibrillar network, whereas alginate had a porous scaffold. FEFEFKFK peptide hydrogel has a nanofibrous structure and the outcome of material on T cells needs to be investigated [302, 307]. In addition, due to its nanofibrous structure it is unknown whether peptide hydrogels could support effective metabolite diffusion and waste product

removal to support T cells activity. Overall, peptide hydrogel's chemical, mechanical and architectural properties on T cells needed to be investigated.

Another question that remains is whether FEFEFKFK type hydrogel can support basic T cell function i.e. induced cell activation by stimuli. One study explored T cell activation by stimulation using OVA peptide conjugated to the nanofiber of the peptide hydrogel (made from RVQV peptide sequence) [335]. DCs processed the OVA-peptide and activated CD8+ T cells in vitro. However, in this study cells were not encapsulated in the material; rather they were mixed in cell culture with fully-formed fibres carrying the OVA-peptide. The purpose of this study was to produce the material suitable for immunisation and deliver peptides to induce an immune response. To date no other literature describes immune cell stimulation within the peptide hydrogels, which could give some indication of the material's influence on cells. Some studies have proven the ability of FEFEFKFK hydrogel to modify other cell line behaviour. For example, Diaz et al. (2016) showed FEFEFKFK hydrogel's ability to support the differentiation of mesenchymal stem cells into osteoblasts in the presence of osteogenic media [312]. Burgess et al. (2021) demonstrated differentiation of cardiac progenitor cells and He et al. (2022) showed hepatocytes' response to cholestatic drugs by altering their production of albumin and urea [308, 324]. These studies were dependent on good supplements or drug diffusions to support stem cells, progenitor cells differentiations, and hepatocyte drug treatment. This indicated FEFEFFKF hydrogel's ability to retain biological activity of added molecules to modify cell behaviour in 3D cultures. In addition, the reported studies cultured

cells for 6 or 12 days, indicating the hydrogel's ability to support good nutrient exchange and waste product removal for the encapsulated cells.

On the basis of 'proof-of-principle' the current aim of this research is to analyse the peptide gels' suitability as a 3D culture system for primary human T cells. First, the viability of T cells under different alkaline conditions was assessed to predict how well T cells can withstand the various pH changes that occur during the formation of gels. Further studies aimed to address the relationship between peptide gel densities and stiffness levels on T cells to identify the optimal FEFEFKFK density able to support active T cell cultures. In addition, peptide hydrogel's effect was tested on both resting and stimulated T cells, as various factors (chemical, mechanical and biological) could influence cell viability, metabolic and phenotypic states [327, 339]. After peptide hydrogel's optimisation for T cell culture, further tests were set up to test T cells' abilities to respond to TCR stimulation and costimulation in a similar way to cells stimulated in 2D cultures, resulting in proliferation and cytokine production.

This study was mainly carried out with CD4+ T cells, for the purpose to analyse the peptide hydrogels' influence on one phenotype of cells and avoid a mixture of responses from different types of T cells. The main purpose of this study was to understand the feasibility of T cell 3D culture in the FEFEFKFK-type hydrogels.

3.2 Results

3.2.1 Determining purity of CD4+ T cells post-isolation

The effectiveness of magnetic cell isolations were routinely determined using antibodies to CD3 and CD4 markers with flow cytometry (Fig. 3.1 (a)). Repeated isolations of T cells from the PBMCs population demonstrated the process to reliably deliver a high-purity single population of cells that were CD3+CD4+. CD4+ T cell purity post-isolation was routinely confirmed before establishing experiments (Fig. 3.1 (b)). Whilst the efficiency of CD4+ isolations varied (i.e. some experiments yielded only 66.4% purity (Figure 3.1 (b)), the majority of isolations had > 90% CD4+ cells and only these were studied further.

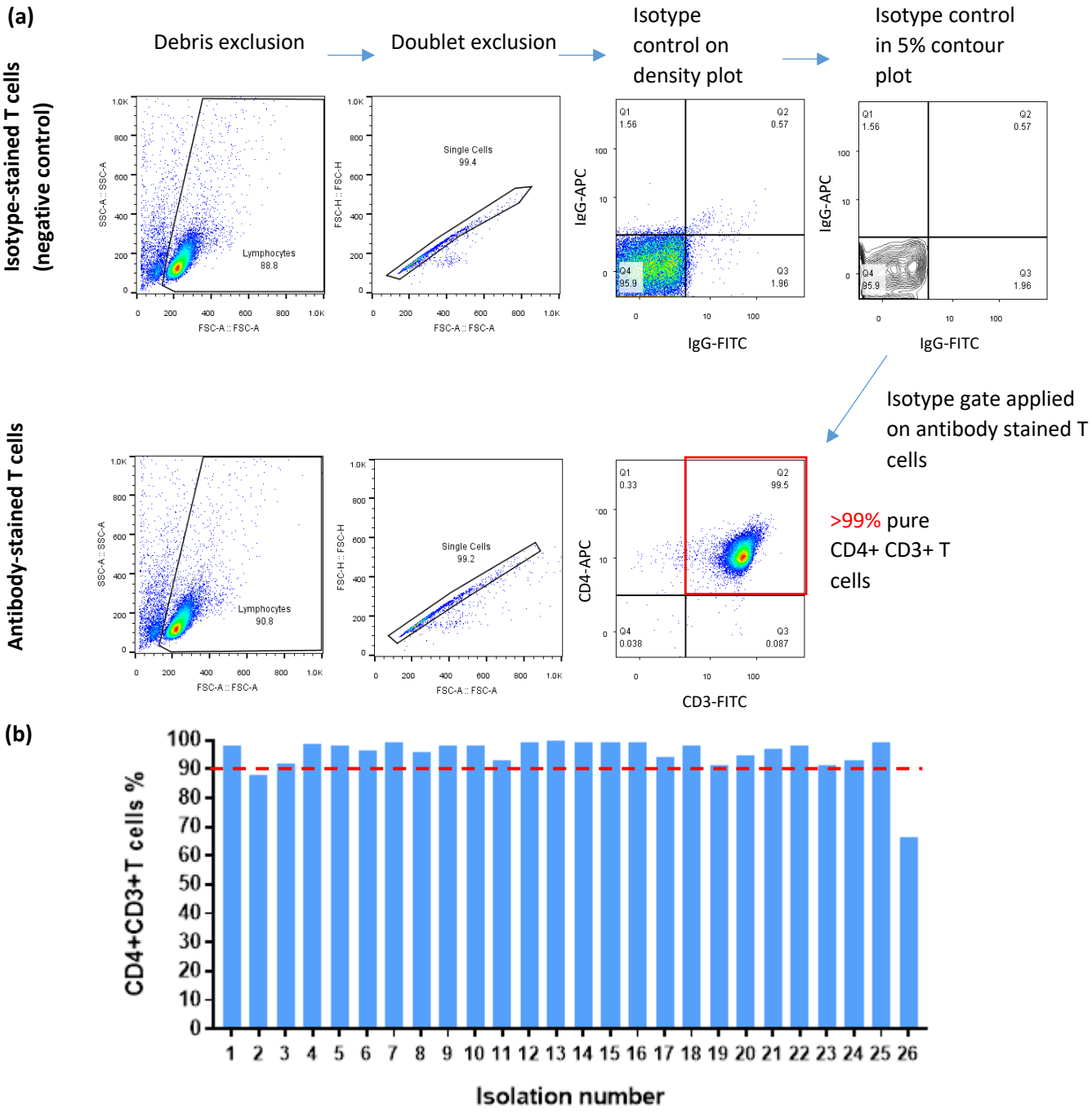

Figure 3.1: The efficiency of isolation of CD4+ T cells from peripheral blood. PBMC cells were isolated from the donated human blood, and further processed with magnetic isolation to obtain a pure CD4+ T cell population. Isolated T cells were labelled with anti-human CD4+ APC and anti-human CD3+ FITC antibodies and analysed by flow cytometry. **a)** Gating strategy for the analysis of the purity of CD4+ T cells. All data was analysed by setting gate-excluding debris, followed by doublets exclusion. The isotype control gates (negative control) were set on the 5% contour boundary and applied on the sample stained with T cell markers. The purity of isolated CD4+ T cells was typically >90%. **(b)** Majority of post-isolations resulted in >90% of CD4+ T cells, anything below (red mark) were excluded from the experiments.

3.2.2 The effect of alkaline pH on the viability of resting T cells

Precursor peptide hydrogels are maintained in contain alkaline conditions (~pH 9.0) to stop the gelation process during the encapsulation of cells in hydrogels. The gelation of the peptide hydrogel occurred at pH 7 (37oC), as rendered by frequent media changes and CO2 presence. It was therefore important to account for the effect of elevated pH on the viability of T cells.

T cells were exposed to the culture media containing alkaline pH, adjusted by the addition of 0.5M of NaOH. Cells were incubated for 24 hours and analysed by propidium iodide stain, which binds the DNA of dead cells, and flow cytometry to assess cells' viability. T cells retained their viability after 24 hours exposure to high pH and viability was not significantly different to the cells incubated at pH 7.4 (Fig 3.2). Subsequent experiments requiring T cells were therefore conducted using this high-pH gelation method.

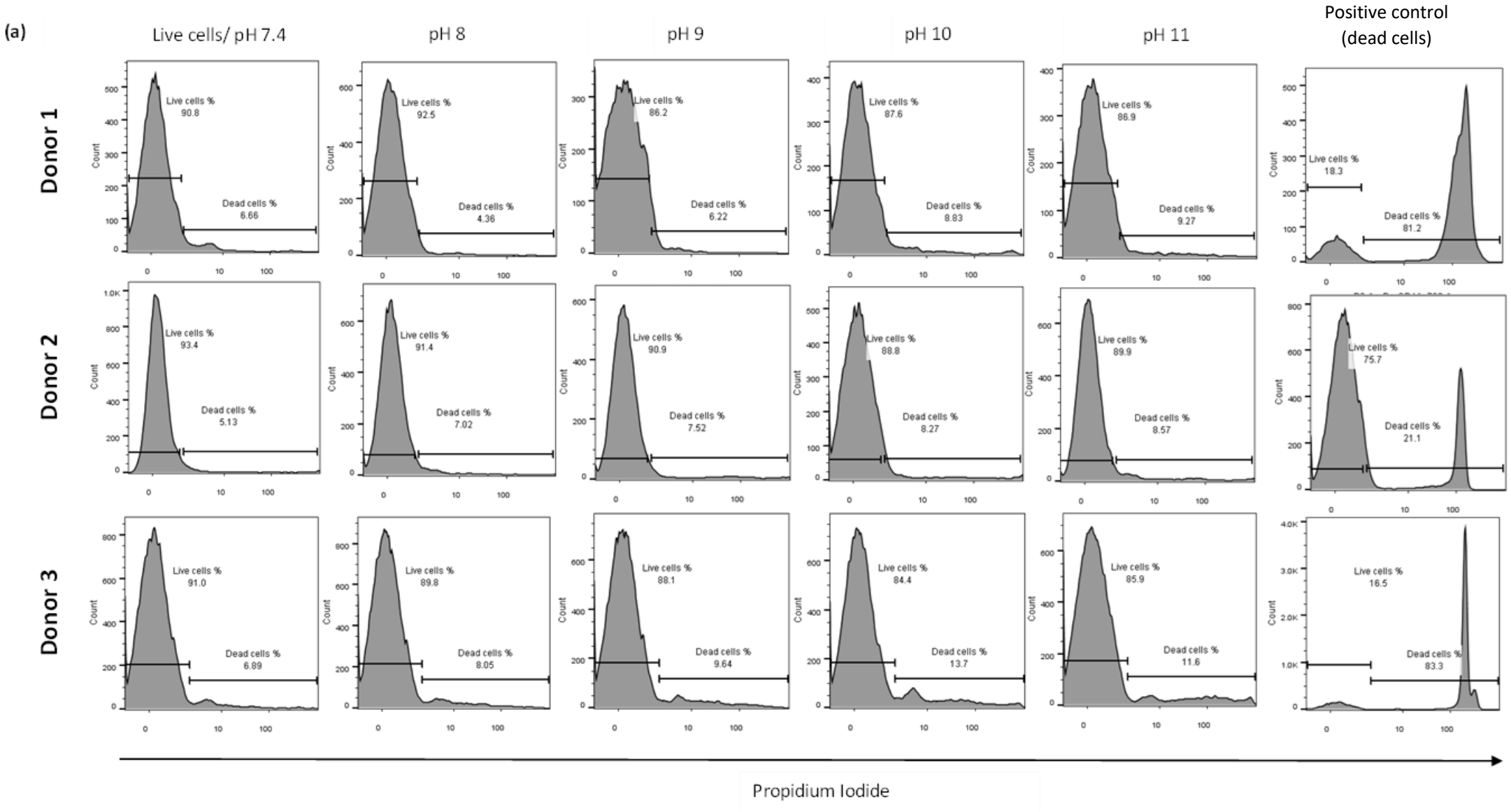
(a)
Live cells/ pH 7.4
pH 8
pH 9
pH 10
pH 11
Positive control (dead cells)
Donor 1
Donor 2
Donor 3
Count
Live cells %
90.8
Dead cells %
6.66
Live cells %
92.5
Dead cells %
4.36
Live cells %
86.2
Dead cells %
6.22
Live cells %
87.6
Dead cells %
8.83
Live cells %
86.9
Dead cells %
9.27
Live cells %
18.3
Dead cells %
81.2
Live cells %
93.4
Dead cells %
5.13
Live cells %
91.4
Dead cells %
7.02
Live cells %
90.9
Dead cells %
7.52
Live cells %
88.8
Dead cells %
8.27
Live cells %
89.9
Dead cells %
8.57
Live cells %
75.7
Dead cells %
21.1
Live cells %
91.0
Dead cells %
6.89
Live cells %
89.8
Dead cells %
8.05
Live cells %
88.1
Dead cells %
9.64
Live cells %
84.4
Dead cells %
13.7
Live cells %
85.9
Dead cells %
11.6
Live cells %
16.5
Dead cells %
83.3
Propidium Iodide

(b)

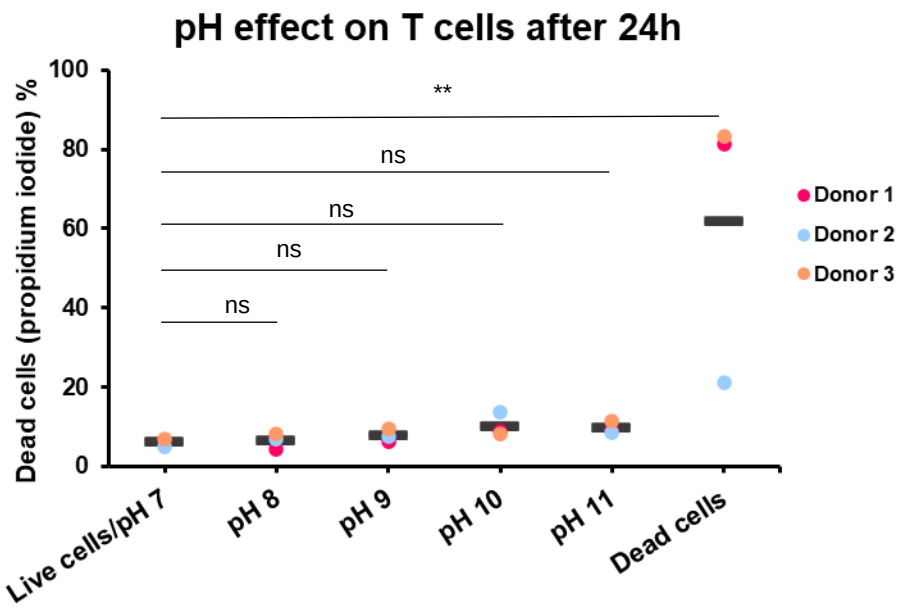

Figure 3.2: The effect of alkaline pH on T cell viability. Resting T cells were incubated for 24 hours (h) in media with alkaline pH, adjusted by 0.5M NaOH. Viability of cells were assessed by propidium iodide and flow cytometry, and compared against live and dead cells (heated for 10 min at 98°C). (**a**) Histogram plots from the flow cytometry presents T cell response to different pH from three donors. (**b**) A summary graph of all donors presents no significant effect of high pH on T cell viability. Statistical analyses was completed by One-way ANOVA with Dunnet's comparison test. Each condition were compared against live cells/pH 7. Data presented as mean+SD, n=3 from three biologically independent donors, $p<0.01$ **.

3.2.3 The impact of the mechanical properties of peptide hydrogel on T cells

The mechanical properties of peptide hydrogel were analysed by bulk oscillatory rheology. First, the optimum strain γ (%) required to be defined, which is the force required to yield a structural deformation of the matrix but still retaining the integrity of the material. If too much strain (%) is applied on the material, it will cause the inner structure to break down (in this case hydrogel's polymer destruction) and cause the material to permanently deform [340]. Thus, excessive strain γ (%) would result in an altered readouts on the material's stiffness level (i.e. storage modulus (Pa)).

Peptide hydrogels may be affected by the presence of serum proteins present in the culture medium, so previously established strain values on the material could not be used [311]. Different peptide hydrogel densities were used to determine the linear viscoelastic region for optimum strain, by using the amplitude sweep test with angular frequency set at 1 rad/s [311]. All hydrogels maintained their storage modulus under 1% strain (Fig. 3.3 (a)) until the increased strain value started to cause the mechanical disruption of the material. Also, the storage modulus values (G') confirmed the elastic (solid) properties of the peptide hydrogels as they were above their corresponding loss modulus values (G''). Further rheology studies on the peptide hydrogels were analysed with the optimum strain set at 1% with an angular frequency of 1 rad/s.

As previously mentioned, peptide hydrogels were formed with the T cell medium (TCM) containing serum. Peptide hydrogel formation involves electrostatic interaction between fibrous peptide networks, and the presence of serum proteins may interfere with the gelation process. The impact of serum protein interactions with the peptides was tested and compared over a range of peptide concentrations (Fig. 3.3 (b-d)). The stiffness level of the hydrogels was not markedly affected by the presence of TCM, and the storage modulus was sustained with no significant difference when compared to the RPMI containing hydrogels. Similar observations were noted across different peptide hydrogel densities, indicating that serum proteins had no marked effect upon gelation.

The storage modulus (G') of the peptide hydrogels was determined before encapsulating T cells to assess the impact of material stiffness on T cell function. The hydrogels were encapsulated with TCM only and analysed 24 hours after the onset of the gelation process, similar to the conditions that T cells would be exposed to in the fully formed gel. The results indicated the level of stiffness (G') increased with higher concentration of peptide gel; however there was only statistical significance between 6 mg/ml and 10 mg/mL hydrogels (Fig. 3.3 (e)). The average values of 6, 8 and 10 mg/ml were 283 Pa, 698 Pa and 871 Pa, respectively. There was some variation observed between experimental repeats as 6 mg/ml had a standard deviation (SD) of 123, which was still a significant difference to 10 mg/ml (SD±393). The most notable variation was present in 10 mg/ml rather than 6 mg/mL and 8 mg/mL hydrogels.

(a)

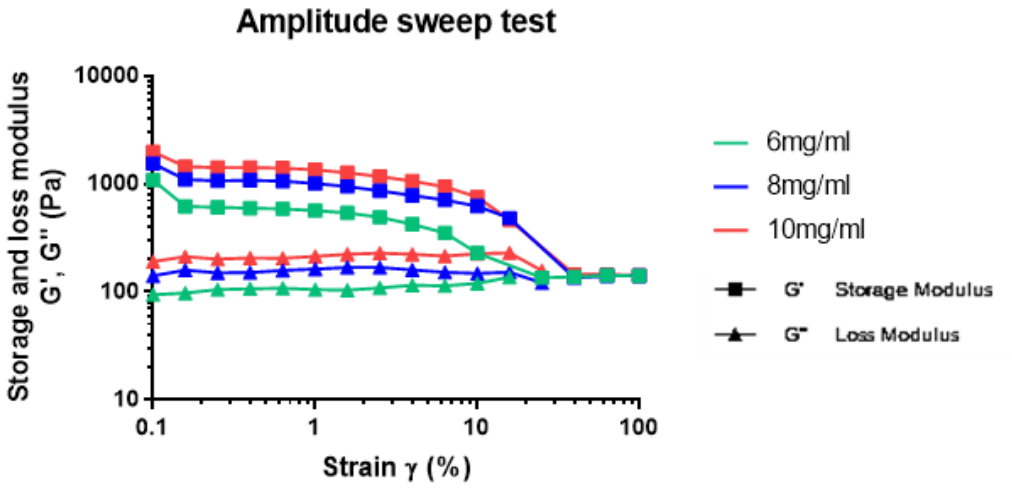
Amplitude sweep test
Storage and loss modulus G', G'' (Pa)
10000
1000
100
10
0.1
1
10
100
Strain γ (%)
6mg/ml
8mg/ml
10mg/ml
G' Storage Modulus
G'' Loss Modulus

(b)

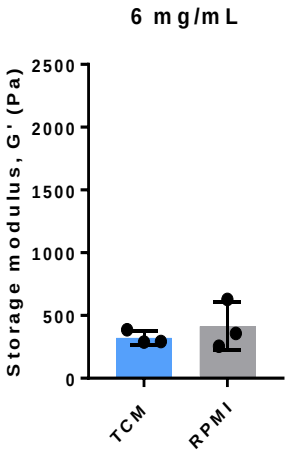
6 mg/mL
Storage modulus, G' (Pa)
2500
2000
1500
1000
500
0
TCM
RPMI

(c)

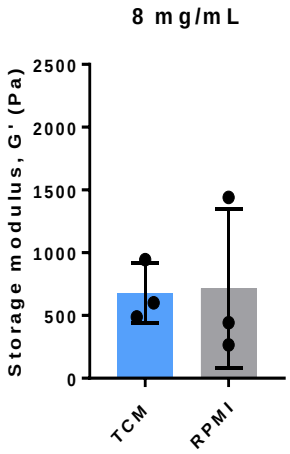
8 mg/mL
Storage modulus, G' (Pa)
2500
2000
1500
1000
500
0
TCM
RPMI

(d)

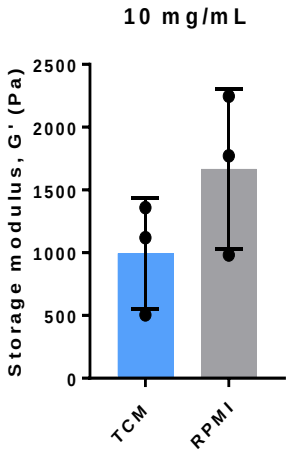
10 mg/mL
Storage modulus, G' (Pa)
2500
2000
1500
1000
500
0
TCM
RPMI

(e)

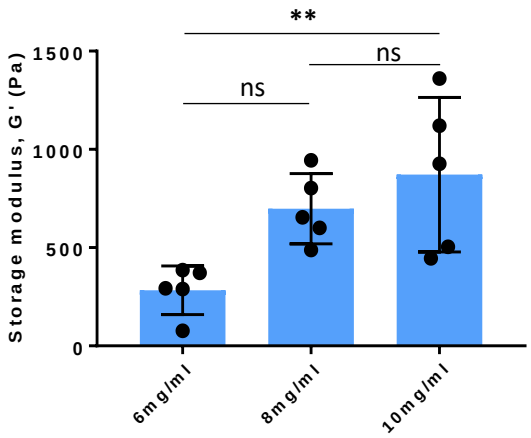
**
ns
ns
Storage modulus, G' (Pa)
1500
1000
500
0
6mg/ml
8mg/ml
10mg/ml

Figure 3.3: Mechanical properties of the peptide hydrogels. Different concentrations (mg/ml) of peptide hydrogel were prepared and tested after 24 hours of gelation process with bulk oscillatory rheology. **(a)** Amplitude sweep test was set up to determine linear viscoelastic regions of the peptide gels and strain γ (%). 6mg/mL **(b)**, 8mg/mL **(c)** and 10mg/mL **(d)** peptide hydrogels (n=3) were encapsulated with TCM (contained serum) and compared their stiffness level against the same density hydrogels but encapsulated with RPMI medium only. No significant difference between two medium were achieved. **(e)** Stiffness level (G') of the peptide hydrogels (n=5) significantly increased between 6 and 10 mg/mL only. Statistical analyses: unpaired t-test **(b-d)** and One-way ANOVA with Tukey's post-hoc **(e)**. Data presented as mean±SD, ** $p<0.01$.

3.2.4 Optimising peptide hydrogel density for T cell culture

Optimal peptide hydrogel density was investigated for T cell culture, since specific cell lines required specific hydrogel density and stiffness level [306, 311, 312]. In this experiment, activated and resting T cells were encapsulated in different peptide hydrogel densities to analyse the material's support on proliferating and quiescent state T cells. Control 2D cultures were established alongside 3D experiments at the same cell density and used to monitor T cells' behaviour under the standard laboratory conditions.

Resting and stimulated T cells were separately encapsulated at 0.5x106/mL in the peptide hydrogels and incubated for 5 days. Prior to the experiment, T cells were stimulated for 12 hours with PMA and Ionomycin; mitogen diffusion through the material was not tested. Microscopic images on day 1 showed relatively homogeneous distribution of encapsulated cells across the hydrogels (Fig. 3.4). On day 5, proliferating clusters of activated T cells were visible in all peptide hydrogels. The material itself was homogenous and without visible debris that could be confused for cells.

Cell viability in the hydrogels were assessed by Live/Dead staining, followed by quantifying data (cell viability %) based on the total number of cells divided by viable cells (green) only (Fig. 3.5. (a-b)). All hydrogels supported resting and stimulated T cell viability with no significant difference by day 1. However, on day 5, resting T cell viability was significantly reduced, in comparison to stimulated cells, across all the peptide hydrogels. Stimulated T cells maintained

their viability in all hydrogels, but it was more evident with the 6 mg/mL hydrogel, which supported more cell viability than other densities. The results were not significantly different, but the trend on increased peptide hydrogel density (above 6 mg/mL) and reduced stimulated T cell viability was evident (Fig. 3.5. (c)).

The final observation on T cell culture in the peptide hydrogel was based on the cell count by flow cytometry. On day 5, cells were released from the peptide hydrogel and the whole sample was processed for the total cell count (Fig. 3.6. (a). Due to poor resting T cell viability in the peptide hydrogels, no cells were detected in the 'cell gate' region based on 2D culture cells. However, stimulated T cells from the peptide hydrogel had occurred in the same dot plot region as the 2D culture cells, and by looking at all donors, T cells were more frequently detected from the 6 mg/mL peptide gel than 8 or 10 mg/mL. In addition, T cell count was significantly greater in 6mg/ml than any other hydrogels (Fig. 3.6. (b). All donor cells were biologically active as indicated in control – 2D cultures (Fig. 3.6. (c).

Overall, the optimal peptide gel density for T cell culture was 6 mg/mL because it supported better viability and expansion of proliferating cells.

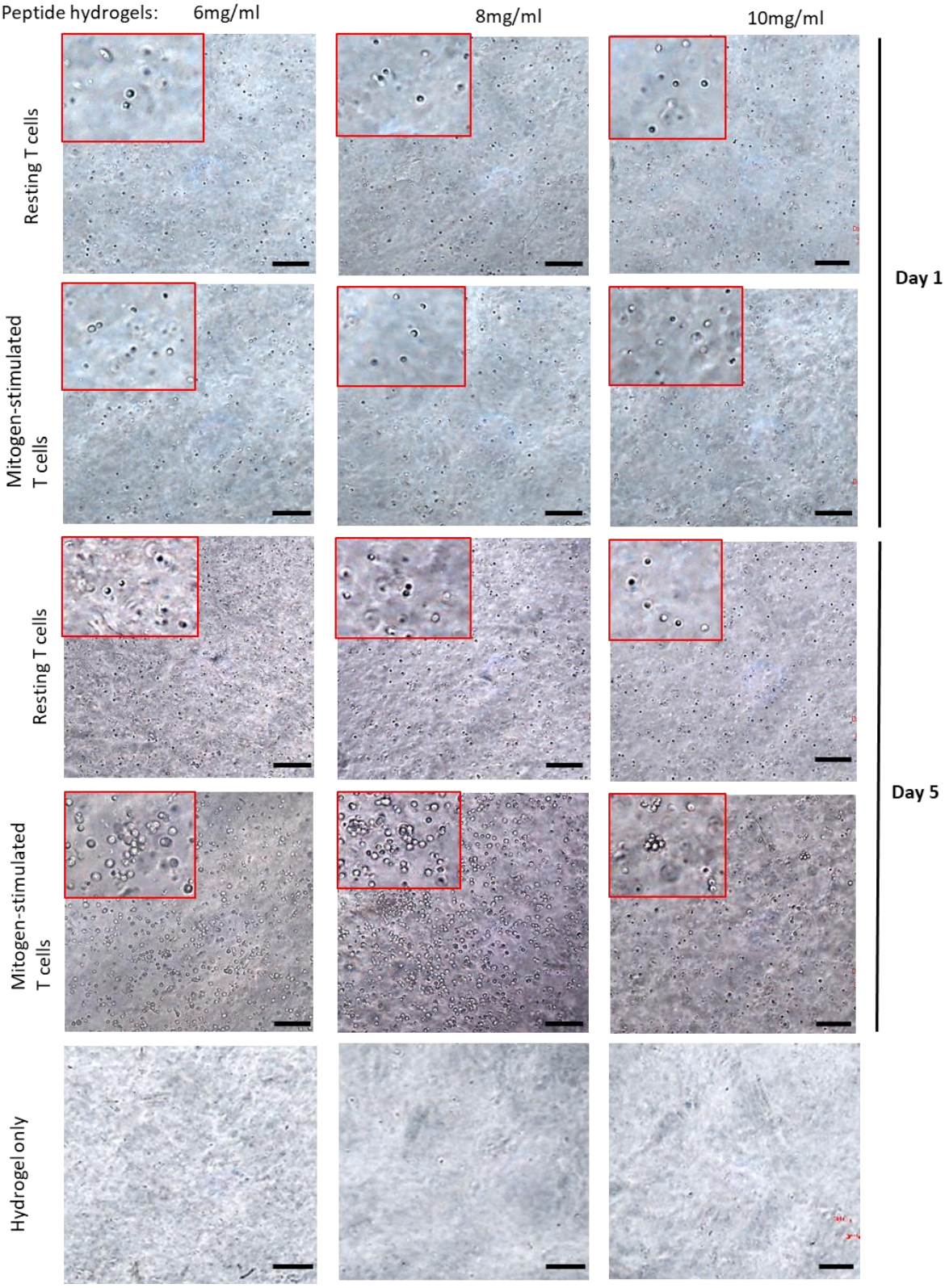

Figure 3.4: Assessing T cell culture encapsulated in the peptide hydrogel. Mitogen stimulated and resting T cells were encapsulated in the hydrogels with different densities (mg/ml) and incubated for 5 days. Brightfield microscopic images of T cells in the hydrogels show the individual cells by day 1, and proliferating clusters of stimulated T cells were visible by day 5. Hydrogels without cell culture provide a homogenous background. Cell culture images contain enlarged image sections (outlined red) to aid the visibility of cells. Images were collected with 10x magnification, scale bars set to **100µm**.

(a)

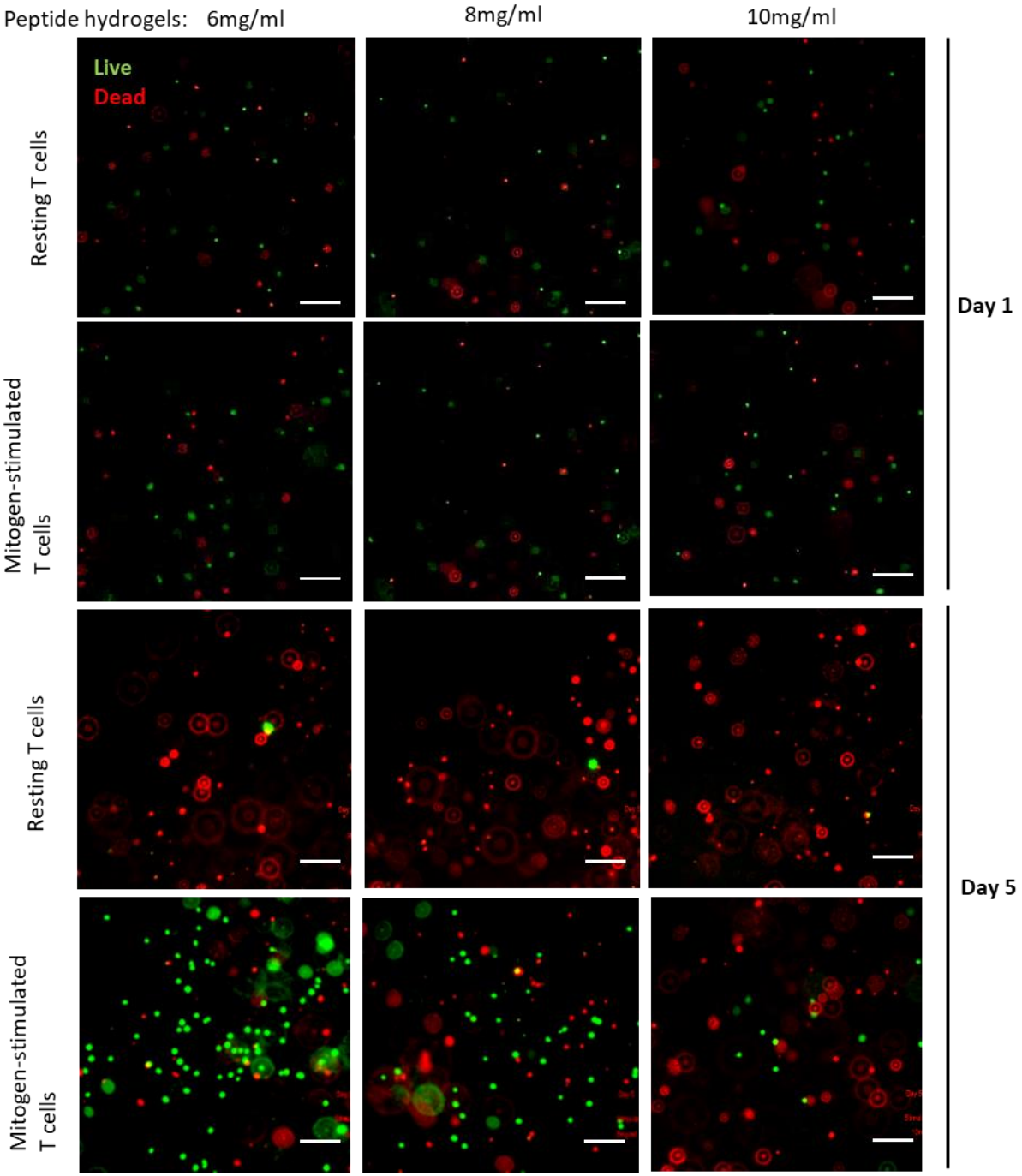
Peptide hydrogels: 6mg/ml
8mg/ml
10mg/ml
Live
Dead
Resting T cells
Mitogen-stimulated T cells
Resting T cells
Mitogen-stimulated T cells
Day 1
Day 5

(b)

(c)

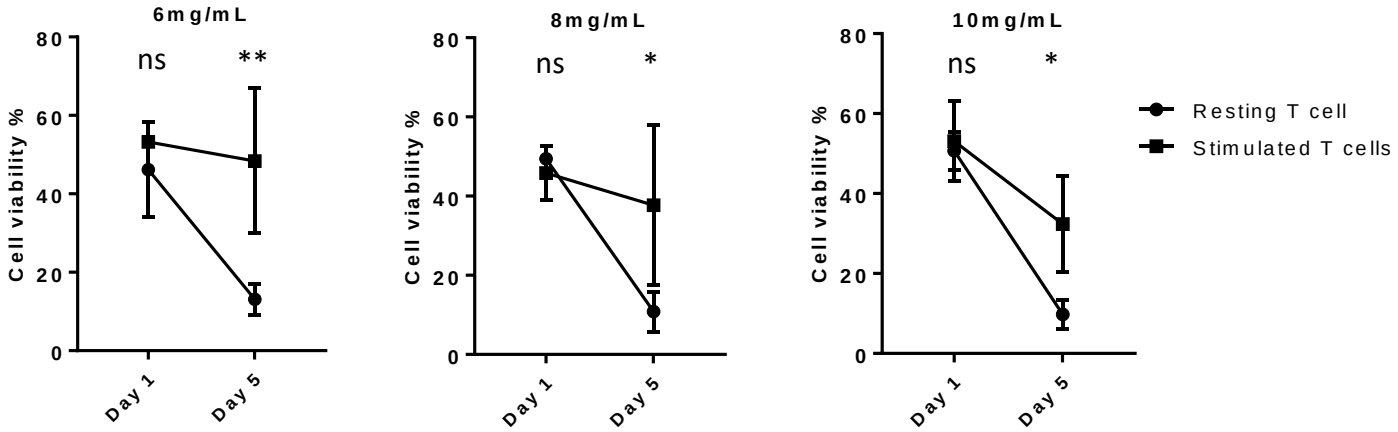
6mg/mL
8mg/mL
10mg/mL
Cell viability %
ns
**
*
Day 1
Day 5
Resting T cell
Stimulated T cells

(c)

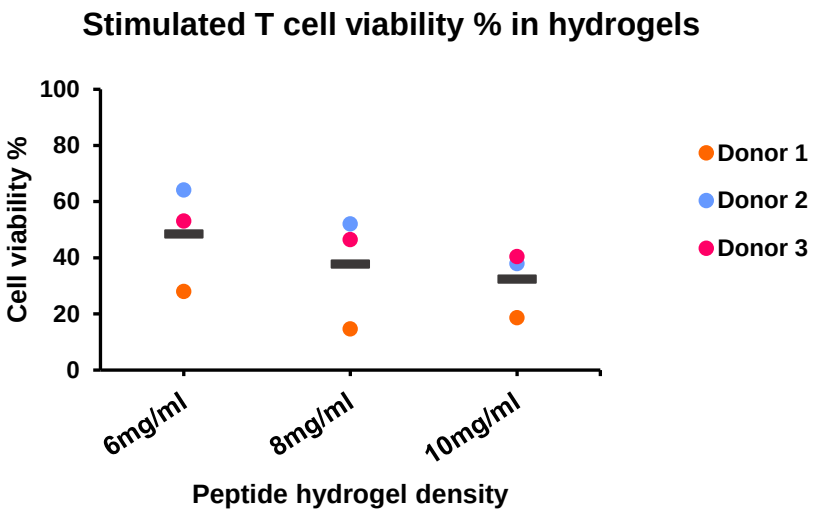

Figure 3.5: Analysing T cell viability (%) in the peptide hydrogel. Mitogen stimulated and resting T cells were encapsulated in the peptide hydrogels with different densities (mg/ml) and incubated for 5 days. **(a)** Fluorescence microscopy images of T cells stained with Live/Dead stain in the peptide gels on day 1 and 5. Cell viability % **(b)** was calculated from fluorescence images, produced from three biologically independent donors. **(c)** Summary graph of cell viability (%) of stimulated T cells across the hydrogels show no significant difference. Statistical significance was determined by with two-way ANOVA with Sidak's comparison test, mean±SD **(b),** and RM One-way ANOVA with Tukey's post-hoc and data presented with mean value only **(c).** Data composed from n=3, *p<0.05, **p<0.01. Scale bars set to **100µm**.

(a)

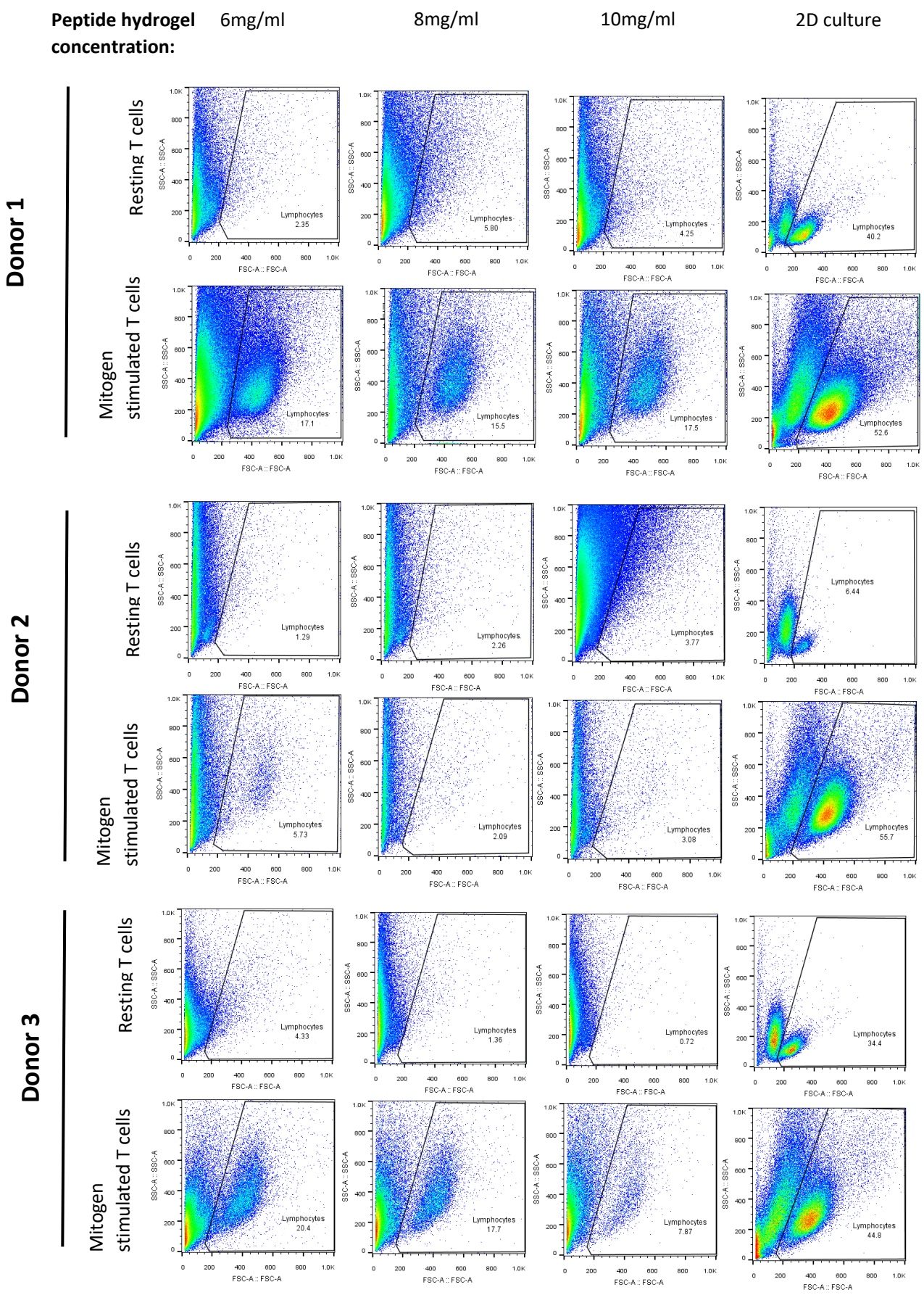
Peptide hydrogel concentration:
6mg/ml
8mg/ml
10mg/ml
2D culture
Donor 1
Resting T cells
Mitogen stimulated T cells
Donor 2
Resting T cells
Mitogen stimulated T cells
Donor 3
Resting T cells
Mitogen stimulated T cells
SSC-A :: SSC-A
FSC-A :: FSC-A
Lymphocytes 2.35
Lymphocytes 5.80
Lymphocytes 4.25
Lymphocytes 40.2
Lymphocytes 17.1
Lymphocytes 15.5
Lymphocytes 17.5
Lymphocytes 52.6
Lymphocytes 1.29
Lymphocytes 2.26
Lymphocytes 3.77
Lymphocytes 6.44
Lymphocytes 5.73
Lymphocytes 2.09
Lymphocytes 3.08
Lymphocytes 55.7
Lymphocytes 4.33
Lymphocytes 1.36
Lymphocytes 0.72
Lymphocytes 34.4
Lymphocytes 20.4
Lymphocytes 17.7
Lymphocytes 7.87
Lymphocytes 44.8

(a) continued

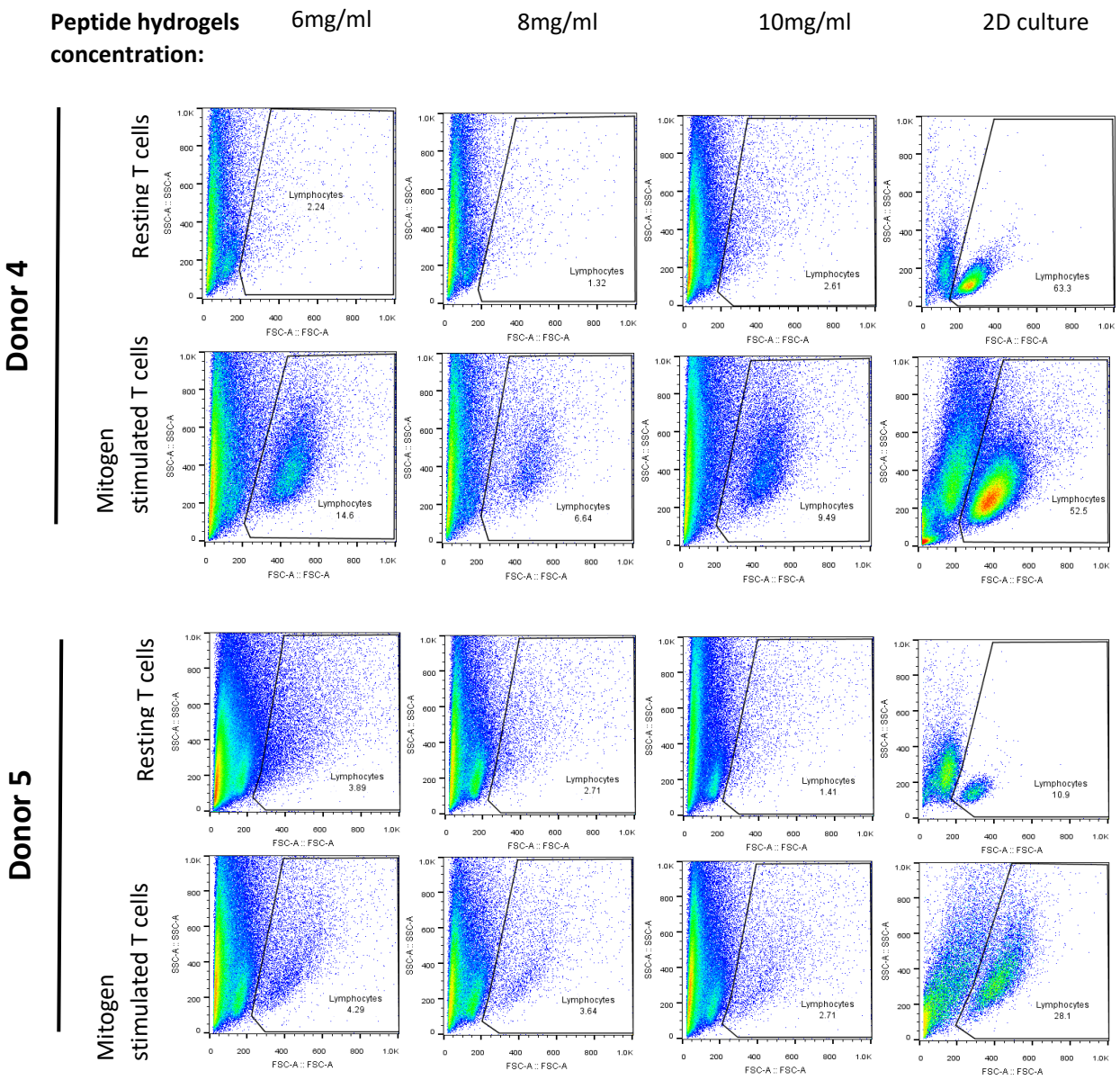

(b)

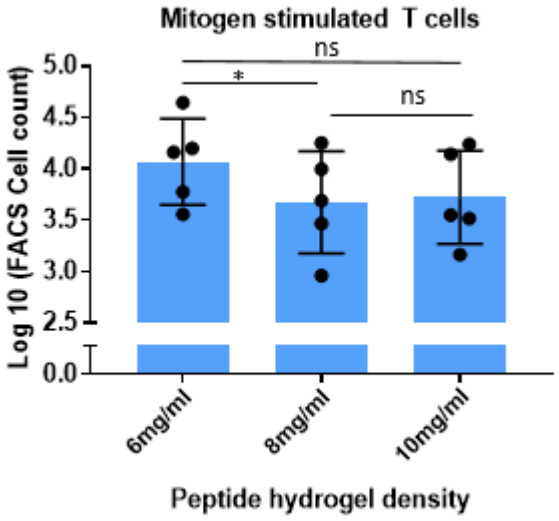

(c)

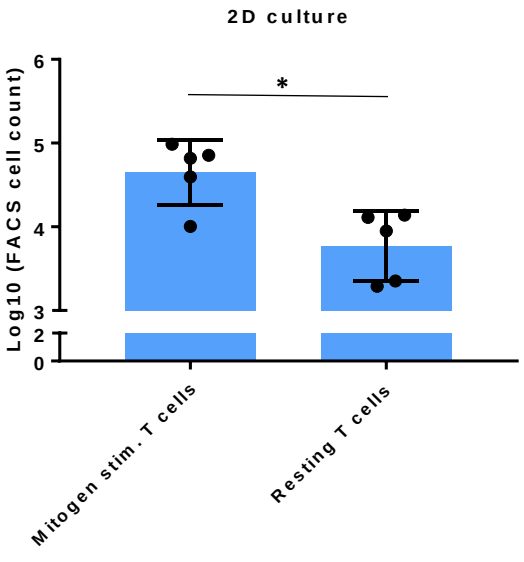

Figure 3.6: Determining the optimal peptide hydrogel density for T cell culture. Mitogen stimulated and resting T cells were encapsulated in the peptide hydrogels with different densities (mg/ml) and incubated for 5 days. On the final day, cells were released from the hydrogel by the TrypLe 1x solution and analysed by the flow cytometry. **(a)** Flow cytometry data presented individual donor's T cells released from the hydrogels on day 5. No population of resting T cells were detected by the flow cytometer, apart from stimulated cells. **(b)** Summary graph of stimulated T cell counts released from the peptide hydrogels, and 2D culture cells **(c)**. Cell counts from hydrogels were analysed by RM One-way ANOVA with Tukey's post-hoc **(b)**, where 2D culture was analysed with two-tail, paired t-test **(c)**, data presented as mean±SD, * $p<0.05$, n=5 from biologically independent donors.

3.2.5 Optimisation of resting T cell density in peptide hydrogel

Previous data has shown poor survival of resting T cells in the peptide hydrogels, irrespective of their density. It is important to retain a viable resting T cell population as future studies rely on T cell stimulation within hydrogels. It was hypothesised that increased resting T cell density could improve T cell survival and retain viable cells for a prolonged incubation period [341, 342].

Resting T cells were encapsulated at various cell densities in 6 mg/mL peptide hydrogels (Fig. 3.7). Over a 5day period, more viable cells were visible in hydrogels containing densities above $1.5x10^6$ cell/mL. Gradual cell death was more evident with T cells seeded lower than $1.5x10^6$ cells/mL in the peptide hydrogels (Fig. 3.7. (a-b)). The effect of increased cell density on the structure of peptide hydrogels was also observed on the same days as the cell viability assay (Fig. 3.7. (c-d)). All cell densities changed the size of the peptide gels by day 5, but most of evident structural deformation was with lower cell densities ($<1.5x10^6$ cells/mL). However, media change could be a contributing factor as well, since hydrogel-only samples (no cells) did not retain their original size from day 1. In conclusion, resting T cell viability can be improved by increased cell density without impairing the material's structure. Resting T cells at $1.5x10^6$ cells/mL in 6mg/ml peptide gel was used for future experiments.

(a)

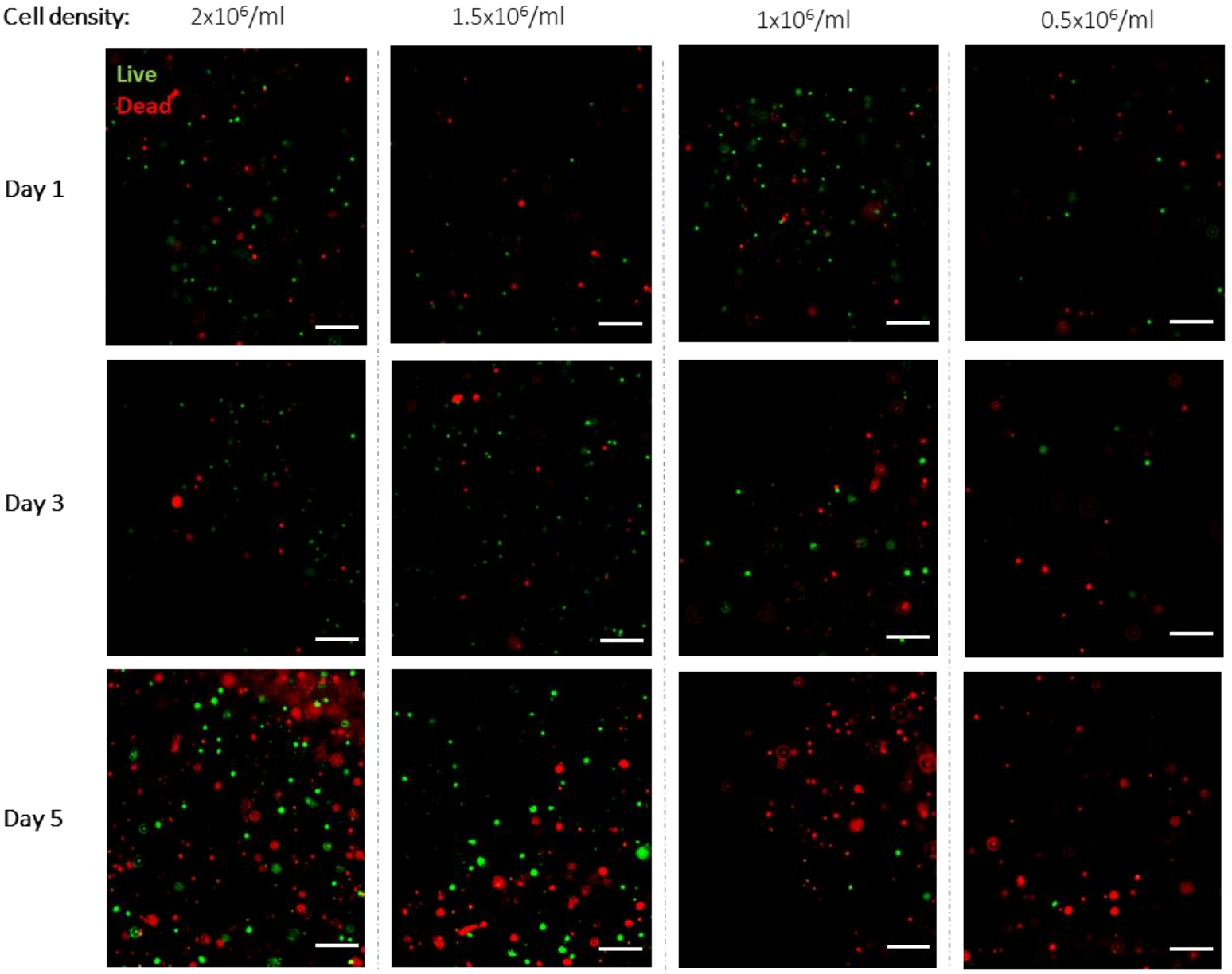
Cell density:
2x10⁶/ml
1.5x10⁶/ml
1x10⁶/ml
0.5x10⁶/ml
Live
Dead
Day 1
Day 3
Day 5

(b)

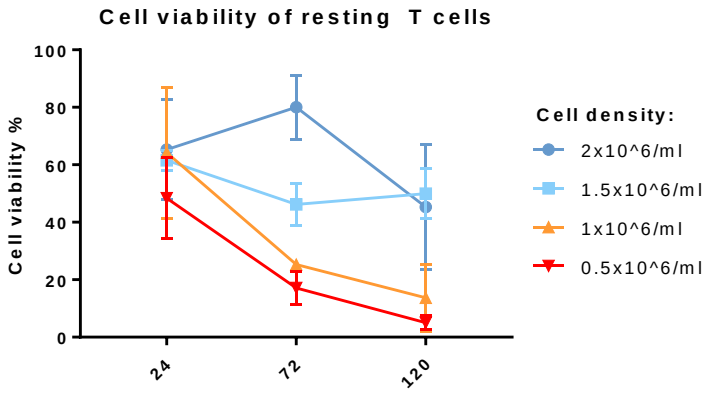
Cell viability of resting T cells
Cell viability %
100
80
60
40
20
0
24
72
120
Time (hours)
Cell density:
2x10^6/ml
1.5x10^6/ml
1x10^6/ml
0.5x10^6/ml

(c)

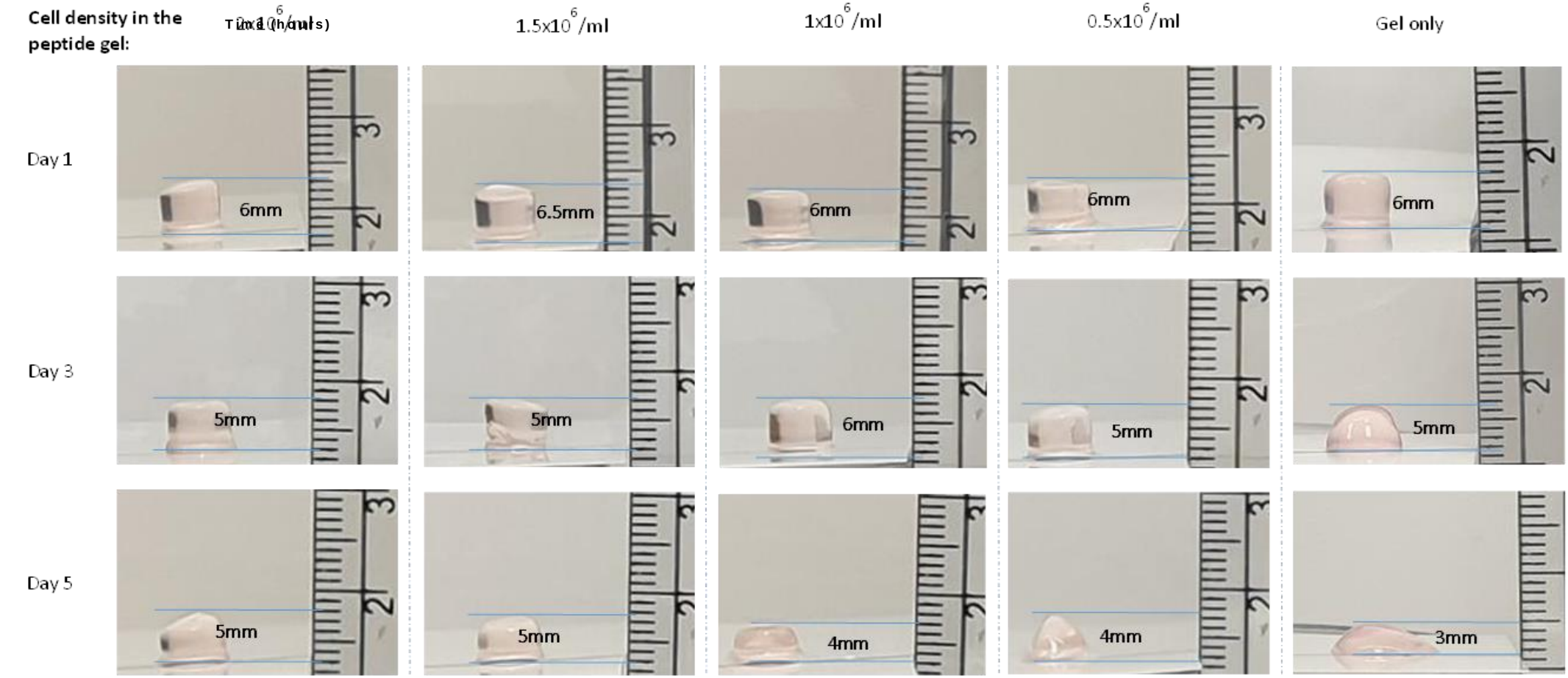
Cell density in the peptide gel:
2x10^6/ml
1.5x10^6/ml
1x10^6/ml
0.5x10^6/ml
Gel only
Day 1
Day 3
Day 5
6mm
6.5mm
6mm
6mm
6mm
5mm
5mm
6mm
5mm
5mm
5mm
5mm
4mm
4mm
3mm

(d)

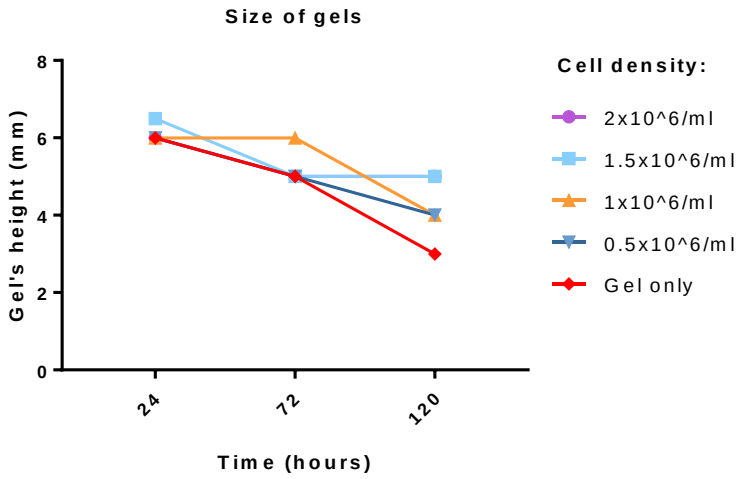

Figure 3.7: Determining optimal resting T cell density in 6mg/mL peptide hydrogel. Resting T cells at various cell densities were encapsulated in 6mg/mL peptide hydrogels and incubated for 5 days. On the final day, cell's viability was observed by Live/Dead assay and fluorescence microscope. **(a)** Fluorescent images of resting T cells indicate live and dead cells in the peptide hydrogel. **(b)** From three different regions of the hydrogel, images were collected to calculate cell viability %. Resting T cells viability % was improved at high cell densities (from $1.5x10^6$ cells/ml) in the material. **(c** and **d)** Images and measurements of the peptide hydrogel structural change. Peptide gels retained their structure even after encapsulating high density of cells. Scale bars are set at **100µm**, data presented as mean±SD, n=1.

3.2.6 Coating polystyrene particles with stimulating T cell antibodies (artificial APC) and testing against alkaline conditions

Classical T cell activation depends on the APC (e.g. dendritic cells) but these are frequently replaced with stimulating antibodies coated on to polystyrene beads or culture plates for 2D culture studies [328, 343, 344]. In this study, polystyrene particles (size 10μm) were coated with CD3 and CD28 antibodies to induce full T cell activation, and they are defined as artificial APC. There was a concern that the alkaline conditions of the precursor hydrogel could affect the biological activity of antibodies during the encapsulation process. Powdered hydrogel is dissolved at high pH (> pH 9), by adding NaOH, which prevents the interaction between negatively and positively charged amino acids of FEFEFKFK. At this stage, it allows a better content mixing within the material. Hydrogel gelation is achieved by medium exchange (which contains HEPES buffer, sodium bicarbonate) and the presence of CO_2 gas neutralises excess NaOH and reduces the alkaline to neutral pH 7 [345, 346]. Alkaline pH of the precursor hydrogel may well have an adverse effect on any antibodies, resulting in a failure to stimulate the T cells. We therefore tested the effect of high pH on antibodies targeting CD3 and CD28 activity.

First, by using a passive adsorption method, polystyrene particles were coated with 10 μg/ml of CD3 and 10 μg/ml of CD28 antibodies. The next batch contained higher concentration of stimulatory molecules, where they have been coated with 30 μg/ml of CD3 and CD28 antibodies [317]. Eventually, two batches of

artificial APC were prepared with high or low concentrations of stimuli, to indicate whether they could withstand alkaline pH and remain functional. The presence of antibodies on the particles were detected by using secondary anti-mouse antibodies and flow cytometry. The percentage of coated particles with antibodies were analysed by using a gating strategy set on the particles only (0 µg/mL of antibodies) (Fig. 3.7. (a)). 93.4% of particles were positive for antibodies coated with 10 µg/mL, whereas 30 µg/mL achieved up to 97.8% (Fig. 3.7. (b)). In addition, the MFI value of 10 µg/mL concentration (MFI: 54.9) was lower than the particles coated with 30µg/ml (MFI: 78.5). It is evident that by increased antibodies' concentration, the fluorescence intensity increases too, indicating more bound antibodies on the particle's surface. Particles (0 µg/mL) were only coated with a blocking buffer containing 0.05% of FCS serum in PBS.

The alkaline pH effect on the antibodies was tested with the same method used to indicate the effect on T cells' viability (Fig. 3.2). In this instance, after the exposure to an alkaline medium, the artificial APC were collected, washed and incubated with T cells for 4 days in 2D culture. On day 3 (Fig. 3.7. (c)), the proliferated blasts of T cells were visible after the stimulation with 10µg/mL and 30µg/mL artificial APC in comparison to 0 µg/mL particle control. It was evident that 30 µg/mL artificial APC caused greater proliferating blasts than 10 µg/mL coated beads. On day 4, the observation was confirmed by 3H-Thymidine assay confirming greater T cell proliferation response to 30µg/mL than 10µg/mL coated particles (Fig. 3.7. (d)). In regards to pH effect on antibodies, there was no noticeable change on T cell proliferation to the beads being exposed to

alkaline pH (Fig. 3.7. (d)). The level of T cell response was close to the particles exposed to neutral pH 7, which indicates the alkaline pH (above pH 7) did not affect the biological activity of antibodies, and artificial APC will retain their function in the hydrogel.

(a)

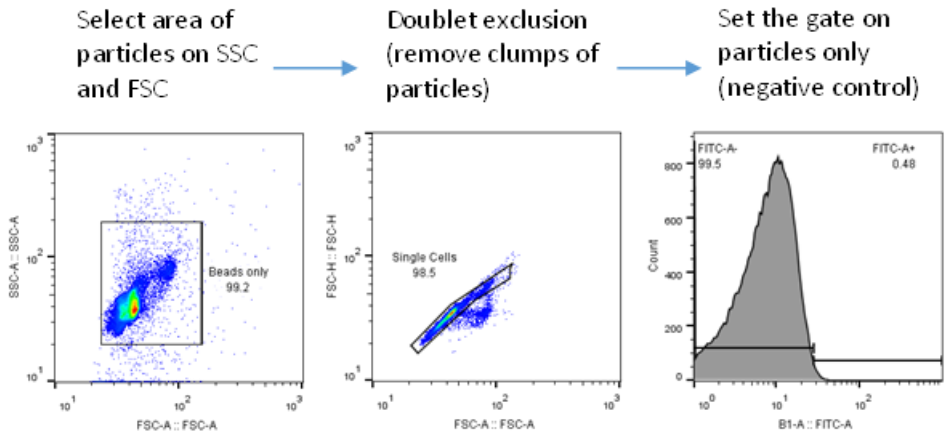
Select area of particles on SSC and FSC
Doublet exclusion (remove clumps of particles)
Set the gate on particles only (negative control)
SSC-A :: SSC-A
FSC-A :: FSC-A
Beads only
99.2
FSC-H :: FSC-H
Single Cells
98.5
FITC-A-
99.5
FITC-A+
0.48
Count
B1-A :: FITC-A

(b)

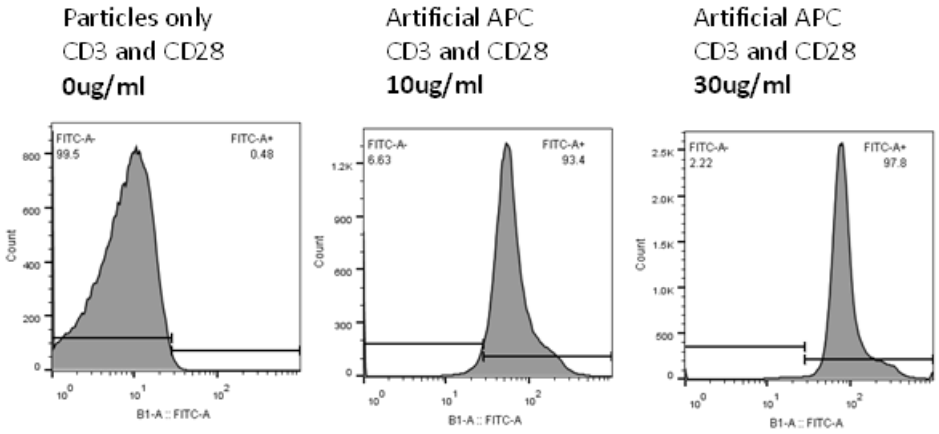
Particles only
CD3 and CD28
0ug/ml
Artificial APC
CD3 and CD28
10ug/ml
Artificial APC
CD3 and CD28
30ug/ml
FITC-A-
99.5
FITC-A+
0.48
FITC-A-
6.63
FITC-A+
93.4
FITC-A-
2.22
FITC-A+
97.8
Count
B1-A :: FITC-A

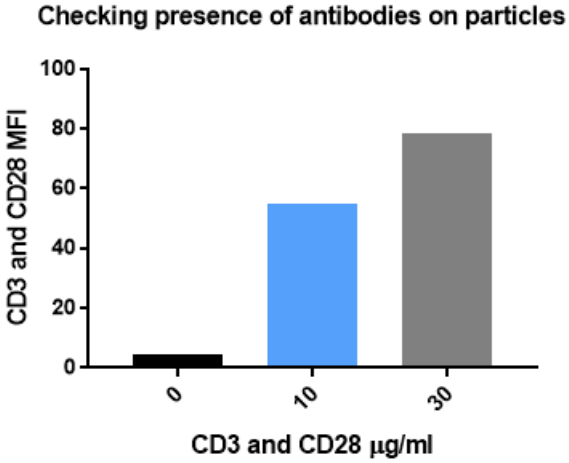
Checking presence of antibodies on particles
CD3 and CD28 MFI
100
80
60
40
20
0
0
10
30
CD3 and CD28 µg/ml

(c)

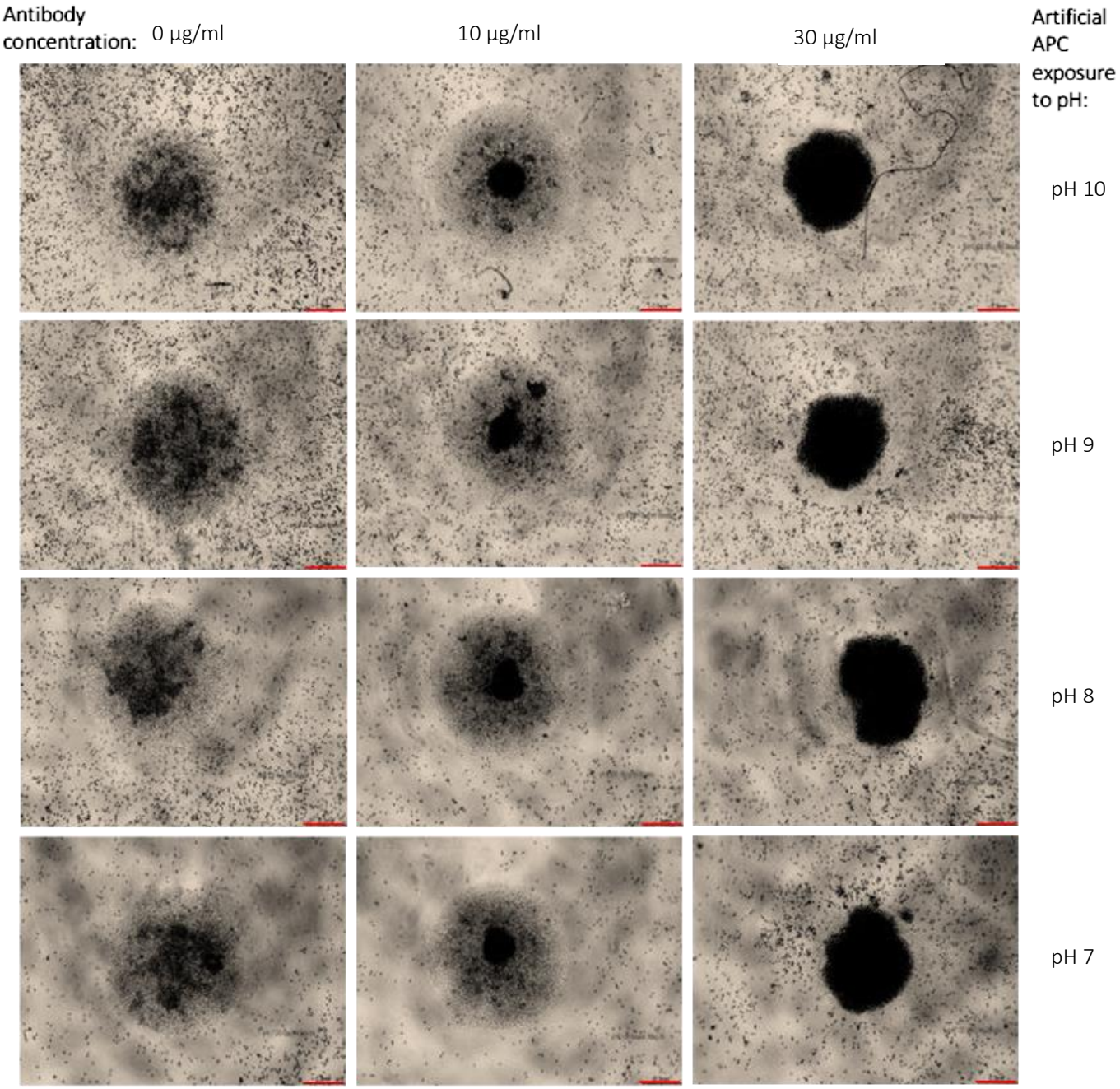
Antibody concentration:
0 µg/ml
10 µg/ml
30 µg/ml
Artificial APC exposure to pH:
pH 10
pH 9
pH 8
pH 7

(d)

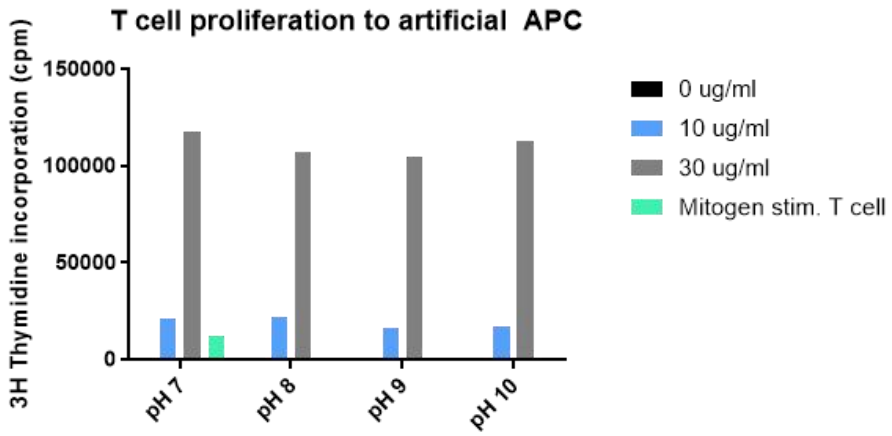
T cell proliferation to artificial APC
3H Thymidine incorporation (cpm)
150000
100000
50000
0
pH 7
pH 8
pH 9
pH 10
0 ug/ml
10 ug/ml
30 ug/ml
Mitogen stim. T cell

Figure 3.7: The effect of alkaline pH on artificial APC. Particles were coated with different concentrations of CD3 and CD28 antibodies (artificial APC) and incubated for 24 hours in the media buffered to different alkaline pH with 0.5 NaOH. After 24 hours the artificial APC were washed and incubated with T cells at 2:1 ratio (APC:T cells) for 4 days. **(a)** The gating strategy for detecting the presence of antibodies on the polystyrene particles by the flow cytometer. **(b)** The % of coated particles were detected by gate set on blank (0µg/ml) sample, and the antibodies' levels were compared with MFI values. **(c)** Light microscopy images of cells proliferating clusters responding to artificial APC on day 3. **(d)** 3H Thymidine incorporation assay were used to analyse T cell stimulation by artificial APC. On day 3, 3H-Thymidine (2uCi/ml) were added and incubated for 18 hours. Thymidine incorporation was measured by scintillation counting. **MFI = median fluorescence intensity**, scale bars were set at **300µm**, n=1 experiment with no repeats.

3.2.7. Modifying T cell response with different co-stimulation signals on artificial APC

Typical T cell activation requires Signal 1 (T cell receptor, TCR), Signal 2 (co-stimulation) and Signal 3 (cytokines) to induce full stimulation and differentiation into effector cells. There is a large repertoire of costimulatory molecules that can allow for specific T cell functions under different environmental conditions [105]. Costimulation molecule expression depends on the type of stimulus and tissue environment where the T cells are activated [347]. It is hypothesised that peptide hydrogel permits T cell response to distinctive costimulatory molecules and modulates T cell response.

New artificial APC were formed with different co-stimulatory signals: CD28 and CD55. Costimulation requires CD3 (Signal 1) presence to amplify a T cell response. However, CD3 alone at high concentration (e.g. plate bound antibody above 3 μg/mL) can induce a T cell response and reduce the chance of detecting a co-stimulation effect, thus previously formed APC could not be used for this study due to high CD3 concentration (results 3.2.6) [348]. Artificial APC were first optimised with CD3 antibody to induce a sub-optimal T cell proliferation response. Enhanced responses were then observed with increasing concentrations of costimulatory signals (anti-CD3 and anti-CD28). Artificial APC were tested first under 2D culture settings, to indicate the functional capacity of the stimulus on cells.

T cell proliferation was analysed by CFSE dye dilution and measured by flow cytometry. T cells labelled by CFSE dye will undergo cell division upon stimulation and dilute the fluorescent dye into the daughter cells, which also reduces the CFSE fluorescent intensity [319]. Prior to the experiment, labelled CFSE cells' staining quality and uniformity were checked against the unstained cells (Fig. 3.8. (a)). Proliferation of T cells was reported as divided cells %, where the gate was first set on the resting (unstimulated) T cells (Fig. 3.8. (b)). In some experiments division index is reported as well, which indicates the average number of divisions the cell has gone through, taking into account stimulated and resting T cells (Fig. 3.8. (c-d)).

Polystyrene particles were coated with different (0-30 μg/mL) concentrations of CD3 antibody and analysed by anti-mouse secondary antibody and flow cytometry (Fig. 3.9. (a)). The MFI values increased up to 3.3 μg/mL CD3 concentration, followed by a decrease in higher concentrations. This represents the hook effect more than an actual negative result of antibodies coating the particle. The hook effect is a common problem in immunoassays where high concentration of analyte (in this case CD3) saturates secondary antibodies for flow cytometry and gives a false negative result [349]. CD3 coated particles were incubated with T cells for 5 days in the 2D culture. T cells responded to the various CD3 concentrations, with maximum proliferation response achieved at 3.3 μg/mL and sub-optimal response at 1.1 μg/ml (one donor representation, Fig. 3.9. (b)). CFSE precursor frequency % and division index confirms the

analysis from all three donors (Fig. 3.9. (c)). A CD3 concentration of 1.1μg/ml was selected for artificial APC preparation with costimulating antibodies.

Particles coated with CD28 and CD55 show increasing MFI values alongside the given concentrations (Fig. 3.10. (a-b)). However, by reaching the maximum concentration, both costimulating antibodies' MFI values decreased, which demonstrates the hook effect again. CFSE-labelled T cells were cultured with Ab-particles at a ratio of 2:1 (Ab-particle: cells) for 5 days. One representative donor (Fig. 3.10. (c)) indicated T cell response to the given artificial APC coated with CD28 and CD55 antibodies. CFSE % of divided cells indicated a maximal response was reached by 3.3 μg/ml of CD55 and 10 μg/ml of CD28 (Fig. 3.10. (d)). However, the response from CD28 at 3.3 μg/ml was not far from the maximal (only 5% difference) and therefore, for the consistency of artificial APC preparation, it was decided to coat particles with 3.3 of μg/ml of CD55 and CD28 antibodies. Though, the following analysis of division index (Fig. 3.10. (d)) contradicted the choice of 3.3 μg/ml of CD28 antibodies, as the maximal T cell response was achieved by 10 μg/ml. This also indicated that interpretation of CFSE % of divided cells data needs to be taken with caution.

In conclusion, artificial APC were formed with optimised CD3, CD28 and CD55 antibody concentrations to study the co-stimulation effect on T cells in the peptide hydrogels.

(a)

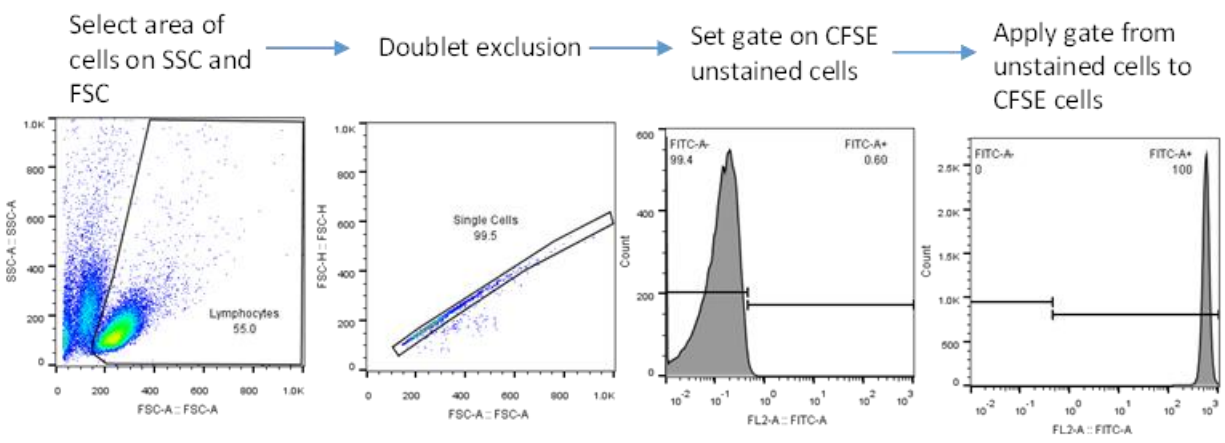
Select area of cells on SSC and FSC
Doublet exclusion
Set gate on CFSE unstained cells
Apply gate from unstained cells to CFSE cells
Lymphocytes
55.0
Single Cells
99.5
FITC-A-
99.4
FITC-A+
0.60
FITC-A-
0
FITC-A+
100
SSC-A :: SSC-A
FSC-A :: FSC-A
FSC-H :: FSC-H
Count
FL2-A :: FITC-A

(b)

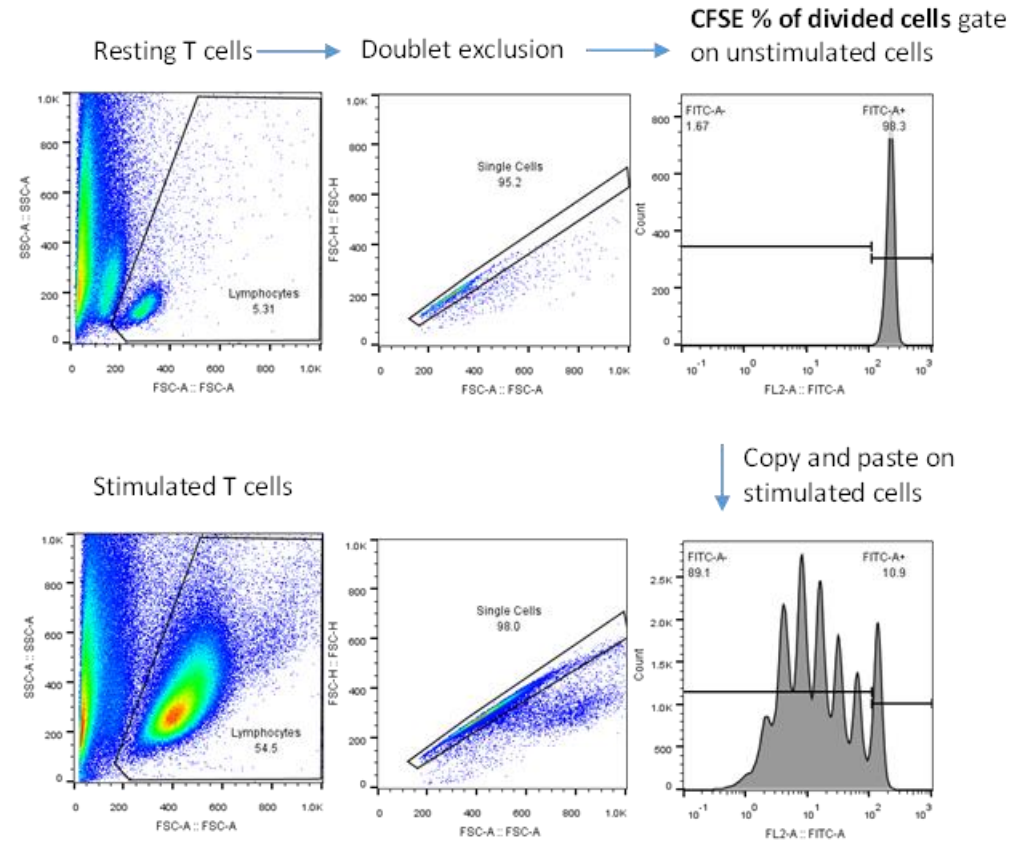
Resting T cells
Doublet exclusion
CFSE % of divided cells gate on unstimulated cells
Lymphocytes
5.31
Single Cells
95.2
FITC-A-
1.67
FITC-A+
98.3
Stimulated T cells
Copy and paste on stimulated cells
Lymphocytes
54.5
Single Cells
98.0
FITC-A-
89.1
FITC-A+
10.9
SSC-A :: SSC-A
FSC-A :: FSC-A
FSC-H :: FSC-H
Count
FL2-A :: FITC-A

(c) **Division index analysis (open Histogram FITC-A (CFSE) under 'Cell proliferation analysis' tool)**

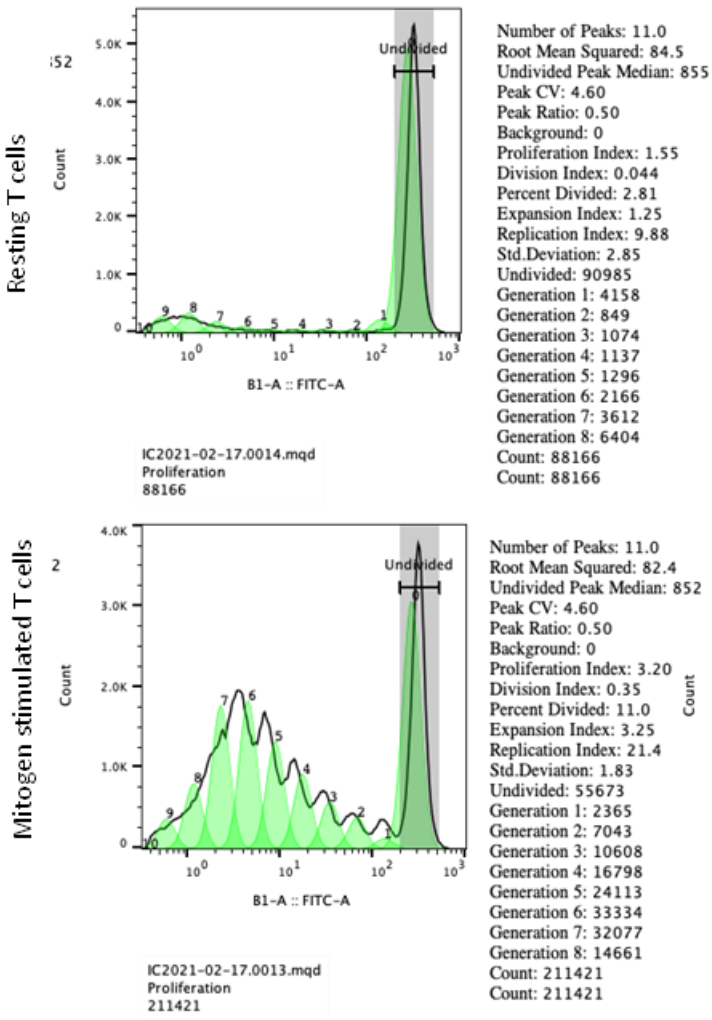

Process of 'Cell proliferation analyses' tool on FlowJo 10.8 data analyses:

Indicated 'Undivided' population on 'Resting T cells' sample

↓

Copy and paste the 'Undivided' gate on 'Positive control – mitogen stimulated T cells'

↓

Fitting computer data to the raw data: count the total number of peaks and add 1+ peak count, adjust coefficient of variance (CV) between 4-7% and peak ratio between divisions (0.4-0.5)

↓

Check the values of **root mean squared (RMS)** value (the lower the value the more agreement between software and raw data)

↓

Apply the same values (i.e. CV%, peak ratio) across the rest of samples

(d)

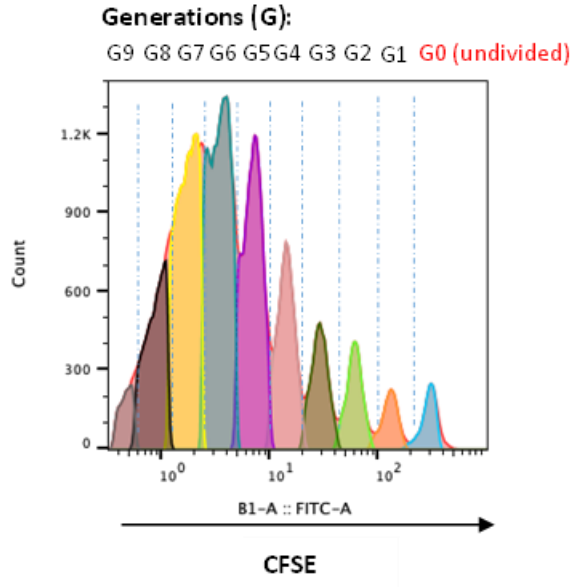

Division index: average cell division number per cell from the whole culture (includes divided and un-divided cells)

By using FACS cell counts (events), **Division index** is calculated:

1) Total nr. of cells at **start of culture** = G0 + (G1/2) + (G2/2) ...
2) Total nr. of **division** = (G1/2)*1 + (G2/2)*2 + (G3/2)*3 ...
3) **Division index** = Total nr. of division / total nr. of cells at start of culture

Figure 3.8: Analysing T cell proliferation with Cell Trace CFSE and flow cytometry. T cell proliferation is assessed with Cell Trace CFSE dye and flow cytometry. **(a)** Prior to the experiment T cells were stained with 1μM CFSE dye, washed and analysed for labelling efficiency against unstained cells. **(b)** Gating strategy for analysing the proliferating T cells, which reports divided cells % by using a negative control gate set on the resting T cells. **(c)** Analysis method of using the 'Proliferation tool' in FlowJo v10.8.1 software to obtain statistical analysis on T cell proliferation. **(d)** Division index (DI) was used to report T cell responses in the peptide gel and the graph explains how the DI value is obtained.

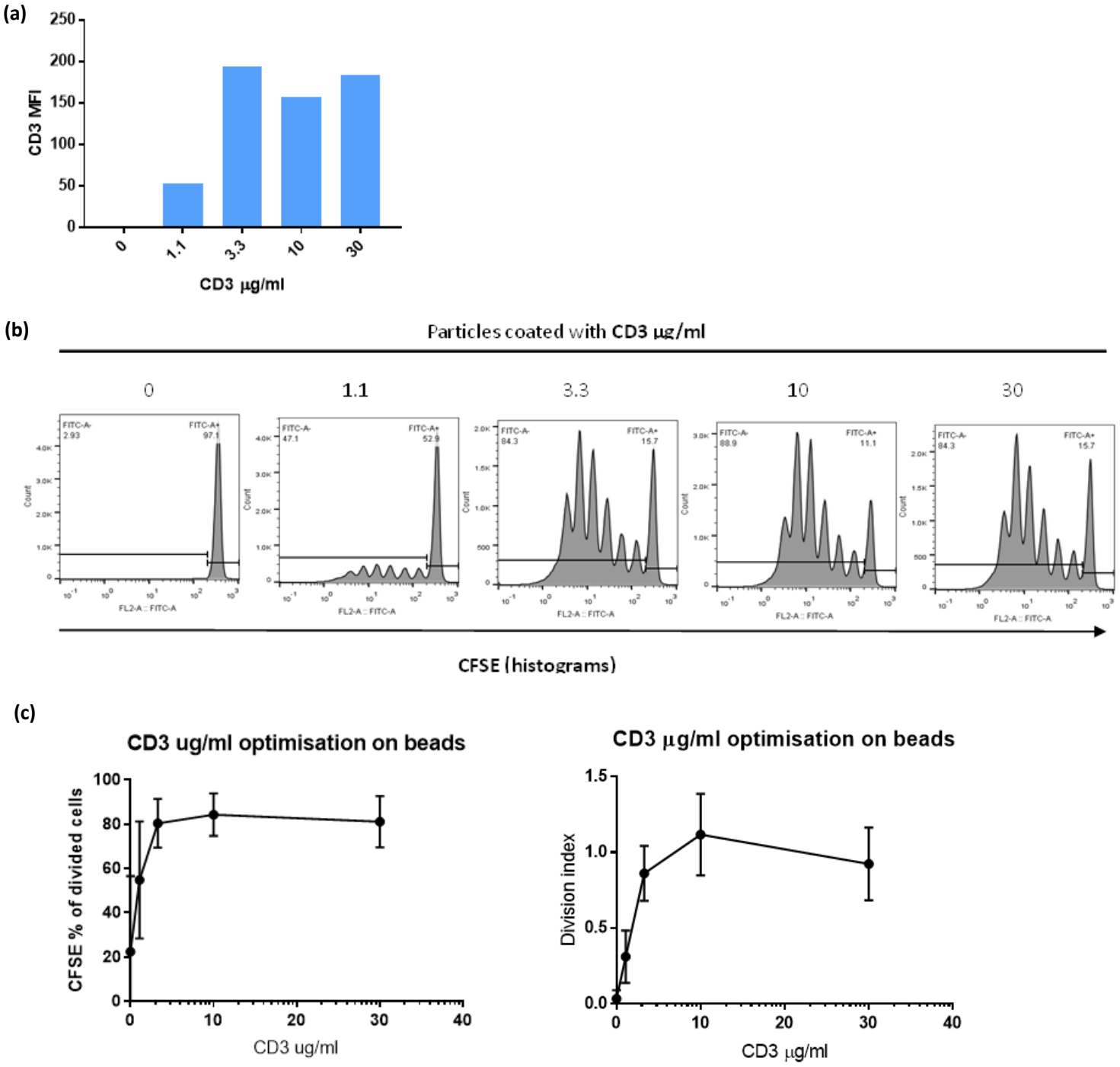

Figure 3.9: Optimisation of CD3 antibody for sub-optimal T cell proliferation. Polystyrene particles were coated with different concentrations of CD3 antibody (µg/mL), and cultured with CFSE labelled T cells at 2:1 ratio (APC:T cells) for 5 days. **(a)** MFI values obtained by flow cytometry, present particles coated with CD3 antibodies at various concentration. **(b)** Histograms from one of the donors represents T cell proliferation in response to changing CD3 concentrations. **(c)** Summary graph from three donors presents CFSE % of divided cells and division index values. Data presents mean±SD, n=3 biologically independent donors.

(a)

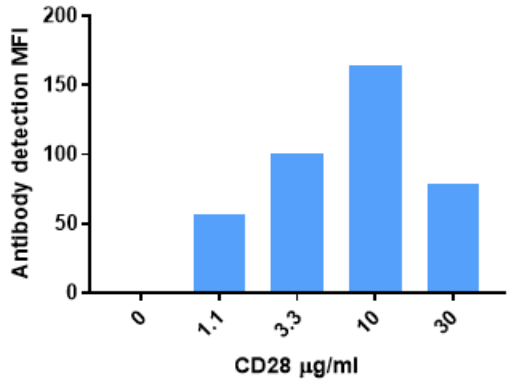

(b)

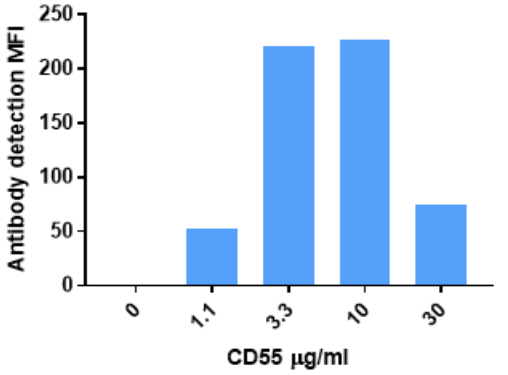

(c)

Co-stimulation of T cells with beads coated with **1 µg/ml of anti-CD3** and a range of concentrations of **anti-CD28** and **anti-CD55**

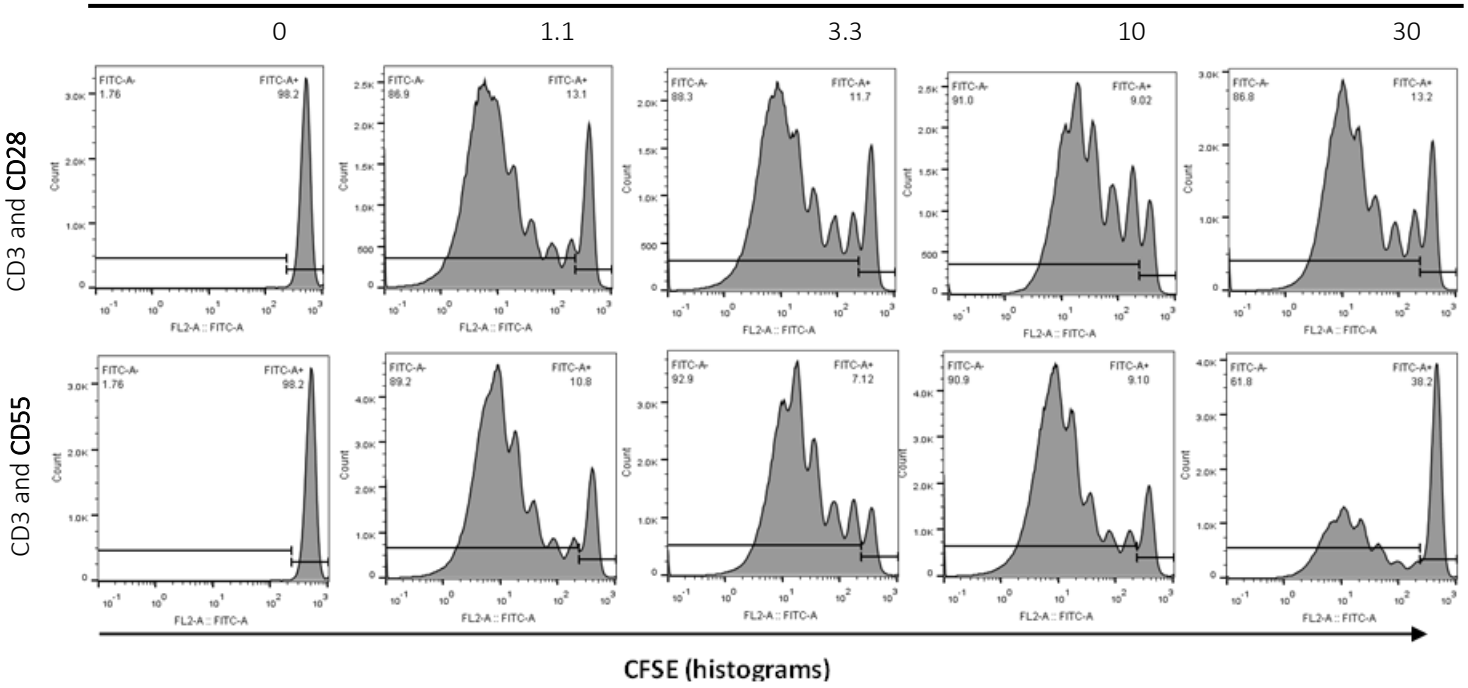

(d)

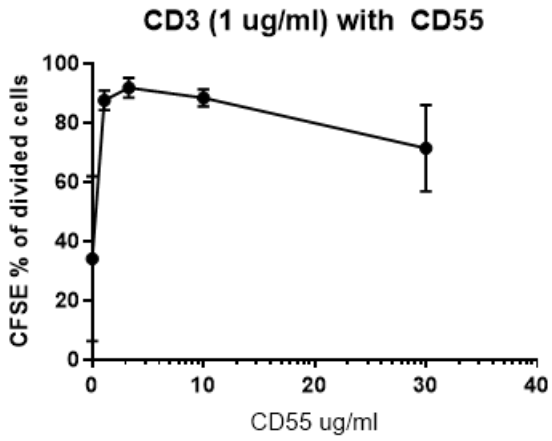

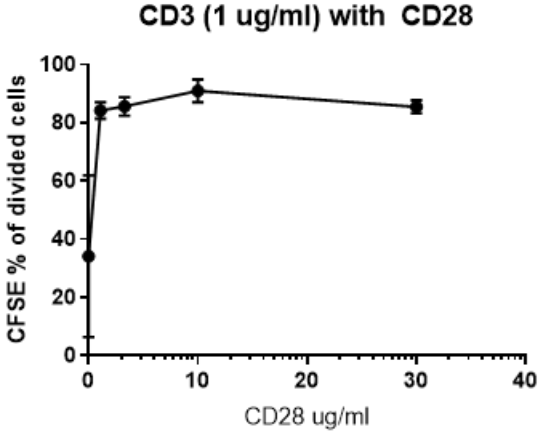

(e)

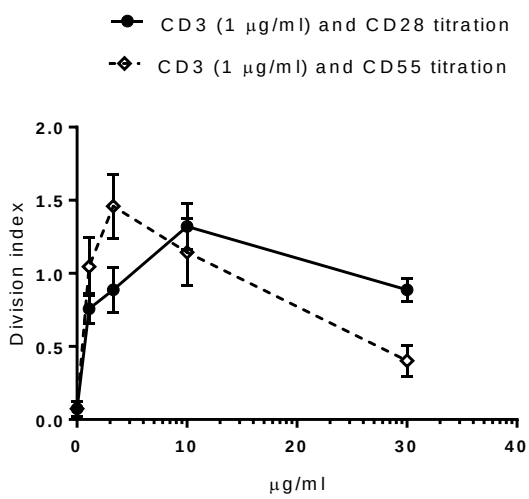

Figure 3.10: Optimisation of CD28 and CD55 antibodies with constant CD3 1µg/ml to induce maximal T cell proliferation response. Polystyrene particles were coated with different concentrations of CD28 and CD55 antibodies in the presence of 1 µg/ml CD3 antibody. Artificial APCs were tested in 2D cultures with CFSE labelled T cells at a ratio of 2:1, and the data was collected on day 5 by flow cytometry. **(a** and **b)** MFI values present particles coated with various CD28 and CD55 antibody concentrations **(c)** Histograms present one donor's T cells proliferation response to artificial APC with various co-stimulating antibody concentrations. **(d** and **e)** Summary graphs of CFSE % of divided cells and division index presented from all three biologically different donors. Data presented here with mean±SD, n=3 biological independent donors.

3.2.8. Modifying T cell function with different co-stimulating signals in the peptide hydrogels

After production of new artificial APC carrying CD3 with CD55 or CD28 costimulatory molecules, T cells (labelled with CFSE) and artificial APCs were encapsulated in the peptide hydrogels. The purpose of this experiment was to analyse peptide hydrogels' ability to support T cell activation and proliferation in presence of different stimuli.

Based on literature, T cells were encapsulated with artificial APC at a 1:2 ratio in 6 mg/mL peptide hydrogel and incubated for 7 days [350]. Alongside the 3D culture, T cells from the same donor were set in a 2D culture as well, with the same parameters (i.e. total volume of medium, final cell and particle densities per well) as the T cells in the hydrogel. This was mainly to observe T cell responses to the artificial APC in the absence of hydrogel. Before encapsulating cells with artificial APC, the presence of the antibodies was checked by the flow cytometry. It was evident that by forming artificial APC for each experimental repeat, the MFI varied amongst different batches (Fig. 3.11. (a)). However, by culturing T cells (white phase) with artificial APC (dark phase), each batch had no issue in activating cells in 2D culture settings, as clusters of cells were visible under the microscope (Fig. 3.11. (b) of one representative donor). Whereas clusters of cells were barely detectable in the peptide hydrogels. Costimulation effect was detected by overlaying CFSE proliferation histograms for each stimulus and controls per donor (Fig. 3.11. (c)). Each donor in the 2D culture presented T cell proliferation on days 5 and 7 according to the given stimulus,

and showed the sub-optimal proliferation to CD3 and enhanced response to CD28 and CD55 (Fig. 3.11. (d)). In addition, two donors' T cells responded to CD55 with greater response than CD28 costimulation. In contrast to the 2D culture, all donors' cells showed a poor response to the artificial APC in 3D culture. Due to weak response in the 3D culture, the expansion index was reported from the whole culture rather than individual cells. Expansion index indicated a fold-expansion of the whole culture (including undivided cells) in response to stimuli (Fig. 3.11. (e)). The summary graph indicates the increased T cell proliferation response upon exposure to stimuli, but no significant difference between stimulated and resting T cells was achieved in the peptide hydrogel (Fig. 3.11. (f)). Moreover, 2D culture T cells also responded to the artificial APC with CD3 and costimulatory molecules, but there were only significant results between CD3 with CD28 stimulus against resting T cells (Fig. 3.11. (g)). Overall, there was an indication of T cells responding to given stimuli, but due to wide data distribution obtained from different donors, no statistical significance was achieved.

The supernatants from the same experiments were collected to analyse IFNγ and IL-10 cytokines, to confirm different costimulatory molecules' effect on T cells. Cytokine secretion data was presented from one donor only, as no cytokines were detected from other tested donors in the peptide hydrogel (Fig. 3.11. (h)). During 7 days of the experiment, the highest amount of cytokines (IFNγ and IL-10) were detected by day 3 in 2D cultures. However, different kinetics were found in the peptide hydrogel as T cells gradually secreted the

cytokines without reaching the optimal peak. Both culture systems confirmed CD28 costimulatory molecules had greater influence on T cells to secrete IFNγ than CD55. IL-10 was released at higher levels by T cells in the hydrogel under CD55 costimulation than in 2D culture. In 2D culture, there was a small difference between CD28 and CD55 costimulatory molecules' effect on IL-10 secretion. But the data itself confirms the co-stimulatory effect on T cells, as artificial APC with CD3 only caused the lowest level of two different cytokines release.

In conclusion, costimulation of T cells is feasible in the peptide hydrogel but requires further optimisation of artificial APC suitable for 3D culture rather than 2D culture settings. In this case, further studies are continued with artificial APC coated with high concentration (30 μg/mL) of CD3 and CD28 antibodies in the peptide hydrogel.

(a)

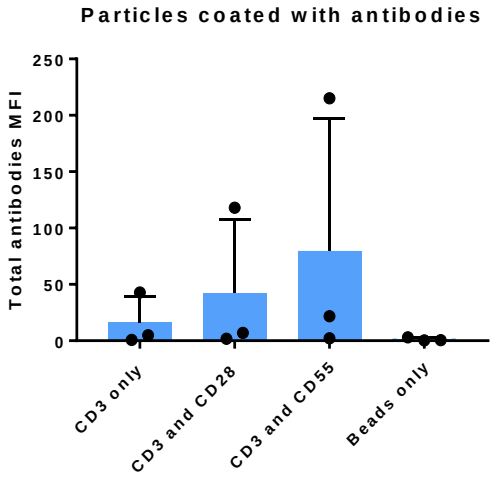
Particles coated with antibodies
Total antibodies MFI
250
200
150
100
50
0
CD3 only
CD3 and CD28
CD3 and CD55
Beads only

(b)

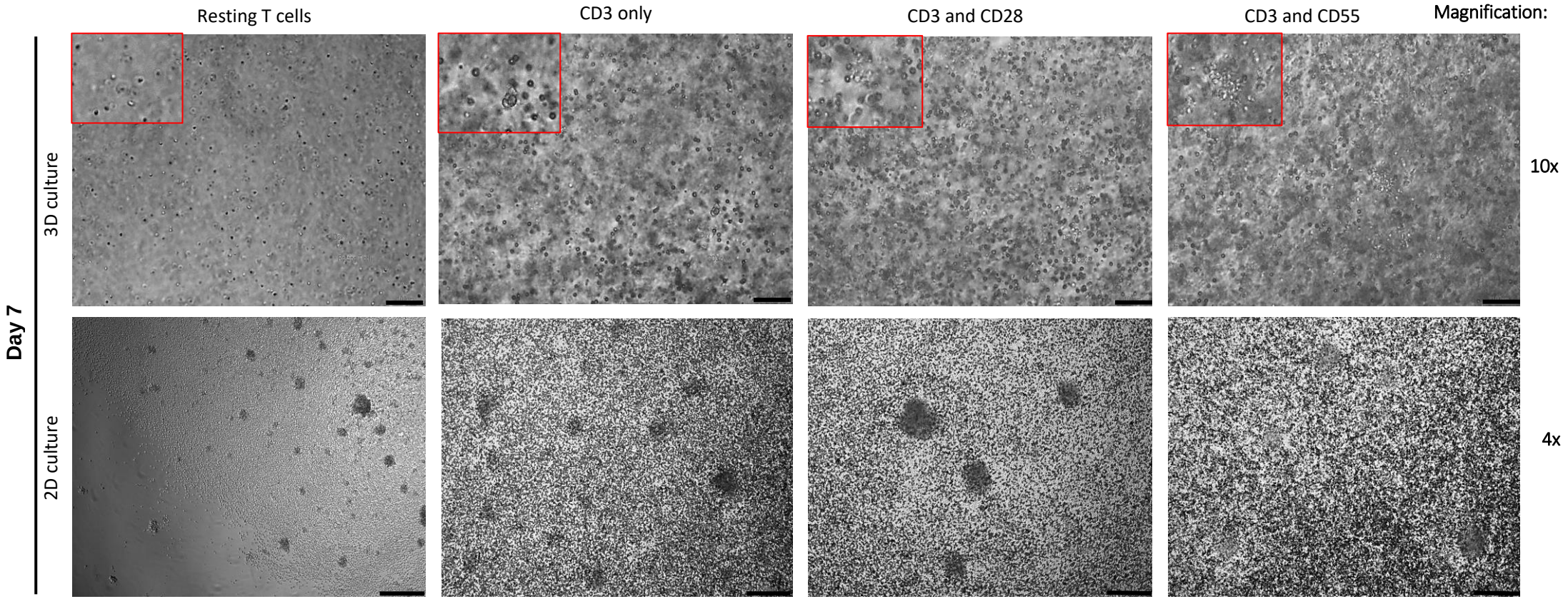
Resting T cells
CD3 only
CD3 and CD28
CD3 and CD55
Magnification:
Day 7
3D culture
2D culture
10x
4x

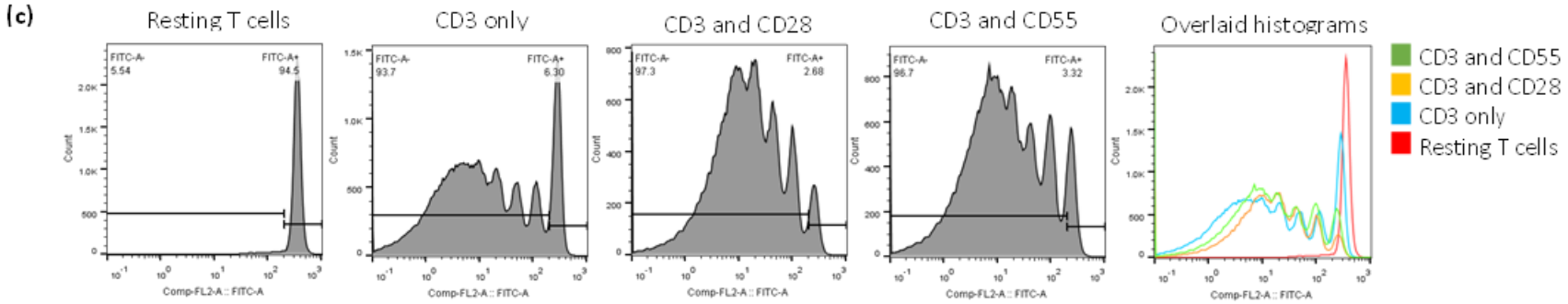
(c)
Resting T cells
CD3 only
CD3 and CD28
CD3 and CD55
Overlaid histograms
CD3 and CD55
CD3 and CD28
CD3 only
Resting T cells

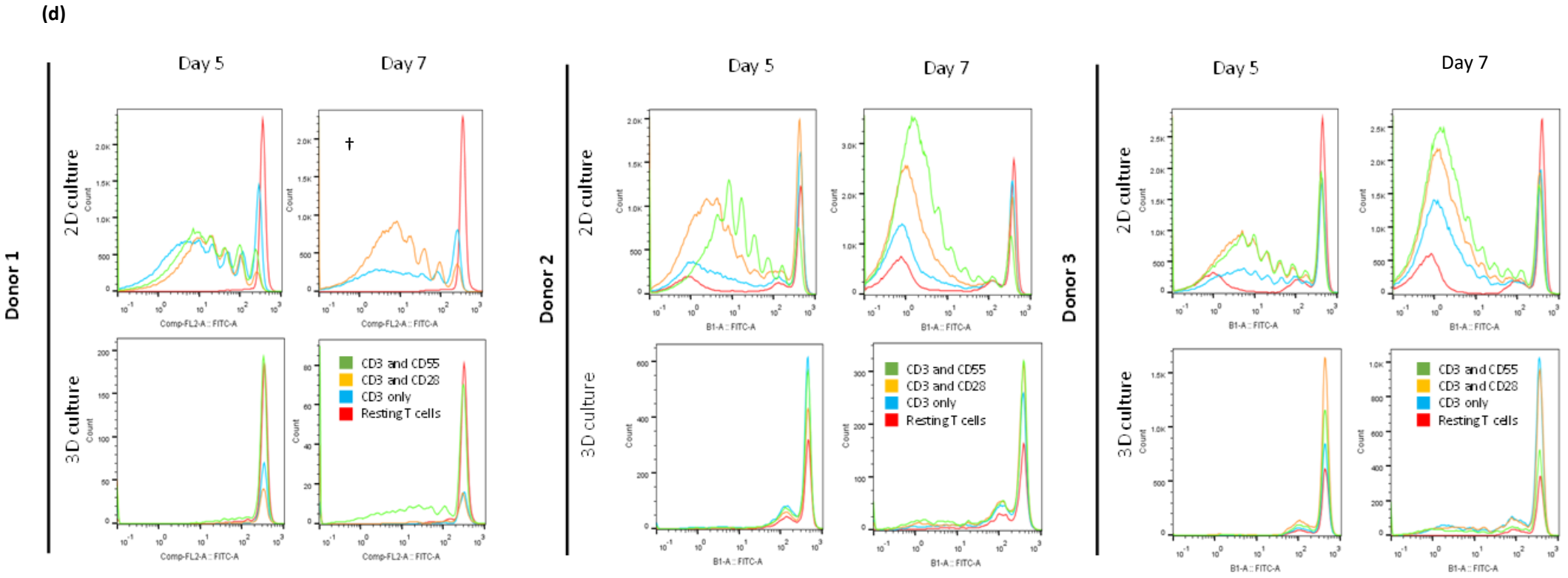
(d)
Donor 1
Donor 2
Donor 3
Day 5
Day 7
2D culture
3D culture
†
CD3 and CD55
CD3 and CD28
CD3 only
Resting T cells

(d) Cont.

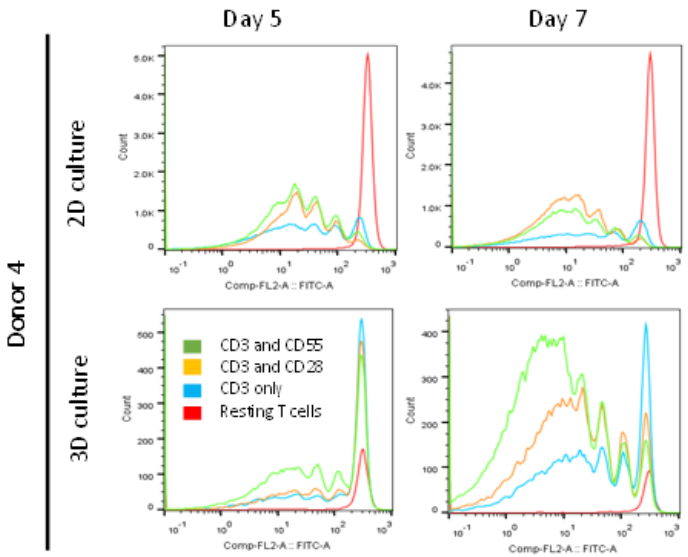

(e)

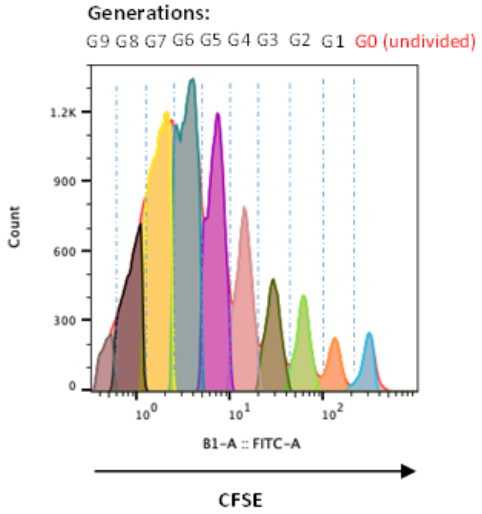

Expansion index: indicates the fold-expansion of the whole culture (includes divided and un-divided cells)

By using FACS cell counts (events), **Expansion index** is calculated:

1) Total nr. of cells = G0 + G1 + G2 ...
2) Total nr. of cells at **start culture** = (G1/2) + (G2/2) + (G3/2) ...
3) **Expansion index** = Total nr. of cells / total nr. of cells at start of culture

(f)

Day 7 – 3D culture

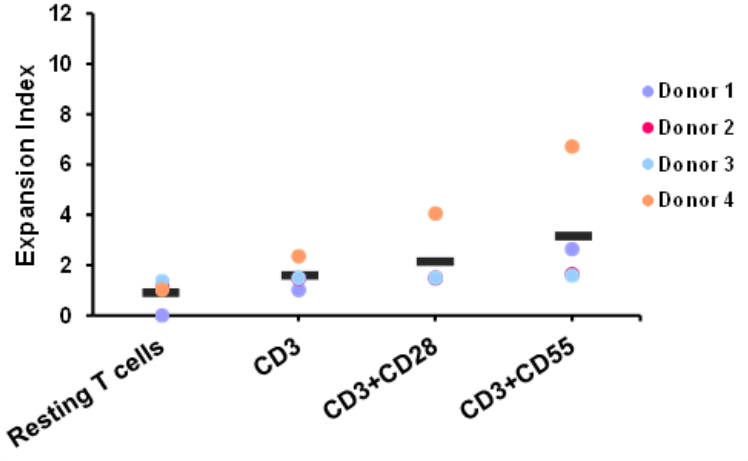

(g)

Day 7 – 2D culture

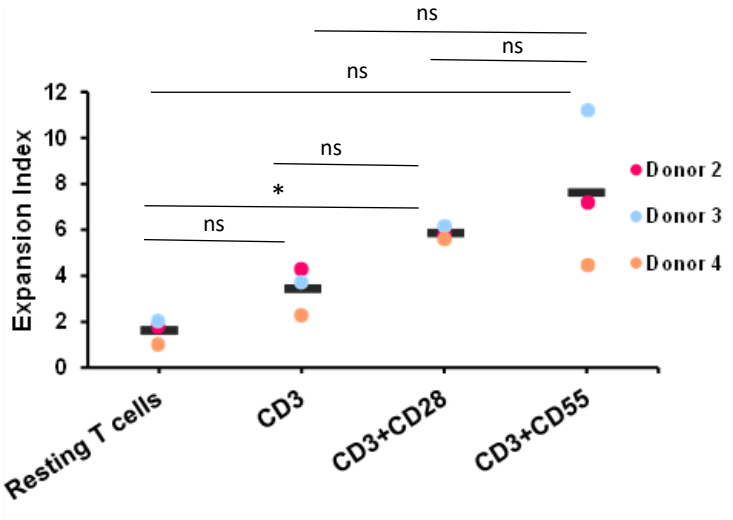

(h)

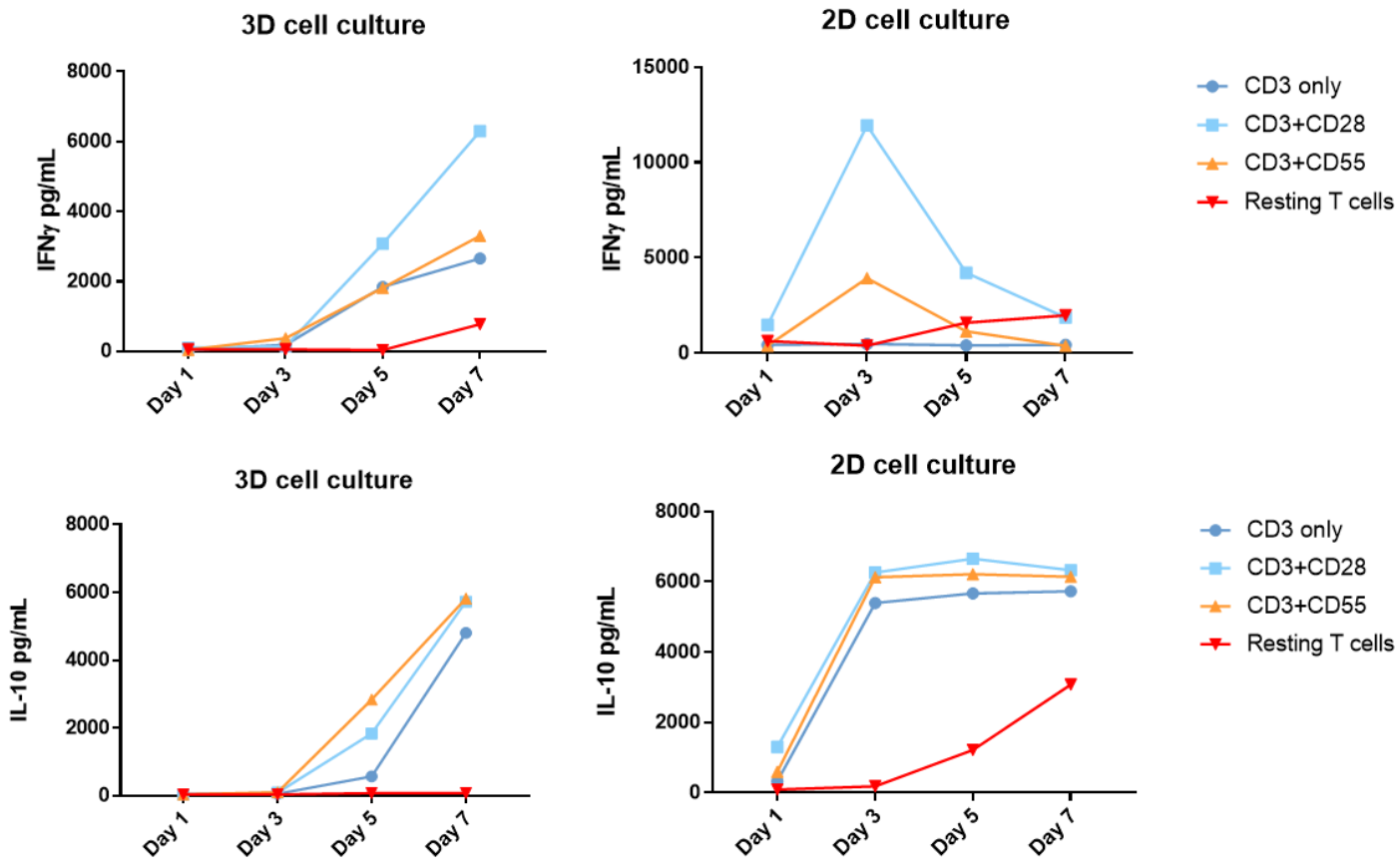

Figure 3.11: Costimulation of T cells by CD55 and CD28 antibodies in the peptide hydrogels. T cells were encapsulated with artificial APC in 6mg/mL hydrogels coated with optimised with CD3, CD28 and CD55 concentrations. Artificial APC and T cell ratio was 2:1, and data was collected on days 5 and 7 to compare the stimulation effect of T cells between 2D and 3D cultures. **(a)** The graph reports MFI values of each batch of produced artificial APC and the presence of stimulatory antibodies. **(b)** Brightfield images present APC (dark phase) and T cells (white phase) in both culture settings, and clusters of cells were more visible in 2D culture than 3D culture systems. **(c)** The costimulation effect amongst different artificial APC were compared by overlaid histogram data, reporting T cell proliferation. **(d)** Histograms reported donor responses in two culture systems on different days. **(e)** T cell proliferation response was reported as the expansion index, and summary graphs were generated from all donors in 3D culture, which show no significant results **(f).** Same donor cells were also set up in 2D culture for comparison to 3D culture on the same day **(g)**. **(h)** The supernatant from the donor 4 was analysed by ELISA for IFNγ and IL-10 cytokines secreted by T cells under influence of costimulatory molecules. Scale bars in 3D culture are set at **100µm**, 2D culture **300µm**. Data for artificial APC presented with mean+SD (n=3). Expansion index data is reported with mean value only. Statistical analyses completed with RM One-way ANOVA with Tukey's post-hoc, **p<0.01. Expansion index for 2D culture contains n=3, and 3D culture of n=4 of biologically independent donors. † - indicates missing CD55 data.

3.2.9. Stimulation of T cells in the peptide hydrogel with artificial APC

Previous studies (Fig. 3.11) demonstrated that optimised artificial APC required more work to induce effective T cell response in the peptide hydrogel. For this, high antibody concentration of CD3 and CD28 (30µg/ml each) coated particles was used to stimulate T cell response in the peptide hydrogel. Extra artificial APCs were also prepared with CD3 only at 30µg/ml, to indicate whether the T cell could detect Signal 1 on its own [89]. It is important to highlight that this experiment was set up before the cell density optimisation experiment (Fig. 3.5) and the hydrogels contained $1x10^6$ cells/ml, which was based on the literature review [328]. Particles were successfully coated with antibodies as the majority of them (>99%) were positive for CD3 and CD28 (Fig. 3.12. (a)). The MFI values confirmed the presence of single and combined antibodies on the surface of particles, which indicated the full formation of artificial APC presenting Signal 1 and Signal 2 ligands (Fig. 3.12. (a)).

T cells were encapsulated with artificial APC in the peptide hydrogels and observed every day for proliferating clusters of cells (Fig. 3.12. (b)). On day 1, artificial APC and resting T cells appeared to be separated in the hydrogel and by day 5, clusters of cells were visible under the microscope. Proliferation, as measured by 3H-Thymidine assay confirmed T cell response (measured by CFSE) to the artificial APC (Fig. 3.12. (c)), as CD3 or CD3 and CD28 stimulated cells were significantly ($p<0.0001$) different from the resting T cells. T cells were also able to respond accordingly to the given stimuli, as presence of co-stimulation (CD28)

induced significantly higher response than CD3 on its own. The incorporation of 3H-Thymidine was similar to the positive control (mitogen-activated T cells) indicating the peptide hydrogels' ability to sustain stimulus and support T cell proliferation.

Over a 5-day period in the peptide hydrogel, T cells stimulated by CD3 and CD28 secreted higher IFNγ cytokine concentration than CD3 on its own (Fig. 3.12. (d)). No other factors interfered with T cell responses, as resting T cells did not secrete any detectable cytokines. This confirmed the peptide hydrogels' ability to support T cell function by artificial APC.

(a)

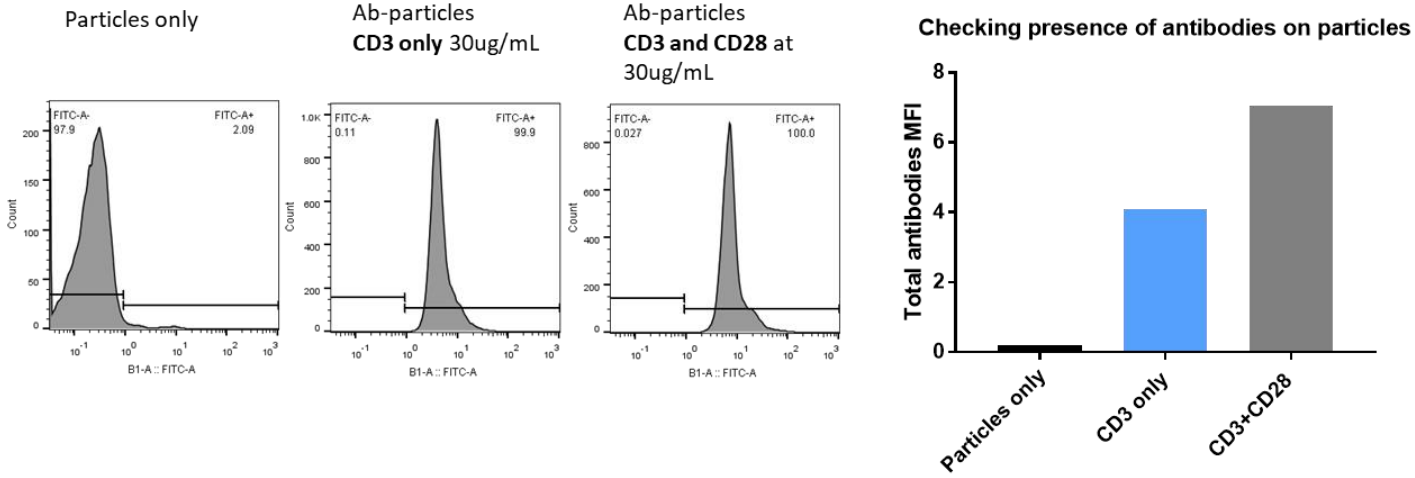
Particles only
Ab-particles
CD3 only 30ug/mL
Ab-particles
CD3 and CD28 at
30ug/mL
FITC-A-
97.9
FITC-A+
2.09
FITC-A-
0.11
FITC-A+
99.9
FITC-A-
0.027
FITC-A+
100.0
Count
B1-A :: FITC-A
Checking presence of antibodies on particles
Total antibodies MFI
0
2
4
6
8
Particles only
CD3 only
CD3+CD28

(b)

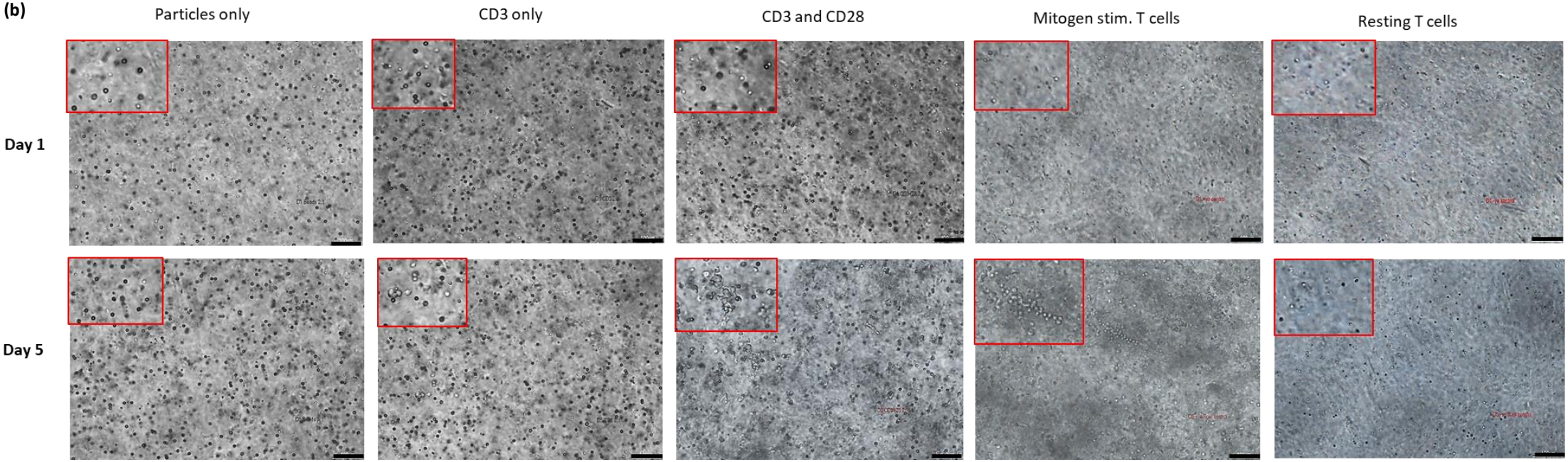
Particles only
CD3 only
CD3 and CD28
Mitogen stim. T cells
Resting T cells
Day 1
Day 5

(c)

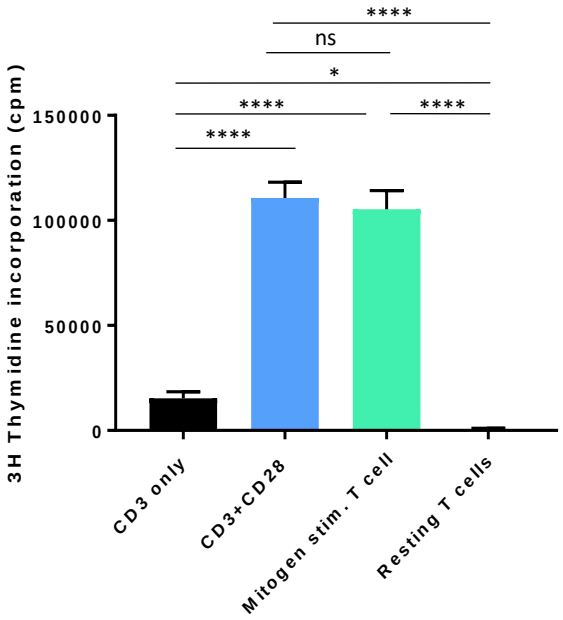

(d)

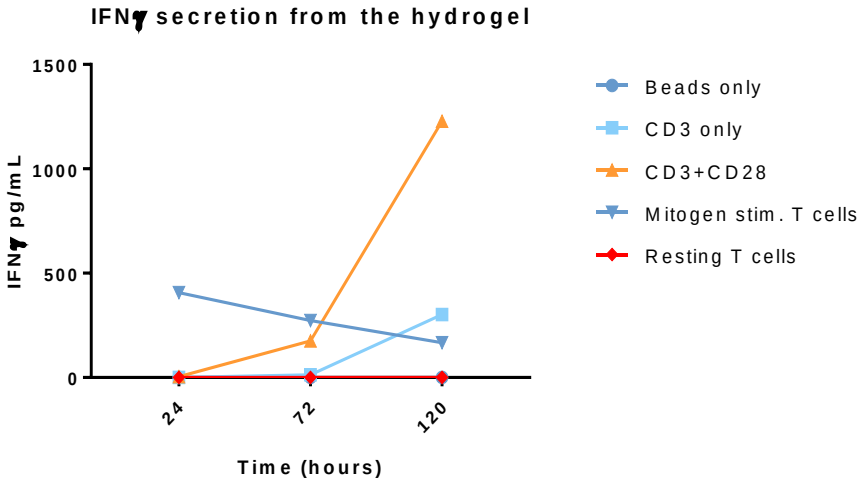

Figure 3.12: T cell stimulation by artificial APC in the peptide hydrogel. Resting T cells were encapsulated in the peptide hydrogel with artificial APC at ratio 1:2 (T cells: APCs) and incubated for 6 days. Positive control was prepared by stimulating T cells with mitogens for 12 hours prior to encapsulation. **(a)** Flow cytometry analyses indicated the presence of stimulatory antibodies on the polystyrene beads. **(b)** Artificial APCs were encapsulated in hydrogels with cells, and brightfield images showed the distribution of artificial APC and T cells across the hydrogel from day 1. By day 5 proliferating clusters of T cells were visible in the hydrogel. **(c)** 3H-Thymidine incorporation assay was used to measure T cell proliferation response. **(d)** Secreted IFNγ cytokines over 5 day period from the culture were assayed by ELISA IFNγ kit. Scale bars are set at **100µm**. Data presented with mean+SD, statistical test completed by One-way ANOVA with Tukey's post-hoc test, $p<0.05$*, $p<0.0001$ ****, n=4 repeats from 1 experiment.

3.2.10. The optimal time point to analyse T cell response to artificial APC and ratio in the hydrogel

Previous experiments indicated the hydrogel's ability to support T cell stimulation without any adverse effects. However, the experiment approach was based on literature that mainly used different culture settings rather than self-assembling peptide hydrogels [328, 350]. This mean the appropriate ratio between T cells and artificial APCs still needs to be investigated, especially to define the optimal ratio, which could guarantee 3D T cell responses and overcome possible donor-to-donor variations. In this experiment, T cells were encapsulated with different densities of artificial APC (coated with 30µg/ml of CD3 and CD28) to find the optimal ratio for cell stimulation. Alongside investigating optimal cell ratios, the optimal day of T cell proliferation under 3D culture settings was also observed. This was to indicate the best point in time to study T cell responses in the hydrogel.

T cells were encapsulated at constant cell density (1.5x10^6 cells/ml) at various ratios with artificial APC and incubated for a 7-day period. To find the day when the T cell proliferation peak occurred in the peptide hydrogel, T cell proliferation was presented as a percentage of divided cells. T cells were released from the hydrogel and divided cells (%) were analysed on days 3, 5 and 7 by flow cytometry (Fig. 3.13. (a)). Day 1 data was missed as previously observed results (Fig. 3.12. (d)) have shown no detectable T cell responses. T cells from all three donors gradually increased their proliferation in response to all given ratios over a 7-day period (Fig. 3.13. (b)). The highest ratio of artificial APC to T cells (4:1)

was detectable from one donor by day 3 whereas others were detectable by day 5. On day 7, all donors' T cells had responded to the different quantities of stimuli in hydrogels, including the lowest ratios of artificial APC to cells (Fig. 3.13. (c)). It should be noted that there was differences on the level of responses between donors. For example, at a 0.1:1 ratio the level of proliferation varied amongst donors: absence (Donor 1), moderate (Donor 3) and maximum proliferation response (Donor 2) (Fig. 4.7. (b)). Ratio at 4:1 was selected to determine the optimal timepoint with statistical significance to analyse T cells response in hydrogel. At this ratio, all donors showed the highest response in the hydrogel (Fig. 3.13. (b) and (c)). There was a significant difference of T cells' proliferation response in hydrogel at days 5 and 7 in contrast to day 3, with no significant difference between days 5 and 7 (Fig. 3.13. (d)). For the subsequent experiments, T cell functions in the peptide hydrogel would be observed on day 7, as at this time T cell response is detectable with a small variation amongst different donors.

The optimal ratio of T cells to the artificial APC was analysed by day 7. However, this time T cell proliferation is reported as division index (DI) and the generations of daughter cells from every ratio and donor were colour-coded by the FlowJo software. It is important to note that by decreasing the ratio of artificial APC to T cells, it increases the quantity of non-responded cells (blue peaks) (Fig. 3.14. (a)). This is why the division index was reported to also take unstimulated cells into account. Overall, all three donors showed a gradual DI increase upon increasing ratios of artificial APC (Fig. 3.14. (b)). Donor-to-donor variation was

evident in this experiment, as cells under the same parameters showed variable responses. However, there was no statistical significance between stimulated cells with artificial APC and resting T cells in the hydrogel in this limited set of experiments. There was a clear difference between stimulated T cells' proliferation response to the negative control. The optimum T cell stimulation was achieved by a 2:1 ratio and therefore this ratio was chosen for future studies. This was because the highest ratio of artificial APC to the T cells did not improve overall response, whereas 1:1 ratio could risk other future studies by not delivering T cell response.

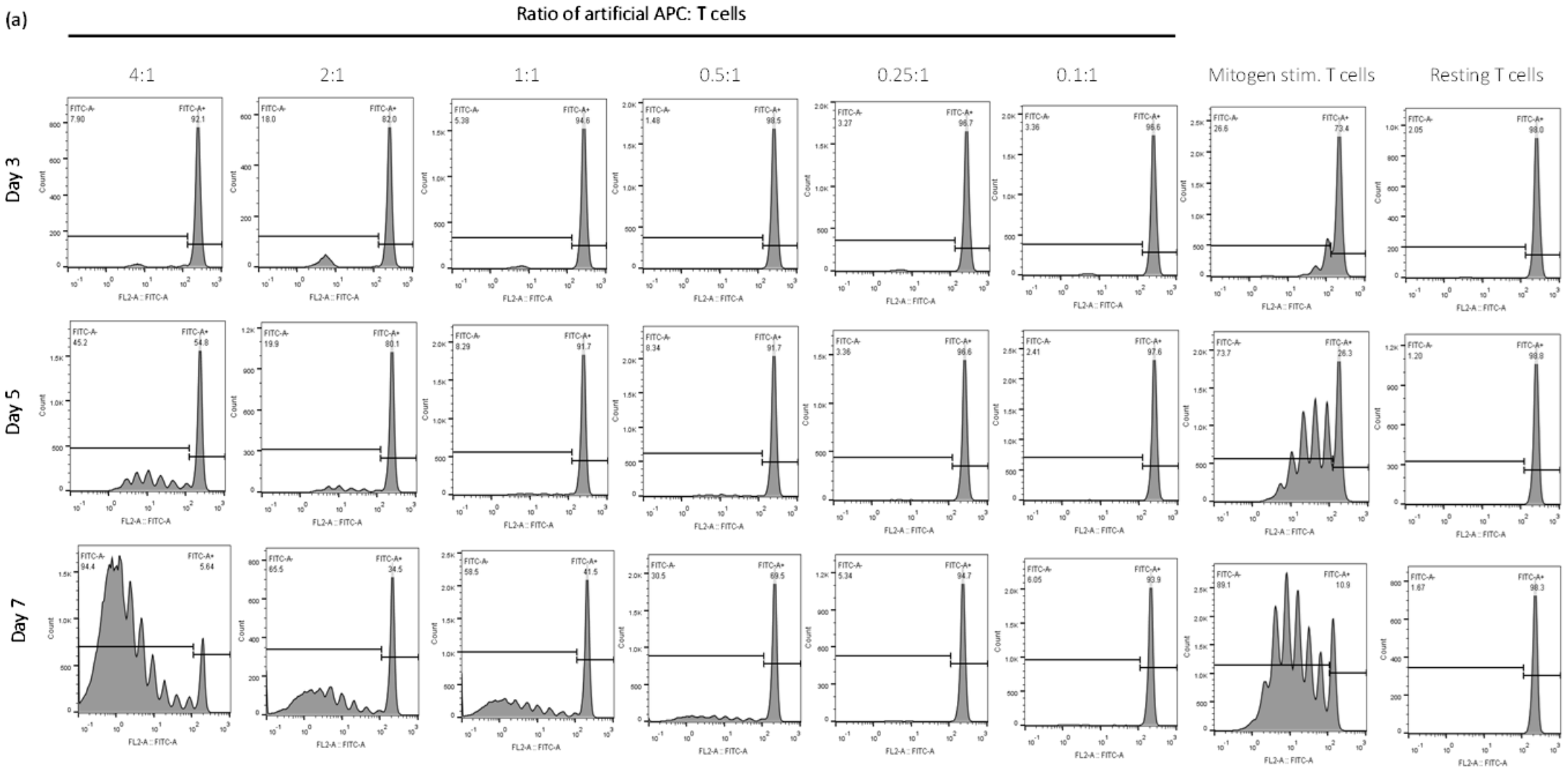
(a)
Ratio of artificial APC: T cells
4:1
2:1
1:1
0.5:1
0.25:1
0.1:1
Mitogen stim. T cells
Resting T cells
Day 3
Day 5
Day 7
FITC-A-
FITC-A+
Count
FL2-A :: FITC-A

(b)

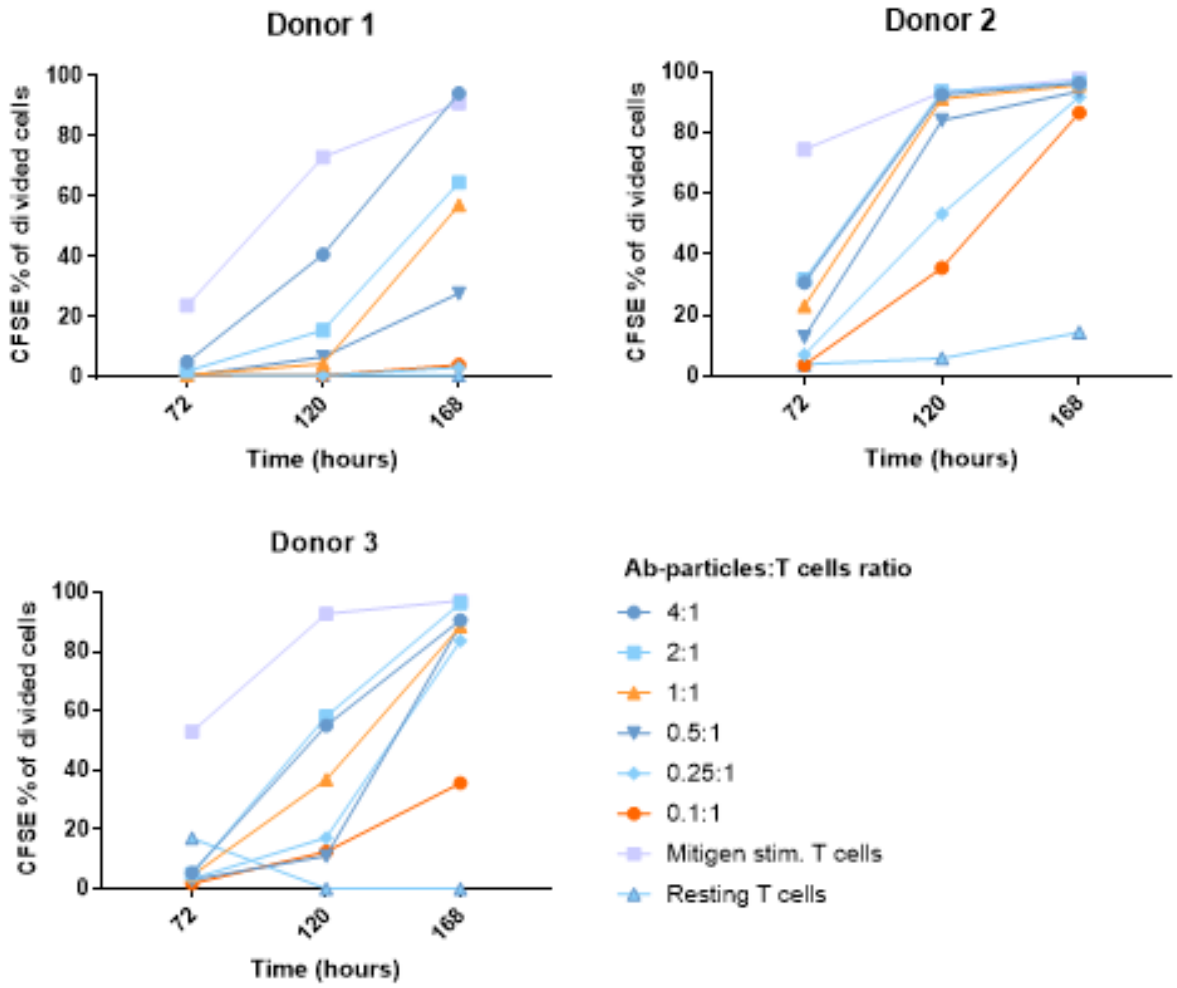
Donor 1
Donor 2
Donor 3
CFSE % of divided cells
Time (hours)
72
120
168
0
20
40
60
80
100
Ab-particles:T cells ratio
4:1
2:1
1:1
0.5:1
0.25:1
0.1:1
Mitigen stim. T cells
Resting T cells

(c)

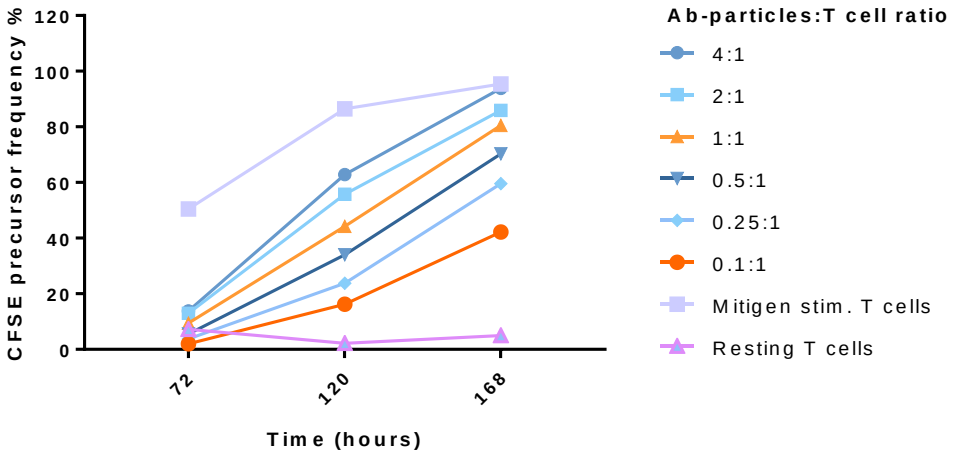
CFSE precursor frequency %
Time (hours)
72
120
168
0
20
40
60
80
100
120
Ab-particles:T cell ratio
4:1
2:1
1:1
0.5:1
0.25:1
0.1:1
Mitigen stim. T cells
Resting T cells

(d) **T cell stimulation at 4:1 in hydrogel over time (hours)**

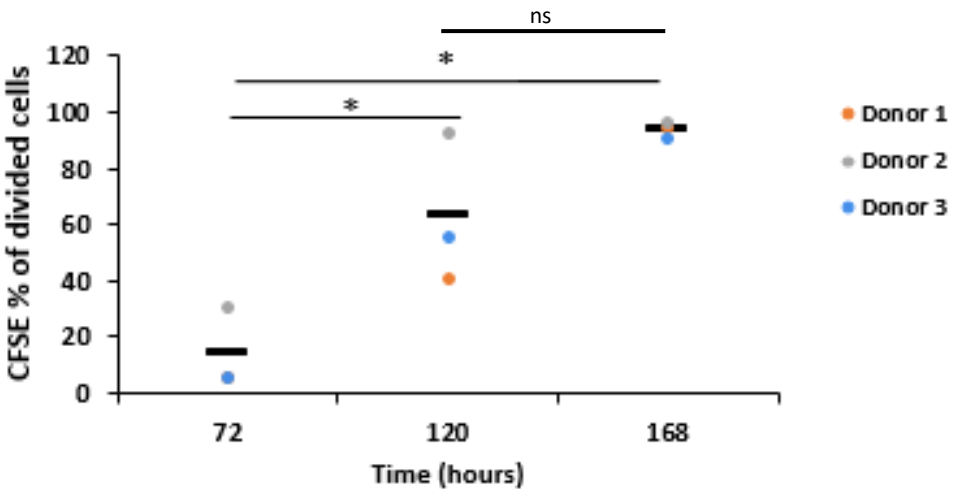

Figure 3.13: Time-point (day) for detectable T cell responses in the peptide hydrogel. CFSE labelled T cells were encapsulated at constant 1.5x10^6 cells/ml density with various ratios of artificial APC (in graphs identified as Ab-particles) coated with 30 µg/ml of CD3 and CD28 in the hydrogels and incubated for 7-days. Cells were released from the hydrogel on the selected days and analysed by flow cytometry. **(a)** Histograms represent one donor analysis of CFSE % divided cells over the 7 day period of the experiment. **(b)** Each donor T cells proliferation is plotted over a 7 day period, and the summary graph reports a mean value **(c)** from all three biologically independent donors (n=3). **(d)** At ratio 4:1, detectable T cells' proliferation was on day 5 (120 h) and 7 (168 h), which were both significant different to the day 3 (72 h) timepoint. Data presented as mean values only, n=3, RM One-way ANOVA with Tukey's post-hoc, * $p<0.05$.

(a)

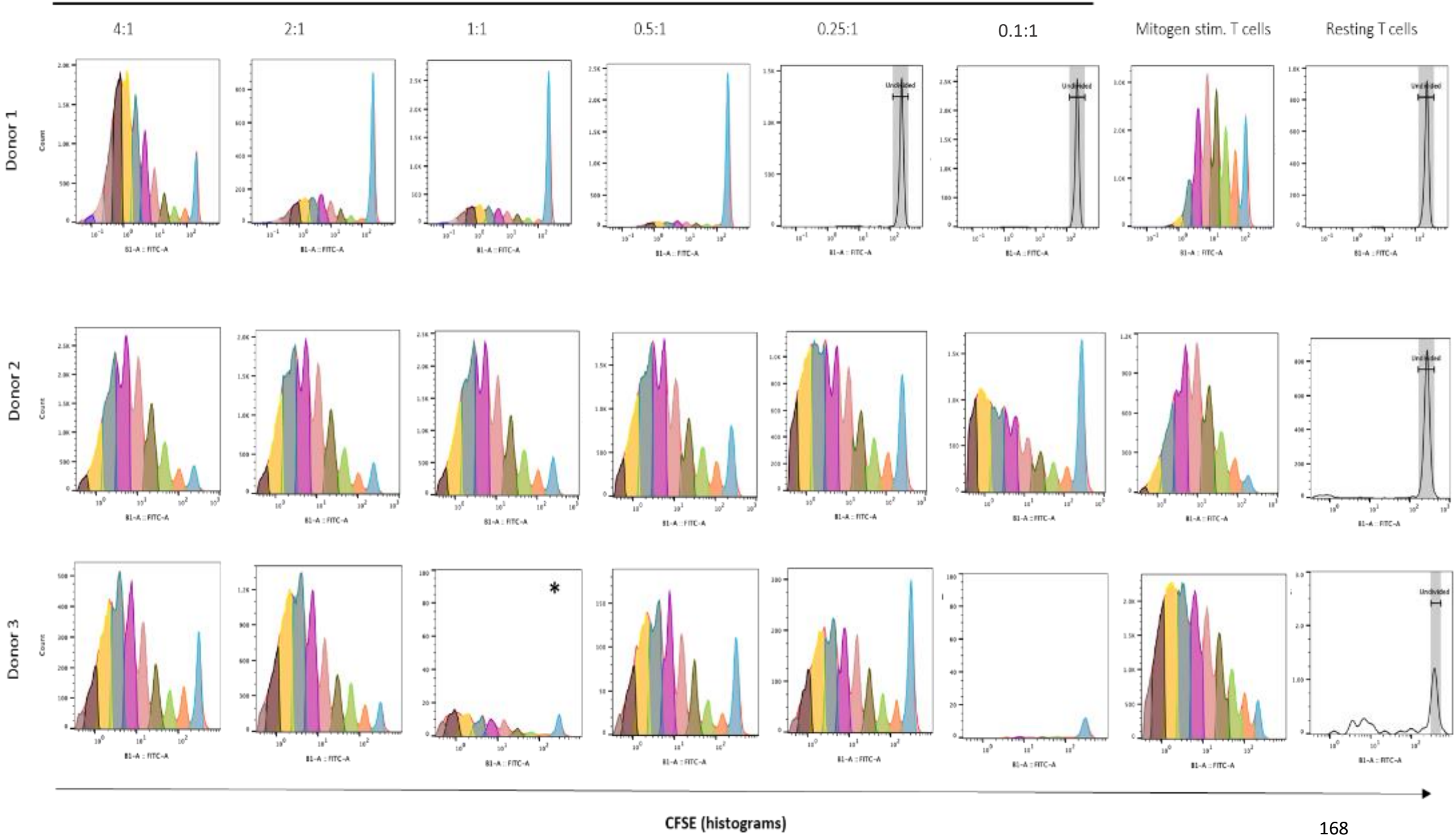
Ratio of artificial APC:T cells
4:1
2:1
1:1
0.5:1
0.25:1
0.1:1
Mitogen stim. T cells
Resting T cells
Donor 1
Donor 2
Donor 3
Count
B1-A :: FITC-A
Undivided
*
CFSE (histograms)

(b)

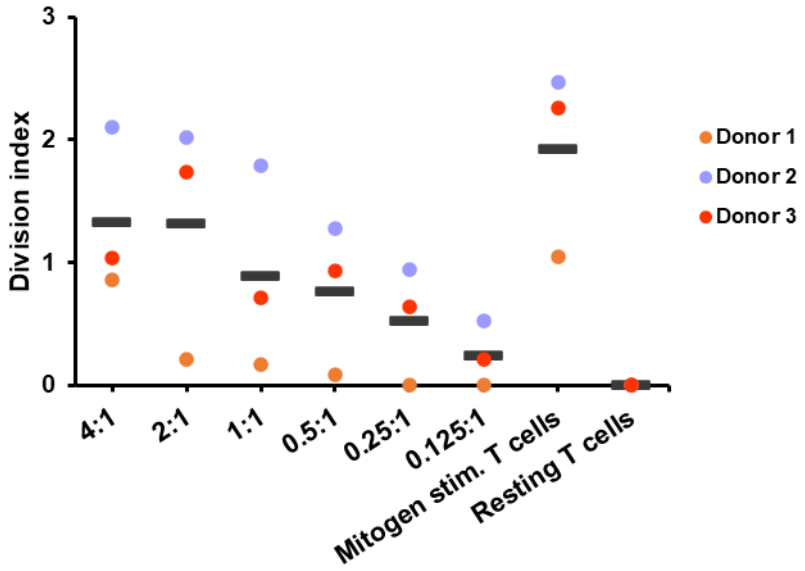

Figure 3.14: Determining the optimal ratio between artificial APC and T cells for T cell stimulation in the hydrogel. CFSE labelled resting T cells ($1.5x10^5$ cells/ml) were encapsulated with different ratios of artificial APC in the peptide hydrogels and incubated for 7-days. On day 7 cells were released from the hydrogel and analysed by flow cytometry. **(a)** Histograms represent each donor's T cell proliferation in response to stimuli on day 7, and generations of daughter cells are identified by distinctive colours. * indicates the experimental error occurring during data collection. **(b)** Summary graph present division index from all three biologically independent donors (n=3) with no significant results. Data presented as mean, and analysed by RM One-way ANOVA with Dunnet's multicomparison test, where each group was compared against resting T cells control.

3.2.11. T cells express activation and proliferation markers in the peptide hydrogel

After establishing the T cell ratio to the artificial APC in the peptide hydrogel, other dynamics of T cell activation-related features were analysed. Upon stimulation, CD25 (latent activation marker) was analysed on T cell's surface and Ki67 (proliferation marker) expression. T cells were encapsulated with artificial APC or particles coated with serum only (as a negative control) at ratio 2:1. After 7 days of incubation, T cells were released and stained with antibodies recognising the CD25+ marker. To analyse specific marker expression from the peptide hydrogels by flow cytometer, two control samples were prepared to set the CD25-isotype gate (negative) and exclude hydrogel debris from the analyses (Fig. 3.15. (a)). After 7 days, T cells responded to the stimulus in the hydrogel and expressed CD25+ on their surface, compared to the resting T cells and serum-coated particles (Fig. 3.15. (b and c)). Matching donors were set up in 2D culture as well and delivered the same trend of CD25 expression as the 3D culture cells (Fig. 3.15. (d)). Although there was no significant difference between stimulated and resting cells in the 3D culture, there was evident increased response to artificial APCs from all donors. Even T cells under 2D culture responded to stimuli by increased CD25 expression, but with no significance to the resting T cells (Fig. 3.15. (d)).

The Ki67 marker expression was analysed by confocal microscopy to observe proliferating clusters of cells in the intact hydrogel (Fig. 3.15. (e)). On day 7, CFSE-labelled T cells were present in the hydrogel, but proliferating clusters of cells

were not visible under the microscope. Proliferating clusters of T cells were detected by observing bright-field images combined with Ki67 together, which showed artificial APCs were surrounded by immune cells. Under the same colour as Ki67, CD3 and CD28 were also detected on the particles as all the of antibodies were derived from mice. To distinguish CD3 and CD28 from Ki67 signals, merged brightfield images showed CD3 and CD28 as dark phase particles, whereas Ki67 were white phase – T cells. As expected, no proliferating clusters of cells were detected in T cells encapsulated with particles only. Overall, T cells after stimulation showed phenotype of activated T cells, which also indicated the biocompatibility of the peptide hydrogels.

(a)

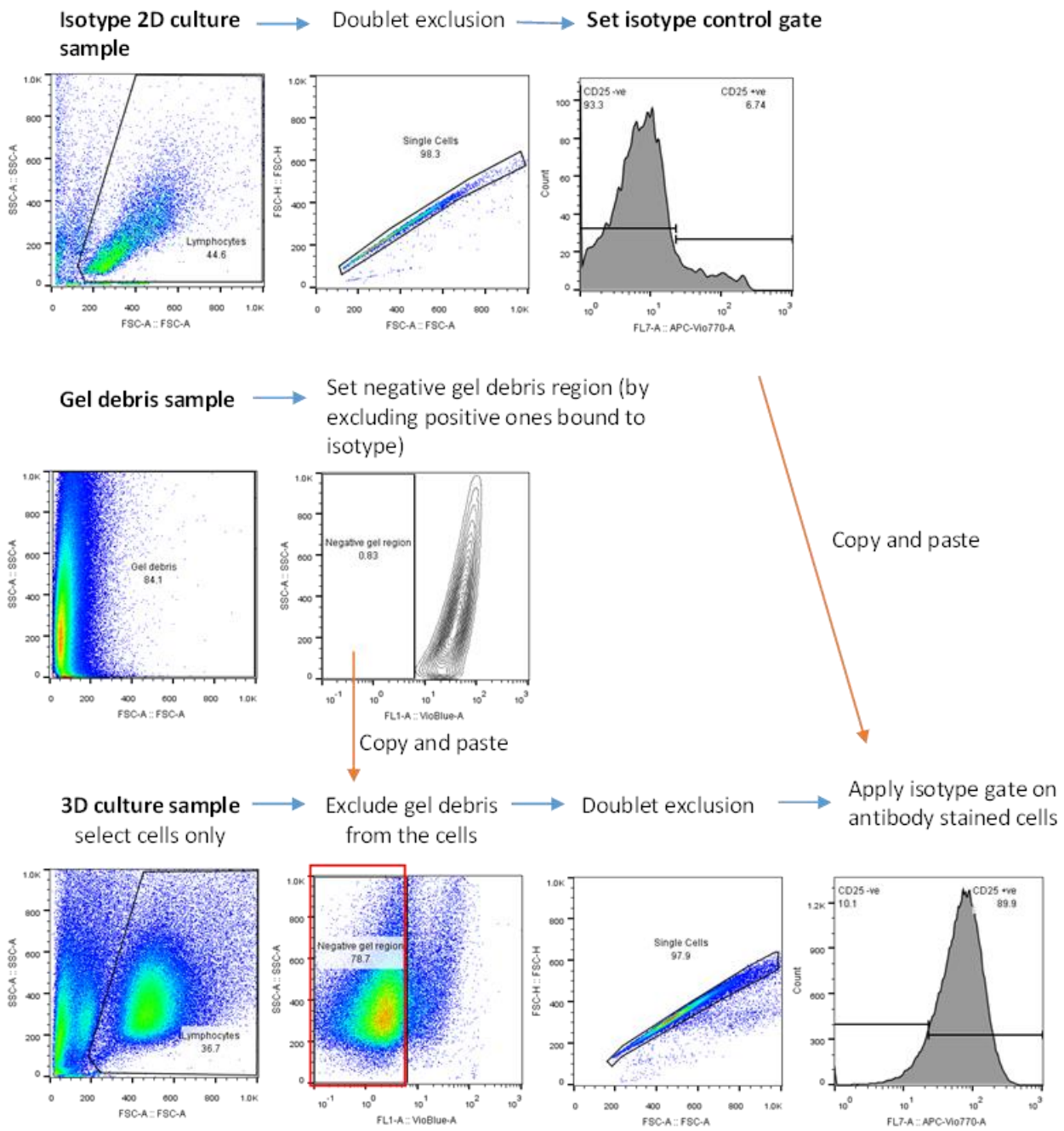
Isotype 2D culture sample
Doublet exclusion
Set isotype control gate
Lymphocytes 44.6
Single Cells 98.3
CD25 -ve 93.3
CD25 +ve 6.74
Gel debris sample
Set negative gel debris region (by excluding positive ones bound to isotype)
Gel debris 84.1
Negative gel region 0.83
Copy and paste
Copy and paste
3D culture sample select cells only
Exclude gel debris from the cells
Doublet exclusion
Apply isotype gate on antibody stained cells
Lymphocytes 36.7
Negative gel region 78.7
Single Cells 97.9
CD25 -ve 10.1
CD25 +ve 89.9

(b)

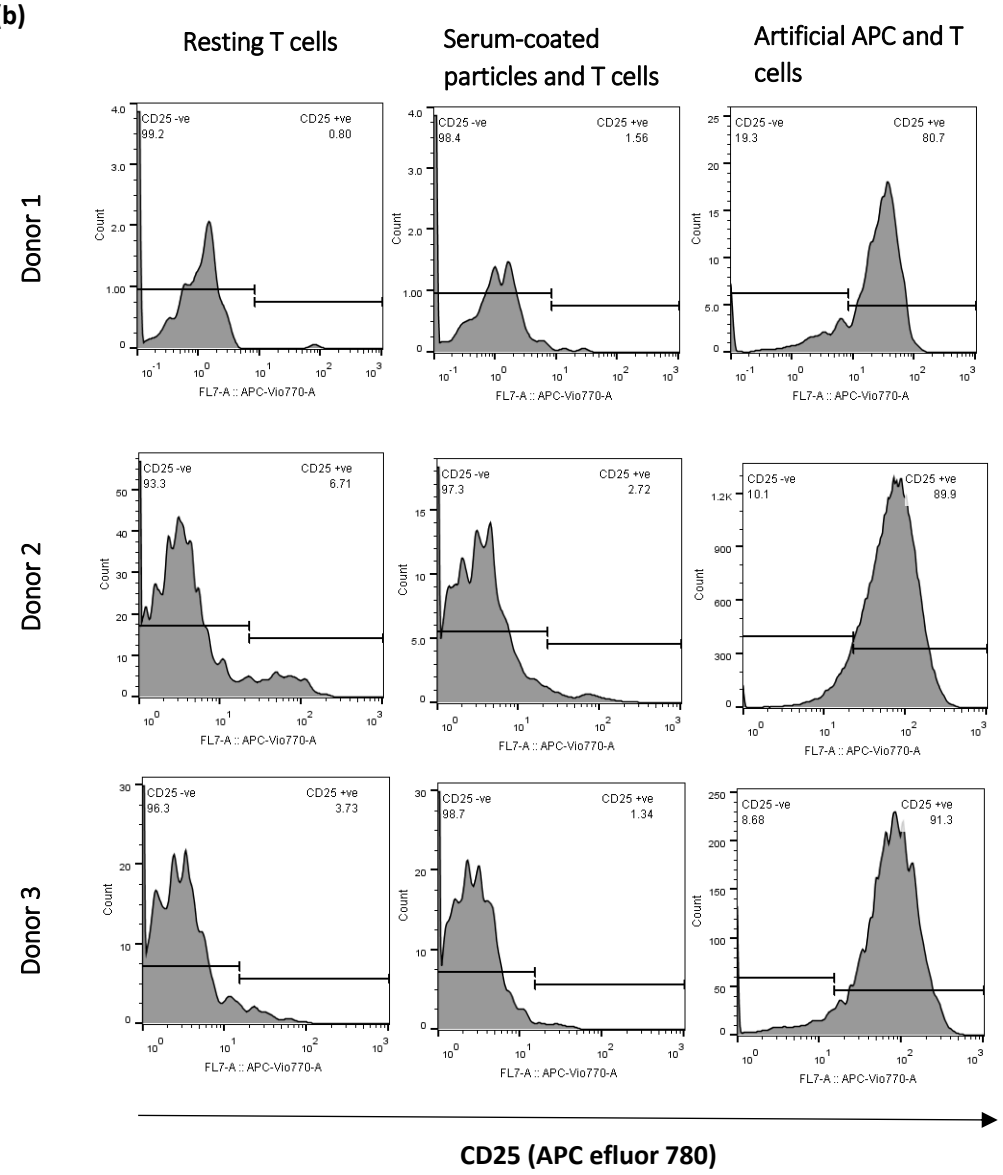
Resting T cells
Serum-coated particles and T cells
Artificial APC and T cells
Donor 1
Donor 2
Donor 3
CD25 -ve
CD25 +ve
99.2
0.80
98.4
1.56
19.3
80.7
93.3
6.71
97.3
2.72
10.1
89.9
96.3
3.73
98.7
1.34
8.68
91.3
Count
FL7-A :: APC-Vio770-A
CD25 (APC efluor 780)

(c)

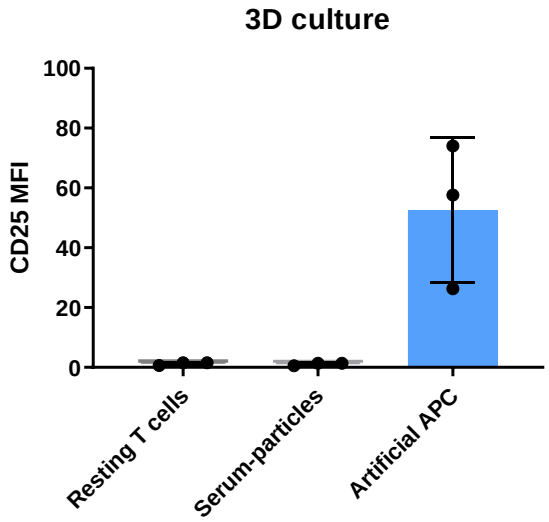
3D culture
CD25 MFI
100
80
60
40
20
0
Resting T cells
Serum-particles
Artificial APC

(d)

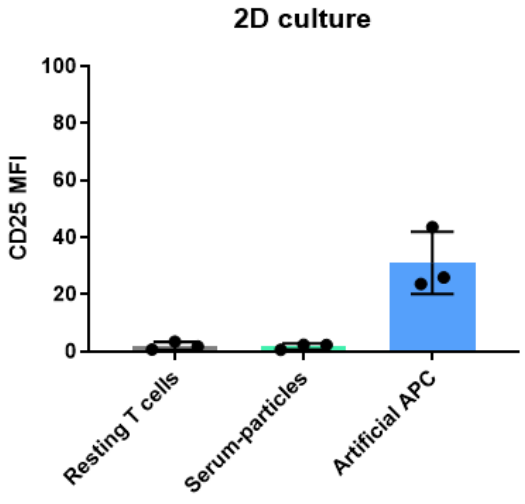
2D culture
CD25 MFI
100
80
60
40
20
0
Resting T cells
Serum-particles
Artificial APC

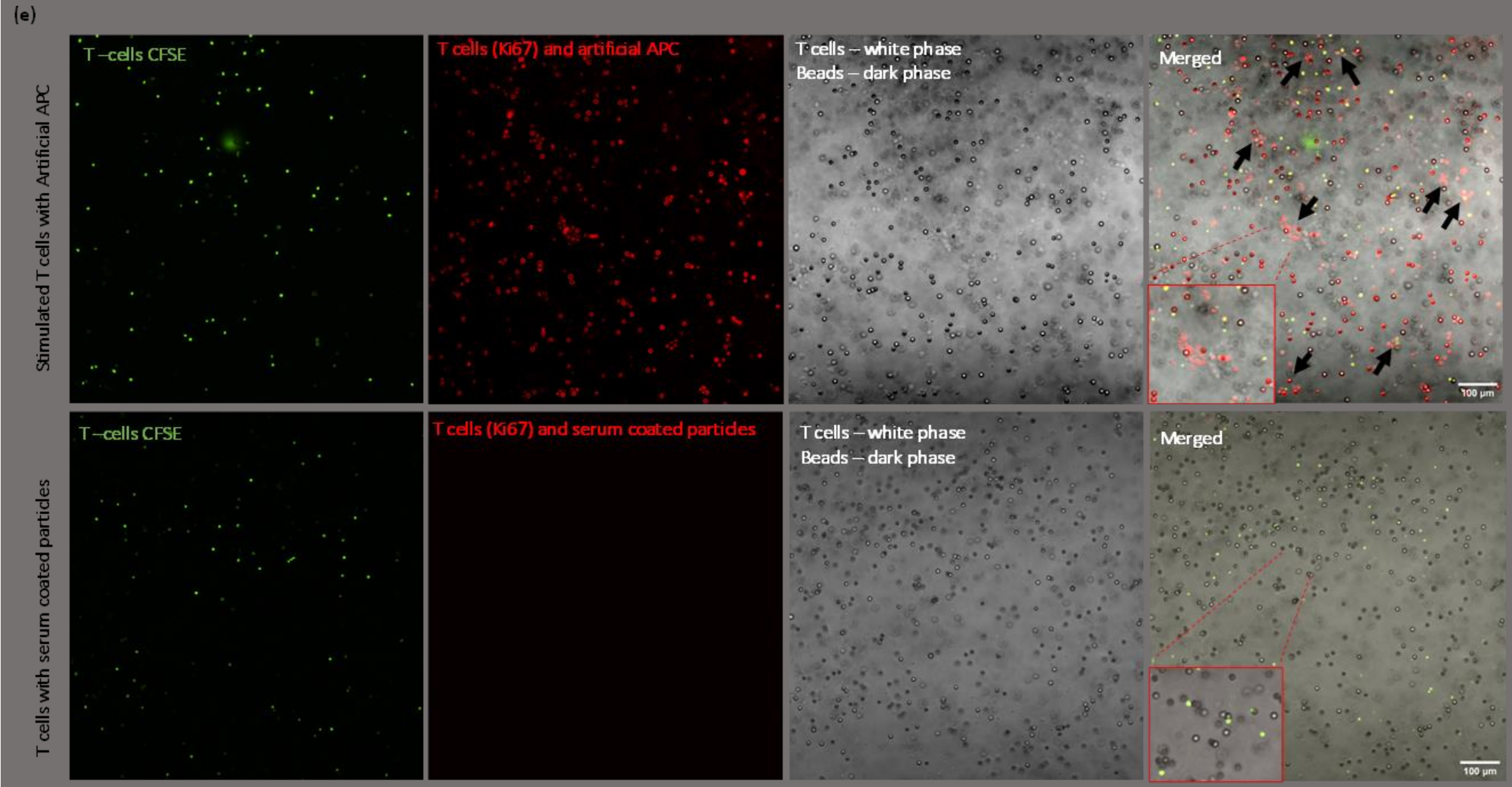
(e)
Stimulated T cells with Artificial APC
T –cells CFSE
T cells (Ki67) and artificial APC
T cells – white phase
Beads – dark phase
Merged
100 µm
T cells with serum coated partides
T –cells CFSE
T cells (Ki67) and serum coated partides
T cells – white phase
Beads – dark phase
Merged
100 µm

Figure 3.15: T cells express activation and proliferation markers after Ab-particle stimulation in the peptide gels. T cells were encapsulated with artficial APCs or serum coated particles in the peptide hydrogel at ratio 2:1 (artificla APC: T cells) and incubated for 7 days. On the final day of experiment, peptide hydrogels for CD25 expression were degraded and analysed by flow cytometry. For Ki67 expression, CFSE labelled T cells in the hydrogel were analysed by confocal microscope. **(a)** Gating strategy to detect CD25 expression (activation marker) on released T cells from the peptide hydrogel. Isotype control gating for CD25 was set on the 2D culture sample. A separate sample was prepared with gel debris only and stained with a different isotype (IgG-APC) which is irrelevant to the cells and marker detection. Gel debris interacted with isotypes, and the region negative for gel debris with IgG-APC was selected. Sample of T cells released from the hydrogel were stained with CD25 antibody and IgG-APC. Sample debris were excluded from T cell gating, followed by the gel's debris exclusion. T cells were analysed for CD25 expression with isotype gate control. **(b)** Histograms present each donor's T cells released from the hydrogels and analysed for CD25 expression. Summary graphs of CD25 MFI values are presented in 3D culture **(c)** and 2D culture **(d)** with no significant results, from all three biologically independent donors (n=3). **(e)** Confocal microscope images of T cells and artificial APC in hydrogels. T cell proliferation was assessed with Ki67 protein (proliferation marker) expression. Data presented here as mean+SD, statistical analyses were done by RM One-way ANOVA with Dunnet's multicomparison test to the resting T cells. Scale bars are **100 μm**.

3.3 Discussion

Self-assembling FEFEFKFK peptide hydrogel supported human primary T cell cultures under 3D culture settings. T cells retained their viability, responded to the given stimuli and proliferated under these novel *in vitro* culture conditions indicating the potential suitability of peptide hydrogel as a new biomaterial for 3D T cell studies.

Initial experiments demonstrated the robustness of T cells to withstand alkaline conditions in medium and peptide hydrogels. In this study resting CD4+ T cells were used, as these cells at 'quiescent state' tend to be more sensitive to intrinsic- or extrinsic- induced stresses than activated cells [351, 352]**.** This is due to the lack of DNA damage repair machinery in resting T cells, which causes accumulation of DNA lesions and cell death under stressful conditions. On the other hand, stimulated/proliferating T cells have relaxed chromatin structures and active gene expression for DNA repair mechanisms, which prevent cells from apoptosis [351]. High pH levels (7.4 – 11pH) had no significant effect on resting T cell viability, indicating cells' abilities to survive given precursor hydrogel conditions. It is important to take into account that the medium used for T cell culture contained sodium bicarbonate, HEPES buffering agent and exposed to 5% CO_2 which neutralised pH of hydrogel during the gelation process . However, T cells were found in tissues with high pH e.g. cells detected in urine from patients with lupus nephritis and chronic wounds indicating T cells ability to withstand alkaline conditions [353, 354].

T cells cultured in hydrogels with different peptide densities showed a preference to material with the lowest stiffness level (i.e. 283 Pa). This part of the study looked only from mitogen-stimulated T cells perspective, as these cells, once they are activated, undergo expansion by proliferation to deliver the immune response. As predicted, high density of the peptide hydrogel (i.e. stiffness) created limitations for T cell culture, whereas material with the lowest density supported better T cell viability and proliferation response. T cells relies on loose tissues networks which allows them to migrate and induce their function [177, 217, 355, 356]. However, during the disease increased tissue's stiffness level (e.g. metastatic lymph node (330 Pa), breast cancer (> 5 kPa), liver fibrosis (1.6 kPa)) known to impair T cell's function [177, 355, 357-359]. For example, co-infected liver by hepatitis C virus (HCV) and human immunodeficiency virus (HIV) with increased stiffness >7.1kPa had high levels of activated and dysfunctional 'exhausted' T cells, and created imbalance of T cells populations possibly further the liver injury [360]. The negative impact of stiffness is normally down to the excessive deposition of extracellular matrix components (ECM), and the peptide hydrogel mimics its nanofibrous structure [4, 184, 298, 356]. By comparing peptide hydrogel results with other studies, the similar negative effect of high-density tissues or hydrogels on T cells is notable.

Some studies reported different results, and showed a positive impact of high stiffness level on T cell responses. For example, T cells cultured on poly-acrylamide gels had increased proliferation, cell cycle progression and migration on stiffer (100 kPa) than the soft material (0.5 kPa) [361]. This could be

attributed to the porous hydrogels (i.e. large empty spaces), which did not restrain T cells expansion as it would happen in encapsulated nanofibrous structures. Another study, showed cultured T cells greatest proliferation on 50-100 kPa PDMS silicone elastomer than on >2.3 kPa [362]. Once again cells were cultured on the surface of PDMS, rather than being encapsulated. Altogether, the comparison between biomaterials and the mechanical properties effects on T cells should be minded cautiously due to material differences in the architecture and culture dimensions (i.e. 2D versus 3D) [161, 180, 339, 361, 362]. At this point, the peptide hydrogel had an advantage by providing a nanofibrous network which is commonly found in tissues, and with adjusted stiffness level made the 3D T cell culture studies more realistic under in vitro settings.

Opposite to the activated T cells, resting T cells showed poor survival across different hydrogel densities. One of the possible reason was a low T cell concentration in 3D culture. By increasing the number of encapsulated T cells in the peptide hydrogel, the survival of resting T cells evidently improved. Resting T cells are normally cultured at $1x10^6$ cell/ml in the 2D culture settings, whereas current peptide hydrogel experiments used $0.5x10^6$ cells/ml [328, 363, 364]. Miranda-Caru's study (2005) highlighted the importance of T cell contact to maintain their survival via homeostatic proliferation [341]. This was down to an autocrine and juxtacrine method of sharing IL-15 cytokine amongst the cells. Another study argued the importance of high cell density for T cell activation, as anything below $1x10^6$ cells/ml in 2D culture settings resulted in low or absent

activation response [342]. Clearly, the given peptide hydrogels dimension reduced resting T cell survival as T cells are dispersed through 3D space, reducing their of cell-cell contacts. However, T cell viability could also be influenced by other factors such as cells e.g. fibroblastic reticular cells which secrete IL-7, or matrix components such as hyaluronic acid which promote Th1 T cell subtype and survival [127, 365]. This could explain why T cell proliferation and culture expansion was more favoured in Matrigel (hydrogel composed from ECM derived from Engelbreth-Holm-Swarm mouse sarcoma) than polystyrene 3D scaffold when cells were seeded at the same cell density ($1x10^6$ cells/ml) [328]. Future work could consider including extra factors to support T cell survival, but at this point increased cell density in hydrogel was enough to continue the studies.

Moving forwards with 3D T cell culture in the peptide hydrogel, the material's susceptibility to degradation has to be taken into account. In this study, peptide hydrogel stability was affected by an increased number of dead cells and media change process. Due to the nature of the material, where peptides assemble together via non-covalent interactions (i.e. Van der Waals forces, electrostatic interactions) it can be affected by build-up of lactic acid from cells due to increased aerobic glycolysis, or even by accumulation of lysosomal enzymes released by necrotic cells [366-368]. These factors need to be taken into account to control the peptide hydrogel degradation and secure spatiotemporal studies of T cells.

Another challenge associated with the material was the variability of mechanical properties of the peptide hydrogel. It was noted, across many repeats at the same peptide concentration, the hydrogel does not always achieve the same level of stiffness. It is unknown what specific factors could influence the different results, but it is possible that day-to-day hydrogel formation, reagent batch-to-batch difference or even newly prepared media with FCS serum could contribute to the different stiffness levels. Even different repeats with 6 mg/ml peptide hydrogel could cause different T cells responses. As one study reported, T cells express YAP - a mechanosensor in cells [180]. Increased stiffness of tissues i.e. lymph nodes, activate YAP in stimulated T cells which suppresses cell's metabolism, activation and proliferation [180]. This worked as a negative regulation on T cells, where towards the end of infection T cells response is not needed. In addition, YAP suppresses T cells activity against solid tumours, which is likely to due to increased stiffness level limiting cell infiltration [369]. Current results already show reduced T cell proliferation amongst different peptide gel densities (6-10 mg/ml) which support previous studies observations. Small stiffness variation amongst the repeats may have a marginal effect on T cells and deliver reproducible results.

Further studies looked into hydrogel's ability to support resting T cells activation by stimuli. At first, it was decided to use antibody-coated polystyrene particles (i.e. artificial APC) rather than actual cells to stimulate T cells. As at this point, it is unknown how other immune cells such as dendritic cells could react to novel culture conditions provided by the hydrogel. However, antibodies present on

artificial APCs are protein molecules, their stability and biological function could be affected by alkaline conditions of the precursor hydrogel that carried a negative charge (-2) due to high pH (i.e. pH 9) [308, 370, 371]. In exposure to alkaline medium, CD3 and CD28 antibodies functions were not affected, as part of the artificial APC function the antibodies induced T cell activation. Cells had responded to the given stimuli, indicating the robustness of the antibodies to withstand high pH. This also indicates the biocompatibility of the hydrogel as it retains other proteins' biological activity. The addition of media, HEPES buffer agent, frequent media changes and low peptide gel concentration could be all the contributing factors to reduce detrimental effect on the antibodies.

Before T-cell stimulation in the hydrogel, artificial APCs were optimised with antibodies targeting CD3 to deliver 'Signal 1,' and CD28 or CD55 for 'Signal 2' co-stimulation response. Since CD28 is a potent costimulator of T cells, it is important to see if other costimulatory molecules can induce distinctive T cells responses in hydrogel's system. Both co-stimulatory signals target the primed (antigen experienced, memory cells) and naïve T cells populations [348, 372, 373]. CD28 is expressed by 80% of CD4+ T cells, whereas CD55 is found on various cells [374-376]. CD55 (also known as decay-accelerating factor (DAF)) is a complement protein which prevents host cells from proteolytic activity induced by MAC complex formation [348, 377]. Both costimulations are known for their ability to induce the release of pro-inflammatory IFNγ (e.g. Th1) and anti-inflammatory IL-10 cytokines (e.g. Tregs) [348, 378]. However, CD55 induces Tr1 type cells to secrete IL-10, whereas CD28 mainly effects nTregs [363,

375, 379, 380]. Overall two different costimulatory molecules were tested in the peptide hydrogel to indicate the material's support on their function and activation of T cells. In the end, CD3-induced proliferation and cytokine secretion response were amplified by CD28 or CD55 costimulatory molecules.

Artificial APC were carefully produced to allow maximal CD28 and CD55 stimulated T cell response. First, antibody CD3 were optimised to induce sub-optimal T cell proliferation response, followed by full stimulation provided by costimulatory molecules. Memory T cells are known to respond well to CD3 on their own, whereas naïve T cells will only last for a short period of time due to the absence of costimulation signals [381]. In this study, only low concentrations of CD55 and CD28 were needed to induce maximal T cell reaction, as at any higher concentration there was no improved proliferative response. Not many studies have explored the hydrogel system with different costimulation molecules; furthermore, the majority of them only concentrated on CD3 and CD28 combinations [161, 277, 328, 347, 382].

T cells' responses to optimised CD3 and CD28/CD55 stimuli were observed in the peptide hydrogel. But the level of response from 3D culture cells was lower in comparison to the 2D culture. This could be explained by the amount of signal T cells received, as T cells in the 2D culture were surrounded by the APCs i.e. multiple exposure to the stimuli, whereas in 3D culture cell encounter with APCs was limited (based on microscopic image observation). T cell activation occurs once the threshold level is reached by the intracellular signalling events (tyrosine

phosphorylation, MAPK activation, and calcium release) induced by TCRs and CD3 complex [383, 384]. The signalling events accumulate proportionately to the number of TCRs interacting with MHC:peptides presented by the APC, thus this determines T cell activation [385]. A high level of immobilised anti-CD3 will induce T cell activation in a short time space, due to accumulated signalling events in cells. In the presence of co-stimulation, less TCRs/CD3 complex needed to be triggered, as co-stimulation will amplify the signalling events [385]. In the hydrogels, a low concentration of antibodies and low interaction between particles and cells might result in insufficient stimulation response. Whereas in 2D culture, due to given dimensions T cells are surrounded by APC, which eventually provides multiple CD3 binding sites to TCR, giving a bigger stimulation response. A clear distinction between T cell behaviour in 2D and 3D culture was highlighted in Majedi et al. studies (2020), where T cells had higher activation response and IL-2 and TNFα secretion in planar culture than alginate hydrogel [161]. This was due to T cells' frequent encounters with APC in planar surface culture compared to the hydrogel system. Future studies in the peptide hydrogel should consider testing a higher ratio of artificial APC to T cells or further optimisation of the antibodies' concentrations suitable for 3D culture only.

T cells were eventually activated by the artificial APC in the peptide hydrogel, but only if they were exposed to artificial APC coated with 30 μg/mL of CD3 and CD28 antibodies. These antibody concentrations were higher than previously tested ones (i.e. 1 μg/mL CD3 with 5 μg/mL CD28), which indicated T cell stimulation requirements in the hydrogel were different to that in the 2D

culture. T cell stimulation in the hydrogel was evident by proliferation and secreted IFNγ content, and the combination of CD3 with CD28 surpassed the CD3 only response. CD28 co-stimulation amplifies T cell response to CD3, which also improves cell survival (increase of anti-apoptotic proteins e.g. BCL-XL), increases cell cycle progression, metabolism, proliferation and differentiation into effector cells [363, 375, 381, 384, 386]. T cells secreting IFNγ are known as Th1 type cells, and the presentation of CD28 is essential for continued Th1 cell expansion [378]. Other hydrogel-related studies used the same form of stimuli for T cell activation, which approves the FEFEFKFK peptide hydrogel suitability for T cell culture [161, 328, 387].

The time to achieve noticeable T cells' stimulation response in the peptide hydrogels was different to the typical 2D culture settings. Normally under 2D culture settings, combination of CD3 and CD28 induced detectable T cell response over a 1-3 day period, whereas in this hydrogel-based study it took around 7 days [180, 343, 348, 388]. Again, this could be attributed to the given culture dimensions, where T cells in the hydrogel were more dispersed and had reduced the number of contacts with stimuli and cells. However, current results were compared to other tested hydrogels which used CD3 and CD28 antibodies as well for T cell stimulation: a Matrigel and polystyrene hydrogel system took 6 days; alginate hydrogel around 3 days; 5 days in hyaluronic acid hydrogel; and 7 days in the polyethylene glycol (PEG) hydrogel with fibronectin peptides [328, 378, 382, 387]. The difference in T cell responses could be explained by the architecture, biochemical and mechanical properties differences amongst

tested hydrogels. However, FEFEFKFK hydrogel culture fits the time range of T cells stimulation under 3D culture settings, as the majority of reported studies with different hydrogels required longer incubation periods than simple 2D culture systems.

The study was also set up to indicate the required amount of artificial APC to induce the optimal T cell stimulation in the peptide hydrogel. Most of the conditions gave a non-significant difference amongst different ratios of artificial APC to T cells, however the trend of the response (division index) was evident amongst different T cells' donors. The optimum ratio between artificial APC and T cells was reached at ratio 2:1 (APC and cells), as any extra stimuli (i.e. ratio 4:1) did not improve T cell response. The unchanged response at higher concentrations could be explained by the 'restimulation induced cell death', where T cells undergo apoptosis after strong stimulation (in this case high quantity of CD3 and CD28 stimuli), which is thought to be a protective mechanism from creating autoreactive cells [389, 390]. Another explanation could be due to the depletion of available nutrients and build-up of metabolic waste in the hydrogel, essentially 'stalling' the progressive T cell response. During the activation process, T cells increase their glucose, fatty acids and amino acids uptake, and produce lactic acid as a waste product which is known for its inhibitory effect on proliferating cells [386, 391, 392]. However, during the experiments media surrounding hydrogel was changed regularly to maintain cell culture, and prevent accumulation of lactic acid to reduce hydrogel's degradation process. Based on these technical challenges and 'restimulation-

induced cell death', ratio 2:1 of artificial APC to T cells was selected for further studies in the peptide hydrogel.

The selected ratio between APC and T cells is unique to the peptide hydrogel, as other studies with similar stimuli (CD3 and CD28) used different ratios for T cell stimulation. For example: ratio 1:1 of Dynabeads (ThermoFisher scientific) to T cells was used in the Matrigel and polystyrene hydrogel; alginate stimulating particles were seeded at 1:1 ratio to T cells in alginate-RGD functionalised gel; gold nanoparticles with CD3 only were set up at a 1:1 ratio in the PEG hydrogel with fibronectin; and a 1:1 ratio of Dynabeads in PEG hydrogel with heparin [161, 277, 328, 382]. However, some of those studies used functionalised hydrogels with ECM components (i.e. ECM in Matrigel, alginate with RGD sequence, fibronectin peptides and heparin) which could enhance T cell responses as well. For example, fibronectin enhanced T cells binding to the stimuli (i.e. anti-CD3), or heparin bound CCL21 chemokines facilitated better migration and proliferation of T cells within material [277, 393]. Selected ratio 2:1 sustained T cells response in non-functionalised peptide hydrogel, but there is possibility of adjusting the ratio again depending on whether additional biological motifs are added to the material.

In conjunction with this, there was a clear difference in donor-to-donor T cell responses, especially in the magnitude of delivered responses. T cells from different donors still presented the same pattern of results, just some of them were more robust than others. This was especially evident from activated T cells

cultured in different peptide hydrogel densities, as some donors tolerated the new material and proliferated well whereas others delivered a weak or delayed response. T cells were collected from healthy human donors, however age difference, exercise status and diet are known to affect T cell diversity and their function. For example, ageing reduces the naïve T cell pool, exercise promotes high T cell proliferation and cytokine secretion, and a calorie-restricted diet increases CD4+ memory T cell development [394-396]. T cell diversity and function status in healthy donors could be another confounding factor in this research, alongside the effects created by varying properties of the peptide hydrogels. Due to this, careful observations should be made during the research and multiple experimental repeats with different biological donors should be carried out.

Overall, the current results show the T cells ability to adapt to new 3D culture settings and accept the peptide hydrogel as a new culture system. Several challenges related to the hydrogel and T cell culture requirements were dealt with, which also helped to understand the capacity of the material for culturing primary immune cells. The desired results for culturing complex cells can be achieved due to hydrogel's biocompatibility, low-toxicity, and adjustable mechanical properties. For instance, the material supported T cells stimulation by artificial APC which was evident by increased proliferation and secreted cytokines. This was achieved without additional ECM components that are commonly incorporated in other hydrogels for T cell function [277, 382, 387, 397]. Moreover, activated T cells by artificial APC were phenotypically (CD25 and

Ki67) and functionally no different to the T cells cultured in planar culture. It is also important to note that T cells were not activated by negative controls (i.e. beads only, resting T cells), which indicates there are no foreign particles in the hydrogel which could trigger a higher background of T cell response. Nevertheless, future studies should take extra caution of making comparisons between 3D and 2D culture systems. As there were evident differences in time of stimulation, required amount of artificial APC and working antibody concentrations between the two culture systems. Still, the acquired data showed peptide hydrogels compatibility as the novel *in vitro* system which supported viable and functional cells.

Chapter 4 T cell stimulation by dendritic cells in the peptide hydrogel

4.1 Introduction

Normal T cell activation occurs once they interact with APC. T cell's TCR interacts with a cognate antigen presented by MHC Class II found on APC such as B cells, macrophages and dendritic cells (DC) [90]. On the other hand, CD8+ T cells interact with MHC Class I, which is presented by all nucleated cells. APC presents additional co-stimulatory molecules (e.g. OX40L, ICAM1, CD70) and secretes cytokines (e.g. IL-12 for CD4+ Th1 type response) that induce full T cell activation and differentiation into effector cells [347, 398]**.** A current study, demonstrated T cells' activation by artificial APC (antibody CD3 and CD28 coated particles) in the peptide hydrogel. Since T cell stimulation under 3D culture settings proved to be possible, the next study will investigate T cell stimulation by DC, also known as 'principle professional APC' [399, 400].

The primary site of T cell activation occurs in the SLOs such as the lymph node, spleen and mucosa-associated lymphoid tissues [82, 84, 401, 402]. At first, DC exist in an immature state where they constantly 'sample' the environment by increased phagocytosis and micropinocytosis [398, 402]. Once they encounter the antigen, DC become mature cells that upregulate MHC, co-stimulatory molecules and cytokine secretions for T cell activation. Mature DC migrate to

the nearest lymph node from the peripheral tissues to present the antigens to T cells [402]. There are circumstances where T cells and DC interact in non-lymphoid tissues, when instant T cell activation response is required. For example, DC differentiated from blood-derived monocytes activate resident memory T cells (antigen experienced) to eliminate herpes simplex virus infection in sensory dorsal root ganglia [403]. Other studies report non-migrating mature DC in the cancer environment to maintain activated T cell antitumour response [404-406]. In some cases, tertiary lymphoid organ tissue can form in the peripheral tissues, which resemble the lymph node by containing HEVs, and activation zones for T cell and B cells [407]. This mainly occurs in chronic inflammations such as kidney injuries, rheumatoid arthritis and cancer, where they have protective or pathogenic roles [407-410].

The location of T cell encounter with APC occurs in various tissues and 2D *in vitro* studies underrepresent the environment for cells. There are a variety of biomaterials which can be selected to represent specific tissue models to study T cell communication with other cells. Aung et al. (2020) used gelatin hydrogel in a tumour-on-a-chip device to study T cell recruitment mediated by chemokines in presence of monocytes and breast cancer cells [397]. Another study used collagenous extracellular matrix hydrogel as a 3D skin model to analyse dermal fibroblast, keratinocytes and CD4+ T cell communication in response to fungal infection [411]. Furthermore, Daneshmandi et al. (2015) highlighted the differences between the collagen-chitosan scaffold and 2D culture system for DC and T cell interaction [412]. The study showed that DCs in

scaffold upregulated their maturation markers and activated T cell response, which was better than 2D culture [412]. The complexity of tissues cannot be replicated exactly in the biomaterials, but some of the tissue-relevant features can be incorporated to improve *in vitro* studies. To this date no research has studied co-culture between T cells and APC in the self-assembling peptide hydrogels. And the hydrogel itself at 6mg/ml provides the dimensions and stiffness level, which improves current *in vitro* studies [177, 179, 194, 298, 413]. Before establishing the 3D in vitro culture with the peptide hydrogel, it is important to identify if cell-cell interactions are feasible in the biomaterial.

The following hypothesis will test whether peptide hydrogel can host MLR between DC and T cells. Studies will first analyse DC viability in the peptide hydrogel, followed by the 'immunogenicity' studies to indicate whether the material is inert to DC. There is a possibility that the octapeptide could be recognised by DC as a danger/foreign particle that could induce a non-specific immune response. If the hydrogel does not activate DCs, further studies will explore the optimal ratios between cells and whether T cell function can be modulated by conditioned DCs.

4.2 Results

4.2.1 Dendritic cells' viability in the peptide hydrogel

The first step of the research was to understand whether DCs can adapt and retain their viability in the peptide hydrogel before setting up a co-culture study

with T cells. DCs were encapsulated in the 6mg/ml peptide hydrogel and incubated for 7 days. Cells were tested under 3D culture parameters suitable for T cells only, as separate optimisation experiments for DCs were not conducted. This was due to peptide hydrogel's possible modifications towards DCs requirements rather than T cells. DCs were seeded at 10-fold less concentration than T cells following the common ratio 1:10 (DC:T cells) used in the related studies [414, 415]. Two phenotypes of DCs were encapsulated in the peptide hydrogel: immature and mature states. This was to indicate whether DCs at different activation states handle the hydrogel differently.

DCs were obtained from the differentiated monocytes cultured with GM-CSF and IL-4 over 5-7 days. After 5-7 days of differentiation, DCs were further stimulated by Poly:I:C and R848 (viral analogs) for 24 hours to make mDCs, whereas iDCs were rested in medium only. After 24 hours DC were encapsulated in the peptide hydrogel and their viability was assessed with Live/Dead staining.

The encapsulation process of DC was successful, as iDCs and mDCs were viable after 24 hours in the peptide hydrogel (Fig. 4.1 (a)). Cell viability % (mean±SD) was calculated from three distinctive donors, and iDCs retained their viability over the 7 days in the peptide hydrogel (91.43±5.71, Fig. 4.1 (b)). mDCs from some donors showed a decrease of viability by day 7 (56.84±16.59) but with no significant difference to day 1. mDCs secreted IL-12 to initiate the immune response, and the cytokines were detected from the surrounding media of the hydrogel, indicating functional DCs in the biomaterial (Fig. 4.1 (c)). At the

beginning of the studies, IL-12 was detected (mean±SD) from all donor mDCs at low concentrations (12.66±7.40), but by day 7, cytokine levels were diminished. Two donors' iDCs secreted IL-12 at the beginning of the study, however, they were not detectable at a later time point.

Overall, this study indicated the peptide hydrogel's ability to support DCs over 7 days, regardless of their phenotypic states. This suggested T cell stimulation by actual APC is possible, as DCs retained their viability and function in the peptide hydrogel.

(a)

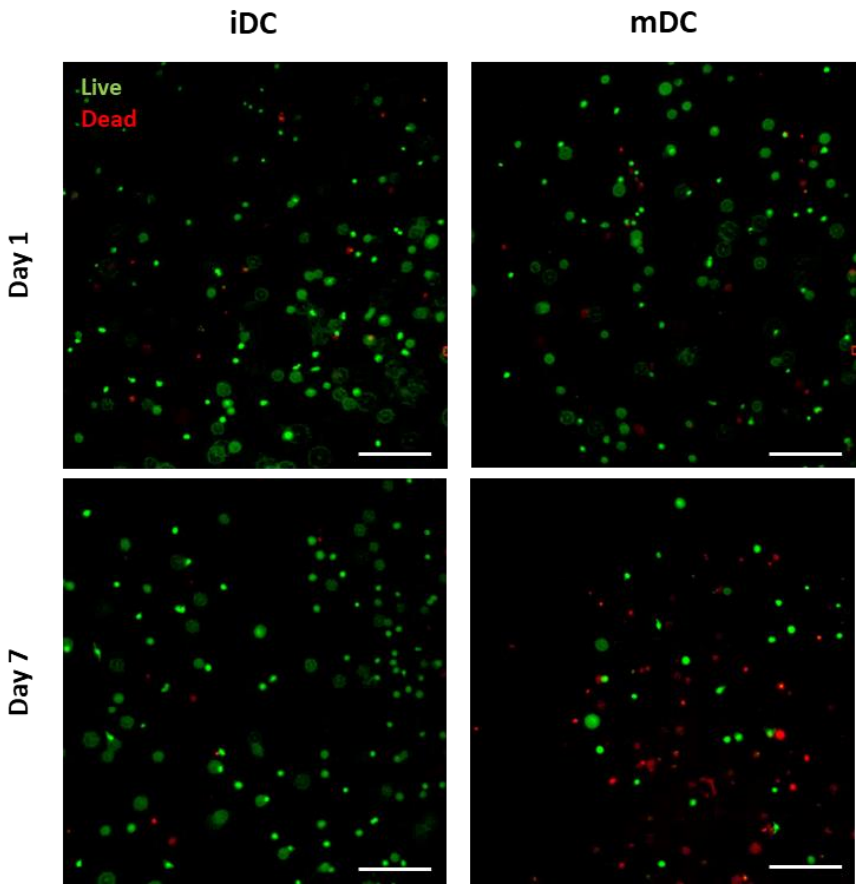
iDC
mDC
Live
Dead
Day 1
Day 7

(b)

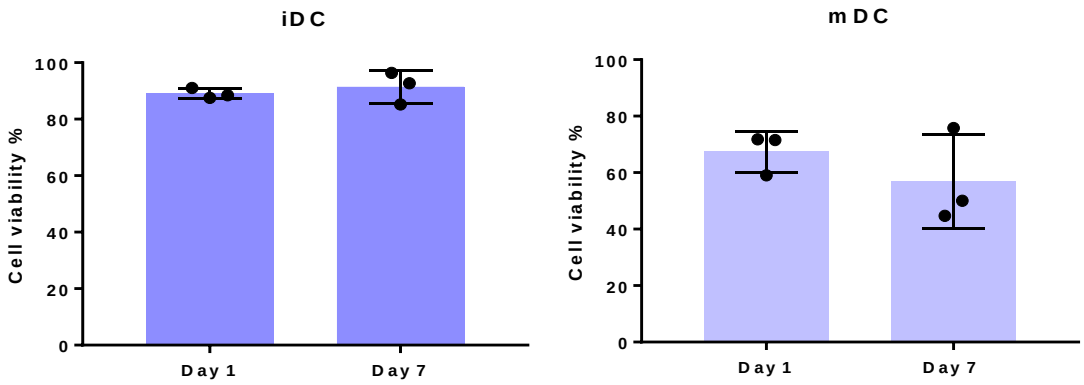
iDC
mDC
Cell viability %
100
80
60
40
20
0
Day 1
Day 7

(c)

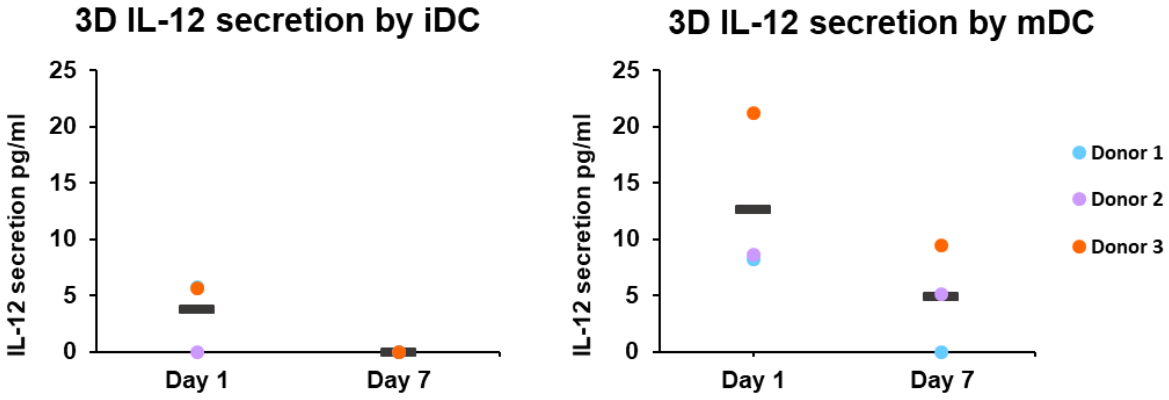
3D IL-12 secretion by iDC
3D IL-12 secretion by mDC
IL-12 secretion pg/ml
25
20
15
10
5
0
Day 1
Day 7
Donor 1
Donor 2
Donor 3

Figure 4.1: Dendritic cells' (DC) viability and cytokine secretion from 6mg/ml peptide gel. mDCs and iDCs were encapsulated in the peptide hydrogel and incubated for 7 days. On days 1 and 7 DC viability was assessed with Live/Dead staining, whereas surrounding media were used for IL-12 cytokine detection. **(a)** Fluorescence microscopic images of encapsulated DC in the hydrogel indicated live and dead cells on day 1 and 7. **(b)** Cell viability % was calculated from three biological independent donors based on Live/Dead fluorescence images, and showed no significant results. **(c)** IL-12 presence in the supernatants were detected by ELISA, with no significant results. Data reports mean±SD in figure **(a)** and only mean in **(c)**. Statistical analyses were set with paired two-tail t-test, scale bars are set at **300μm**, n=3 three biologically independent donors.

4.2.2 Assessing peptide gel ability to induce non-specific immune response

DCs in the immature state constantly 'sample' the environment for the presence of pathogens or danger-related particles which could threaten the system [398]. Some biomaterials could be recognised as the 'non-self' particles and induce DCs maturation response [156]. Conventional T cells are mainly activated by DCs presenting peptide derived antigens [416]. Since the self-assembling peptide hydrogel is composed from the octapeptides, it could be processed and presented by DCs as the 'foreign' particle, and induce T cells' response. If peptide hydrogel has 'immunogenic' (i.e. induces immune response) properties, it will limit further studies due to non-specific immune response to the material. Current experiment indicated whether the peptide hydrogel was inert material and whether the co-culture studies between actual APC and T cells were feasible.

The first part of the study was to investigate whether peptide hydrogel fragments were able to stimulate DCs. 6mg/ml peptide hydrogel with a total volume of 200µL was produced and degraded by constant pipetting to break down the material's structure into fragments. iDCs were cultured in the 96-well plate, and the solution of degraded hydrogel (50µL) was added to the wells. Cells were incubated for 24 hours before further analysis. DCs' response to the hydrogel was analysed by flow cytometry for HLA-DR and CD86 marker expression, which are only upregulated upon DCs' stimulation response [417].

One donor presentation (Fig. 4.2. (a)) of DC population expressing both markers showed that the majority of iDCs incubated with hydrogel fragments showed no upregulation of HLA-DR and CD86 markers. DC with hydrogel fragments retained the same immature phenotype as iDC on their own. The summary graph from three different donors supported the initial observation (mean±SD) and confirmed non-significant difference between iDCs with hydrogel fragments (CD86 0.76±0.19, HLA-DR 19.13±6.97) and iDCs only (CD86 0.6±0.26, HLA-DR 18.6±8.80, Fig. 4.2. (b)). The experiment was also set up with DCs stimulated with Poly:I:C and R848 for 24 hours, which confirmed that all donor cells were functional mDCs. Alongside these studies, media were tested for IL-12 presence. The cytokine was only secreted by mDCs stimulated with viral analogs, whilst nothing was detected from iDCs incubated with hydrogel fragments (Fig. 4.2. (c)).

Another similar question was raised for the encapsulated DCs to indicate whether the intact hydrogel could induce cells' response. This time IL-12 secretions were analysed from the surrounding media and hydrogel itself to analyse any entrapped cytokines (Fig. 4.2. (d)). The IL-12 results confirmed the previous observation, as no cytokines were detected from iDCs cultured in the hydrogel. In contrast, encapsulated mDCs from all donors had secreted the IL-12, but no significant difference was reached to iDCs. This could be explained by donor-to-donor variation, which showed a heterogeneous mDCs response. In addition, mDCs were first stimulated by viral analogues for 24 hours before peptide hydrogel encapsulation. During the encapsulation process cells were

removed from the medium containing stimuli, and cultured without stimuli in the hydrogel. mDCs in the hydrogel 48 hours post-stimulation were unable to secrete as high levels of IL-12 as the 24-hour stimulated (2D culture) mDCs (mDC 24h versus mDC 48h, Fig. 4.2. (c)). Donor-to-donor variation and low IL-12 secretion by mDC could explain the interpretation of the statistic as non-significant results.

In conclusion, peptide hydrogel is an inert material to the DCs. The immature status of the cell was maintained across studies after exposure to the fragmented or intact material. This indicates T cell stimulation response will depend on mature DCs presenting specific stimuli rather than actual peptide hydrogel.

(a)

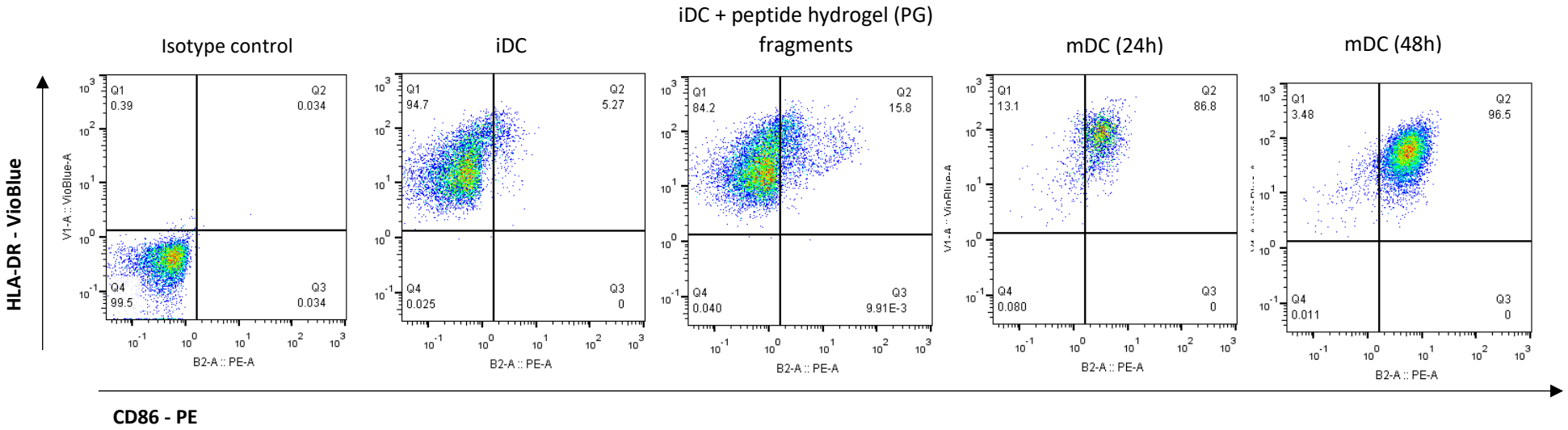
Isotype control
iDC
iDC + peptide hydrogel (PG) fragments
mDC (24h)
mDC (48h)
HLA-DR - VioBlue
CD86 - PE
Q1 0.39
Q2 0.034
Q4 99.5
Q3 0.034
Q1 94.7
Q2 5.27
Q4 0.025
Q3 0
Q1 84.2
Q2 15.8
Q4 0.040
Q3 9.91E-3
Q1 13.1
Q2 86.8
Q4 0.080
Q3 0
Q1 3.48
Q2 96.5
Q4 0.011
Q3 0
B2-A :: PE-A
V1-A :: VioBlue-A

(b)

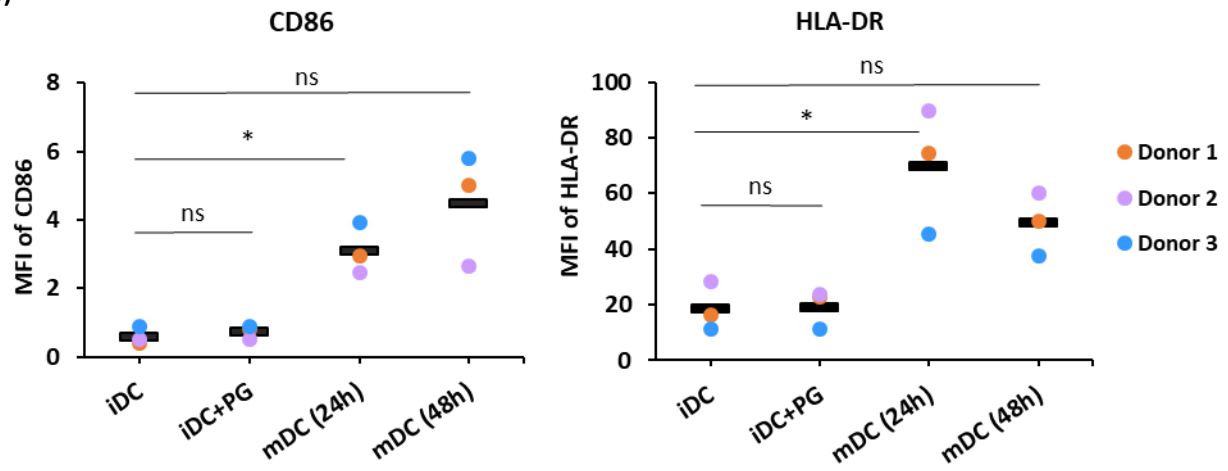
CD86
HLA-DR
MFI of CD86
MFI of HLA-DR
ns
*
ns
iDC
iDC+PG
mDC (24h)
mDC (48h)
Donor 1
Donor 2
Donor 3

(c)

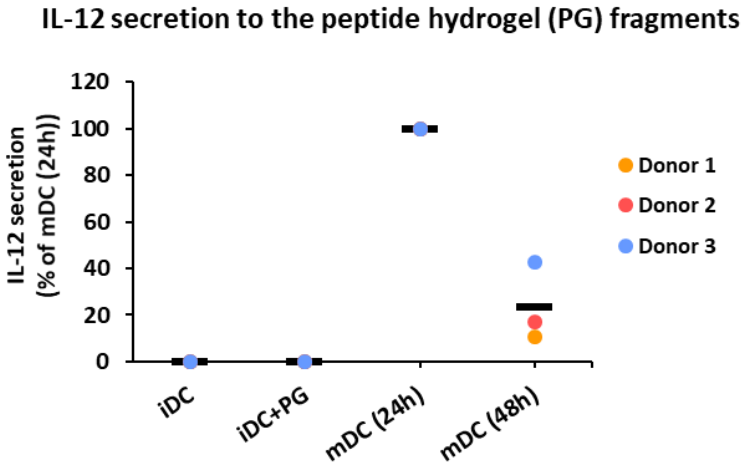
IL-12 secretion to the peptide hydrogel (PG) fragments
IL-12 secretion (% of mDC (24h))
iDC
iDC+PG
mDC (24h)
mDC (48h)
Donor 1
Donor 2
Donor 3

(d)

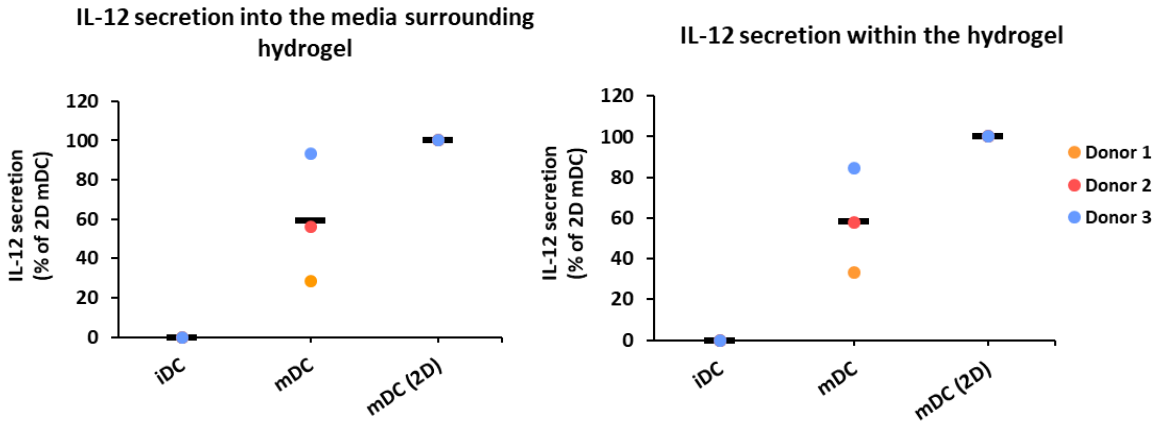

Figure 4.2: Analysing immature DC (iDC) response to the peptide gel. iDCs were incubated in medium culture with peptide hydrogel (PG) fragments or encapsulated in hydrogel for 24 hours. iDCs' response to hydrogel was compared against already stimulated DC (mDC) with viral analogues and iDCs on their own. **(a)** One donor presentation from flow cytometry analyses of CD86 and HLA-DR marker upregulation in response to the hydrogel fragments. **(b)** Summary graphs from three biologically independent donors were reported with MFI values for CD86 and HLA-DR expression. **(c)** IL-12 cytokines presence from DCs cultures were analysed by ELISA, with no significant results. **(d)** iDCs were encapsulated in the peptide hydrogel, and after 24 hours IL-12 were detected from the surrounding media and hydrogel itself, although with no significant results. **MFI = median fluorescence intensity,** statistical test was completed with RM One-way ANOVA with Dunnett's comparison test, and groups were compared against iDC only controls. Data contains mean values only, and $p<0.05$*, from n=3 three biologically independent donors.

4.2.3 Optimal time point for T cell stimulation in response to DC cells in the peptide hydrogel

The peptide hydrogel proved to be biocompatible and inert to DCs, which confirms the continuity of studies without a non-specific immune response. The first question in the co-culture studies is to indicate the optimal time (day) to analyse T cell response to DCs in the peptide hydrogel. As T cells are surrounded with other immune cells, especially live stimulating cells, the stimulation process could be more rapid in the peptide hydrogel than previously tested artificial APCs (antibody coated particles, Fig. 3.14).

The experiment was set up with allogeneic (different donor) immune cells to increase the chance of T cell stimulation by the DC. iDCs and mDCs were prepared with the same procedure as in previous DC-related experiments. T cells (labelled with CFSE) were encapsulated in the peptide hydrogel at constant cell density, whereas DCs density was changed to meet a specific ratio between cells. The reported ratio is based on the number of T cells exposed to one DC (e.g. 1:20, 1 DC to 20 T cells). It is important to note that the established ratios between T cells and artificial APC (Fig. 3.14) for this experiment were not used due to the limited number of DCs that could be obtained from the donor's blood. In addition, live APCs could enhance the peptide hydrogel's degradation process, which could limit the time for 3D cell culture analyses. T cells and mDCs were encapsulated at various ratios, whereas T cells with iDCs were only encapsulated at a 1:10 ratio (Fig. 4.3). This is because iDCs do not stimulate T cells and were used as a negative control to distinguish T cells' response to mDCs. Cells were

encapsulated for 7 days and proliferation was observed by flow cytometry and CFSE dye dilution process.

T cells and DCs were encapsulated in the 6mg/ml peptide hydrogel and after one day of incubation, individual cells were visible in the hydrogel (Fig. 4.3. (a)). T cell's proliferation response to various mDC ratios were confirmed by the flow cytometry (Fig. 4.3. (b)). FSC/SCC pseudocolour plots confirmed T cell induced response by mDC as the cell count gradually increased over the 7 days. However, the T cell response was analysed as CFSE precursor frequency (% of low CFSE, divided cells) with the gate set on the resting T cells (Fig. 4.3. (c)). This was because T cells stimulated by mDCs did not produce distinctive divisional peaks as previously reported T cell response to artificial APC (Fig. 3.14). T cells evidently responded to the mDC as 'CFSE low' peaks appeared by day 7. The summary graph indicates gradual increase of T cell proliferation response to various ratios of mDCs (Fig. 4.3. (d)). Before day 7, T cells across various ratios appeared to be at a resting-unstimulated state, and by day 5 stimulated cells began to appear in response to DCs (Fig. 4.3. (b)). T cells also produced a low response to iDCs, but the same ratio of T cell response to mDC was superior to iDC, confirming T cell stimulation by mDCs in the hydrogel.

Overall, T cells responded to various mDCs ratios in the peptide hydrogel, and the current data agrees with the previous observations made with artificial APC (Fig. 3.13) that the most visible T cell response under 3D culture settings occurs by day 7.

(a)

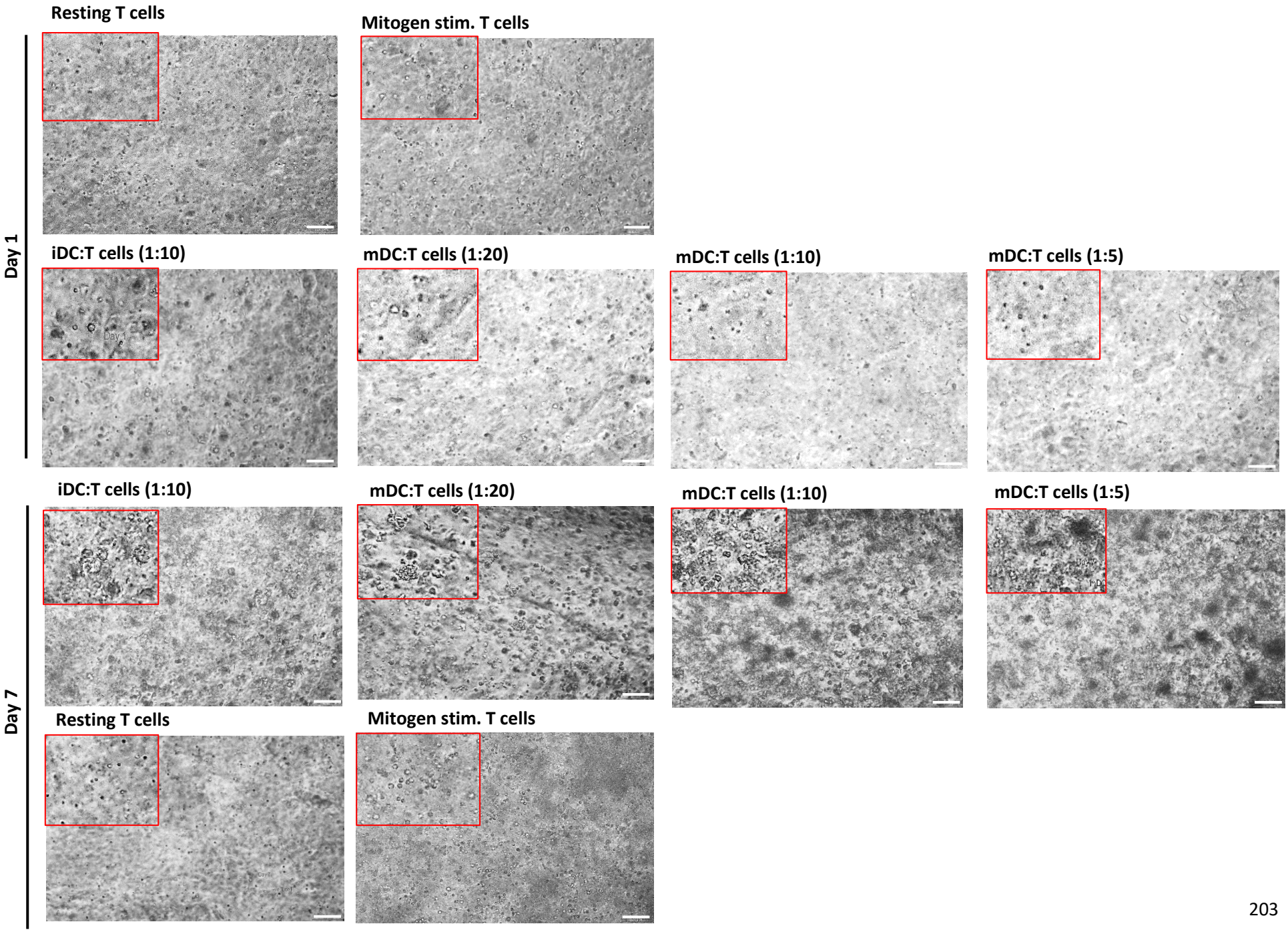
Resting T cells
Mitogen stim. T cells
Day 1
iDC:T cells (1:10)
mDC:T cells (1:20)
mDC:T cells (1:10)
mDC:T cells (1:5)
iDC:T cells (1:10)
mDC:T cells (1:20)
mDC:T cells (1:10)
mDC:T cells (1:5)
Day 7
Resting T cells
Mitogen stim. T cells

(b)

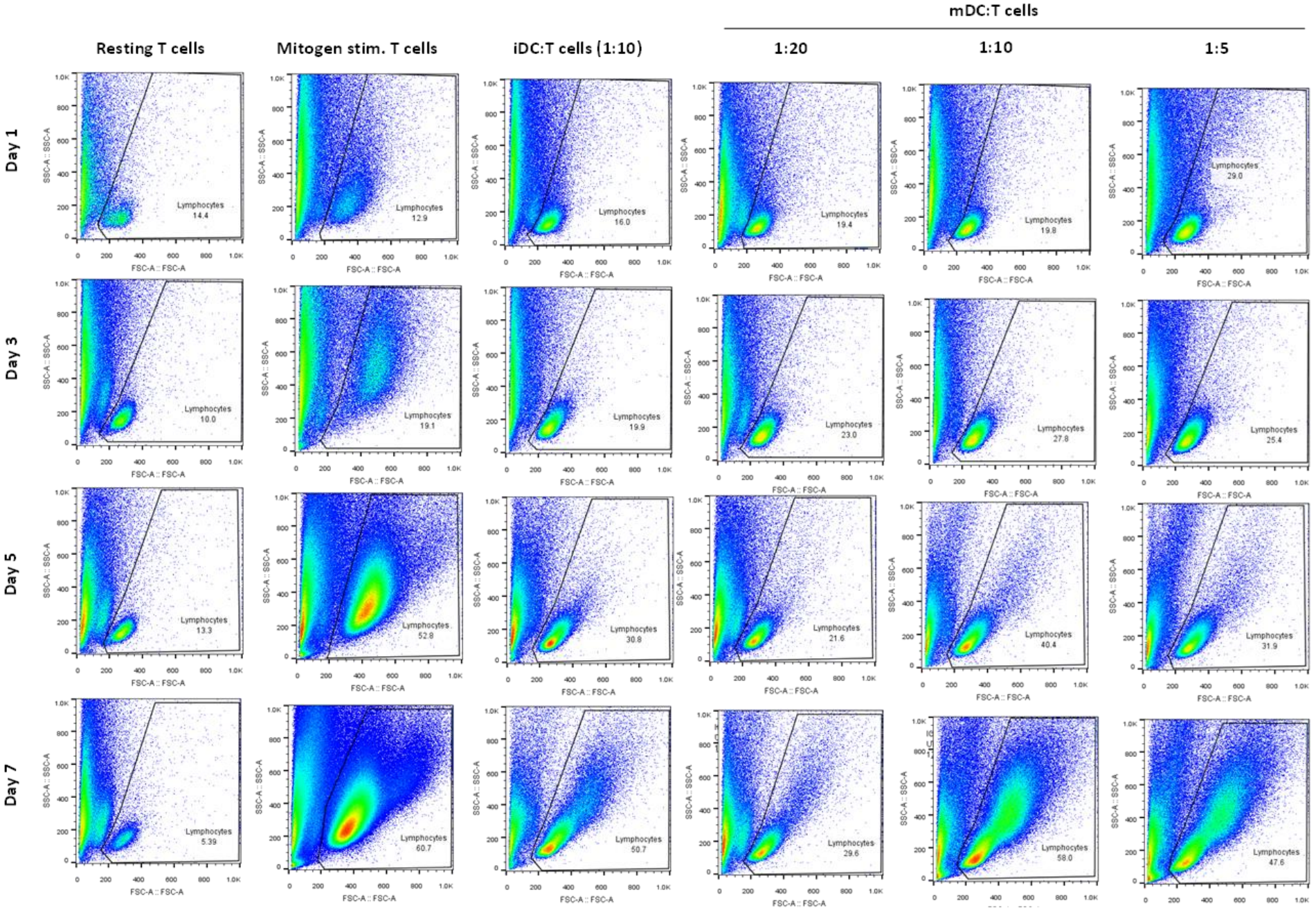
mDC:T cells
Resting T cells
Mitogen stim. T cells
iDC:T cells (1:10)
1:20
1:10
1:5
Day 1
Day 3
Day 5
Day 7
SSC-A :: SSC-A
FSC-A :: FSC-A
Lymphocytes 14.4
Lymphocytes 12.9
Lymphocytes 16.0
Lymphocytes 19.4
Lymphocytes 19.8
Lymphocytes 29.0
Lymphocytes 10.0
Lymphocytes 19.1
Lymphocytes 19.9
Lymphocytes 23.0
Lymphocytes 27.8
Lymphocytes 25.4
Lymphocytes 13.3
Lymphocytes 52.8
Lymphocytes 30.8
Lymphocytes 21.6
Lymphocytes 40.4
Lymphocytes 31.9
Lymphocytes 5.39
Lymphocytes 60.7
Lymphocytes 50.7
Lymphocytes 29.6
Lymphocytes 58.0
Lymphocytes 47.6

(c)

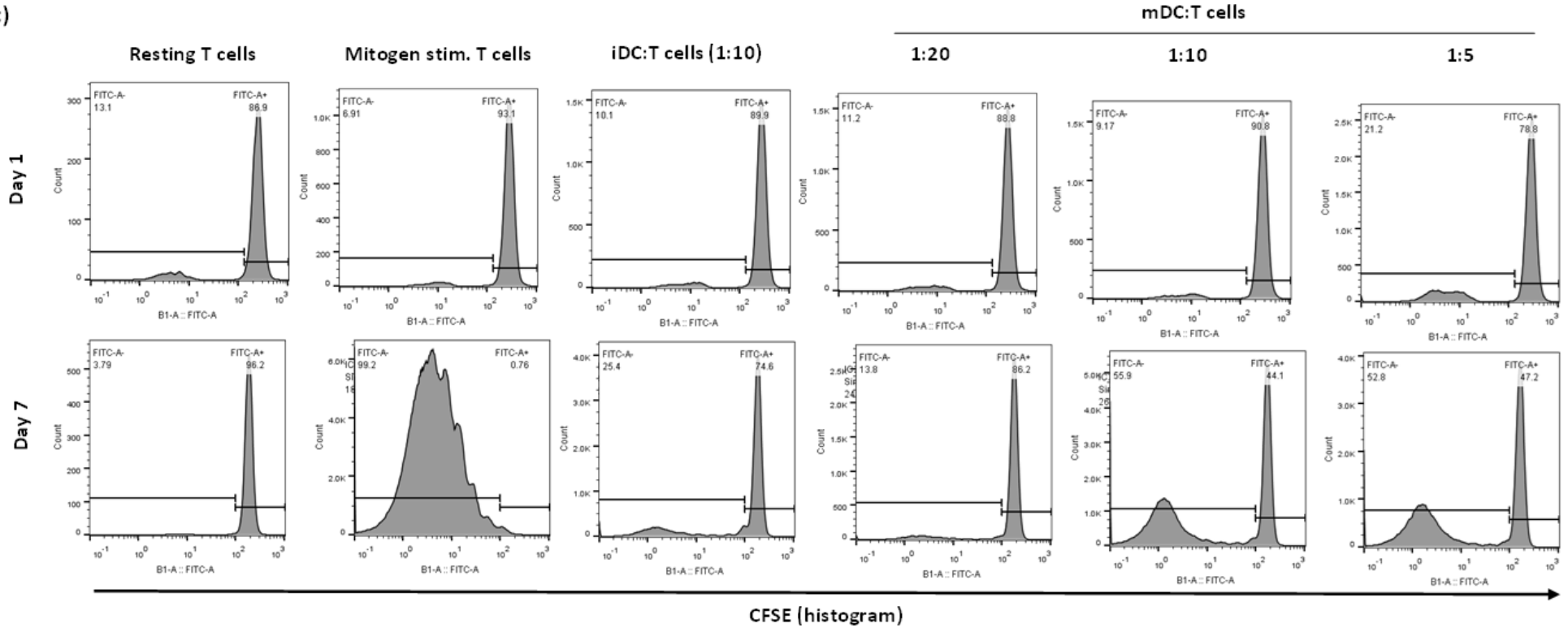
mDC:T cells
Resting T cells
Mitogen stim. T cells
iDC:T cells (1:10)
1:20
1:10
1:5
Day 1
Day 7
Count
B1-A :: FITC-A
CFSE (histogram)

(d)

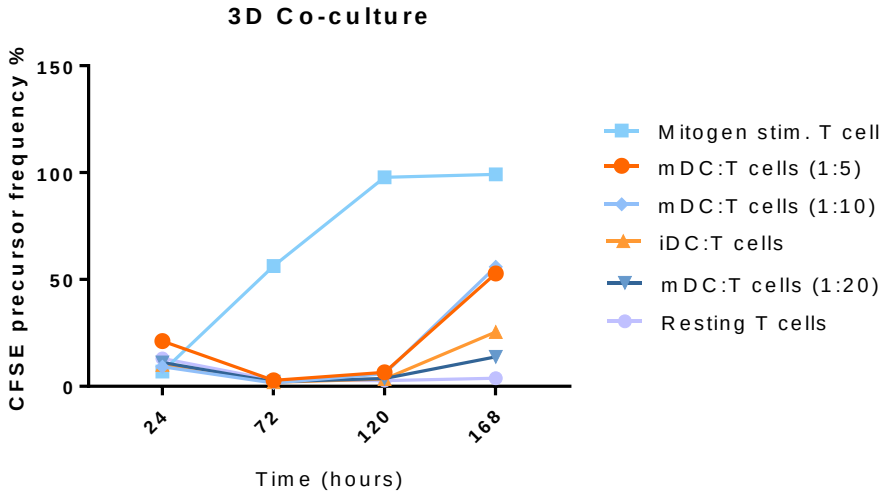
3D Co-culture
CFSE precursor frequency %
150
100
50
0
24
72
120
168
Time (hours)
Mitogen stim. T cell
mDC:T cells (1:5)
mDC:T cells (1:10)
iDC:T cells
mDC:T cells (1:20)
Resting T cells

Figure 4.3: Time point (day) for detectable T cell response to DCs in the peptide hydrogel. DCs were stimulated with viral analogs (mDC) and encapsulated in the peptide hydrogel with CFSE labelled T cells. mDCs were encapsulated at different cell densities to meet the specific ratio to T cells. Hydrogel with co-culture were degraded on the specific days and T cell proliferation was analysed by flow cytometry. **(a)** Light microscopy images of co-culture in the peptide hydrogel on days 1 and 7. **(b)** Cells were released from the hydrogel over 7 days, and proliferation response **(c)** was analysed by CFSE precursor frequency %. **(d)** T cell response to mDC was detected by day 7 (168 hours). The experiment was completed one time. Scale bars represent **100µm**.

4.2.4 Optimal ratio between DCs and T cells in the peptide hydrogel

The previous experiment demonstrated T cells' response to DCs in the peptide hydrogel. T cells were encapsulated at various ratios with mDCs and showed a gradual increase of proliferation response upon decreasing mDCs ratio to T cells (i.e. 1:5 of mDCs to T cells). However, no optimal ratio between different cells was determined in the peptide hydrogel. This study explored different ratios between mDC and T cells in the peptide hydrogel, which guaranteed T cell response no matter the donor variations. The optimal ratio between cells was also determined based on the peptide hydrogel degradation, as co-culture between T cells and APC could cause the hydrogel's structural collapse and limit further 3D culture studies.

The experiment was set up in the same format as previous studies; however, the extra ratio of mDC:T cells (1:2.5) was included as well. This was to increase the chance of detecting the ratio that provided constant T cell response no matter the donor differences in hydrogels. The co-culture studies were set up with allogeneic T cells and DC (different donor cells) in the peptide hydrogel and incubated for 7 days. One donor presentation showed a gradual increase of T cell response by a low T cells ratio to one mDC in the hydrogel (Fig. 4.4 (a)). Most donors presented this gradual increase in T cell stimulation response, except for 'donor 3' cells, which showed no difference amongst various ratios (Fig. 4.4. (b)). However, no significant difference was achieved amongst different co-culture ratios to the resting T cells control. Based on the plotted data from the different

donors, T cell proliferation was increased from 1:10 to 1:2.5 ratio in the peptide hydrogel.

The final decision on the optimal co-culture ratio was based on the structural integrity of the hydrogel. The increased number of encapsulated mDCs to T cells increased the chance for cell-cell encounters, presumably resulting in a greater T cell response. The high T cell response in the peptide hydrogel was reflected by 1:5 and 1:2.5 ratios, which caused a complete structural collapse (Fig. 4.4 (c)). Whereas the ratio at 1:10 retained the hydrogel's structure to a similar level as the peptide hydrogels bearing resting T cells only.

In addition, T cells showed a proliferation response to iDC (1:10) at the same level as T cells cultured with mDC at a 1:5 ratio (Fig. 4.4. (b)). Upon T cells' response to the iDCs, it degraded the hydrogel to the same level as mitogen-activated T cells control (Fig. 4.4 (c)).

In summary, the co-culture between DCs and T cells in the peptide hydrogel was determined to be at 1:10. At this ratio, T cells proliferation and stimulation surpassed the resting T cells control and prevented peptide hydrogels from complete structural collapse.

(a)

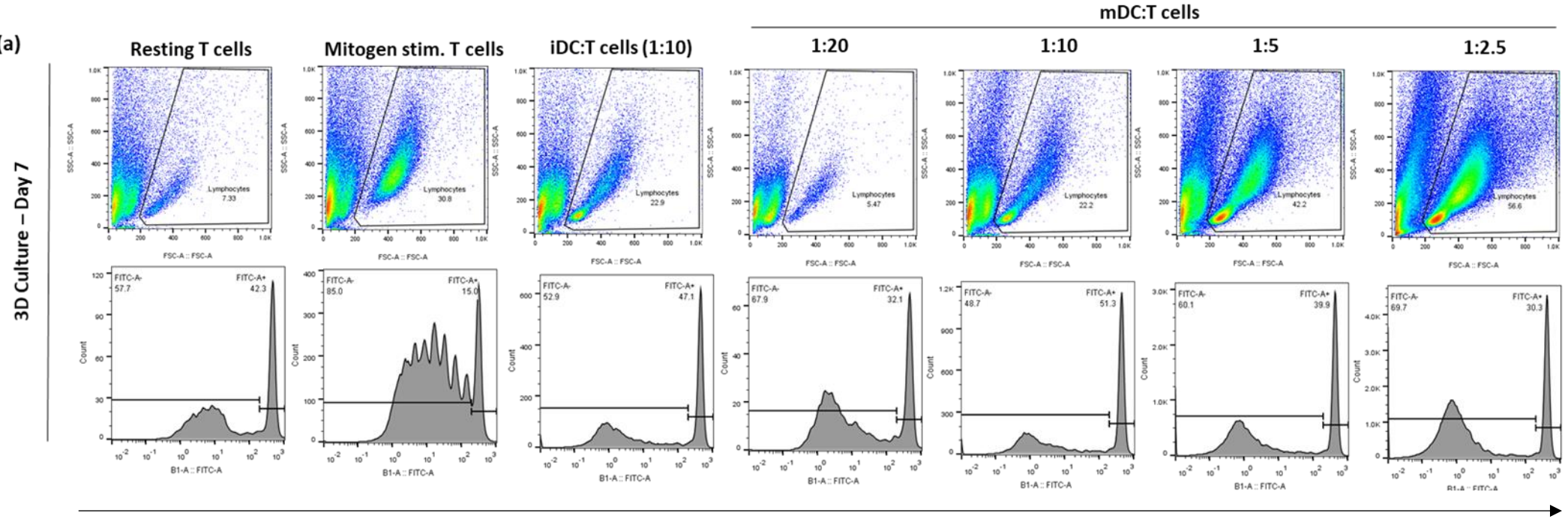
mDC:T cells
Resting T cells
Mitogen stim. T cells
iDC:T cells (1:10)
1:20
1:10
1:5
1:2.5
3D Culture – Day 7
CFSE (histograms)

(b)

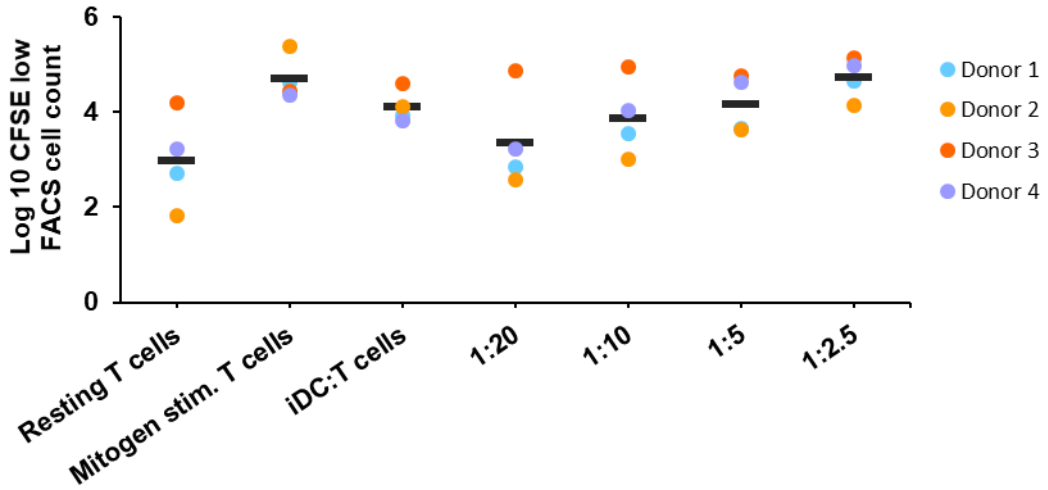
3D MLR - Day 7
Log 10 CFSE low FACS cell count
Donor 1
Donor 2
Donor 3
Donor 4
Resting T cells
Mitogen stim. T cells
iDC:T cells
1:20
1:10
1:5
1:2.5

(c)

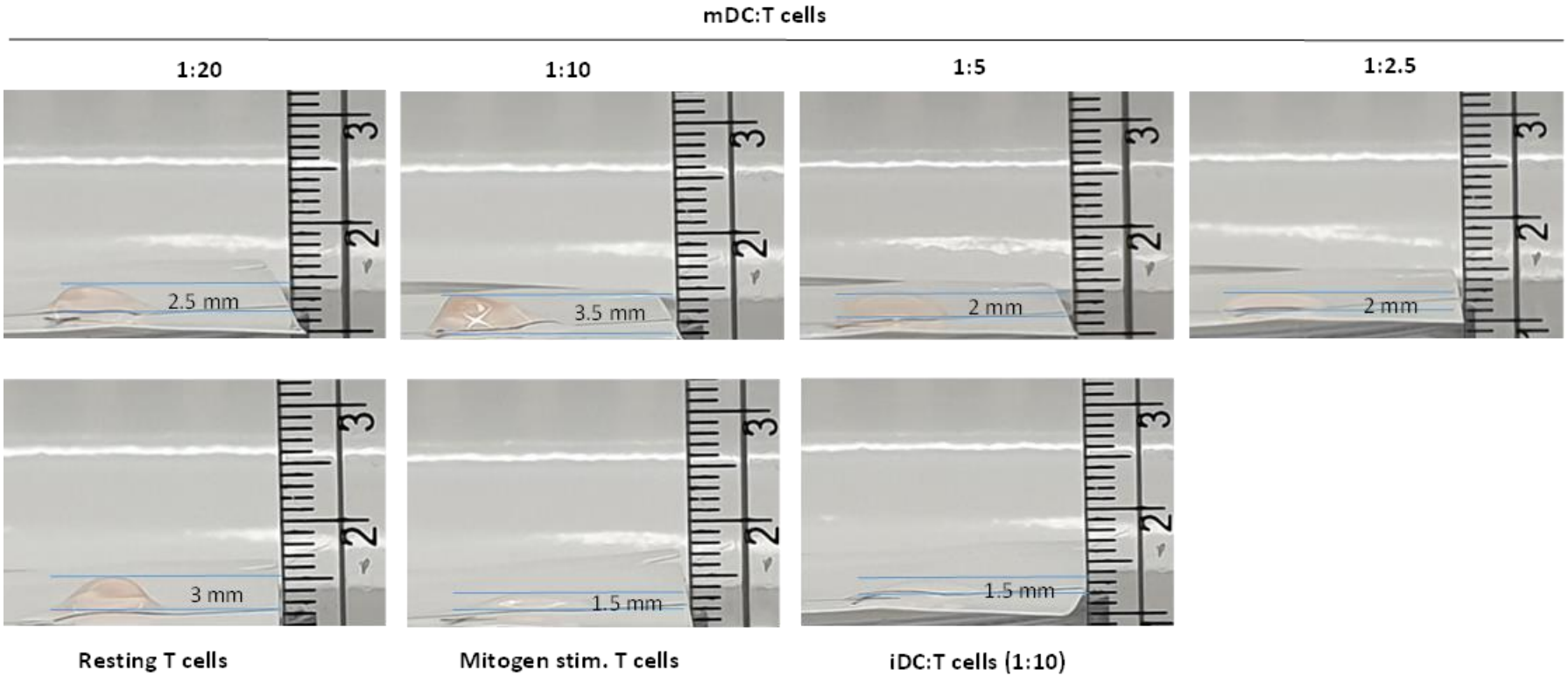

Figure 4.4: Determining the optimal ratio between T cells and DCs in the peptide hydrogel. CFSE labelled T cells and DCs were encapsulated in the peptide hydrogel at various ratios and incubated for 7 days. On the final day, hydrogel's were degraded to release T cells and analysed CFSE dye dilution by flow cytometry. **(a)** One donor flow cytometry data presented T cells response to mDCs at different ratios in the peptide hydrogel. **(b)** Summary graph from four biologically independent donors indicated T cell proliferation response to the mDC cells, with no significant results. **(c)** Images of the peptide hydrgel removed from the inserts on day 7, represented peptide gel's structural degradation due to high T cell proliferation. Statistical analyses were done with RM One-way ANOVA with Dunnett's comparison test to the resting T cells only. Data presented with mean values only, and experiment completed with n=4 biologically independent donors.

4.2.5 Distribution of DC and T cell culture across the peptide hydrogel

Peptide hydrogel supported the co-culture between T cells and DCs, which resulted in T cell proliferation response. However, to this point, there is no indication of whether the cells were equally distributed across the hydrogel, and whether all cells had an equal encounter with DCs in the peptide hydrogel. As the peptide hydrogel 'hosts' different cell types with different phenotypic states (active versus resting T cells; immature versus mature DC), the distinctive cell behaviour could dictate their location in the 3D culture system. Cell distribution across the material could indicate where the initial T cell stimulation response occurs.

The analyses of cell distribution across the intact hydrogel required the fluorescently labelled cells. Before encapsulation in the hydrogel, T cells were labelled with CFSE, whereas DCs were stained with PKH26 dye. The co-culture of cells was incubated for 7 days and analysed by a confocal microscope. Z-stack images were collected from the surface of the hydrogel towards the middle part by 500 µm depth. This was just the portion of the material, as a typical height of the hydrogel (considering some degradation due to T cell proliferation by day 7) ends up around 3000-3500µm (Fig. 4.4 (c)). In addition, cell sizes vary upon activation status and cell types, for example: resting T cells size (in diameter) range from 5-7µm, activated T cells size changes to 12µm, whereas DC ranges from 15-20µm [388, 418, 419]. Considering the cells' sizes, the analysed portion

of the peptide hydrogels is sufficient enough to observe cell distribution across the hydrogel (Fig. 4.5).

The z-stacks were converted first into binary images to demonstrate the distribution of all cells across 500µm peptide hydrogel (Fig. 4.5. (a)). Each cell type controls at different phenotypic states were evenly distributed across the material, without clustering or leaving unoccupied parts of the hydrogel. The binary images of co-culture between T cells and DCs confirmed the same results. The fluorescent images (same as binary) showed the individual T cells and DC distribution across the hydrogels (Fig. 4.5 (b)). T cells labelled with CFSE dye have appeared with a bright green colour for unstimulated/non-divided cells. T cells in the peptide hydrogel appeared evenly distributed, no matter their activation status. However, some stimulated T cells by mitogen or mDCs appeared with 'faded' CFSE colour, which could indicate the cellular division upon diluted CFSE dye. Due to the reduced CFSE fluorescence intensity of activated cells, z-stack images might not show all the cells that underwent several divisions with further dilution of CFSE dye. Resting T cells as the controls or co-culture with iDCs retained the bright CFSE dye and showed even distribution across the hydrogels. PKH26 stained DCs were visible in all controls and co-culture conditions, and appeared to be evenly distributed across the hydrogels.

In conclusion, z-stack images confirmed an even distribution of T cells and DC across the hydrogels. This indicates T cells had an equal opportunity to interact with DCs in the hydrogels. Further analysis is needed to confirm the location of

all activated T cells, as CFSE dye is not sufficient enough to indicate proliferative T cells that could have diluted CFSE dye to an undetectable level by microscope.

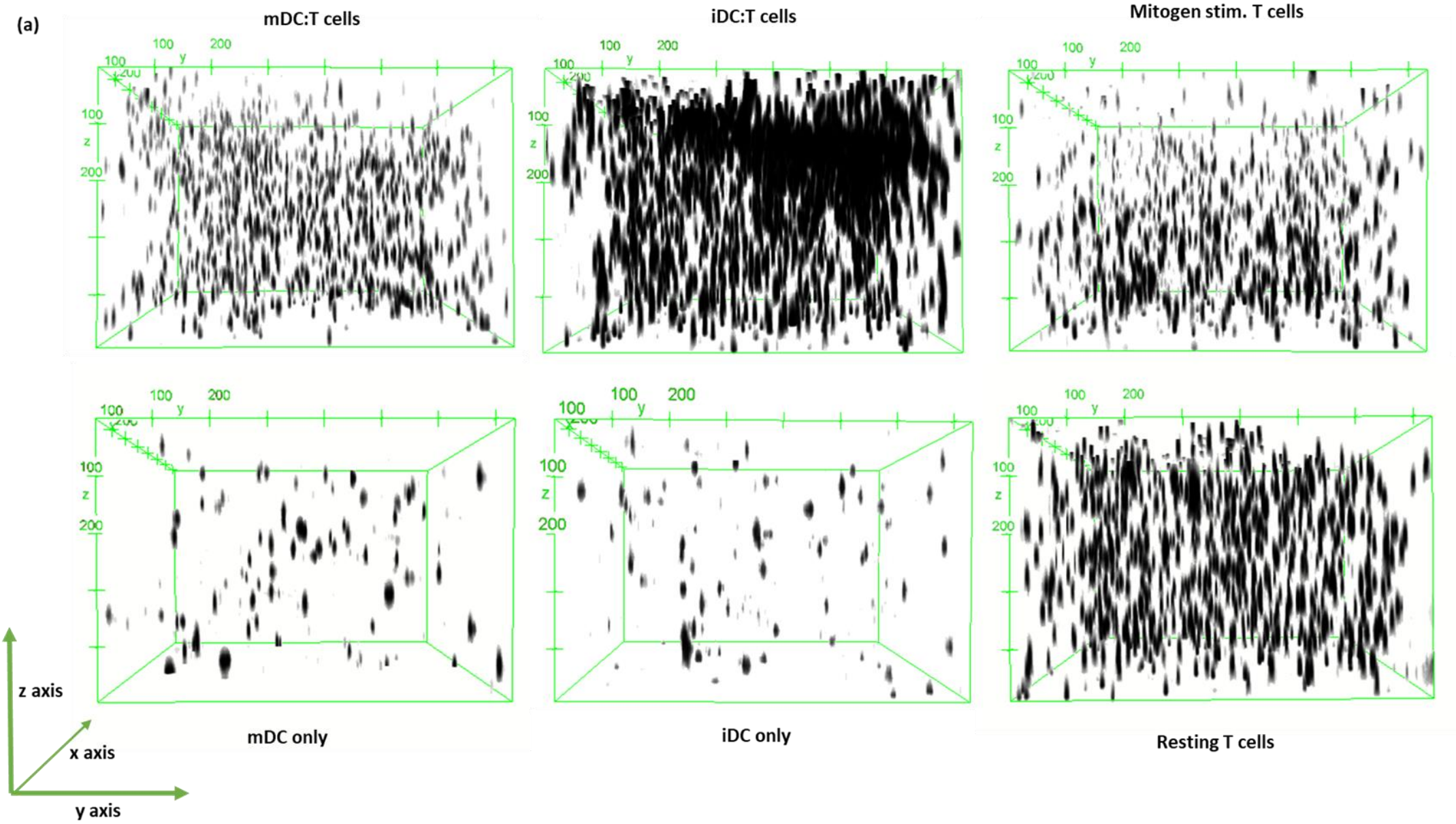
(a)
mDC:T cells
iDC:T cells
Mitogen stim. T cells
mDC only
iDC only
Resting T cells
z axis
x axis
y axis

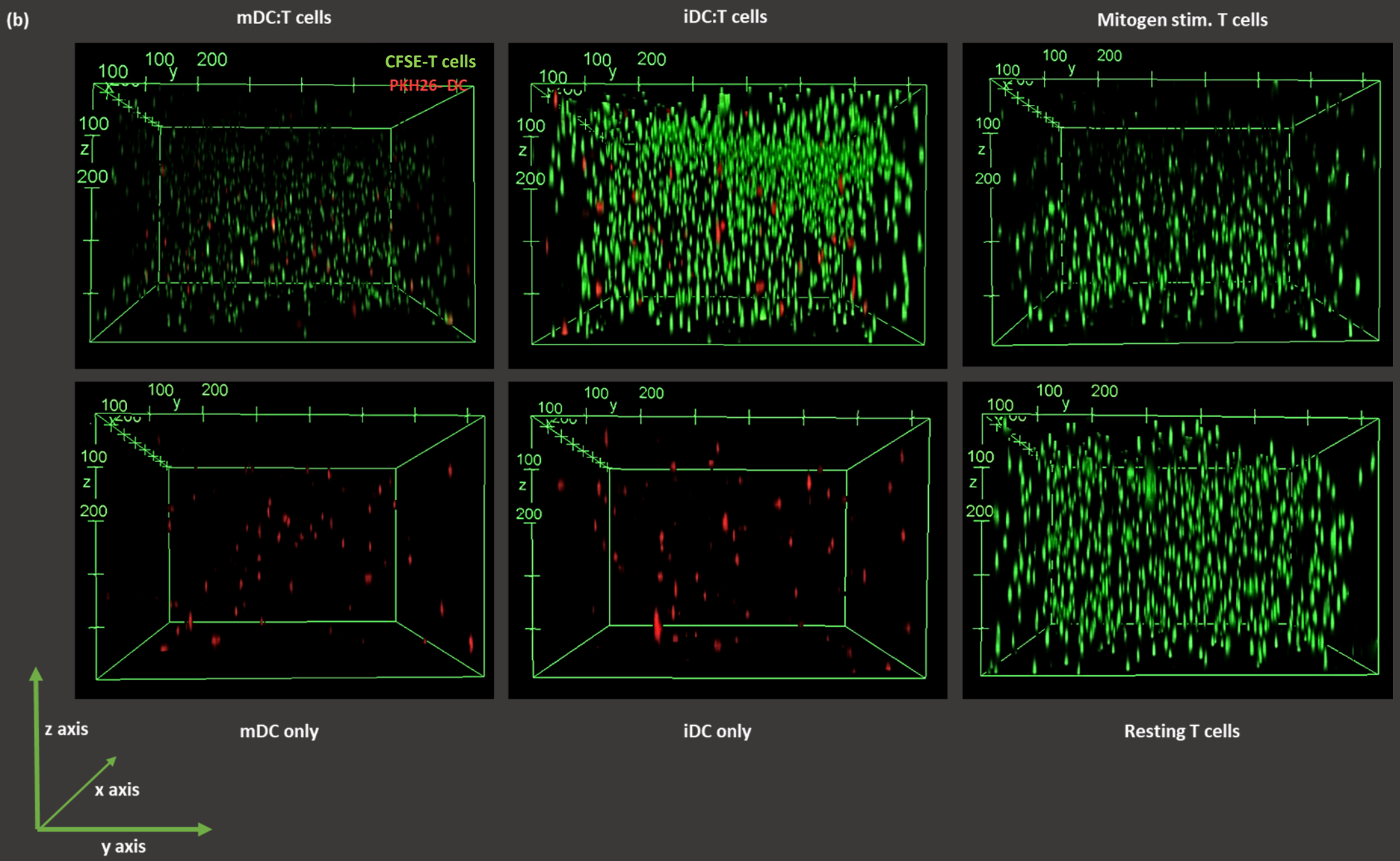
(b)
mDC:T cells
iDC:T cells
Mitogen stim. T cells
CFSE-T cells
PKH26- DC
mDC only
iDC only
Resting T cells
z axis
x axis
y axis

Figure 4.5: Distribution of DC and T cells across 500µm peptide hydrogel. Pre-stained DC (PKH26, red) and T cells (CFSE, green) were encapsulated in the peptide hydrogel at 1:10 ratio and cultured for 7 days. On the final day, peptide hydrogels were removed from the inserts and analysed by confocal microscope with collected z-stacks from the surface towards the middle part of the hydrogel (500µm). **(a)** Binary z-stack image showing all cell distribution across the hydrogel. **(b)** The fluorescence z-stack images indicated DC and T cell distribution in the peptide hydrogel. The experiment was done one time, the coordinates measurements set to µm.

4.2.6 Modulating T cells response with dexamethasone and viral analogs conditioned DC in the peptide hydrogel

Current studies mainly involved mDCs activated with viral analogues, which induced DCs' co-stimulatory marker upregulation and cytokine release for T cell activation. Based on the form of stimuli provided by mDCs, only 'pro-inflammatory' T cell response was analysed in the peptide hydrogel. The 'anti-inflammatory' response on T cells has not been investigated in the hydrogel yet. T cells were cultured with iDCs in the hydrogel, which are also known as tolerogenic cells since they prevent T cells from unnecessary activation response in the absence of pathogen [122]. But to this point, studies have been set up with allogeneic donor cells, where T cell activation against different donor iDCs occurs as well [420]. It is important to see whether the peptide hydrogel permits immunomodulation of T cells by different stimuli delivered by DCs.

In this study, T cells were encapsulated with conditioned DCs, which induced the pro- or anti-inflammatory response of T cells. Before encapsulation, DCs were treated with Poly:I:C and R848 on their own (mDC), or together with Dexamethasone (Dex-mDC), an immunosuppressive drug known to reduce upregulation of costimulatory markers on DC and reduce T cell activation [421]. Autologous (same donor) DCs and T cells were used to determine if T cells purely respond to the given stimulus rather than different donor DCs. Also, instead of pure CD4+ populations, peripheral blood lymphocytes were incubated in the peptide hydrogel so that CD4+ and CD8+ T cell activity could be observed and indicate how widely the hydrogel supports T cell modulation response.

Lymphocytes (stained with CFSE) and DCs were encapsulated at a 1:5 ratio instead of the established 1:10 ratio, to increase the sufficient numbers of CD4+ and CD8+ responding T cells and T cell stimulation by autologous DC.

Before encapsulation in hydrogel, DCs co-stimulatory molecules were checked to detect whether DCs had responded correctly to the distinctive treatments. CD86 and HLA-DR (mean±SD) expression was higher in mDC (CD86 294.66±88.26, HLA-DR 399.66±39.80) and there was a clear reduction of marker expression in mDC treated with dexamethasone (CD86 200±93, HLA-DR 339±28.05, Fig. 4.6. (a-b)). Once DC proved to respond correctly to the drugs, cells were encapsulated with peripheral blood lymphocytes. On day 7, flow cytometry analyses from one donor showed that lymphocytes had responded to the presence of DC, by comparing against resting T cells only (Fig. 4.6. (b)). In each condition, CD4+ and CD8+ were detected and each T cell phenotype was analysed separately for induced proliferation response (CFSE low counts).

T cells responded to the DCs in the peptide hydrogel in comparison to resting T cells only on FSC/SCC pseudocolour plots (Fig. 4.6 (c)). Each co-culture condition had CD4+ and CD8+ populations present, which were further analysed for proliferation response against treated DCs. Only donor 1 showed a distinctive CD4+ and CD8+ T cells response to differently treated DCs cells, especially with reduced response to mDC-Dex treated cells (Fig. 4.6 (d)). Furthermore, donor 2 showed a small difference of T cells responses to mDC-Dex against mDCs only, whereas no distinctive responses were detected from T cells from donor 3. The

mean values from three different donors represented the same trend for CD4+ and CD8+ T cells' responses, but due to heterogeneous responses no significant differences were achieved. This means more repeats with different donors are required to confirm T cells' modulation response in the peptide hydrogel.

From the same donors, media was tested for IFNγ to confirm T cells' modulated response. The summary graph reports the mean value from all three donors and indicates over 5 days T cells' stimulation by mDC-Dex was reduced (Fig. 4.6 (e)). The level of IFNγ secreted by T cells was lower with mDC-Dex than mDCs co-culture. However, there was evident donor variation in this study (Fig. 4.6 (f)), as on day 5 two donors reduced cytokine secretion upon mDC-Dex exposure, whereas donor 1 showed opposite results. Due to donor variations and limited number of repeats, the results were defined as non-significant between mDC-Dex and mDCs cultured T cells.

In summary, the peptide hydrogel showed its ability to host different phenotype T cells, but further studies are needed to confirm T cells' modulation response by pro- and anti-inflammatory DCs. There is indication that T cells responded as expected to mDC-Dex treated cells in the hydrogel, but due to heterogeneous response and donor variations, more repeats are needed to achieve significant results.

(a)

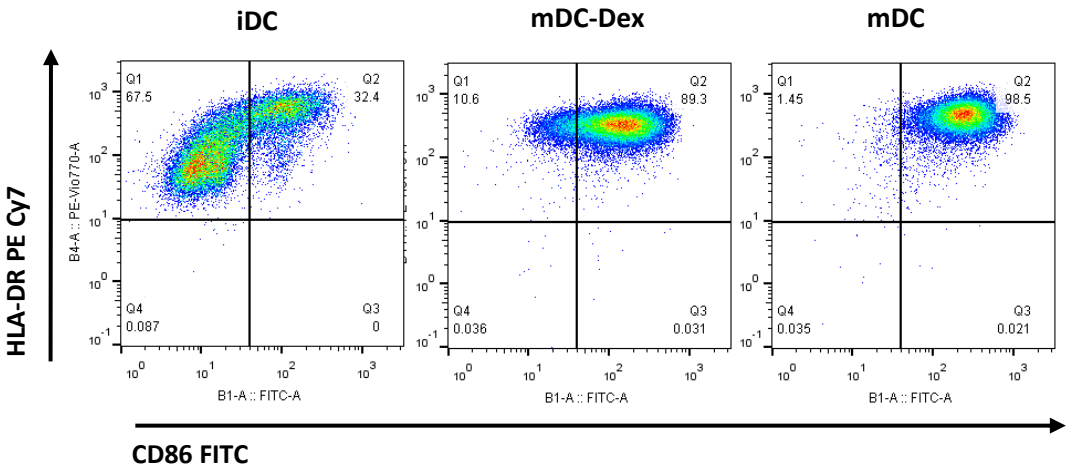
iDC
mDC-Dex
mDC
HLA-DR PE Cy7
CD86 FITC
B4-A :: PE-Vio770-A
B1-A :: FITC-A
Q1 67.5
Q2 32.4
Q4 0.087
Q3 0
Q1 10.6
Q2 89.3
Q4 0.036
Q3 0.031
Q1 1.45
Q2 98.5
Q4 0.035
Q3 0.021

(b)

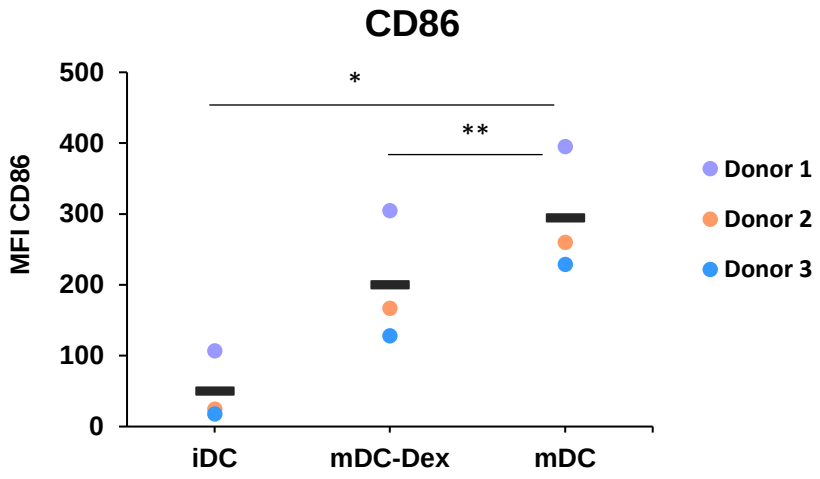
CD86
MFI CD86
500
400
300
200
100
0
*
**
iDC
mDC-Dex
mDC
Donor 1
Donor 2
Donor 3

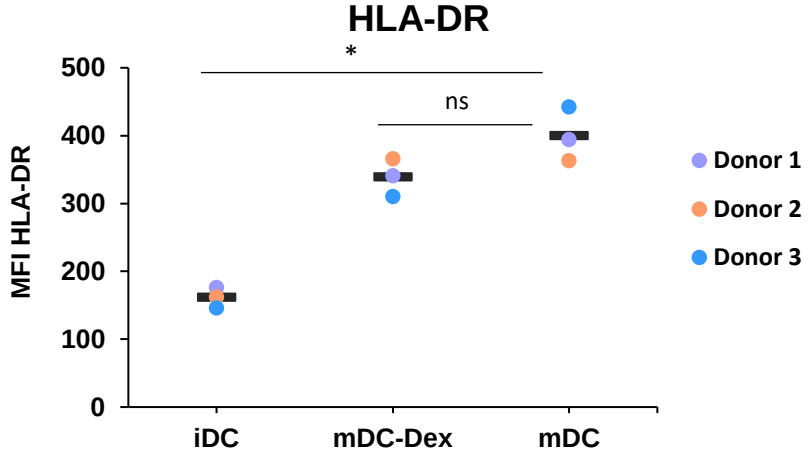
HLA-DR
MFI HLA-DR
500
400
300
200
100
0
*
ns
iDC
mDC-Dex
mDC
Donor 1
Donor 2
Donor 3

(c)

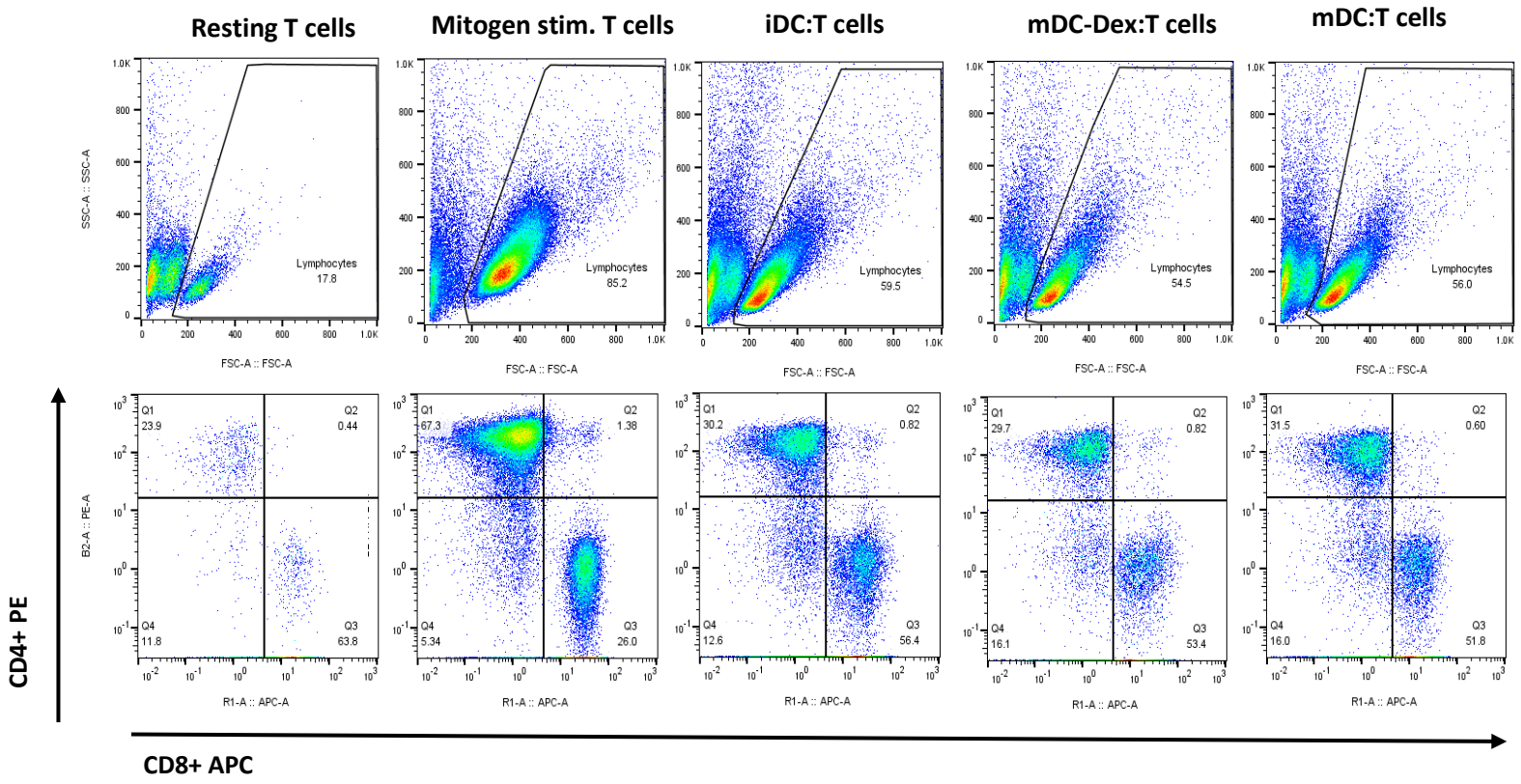
Resting T cells
Mitogen stim. T cells
iDC:T cells
mDC-Dex:T cells
mDC:T cells
SSC-A :: SSC-A
FSC-A :: FSC-A
Lymphocytes
17.8
85.2
59.5
54.5
56.0
B2-A :: PE-A
R1-A :: APC-A
Q1
Q2
Q3
Q4
23.9
0.44
11.8
63.8
67.3
1.38
5.34
26.0
30.2
0.82
12.6
56.4
29.7
0.82
16.1
53.4
31.5
0.60
16.0
51.8
CD4+ PE
CD8+ APC

(d)

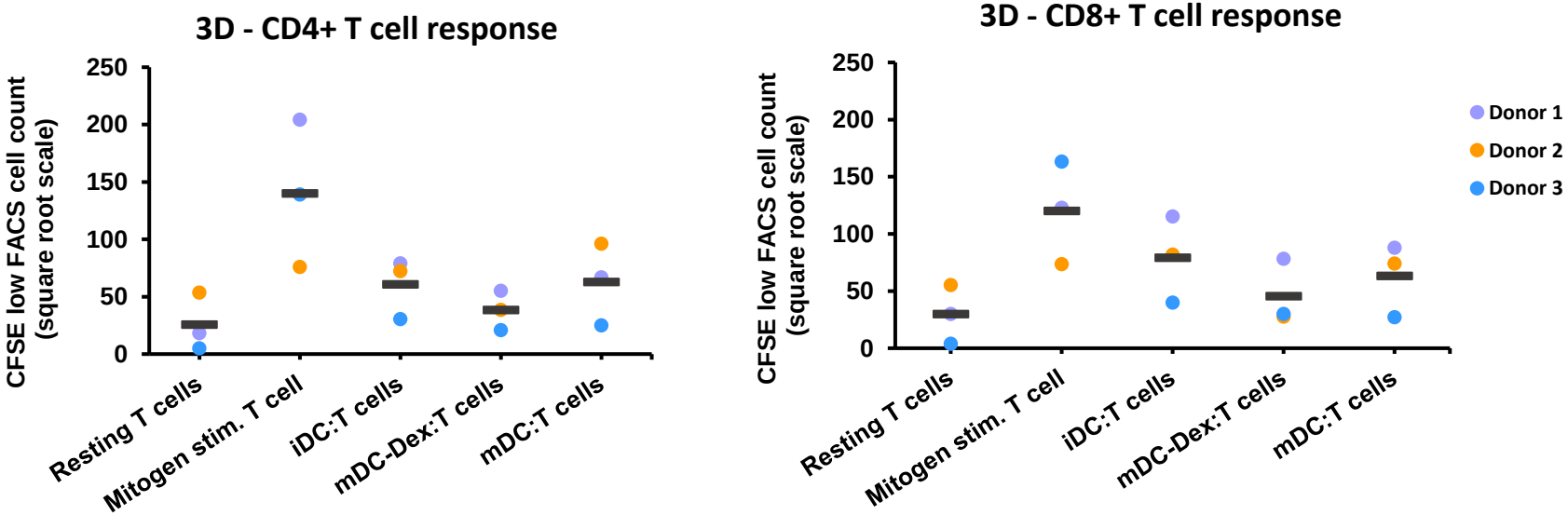
3D - CD4+ T cell response
3D - CD8+ T cell response
CFSE low FACS cell count
(square root scale)
250
200
150
100
50
0
Resting T cells
Mitogen stim. T cell
iDC:T cells
mDC-Dex:T cells
mDC:T cells
Donor 1
Donor 2
Donor 3

(e)

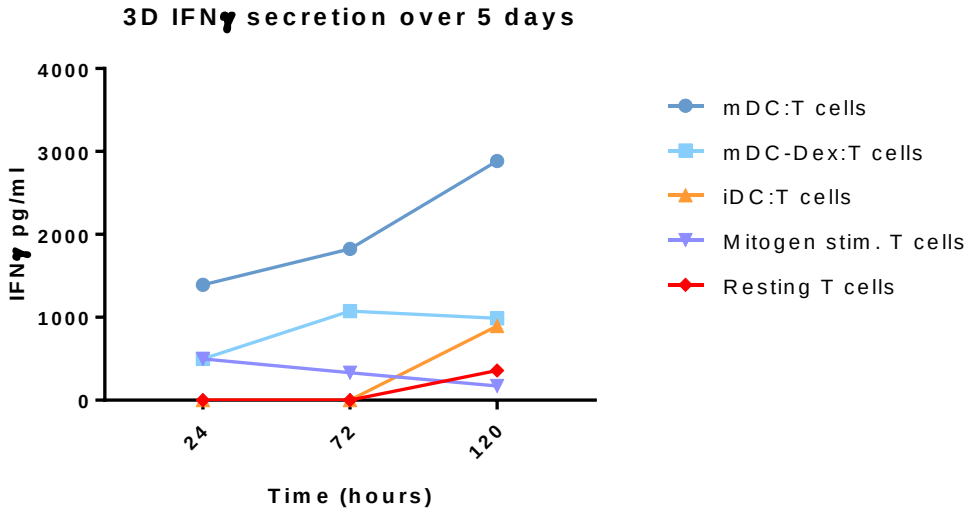

(f)

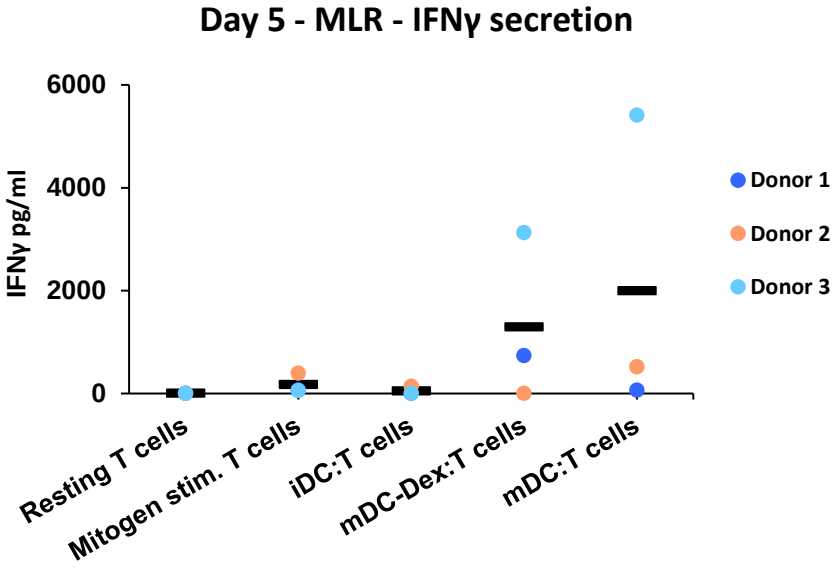

Figure 4.5: Modulating CD4+ and CD8+ T cell function with conditioned DC in the peptide hydrogel. Pre-treated DC were encapsulated with peripheral blood lymphocytes (contain CD4+ and CD8+ T cells) in the peptide hydrogel at 1:5 ratio and incubated for 7 days. **(a)** Before encapsulation the level of HLA-DR and CD86 marker expression were checked on DCs by flow cytometry. **(b)** Summary graphs from three donors showed marker expression level of conditioned DC. **(c)** One donor presentation of released lymphocytes from the peptide hydrogel on day 7, and further analyses of selected cells to define CD4+ and CD8+ T cell population. Each population was separately analysed for proliferation (CFSE low cell count) in response to conditioned DCs. No significant results were achieved amongst the groups. **(d)** Summary graph from 3 donors indicated no significant CD4+ and CD8+ proliferation response to DC. **(e)** Secreted IFNγ was analysed by ELISA over 5 day co-culture incubation. **(f)** Summary graph from all three donors presented individual values of IFNγ cytokine secretion on day 5 with no significant results. **MFI = median fluorescence intensity.** Statistical analyses RM One-Way ANOVA for CD86/HLA-DR expression **(a)** with Dunnett's comparison test to mDC control, and for the rest of data Tukey's multiple comparison test was used. Data presented with mean values only, $p<0.05$*, $p<0.01$ **, from n=3 biologically independent donors.

4.3 Discussion

Current data suggests peptide hydrogels' ability to support complex immune cell co-culture systems, a step closer towards 3D *in vitro* culture studies. The material itself was inert to the DCs, ensuring the absence of non-specific immune response. DCs activated T cells based on the cell's increased proliferation response, commonly found in in vitro and in vivo studies. The biomaterial proved to be biocompatible to various immune cells, indicating great potential for future studies.

Before T cell encapsulation with DCs, a key question was raised in regards to DC behaviour in the hydrogel. DC are a completely different set of immune cells that are phenotypically and functionally distinctive to T cells. However, the peptide hydrogel was not modified to support these professional APCs as it will lose its ability to support basic T cell functions. In this case, it was important to indicate whether the given parameters of the hydrogel were acceptable for the DCs culture. Fortunately, iDC and mDC states proved to be viable in the peptide hydrogel and secreted IL-12 after 7 days of incubation in the hydrogel. There was a minor reduction in mDC viability compared to iDC, which was more so attributed to the cell behaviour rather than the cause of peptide hydrogels. After antigen exposure in the peripheral tissues, mDCs usually last for 1-3 days until they undergo apoptosis [175, 422]. In this short period, mDC migrated to the closest lymph node, activated T cells, lost their motility and eventually committed cell death [175, 402]. This is part of immune tolerance, as persistent activity of mDC could lead to chronic T cell proliferation and the development of

autoimmune disease [423, 424]. By the time the mDCs were encapsulated, cells were post-24h stimulation with the viral analogues, which could also explain why mDCs' viability was lower than iDCs in the peptide hydrogel. Overall, the reduced viability of mDCs is down to the mechanism of immune tolerance response, rather than peptide hydrogel.

Furthermore, mDCs secreted IL-12 in hydrogel but cytokine levels were low in comparison to other in vitro studies [425-427]. IL-12 is important for stimulating T cells, especially for T cell helper type 1 (Th1), which secrete IFNγ to induce pro-inflammatory response [428]. Upon mDCs stimulation, the IL-12 is mostly secreted between 10-18 hours, followed by a gradual decrease at later points in time [429]. This could also influence T cell activation in the peptide hydrogel, since by the time of encapsulation, IL-12 sources are getting exhausted.

Peptide hydrogel itself did not activate DC, which reduced the risks of non-specific T cell response. DC exposed to the peptide hydrogel remained in an immature state without upregulation of costimulatory markers, MHC molecules and IL-12 secretion, which are all important for T cell activation. It is well known that materials can be recognised the by immune system and induce 'foreign body response', thus resulting in cell activation and material's rejection [430, 431]. This phenomenon occurs once specific physical or chemical properties of the material activates DCs, such as: hydrophobic properties of the polylactic acid (PLA), degraded fragments of hyaluronic acid, and spatial properties (pores) of collagen-chitosan scaffold [431-434]. DCs' reaction to the biomaterials occurs

via PRRs, which are conserved sets of receptor-recognising patterns of the pathogen or damage-related molecules. PRRs such as TLR4 recognise lipopolysaccharide (LPS) of the bacterial cell wall, but also recognise fragments of the hyaluronic acid [430, 431]. Chitosan is also known to induce DC maturation due to its ability to interact with TLR4 [435]. Chitosan is also viewed as a potential vaccine adjuvant (enhanced immune response), or as a novel 3D culture system to study DC and T cell interactions [412, 435]. Clearly in some studies, misinterpretation could occur when 3D culture gives a better response than 2D culture, as the actual immune response was induced or enhanced by the material itself. This gives another advantage to the FEFEFKFK based hydrogels, as their inert state leaves the immune response to be initiated by cells only. Moreover, one study tested FEFEFKFK peptide hydrogel activation by macrophages, another APC, which showed a non-inflammatory response [337].

T cells were encapsulated with DC in the peptide hydrogel and required a 7-day incubation to detect a noticeable T cell response. The amount of time T cells required to be stimulated by actual APC was similar to artificial APC (antibody-coated particles) timings, but at a much lower ratio than T cells with artificial APC. As one cell, DC provides more MHC (interacting with T cells' TCR), costimulating molecules and secreting cytokines rather than artificial APC, which explains lower quantity of DC needed to induce T cell activation in the peptide hydrogel [347, 398]. Typical T cell activation in the lymph nodes takes between 3-5 days wherein they then migrate to the peripheral tissues [175, 414, 436]. However, extra time in the peptide hydrogel could be added by the physical

barrier of the gel, delaying cell-cell interaction. It is possible that slight remodelling of material occurred by cells (e.g. degradation due to metabolic waste) allowed T cell and APC interactions. At this point, not many studies have analysed T cell responses after 7 days of incubation to actual APC (i.e. DC). One study incubated cells for 17 hours in the polystyrene scaffold, whereas collagen-chitosan-based scaffold cultured cells for 72 hours [412, 437]. This indicated the co-culture incubation is subjective to the research question and the type of material used.

The peptide hydrogel supported various ratios of T cells and DCs, but the 10:1 ratio was ideal for T cell response and integrity of the hydrogel. Once DCs were added at higher quantities (increasing T cell ratio per DC) the gel underwent structural collapse, losing its 3D culture feature. The explanation relies on the high metabolism of activated T cells (discussed in Chapter 3) and presence of DCs. On the other hand, hydrogel's degradation was noted even at the lowest DC density, where no T cell response was identified. This could be attributed to the dying DC population releasing apoptotic cell's contents with degrading capabilities [419]. Overall, the 10:1 ratio between cells has been used in other 3D and 2D culture systems, indicating the peptide hydrogel's suitability for supporting typical MLR [412, 414, 437].

In the co-culture studies, T cells also seemed to respond to encapsulated iDCs when cultured at the same ratio as mDCs (10:1). Results from iDC-only cultures showed the absence of costimulatory molecules and IL-12 in the peptide

hydrogel. This explanation could rely on several factors: either T cells recognised different donor (allogeneic) self-antigens presented on MHC Class I molecules of DC, which then induced T cells response [420, 438]; there was better iDC viability than mDC, which resulted in a frequent encounter between cells [347, 423]; or the presence of animal-derived serum proteins in media activated iDC and contributed to T cell activation [439]. With consideration of these factors, T cell response to the iDCs should be taken cautiously and not be interpreted on the same level as mDC and T cell co-culture.

From the co-culture perspective, encapsulated DCs and T cells were evenly distributed through the peptide hydrogel. Cell distribution was analysed at the final time point of an experiment to indicate cell location after prolonged incubation. Cells were located from the top of the hydrogel towards the middle, indicating there was an even chance for T cells and DC to interact with each other. In other words, the immune response likely occurred from the entire hydrogel.

One important question that remained unanswered was the location of proliferating cells in the peptide hydrogel. In 3D culture, activated T cells' CFSE dye was noticed to be diluted towards the top surface rather than the middle part of the intact hydrogel, which could indicate cell proliferation in the hydrogel. One study cultured bone marrow stromal cells (OP9-DL) in a microgel made from gelatin and polyethylene glycol, to replicate the thymus environment and induce T cell lineage generation [271]. At the beginning of the experiment,

cells were present within the microgel but by day 7, but most of the cells were allocated towards the surface of the material. It was suspected that cells migrated towards the surface due to greater nutrient exposure and larger surface area for adhesion. In the peptide hydrogel, mDCs could be located more towards the hydrogel's surface due to nutrient, oxygen or adhesion (surface area) requirements and T cells were attracted to the cytokines/chemokines secreted by DCs. This type of T cell behaviour and possible factors influencing cellular organization need to be analysed further.

In addition to co-culture studies, there is preliminary data indicating peptide hydrogels' ability to support immunomodulatory effect by DCs on T cells. Although the results proved to be non-significant due to the low sample number and donor variation, the pattern of response was evident on CD4+ and CD8+ T cells from most donors. Dexamethasone treated DC (mDC-Dex) had affected costimulatory molecule expression and IL-12 secretion, which are both vital components for T cell stimulation [421]. In the presence mDC-Dex, T cells reduced their proliferation and IFNγ secretion showing the immunosuppressive effect in the peptide hydrogel. The initial data indicates peptide hydrogels' ability to support T cell responses according to the given stimuli i.e. DCs, but more studies are needed to confirm the significance of the results.

Various biomaterials have been used to support immune cells' co-culture system under 3D culture settings. But careful selection of material is important, especially when most dynamic and easily polarised cells like T cells and DC are

studied. One example includes alginate cross-linked hydrogels, which relies on Ca^{2+} for the gelation process [440]. Ca^{2+} is important for alginate crosslinking, but any left residues could affect a cell's function since Ca^{2+} is also important for signalling pathways in immune cells. Prior studies have confirmed enhanced dendritic cell maturation via increased cytokine secretion, MHC and co-stimulatory molecules which were attributed to the Ca^{2+}presence [161, 441, 442]. This provides another advantage to the self-assembling peptide hydrogels, as a biomaterial has no factors that could modulate or induce unexpected cell function. In conclusion, observed T cell responses to the conditioned DC were genuinely induced by the immune cells rather than material itself.

Future studies should consider the DC maturation process within hydrogel, and avoid pre-treatment of cells before the encapsulation process. This would help to increase the quantity of viable and functional mDCs for T cells in the peptide hydrogel. This could be done by encapsulating cells with viral peptides or bacterial components (i.e. LPS) which could be processed and presented to the nearby T cells. One previous study used RADA16 self-assembling peptide gels, which encapsulated DC with tumour antigens and anti-PD1 antibodies [332]. The hydrogel was injected into tumour-bearing mice and recruited T cells to induce anti-tumour response. This study proved hydrogels ability to preserve added molecules and allow appropriate immune cell response. Similar methods should be considered with FEFEFKFK peptide hydrogels, where cognate antigens with immune cells are encapsulated together.

In conclusion, peptide hydrogels could be used for 3D co-culture studies. It supported basic T cell interactions with DC, which delivered expected T cells responses. As a material, peptide hydrogel is inert to DC with no adverse chemical/physical factors that could influence cell's responses. The observed T cell responses were genuine to the DC only, which justifies the continuation of studies on T cell functions.

Chapter 5 T cell function in matrix protein functionalised peptide hydrogel (and 3D *in vitro* therapy analyses)

5.1 Introduction

Various studies have used functionalised biomaterials to portray the tissue microenvironment and study their influence on cells [166, 277, 397, 443-446]. The presence of extracellular matrix (ECM) components influence distinctive cell morphology and function when compared to unmodified materials and simple 2D cultures [161, 164, 382]. Furthermore, several investigators examined the effect of functionalised self-assembling peptide hydrogels on cells [300, 305, 308, 447]. However, there is a paucity of similar studies concerning the impact of functionalised FEFEFKFK hydrogels on cells of the immune system. This leaves an open question whether encapsulated immune cells can respond to the environment generated with modified peptide gels.

T cells are found throughout the body and interact with ECM components to mediate their function [323, 448-451]. For example, T cells interact with collagen via integrins, αβ heterodimeric proteins which mediate T cell adhesion and migration through the tissue matrix [196, 452]. The same function of T cells is mediated by fibronectin, a major glycoprotein commonly found in the interstitial tissue matrix [448, 453, 454]. Fibronectin also provides co-stimulatory effect for

T cells by interacting with α4β1 integrin on cells and promote IL-2 and IL-2 receptor synthesis for cells [393, 455, 456]. It also supports effector/memory T cell survival of via α5β1, which known to increase Bcl-2 (anti-apoptotic) molecule and prevent from activation induced cell death (AICD) [323, 457]. Moreover, hyaluronic acid (HA) a glycosaminoglycan (GAG), interacts with CD44 expressed on activated and memory T cells [365, 458]. Depending on the molecular weight of HA, it can regulate T cell migration, proliferation, and tolerance [188, 190]. Other GAG molecules bind to chemokines and cytokines which indirectly affect T cell activity [176, 191, 459]. For example, heparin sulphate in the spleen binds to IL-2 and promotes T cell activation [460]. The list of various ECM components and their influence on T cells is extensive and growing, emphasising the potential impact of functionalising biomaterials to replicate tissue specific environments [461, 462].

A small number of studies have investigated the effect of functionalised biomaterials on T cell biology. Depending on the research question, specific ECM components were either integrated into synthetic biomaterials or the biomaterial itself was made from the ECM component [164, 281, 328, 382, 463]. For example, poly(ethylene)glycol (PEG) was functionalised with heparin to sequester CCL21 to mimic the lymph node environment resulting in enhanced T cell proliferation in comparison to conventional culture [277]. Kim et al. (2015) employed hydrogel made from fibrin-collagen, which promoted T cell interactions with the stromal cells, recreating 'T cell zones' found in the lymph nodes [273]. It is clear from these and other studies that functionalised

biomaterials augment 3D *in vitro* cell culture systems likely by recreating a more physiological microenvironment than standard culture systems [161, 166, 443, 446].

Functionalised self-assembling peptide gels have been used as a platform for various cell lines to generate 3D tissue models [300, 305, 308, 447]. The material proved to be easily modified with ECM components by adding either selected proteins, proteoglycans or even allowing cells naturally to deposit ECM themselves [308, 309, 311, 464]. This trait is a key advantage for 3D culture studies, as peptide gels could be modified with known ECM components to mimic a specific tissue microenvironment. Moreover, the functionalisation process is less complicated by comparing to other hydrogel systems, which commonly require chemical cross-linking or bioconjugation to retain ECM components in the material [287]. In some cases, the functionalisation process is toxic to cells, conferring a further advantage to the peptide gel as it retains viable and functional cells [287, 465, 466].

In this study, peptide gel was functionalised with plasma fibronectin and collagen type I prior to population with T-cells. Fibronectin enhances T cell stimulation and interaction with the nearby cells and promotes survival of activated T cells [467]. During inflammation, plasma fibronectin accumulates in damaged tissue areas and forms networks to restore normal ECM [468, 469]. However, the presence of other ECM proteins can affect the fibronectin structure, for example collagen induces polarisation of fibronectin as well [470-

473]. In this case, hydrogel will be functionalised with both ECM components to provide T cells with tissue's relevant features under in vitro settings.

The main hypothesis of this study is: the presence of ECM proteins in the peptide hydrogel influences T cell function. As previously mentioned, ECM proteins (notably fibronectin) provide co-stimulatory effect for T cells once they are activated by the APC. Therefore, we tested the co-stimulatory effect of Fibronectin and Collagen on T cells stimulated by APC, specifically laboratory-generated monocyte-derived DC. We hypothesised that T cell responses would be modified by the presence of fibronectin or collagen. Lastly, we utilised functionalised peptide gel to support the T-cell response to primary DC, namely peripheral CD1c+ cells. Circulating CD1c+ DC are potent T-cell activating APC that are the subject of recent clinical trial as adoptive immunotherapy for malignant melanoma (EudraCT number: 2019-003391-39, UK).

5.2 Results

5.2.1 The effect of matrix proteins on T cell stimulation

Many studies addressed the influence of fibronectin and collagen on T cell function. Some studies reported inhibitory or stimulatory effects on T cell activity, but due to distinctive forms of stimulation, culture settings (3D versus 2D) and type of biomaterial used there is no defined optimal concentration of both matrix proteins [323, 382, 393, 474, 475]. This complicated the decision of starting concentrations of gel and ECM to be used in the peptide gel as it was

ambiguous weather these variables would exert a positive or negative impact on T-cell responses. To understand to what extent fibronectin and collagen influence T cells behaviour, experiments were initially conducted in 2D culture. The key aim of this experiment was to evaluate whether T cell activation and response to the stimulus was affected by the presence of ECM.

The experiment was set up in a pre-coated plate with fibronectin and collagen proteins at various concentrations. T cells were incubated, with polystyrene beads coated with 1µg/ml anti-CD3 stimulating antibody (an artificial APC), at ratio 8:1 (T cells: artificial APC). The selected lower ratio was used to prevent overstimulation (TCR crosslinking) by large number of APC.

T-cell stimulation by artificial APC was improved in the presence of fibronectin and collagen (Fig. 5.1 (a)). The level of response varied amongst donors, but all of them showed improved stimulation response in presence of matrix proteins. The summary graph of all donors indicates that fibronectin had a greater effect on T cells than collagen (Fig. 5.1 (b)). However, the addition of collagen to a constant fibronectin concentration seemed to diminish the fibronectin effect on cells. For example, fibronectin at 11µg/ml enhanced T cell responses, but collagen reduced this effect. Collagen at 100µg/ml appeared to influence cells on the same level, no matter what fibronectin concentration was present. Except, from the highest fibronectin concentrations (i.e. 100µg/ml), where collagen presence reduced T cell response. But collagen on its own did not achieve significant results compared to fibronectin on its own.

In conclusion, the presence matrix proteins enhanced T cell responses in our study of 2D cultures and matrix proteins therefore may influence T cell functions as described in similar studies [382, 393, 475]. For the peptide hydrogel, fibronectin from 3.6-33µg/ml was selected to be tested with a constant collagen concentration (33µg/ml). Fibronectin at 100µg/ml was not selected for the peptide gel, as 33µg/ml reached significant results. Fibronectin on its own will be also studied in the peptide gel, as it showed an improved T cell response in the absence of collagen.

(a)

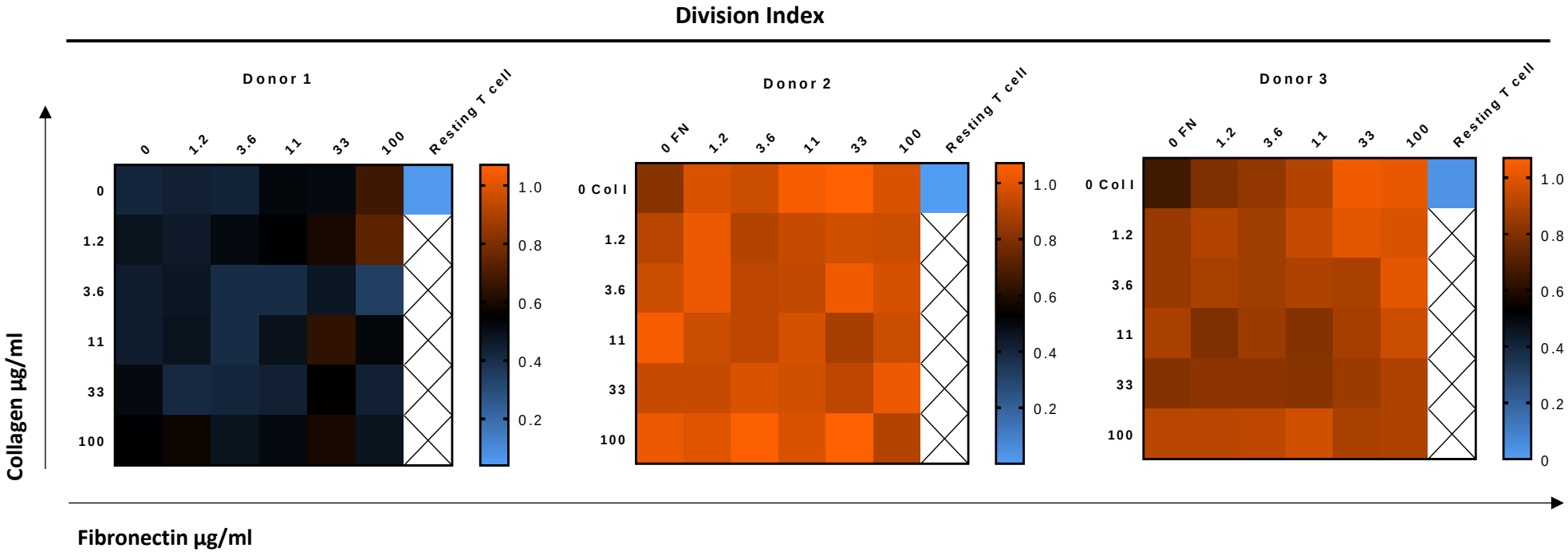
Division Index
Donor 1
Donor 2
Donor 3
0
1.2
3.6
11
33
100
0 FN
0 Coll
Resting T cell
1.0
0.8
0.6
0.4
0.2
0
Collagen µg/ml
Fibronectin µg/ml

(b)

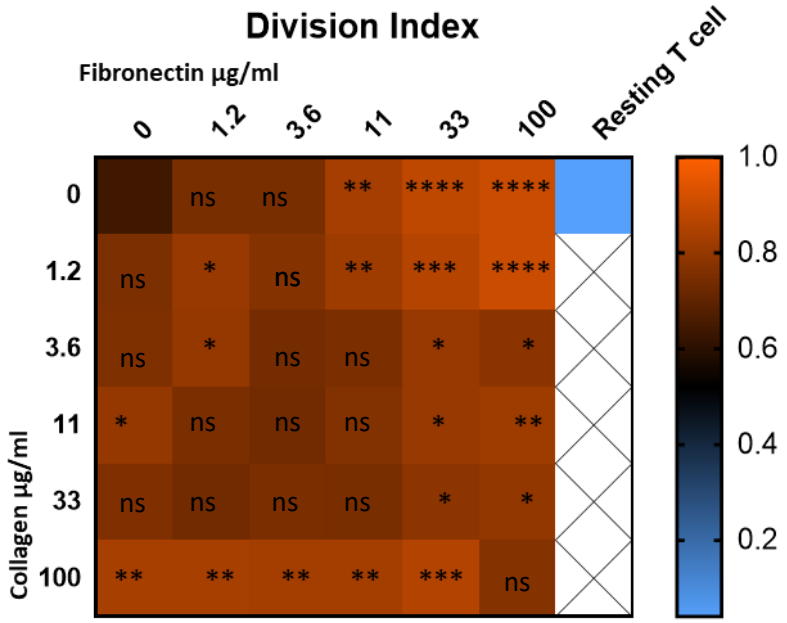
Division Index
Fibronectin µg/ml
0
1.2
3.6
11
33
100
Resting T cell
Collagen µg/ml
ns
*
**
***
****
1.0
0.8
0.6
0.4
0.2

Figure 5.1: Assessing matrix protein influence on T cell stimulation with 1µg/ml CD3 (artificial APC). Culture plates were coated with fibronectin and collagen at the indicated concentrations. CFSE labelled T cells together with artificial APC (ratio 8:1) were cultured for 5 days in presence of matrix proteins. Cell proliferation was analysed by flow cytometry. **(a)** Heat maps present division index values under different matrix protein concentrations from each donor. **(b)** A summary graph of division index from all three donors. Division index is based on the activated and unstimulated cells together, and the value represent the average number of cell divisions the cell has gone through in the whole culture. Statistical analyses were done with RM Two-Way ANOVA, two-tail with Dunnet's comparison test, each group mean was compared against 0µg/mL of fibronectin and collagen.*$p<0.05$, ** $p<0.01$, *** $p<0.001$, ****$p<0.0001$, n=3, three biologically independent donors.

5.2.2 The impact of matrix protein on the physical properties of peptide gel

The gelation of peptide gel occurs by physical crosslinking, starting from octapeptide's hydrophobic regions making fibres to an electrostatic charges creating a nanofibrous network [295, 307]. Such relatively weak interactions could easily be influenced by the presence of other charged proteins. We therefore determined by how much the gel stiffness (i.e. storage modulus) was affected by the presence of collagen and fibronectin matrix proteins and used this information to adjust the peptide gel before populating with T cells.

Initially we analysed the effect of fibronectin on 6mg/ml peptide gel (note, this was carried out prior to analysing the effect of matrix protein on T cells (Fig. 5.1) and 25μg/ml fibronectin was chosen as the trial concentration). In the absence of fibronectin, the storage modulus (G') of gels averaged 551Pa (SD±247.2). However, upon addition of fibronectin (25μg/ml) G' reduced to 263.43Pa (±106.94) (Fig. 5.2 (a)). Whilst not significantly different, it was apparent that the gels had a degree of variability in their rheology, and the presence of fibronectin impacted on the gel's structure.

One key advantage of the peptide hydrogel is the ability to adjust its stiffness level with increased peptide concentration. The peptide gel will eventually end up with an increased peptide stiffness level, but in presence of fibronectin or other proteins the stiffness level could be reduced to meet the original stiffness level. Taking this into account, 8mg/ml peptide gels were produced and

functionalised with 25µg/ml fibronectin to obtain similar stiffness level as found in 6mg/ml (Fig. 5.2 (b)). When fibronectin was added to 8mg/ml peptide gel a corresponding reduction in the stiffness level (307Pa±181.36) was observed. These values were similar and not significantly different to those of non-functionalised 6mg/ml peptide gel (325Pa±63.39).

Having demonstrated the effect of additional proteins on gel stiffness, we further analysed the effect of both collagen and fibronectin. Collagen is known for its ability to increase the stiffness of some materials, whereas fibronectin is documented to have little effect [164, 476]. However, it is presently not possible to predict the effect of combinations of proteins on the physical properties of peptide gel. Therefore, 6mg/ml peptide gels were functionalised with a constant collagen concentration (33µg/ml) and the effect of increasing the level of fibronectin determined (Fig. 5.1). Alterations in matrix protein concentrations resulted in changes in gel stiffness (Fig. 5.2. (c)) however these changes were non-significant.

It is concluded that for the future studies, 6mg/ml peptide gel will be functionalised with both matrix proteins, no matter fibronectin concentration. Due to batch-to-batch gel variation and uncontrolled matrix protein interactions with peptide gel's fibres, it is anticipated that variations will occur in the material's stiffness level. Peptide gels containing combined matrix proteins exhibited similar ranges of stiffness, and the impact of this on T-cell function remained to be determined. However, the future studies with 33µg/ml

fibronectin on its own will use 8mg/ml peptide gel, as 6mg/ml gel could not retain fibronectin at 25µg/ml without structural impairment. Any fibronectin concentrations below 25µg/ml will be encapsulated in 6mg/ml, with prediction that small protein amount would not affect the hydrogels.

(a)

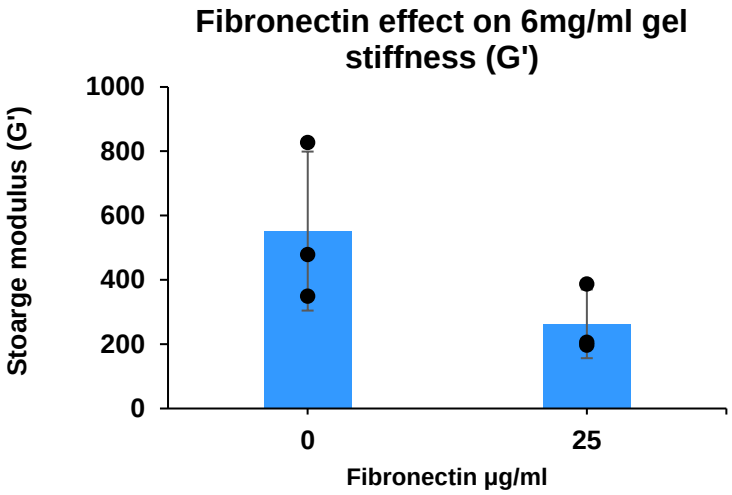
Fibronectin effect on 6mg/ml gel stiffness (G')
Stoarge modulus (G')
1000
800
600
400
200
0
0
25
Fibronectin µg/ml

(b)

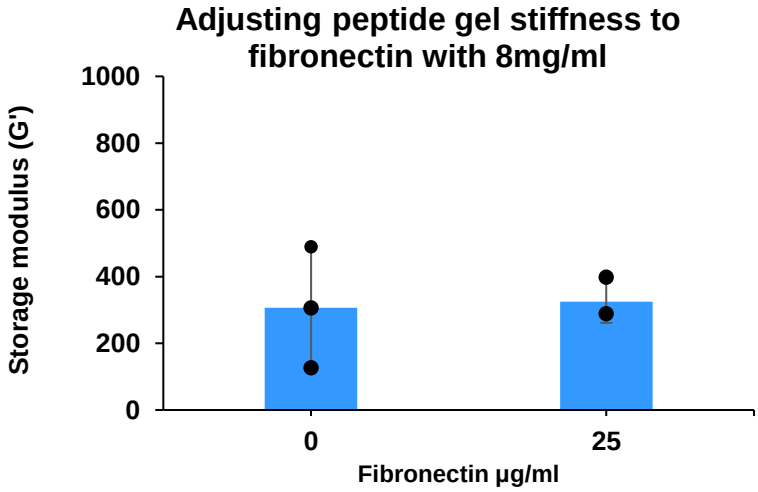
Adjusting peptide gel stiffness to fibronectin with 8mg/ml
Storage modulus (G')
1000
800
600
400
200
0
0
25
Fibronectin µg/ml

(c)

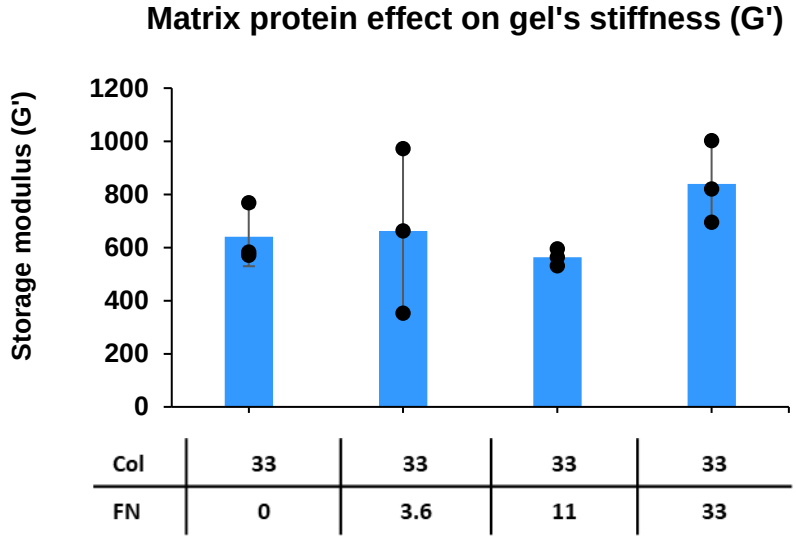
Matrix protein effect on gel's stiffness (G')
Storage modulus (G')
1200
1000
800
600
400
200
0
Col 33 33 33 33
FN 0 3.6 11 33

Figure 5.2: Matrix protein impact on peptide hydrogel's stiffness level. Peptide hydrogels were mixed with matrix protein (μg/ml) and incubated for 24 hours. The stiffness level (storage modulus, G') was measured by bulk oscillatory rheology. **(a)** Fibronectin at 25μg/ml reduced 6mg/ml peptide gel stiffness. **(b)** 8mg/ml took the impact of 25μg/ml fibronectin and reduced the stiffness level matching 6mg/ml non-functionalised peptide hydrogel. **(c)** Presence of collagen (Col, μg/ml) and fibronectin (FN, μg/ml) induced various stiffness level of 6mg/ml. Statistical analyses were carried out with unpaired, two-tail, t-test **(a-b)**, and One-way ANOVA with Tukey's comparison test **(c)**. Data reported with mean±SD, n=3 repeats.

5.2.3 Matrix protein effect on T cells in the peptide gel

Having established a system of functionalised peptide gel with controllable stiffness, we examined the impact of these modified gels on T-cells and their activation through TCR.

In order to conduct the above experiment, it was first necessary to optimise T cell activation with anti-CD3 in the peptide gel system. When polystyrene beads (artificial APC) were coated with 1μg/ml CD3 for co-stimulation purposes, they stimulated T-cell proliferation in 2D-culture, but not in a 3D culture setting (Fig. 3.11). The aim was to identify if artificial APC with 30μg/ml of anti-CD3 is sufficient to partially activate T-cells and reveal both positive and negative effects of matrix proteins. Artificial APC were cultured with T cells in the presence of fibronectin and collagen, which resulted in an improved T cell response (Fig. 5.3 (a)). This confirms the artificial APC suitability as stimuli for T cells in the peptide gel in presence of matrix proteins.

Artificial APC and T-cells were encapsulated in matrix protein-functionalised peptide gel at 1:4 ratio (artificial APC:T cells). This is to prevent excessive stimulation of T cells, which could hide the noticeable effect by the matrix proteins. The addition of fibronectin resulted in a corresponding increase in the proliferation of T-cells (Fib. 5.3 (b-d)) up to a maximum dose of 11ug/ml. However, increased fibronectin concentration to 33μg/ml resulted in a pronounced inhibition of T-cell proliferation to levels lower than control values

obtained with anti-CD3 alone in these 3D cultures. Whilst the absolute proliferation was heterogeneous to the fibronectin only, similar trends were observed across the majority of independent experiments (Fig. 5.3 (c)). The addition of collagen to the hydrogel with fibronectin (3.6-11μg/mL) showed reduced proliferation response (Fig. 5.3 (d)). However, in the presence of high concentrations of fibronectin (33μg/mL) T-cell proliferation was increased in the presence of collagen.

When T-cells were activated by artificial APC with CD3 and CD28 (positive control, in absence of matrix proteins) they secreted significantly enhanced levels of the Th1 cytokine IFNγ in comparison to resting T cells (Fig. 5.3(e)). However cytokine secretion by activated T-cells in peptide hydrogel culture appeared to be modulated by the presence of matrix proteins, although statistical significance was not achieved (Fig. 5.4). Interestingly, whilst not statistically significant, collagen increased IFNγ cytokine secretion, no matter the fibronectin concentrations. There was an increase in IFNγ levels in the presence of 3.6-11μg/mL fibronectin concentrations on its own, but the inclusion of collagen resulted in a modest increase in cytokine secretion. Furthermore, collagen recovered the secretion of IFNγ to levels greater than control in the presence of 33ug/ml fibronectin.

In conclusion, there is preliminary evidence indicating the effect of matrix proteins on stimulated T cells in the peptide hydrogel, but the level of response varied amongst the donors. T cells were able to respond first to the CD3 only

stimulation, which was improved in the presence of fibronectin (3.6-11µg/mL, no collagen). However, upon addition of collagen the majority of donors responded negatively with reduced proliferation response. Yet, the same donor T cells secreted more IFNγ in presence of collagen than fibronectin on its own. This data indicates that both collagen and fibronectin matrix proteins appear to have an effect on on T cells, both in terms of proliferation and cytokine secretion. However further studies are required to consolidate this and provide statistical validity to the data. It may also be important to investigate the apparent and more complex interaction between the two matrix proteins used in these studies as they appeared to influence each others effects.

(a)

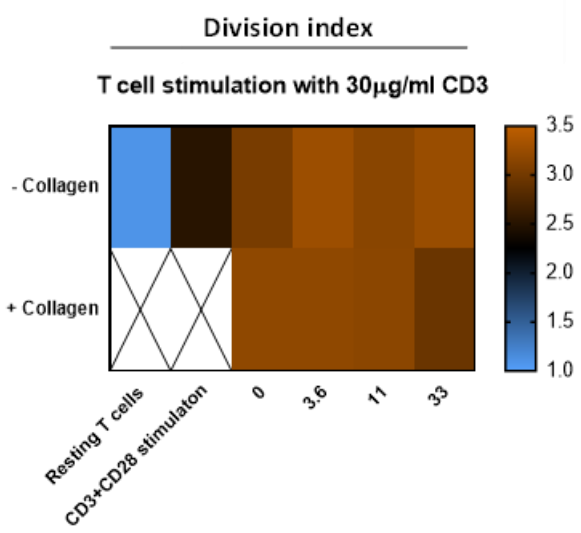
Division index
T cell stimulation with 30µg/ml CD3
- Collagen
+ Collagen
3.5
3.0
2.5
2.0
1.5
1.0
Resting T cells
CD3+CD28 stimulaton
0
3.6
11
33

(b)

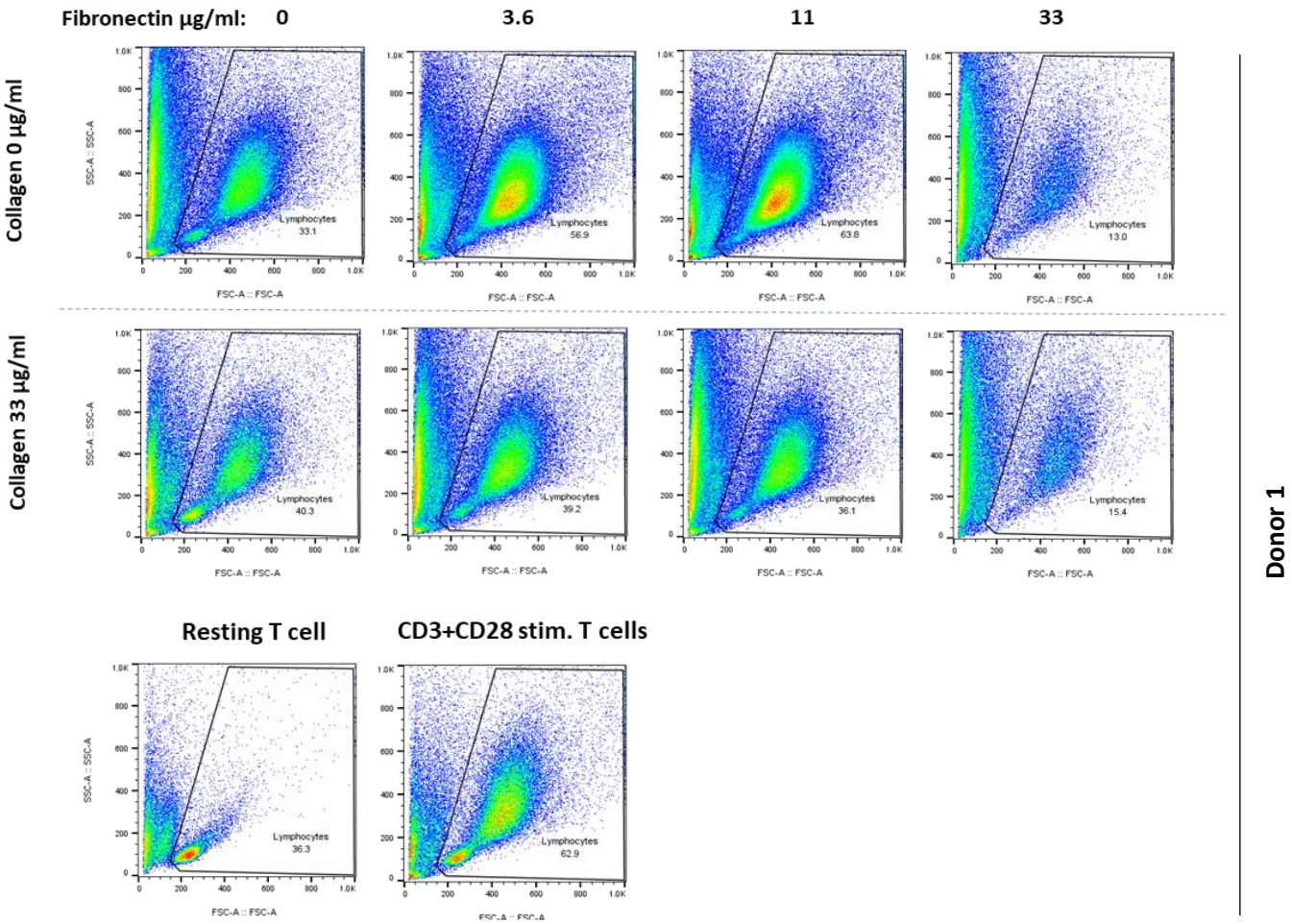
Fibronectin µg/ml: 0
3.6
11
33
Collagen 0 µg/ml
Collagen 33 µg/ml
Lymphocytes 33.1
Lymphocytes 56.9
Lymphocytes 63.8
Lymphocytes 13.0
Lymphocytes 40.3
Lymphocytes 39.2
Lymphocytes 36.1
Lymphocytes 15.4
Resting T cell
CD3+CD28 stim. T cells
Lymphocytes 36.3
Lymphocytes 62.9
FSC-A :: FSC-A
SSC-A :: SSC-A
Donor 1

(b) cont.

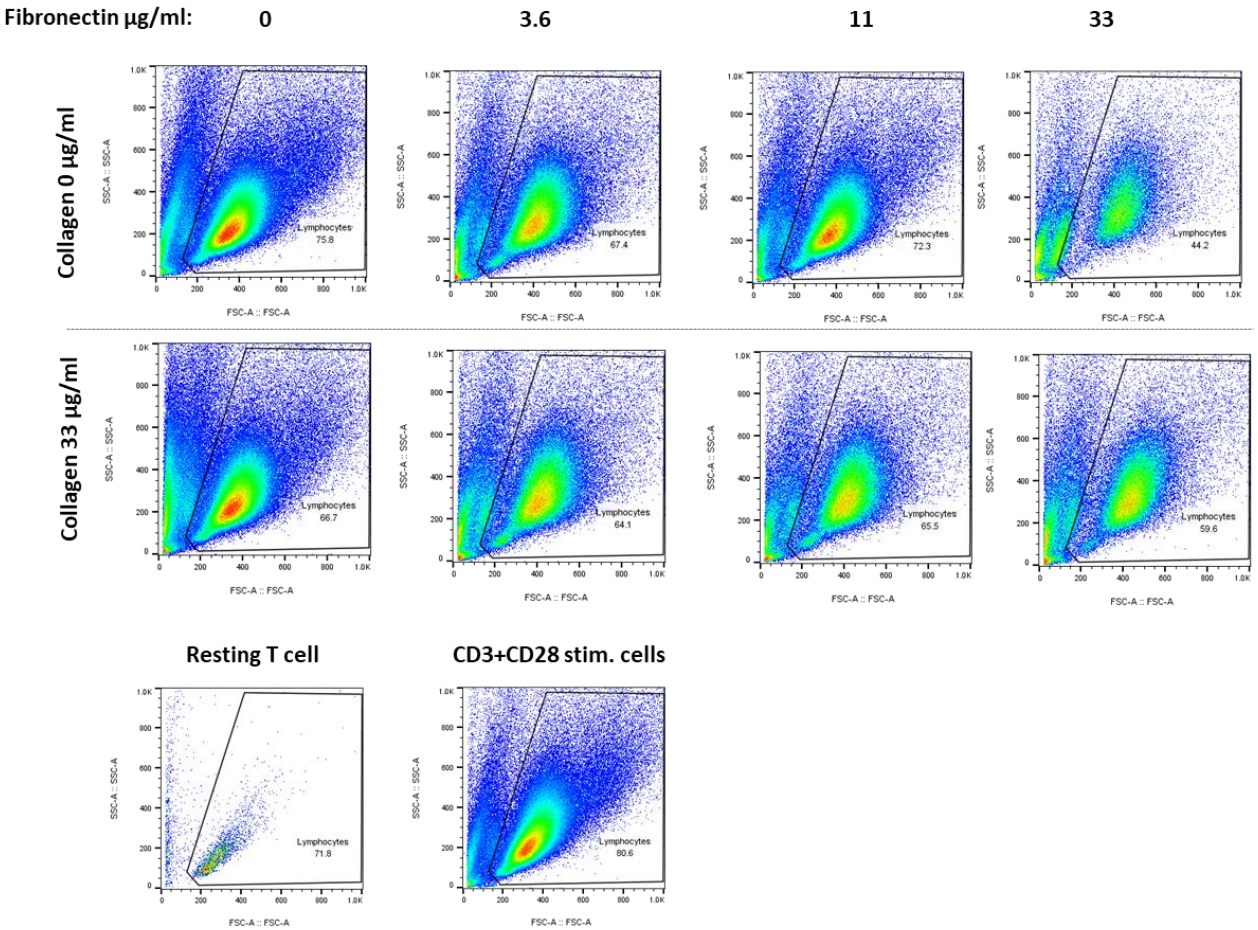
Fibronectin µg/ml:
0
3.6
11
33
Collagen 0 µg/ml
Collagen 33 µg/ml
Lymphocytes 75.8
Lymphocytes 67.4
Lymphocytes 72.3
Lymphocytes 44.2
Lymphocytes 66.7
Lymphocytes 64.1
Lymphocytes 65.5
Lymphocytes 59.6
Resting T cell
CD3+CD28 stim. cells
Lymphocytes 71.8
Lymphocytes 80.6
Donor 2

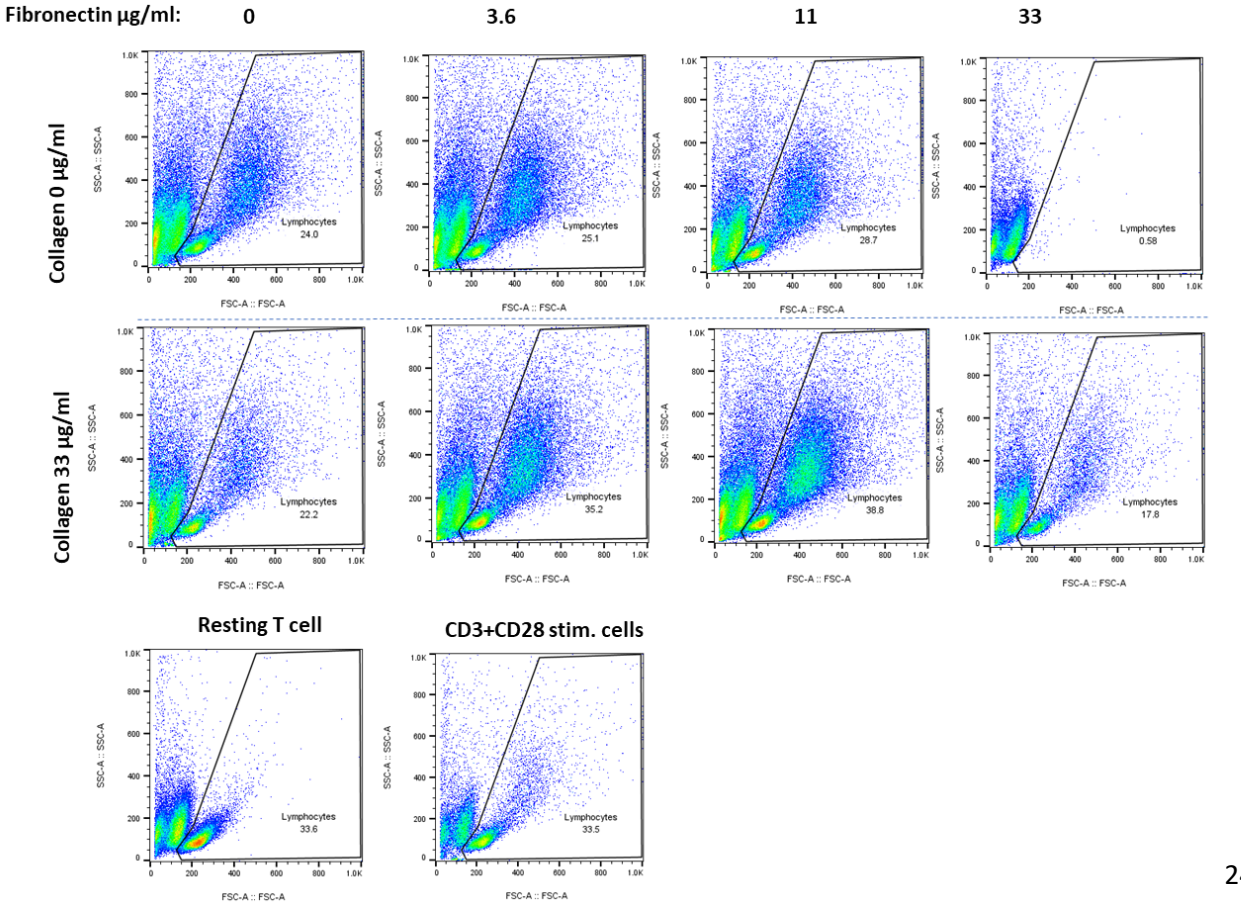
Fibronectin µg/ml:
0
3.6
11
33
Collagen 0 µg/ml
Collagen 33 µg/ml
Lymphocytes 24.0
Lymphocytes 25.1
Lymphocytes 28.7
Lymphocytes 0.58
Lymphocytes 22.2
Lymphocytes 35.2
Lymphocytes 38.8
Lymphocytes 17.8
Resting T cell
CD3+CD28 stim. cells
Lymphocytes 33.6
Lymphocytes 33.5
Donor 3

(c)

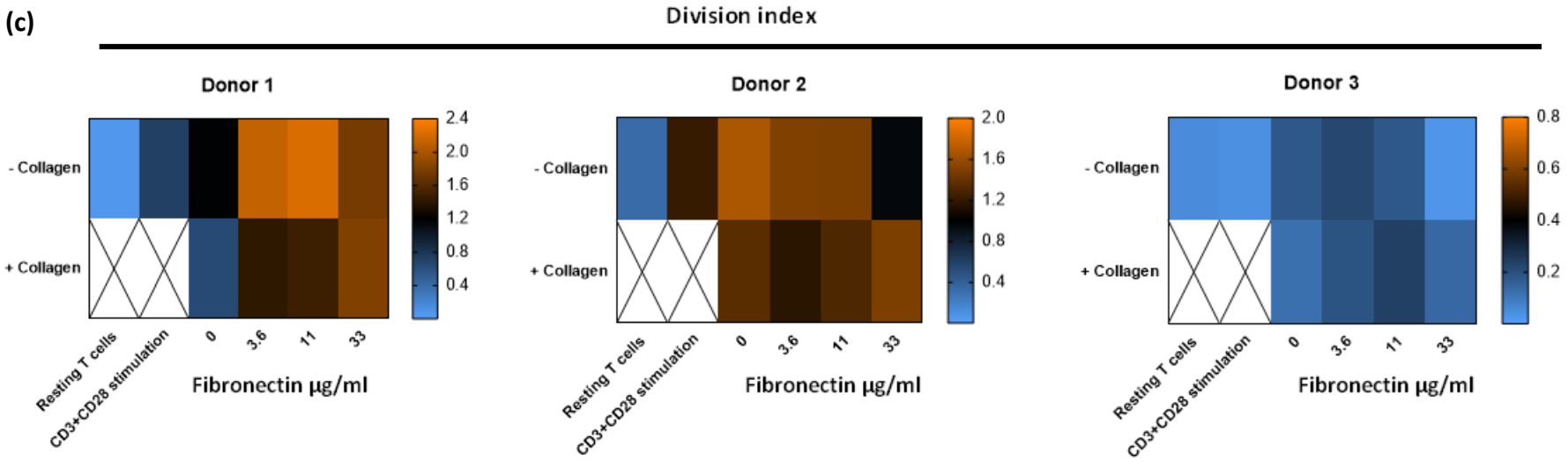
Division index
Donor 1
- Collagen
+ Collagen
2.4
2.0
1.6
1.2
0.8
0.4
Resting T cells
CD3+CD28 stimulation
0
3.6
11
33
Fibronectin µg/ml
Donor 2
- Collagen
+ Collagen
2.0
1.6
1.2
0.8
0.4
Resting T cells
CD3+CD28 stimulation
0
3.6
11
33
Fibronectin µg/ml
Donor 3
- Collagen
+ Collagen
0.8
0.6
0.4
0.2
Resting T cells
CD3+CD28 stimulation
0
3.6
11
33
Fibronectin µg/ml

(d)

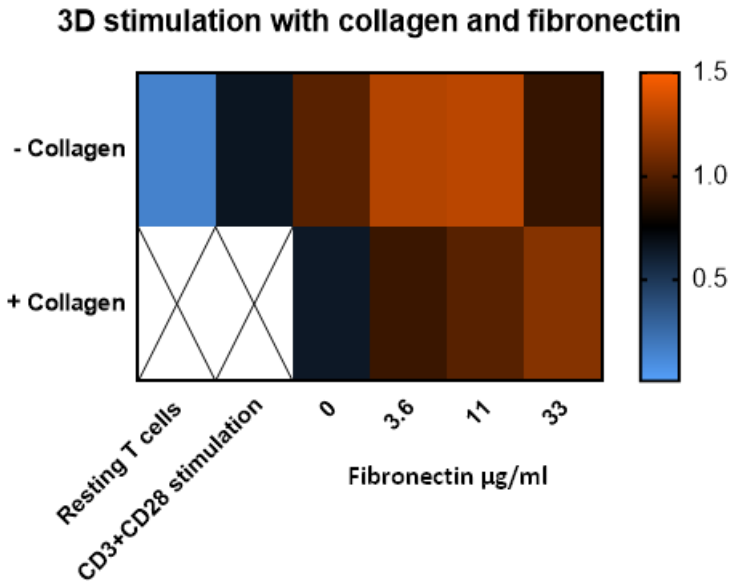
3D stimulation with collagen and fibronectin
- Collagen
+ Collagen
1.5
1.0
0.5
Resting T cells
CD3+CD28 stimulation
0
3.6
11
33
Fibronectin µg/ml

(e)

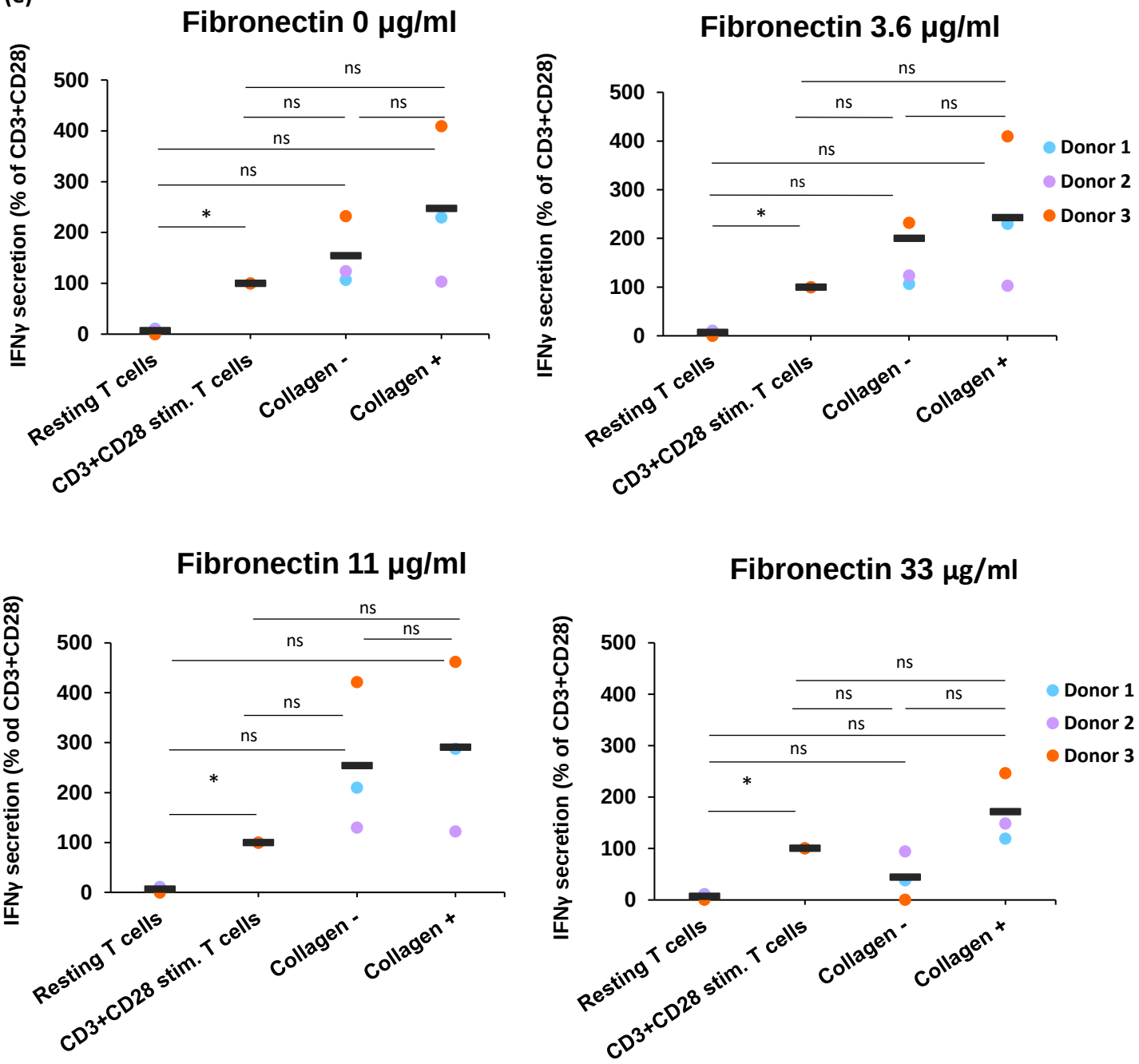
Fibronectin 0 µg/ml
Fibronectin 3.6 µg/ml
Fibronectin 11 µg/ml
Fibronectin 33 µg/ml
IFNγ secretion (% of CD3+CD28)
IFNγ secretion (% od CD3+CD28)
0
100
200
300
400
500
ns
*
Resting T cells
CD3+CD28 stim. T cells
Collagen -
Collagen +
Donor 1
Donor 2
Donor 3

Figure 5.3: Determining collagen type I and fibronectin effect on T cell stimulation in the peptide hydrogel. T cells were encapsulated with 30µg/ml CD3 only APC with matrix proteins in the peptide gel and incubated for 7 days. **(a)** Before encapsulation in the peptide hydrogel, 30µg/ml CD3 APC were tested with T cells (ratio 1:4) in presence of matrix proteins under 2D culture settings (n=1), the reported values are division index. **(b)** Three donors flow cytometer data presentation of T cell stimulation response in presence of fibronectin and collagen in the peptide hydrogel. **(c**) Division index from each donor is plotted as the heatmap, representing T cells response in the peptide gel. **(d)** Summary graph from all donors shows enhanced T cell response in presence of fibronectin only (reported division index), whereas added collagen reduced the effect, although no significant results were achieved. **(e)** The supernatant from 3D cultures were tested for IFNγ secretion by ELISA. RM Two-Way ANOVA with Dunnet's comparison test to 0µg/mL fibronectin and collagen stimulated T cells **(d)**, and the same statistical test for IFNγ secretion but with Tukey's comparison test **(e)**. *$p<0.05$. Data reported with mean value, n=3 three biologically independent donors.

5.2.4 T cell stimulation by Dendritic cells in fibronectin functionalised peptide gel

Having established that fibronectin-functionalised gel modulated T cell responses to artificial APC bearing anti-CD3 (Signal 1) only, we investigated the effect on autologous responses to live dendritic cells.

Autologous T cells and DC (from same donor) were encapsulated at 1:10 ratio in the peptide hydrogel in presence of fibronectin at 11µg/ml, and on day 7 T cell proliferation and IFNγ secretion were analysed.

Fig. 5.4 (a)) showed T cell proliferation response to different DC of a single representative donor. The presence of iDC or mDC shows a similar increase in proliferation to the mitogen-stimulated T cells. It also appears that the presence of fibronectin had no effect on these cultures in this experiment. From the same donors, no significant difference amongst the groups was observed, in terms of secreted IFNγ in presence or absence of the fibronectin. Overall, there is no noticeable change on T cell reaction to DC in the fibronectin or collagen functionalised peptide hydrogel.

(a)

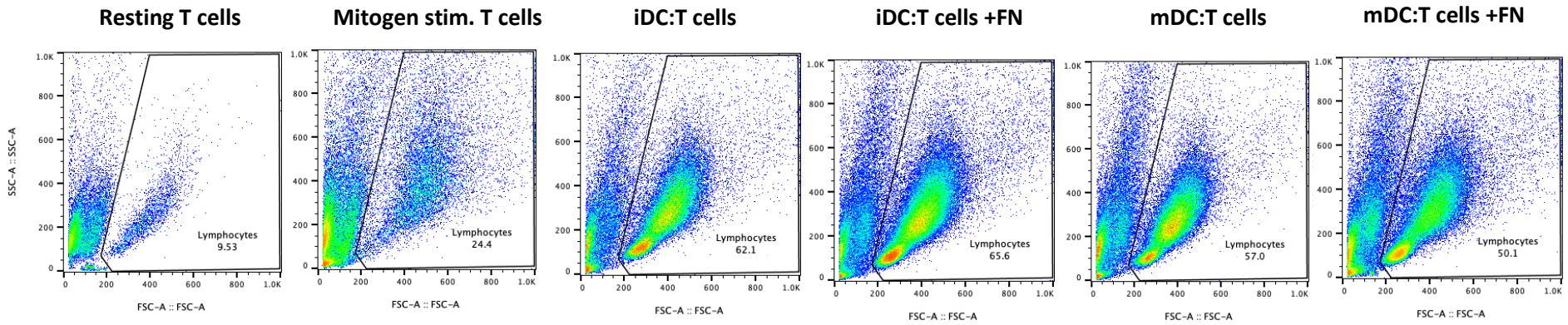
Resting T cells
Mitogen stim. T cells
iDC:T cells
iDC:T cells +FN
mDC:T cells
mDC:T cells +FN
SSC-A :: SSC-A
FSC-A :: FSC-A
Lymphocytes 9.53
Lymphocytes 24.4
Lymphocytes 62.1
Lymphocytes 65.6
Lymphocytes 57.0
Lymphocytes 50.1

(b)

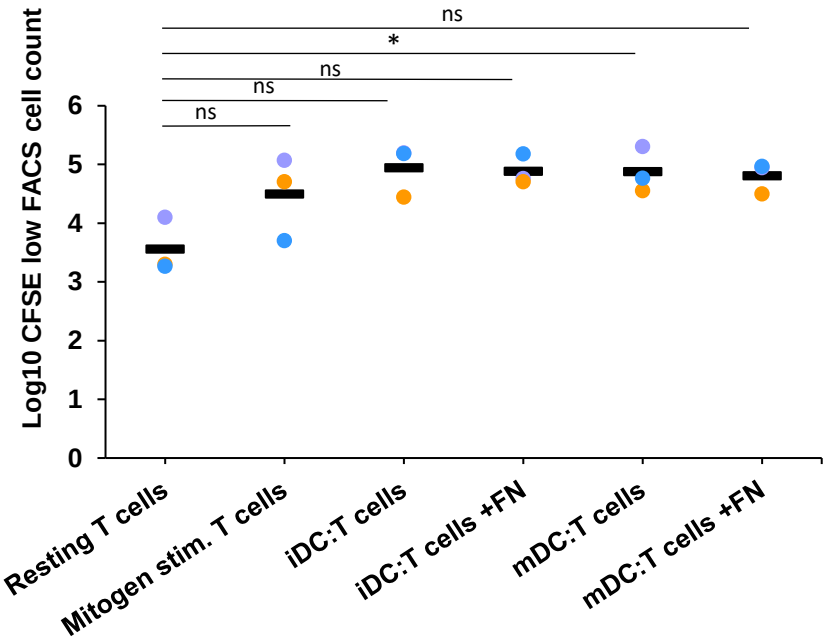
3D MLR response to FN +/-
Log10 CFSE low FACS cell count
ns
*
ns
ns
ns
Resting T cells
Mitogen stim. T cells
iDC:T cells
iDC:T cells +FN
mDC:T cells
mDC:T cells +FN

(c)

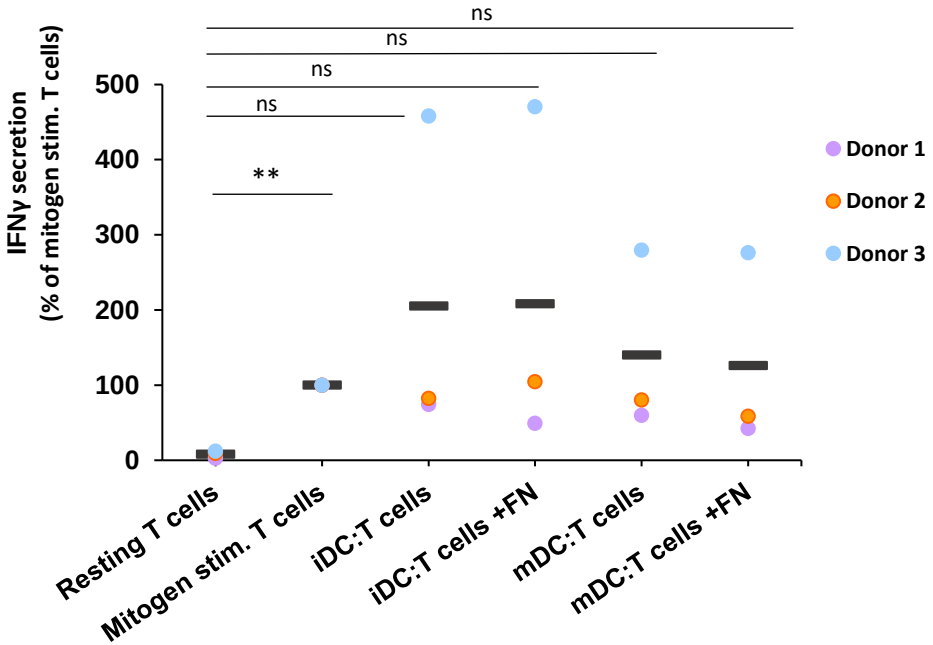
Day 7 - IFNγ secretion from 3D MLR FN +/-
IFNγ secretion (% of mitogen stim. T cells)
ns
ns
ns
ns
**
Donor 1
Donor 2
Donor 3
Resting T cells
Mitogen stim. T cells
iDC:T cells
iDC:T cells +FN
mDC:T cells
mDC:T cells +FN

Figure 5.4: T cell response to DC in fibronectin (FN) functionalised peptide hydrogel. CFSE labelled T cells were encapsulated with iDC or mDC at 1:10 ratio (DC:T cells) with fibronectin (FN) at 11μg/ml in the peptide hydrogel and incubated for 7 days. On the final day, peptide hydrogel was degraded for flow cytometry analyses and culture supernatant for IFNγ detection. **(a)** One donor flow cytometry data presentation of T cells responded to DC in the functionalised hydrogel. **(b)** Summary graph from all three donors reporting T cell proliferation. **(c)** From the same experiment, the supernatants were tested for IFNγ by ELISA. Statistical test RM One-way ANOVA with Dunnet's comparison test to resting T cells, * $p<0.05$, ** $p<0.01$. Data reported with mean value from n=3 three biologically independent donors.

5.2.5 T cell stimulation by primary DC (CD1c+) in functionalised peptide gel

Having successfully established a 3D culture system for T-cell activation by laboratory generated DC we wished to determine if this system could serve as a testbed for T-cell activation by primary human DC. Therefore, we focussed on the major circulating myeloid CD1c+ DC subset which different from moDC in several key ways and are more potent [428, 477]. CD1c+ DC are an increasingly interesting choice for cancer immunotherapy studies, and currently are tested with immunomodulating drugs to sustain immune response in cancer patients [477-479]. We are currently embarking on a first-in-man clinical study of CD1c+ DC (that have had their p38 MAPK modified) for checkpoint-resistance advanced melanoma patients (EudraCT number: 2019-003391-39, UK). As part of the pre-clinical research, the highly selective p38 MAPK inhibitor BIRB196 was employed to upregulate several key CD1c+ DC functions and thus enhance T cell responses [425, 426]. In summary, earlier work in our laboratory has shown that p38 MAPK-inhibited (p38i) cDC1+ DC have markedly increased IL-12p70 and inhibited secretion sufficient to drive strong Th1 responses characterised by high-level IFNg expression. Furthermore, p38i CD1c+ DC displayed high-level CD86 costimulatory molecule expression [426] and have improved chemotactic capacity (unpublished, personal communication Dr. Andrew M. Jackson, University of Nottingham). Previous work on this subject has been limited to classical 2D culture settings. Therefore, we determined to assess autologous T-cells responses to healthy donor CD1c+ DC in the established hydrogel system, investigating if the p38 MAPK inhibited DC behaved similarly in 3D to canonical

experiments, and enquire as to the effect of major matrix proteins on the outcome of the reaction between primary DC and T-cells.

The circulating CD1c+ DC subset are the major myeloid DC subset in human, yet remain a relatively rare population in peripheral blood although their numbers vary amongst different donors [477]. Obtained CD1c+ from one donor were preconditioned to specific stimulus to make cells with different functional status: iDC, mDC, mDC-Dex (immunosuppressed) and mDC-Dex-p38, enhanced DC stimulatory response. Allogenic MLR was set up for 7 days and analysed T cell response.

Distinctive T cell response were evident in the peptide gel in absence of fibronectin. T cell proliferation and IFNγ was induced by iDC and mDC, but the greater response was noted by iDC cells. It was evident by the images of forming cell clusters in the peptide gel (Fig. 5.5 (a), induced T cell proliferation (Fig. 5.5 (b) and cytokine release response (Fig. 5.5 (c)). Moreover, T cells activity were notably reduced by mDC-Dex treated cells, which in comparison to mDC shows the immunosuppressed activity. However, immunosuppressed T cells recovered their response in presence of p38 inhibitor treated mDC-Dex, which surpassed other preconditioned CD1c+ and their MLR response. Enhanced T cell reaction resulted in peptide gel gradual degradation, evident in the microscopic pictures by the ‘cloudy’ appearance of gel (Fig. 5.5 (a)).

In presence of fibronectin there was evident inhibitory effect. No matter the CD1c+ status, T cells overall response were notably reduced. Poor cell cluster formation in the peptide gel and lower number of responder cells imply matrix protein negative effect. It was more evident with p38 inhibitor treated CD1c+ cells, which resulted in substantial decline of proliferating and IFNγ secreting cells.

Overall, the current results in the peptide gel provide typical T cell response to treated CD1c+ cells, which were commonly observed under 2D culture settings. Defined 3D culture system demonstrate the adverse effect of matrix protein on immune response driven by CD1c+ cells, giving a first insight on how tissue specific features could influence cells.

(a)

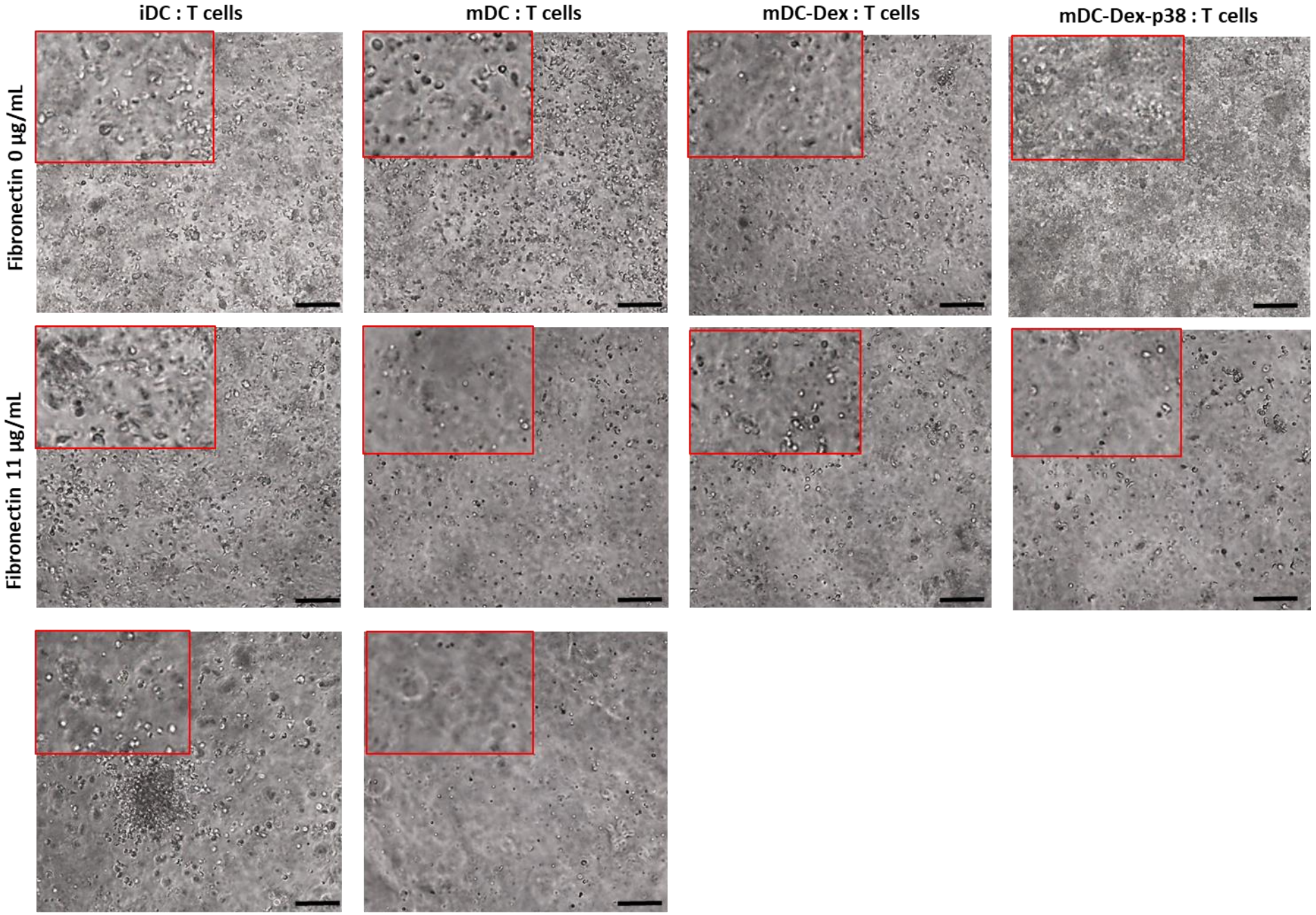
iDC : T cells
mDC : T cells
mDC-Dex : T cells
mDC-Dex-p38 : T cells
Fibronectin 0 µg/mL
Fibronectin 11 µg/mL
Mitogen-stimulated T cells
Resting T cells

(b)

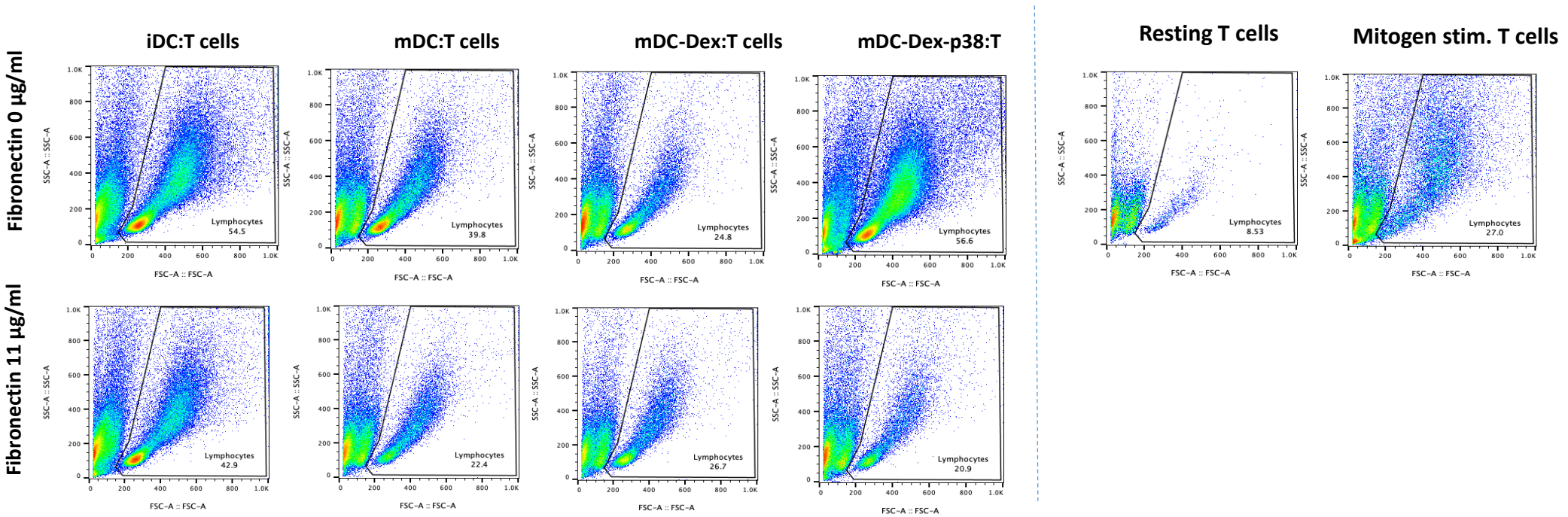
iDC:T cells
mDC:T cells
mDC-Dex:T cells
mDC-Dex-p38:T
Resting T cells
Mitogen stim. T cells
Fibronectin 0 µg/ml
Fibronectin 11 µg/ml
Lymphocytes 54.5
Lymphocytes 39.8
Lymphocytes 24.8
Lymphocytes 56.6
Lymphocytes 8.53
Lymphocytes 27.0
Lymphocytes 42.9
Lymphocytes 22.4
Lymphocytes 26.7
Lymphocytes 20.9
SSC-A :: SSC-A
FSC-A :: FSC-A

(c)

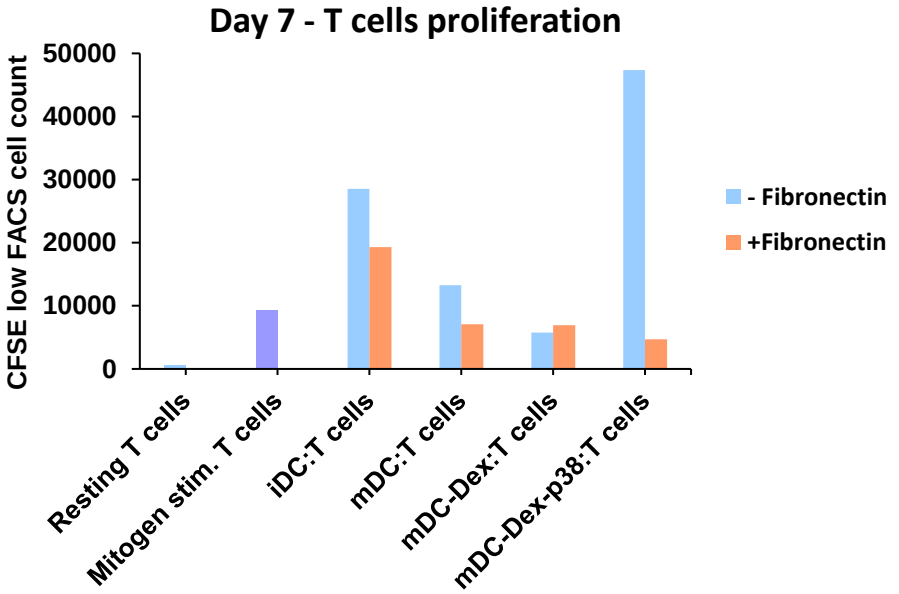
Day 7 - T cells proliferation
CFSE low FACS cell count
50000
40000
30000
20000
10000
0
- Fibronectin
+Fibronectin
Resting T cells
Mitogen stim. T cells
iDC:T cells
mDC:T cells
mDC-Dex:T cells
mDC-Dex-p38:T cells

(d)

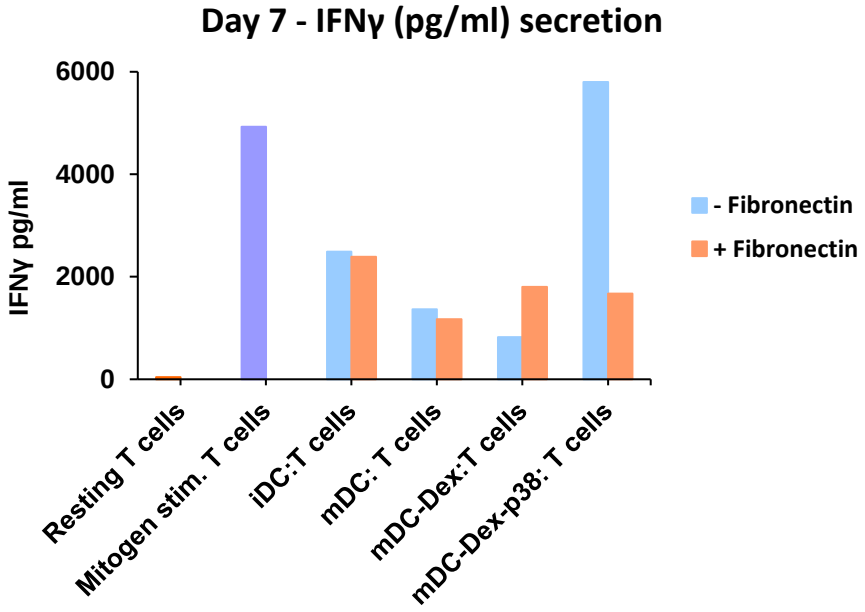
Day 7 - IFNγ (pg/ml) secretion
IFNγ pg/ml
6000
4000
2000
0
- Fibronectin
+ Fibronectin
Resting T cells
Mitogen stim. T cells
iDC:T cells
mDC: T cells
mDC-Dex:T cells
mDC-Dex-p38: T cells

Figure 5.5: Analysing immunomodulatory effect on T cells in the peptide gel. Conditioned CD1c+ Dendritic cells and CFSE labelled T cells were encapsulated at 1:7 ratio in 6mg/ml peptide with or without 11µg/ml fibronectin for 7 days. **(a)** Light microscopy images of cells on day 7 show co-culture of cells in presence or absence of fibronectin. **(b)** Cells released from the hydrogel were analysed by the flow cytometry. **(c)** Summary plot presents CFSE low cell count (proliferated cells). **(d)** Supernatant were tested with ELISA for IFNγ secretion by activated T cells. The reported data here is of a single donor, scale bars in images were set to **100µm**.

5.3 Discussion

The first steps were taken to study T cell behaviour in the modified peptide hydrogel. T cells were able to respond to the different microenvironment provided by the matrix proteins, which highlights the hydrogel's ability to recreate a more realistic 3D culture environment and replace current 2D in vitro studies.

The first choice was made to functionalise peptide hydrogels with fibronectin and collagen, as T cells constantly interact with these proteins in various tissue areas [323, 453, 480]. The importance of fibronectin and collagen for cells was highlighted before, which also explains the commonly made choice in other biomaterial studies [166, 196, 273, 382]. Some studies even just add RGD amino acid sequence, a motif found in collagen and fibronectin to promote T cell interaction with the material as well [161, 330]. Moreover, studies exploring ECM effect on T cells in 2D culture report contradicting results, as in some settings collagen or fibronectin induced a positive effect on T cell stimulations, whereas others argue that it suppresses it [323, 382, 393]. This explains why this current research started from 2D culture settings to explore various fibronectin and collagen effects on T cells, which were later adapted for 3D culture studies.

Interestingly, stimulated T cells showed an improved response in the presence of matrix proteins in 2D culture. T cells responded well to fibronectin on its own than collagen from the proliferation perspective, and nevertheless, there was no

synergetic effect between the two proteins. The explanation could rely on the state of T cells, as several studies pointed out fibronectin's costimulatory effect only on resting T cells, whereas antigen-activated cells benefited more from the collagen [323, 455]. Fibronectin is well reported in various studies to have a costimulatory effect on T cells after CD3 (Signal 1) stimulation [323, 382, 481]. T cells express integrin α4β1 which interacts ICAM-1 on APC and fibronectin in the interstitial matrix [455]. α4β1 via different signalling pathway than CD28 (prominent costimulatory molecule) induces IL-2 cytokine secretion and receptor expression, which promotes T cell proliferation response [455, 482]. Also, the presence of fibronectin could enhance T cell and target cell/stimulus interaction by enhancing the number of TCRs interacting with MHC [483]. α4β1 integrins on T cells modulate actin organization to rearrange cell's synapse and increase the interaction between cells and stimulus [455, 484]. This could explain why resting T cells mainly benefited from fibronectin than collagen on its own during the stimulation process.

From collagen perspective, only high concentration (100μg/mL) under 2D culture enhanced T cell response to the stimulus. This could be attributed to the enhanced motility of T cells which increased encounter frequency between T cells and APC, and greater synapse formation by T cells activating multiple TCR's on cells [323, 449, 455]. Also, activated T cells upregulate β1 integrins (i.e. α1β1, α2β1) which are known for induced costimulation response [455, 482]. However, the costimulation effect is mainly reported on antigen-activated cells rather than resting T cells [172, 323, 475]. The collagen costimulation effect is

only noted in non-lymphoid tissues, as T cells interact with protein mainly in the inflamed tissue areas rather than lymph nodes [151, 166, 475, 480]. Lymph nodes are the main activation site for T cells, but collagen itself is 'hidden' from T cells by FRC leaving T cell migration to be mitigated by chemokine and fibronectin cues only [323, 485]. This could explain why resting T cells in presence of stimulus did not give a significant proliferation response in collagen environment, as only already activated or memory cells benefit from this type of protein.

The similar pattern of T cell behaviour in presence of ECM proteins in 2D culture was also noted in the peptide hydrogel. Fibronectin on its own at moderate levels and in the absence of collagen-induced better T cell proliferation response. The excess of ECM protein reported to have a negative effect on immune response in various diseases [211, 357, 486]. Kuczek et al. (2019) reflected this scenario in the collagen hydrogel, where reported high collagen density limited T cell proliferation in comparison to low-density gel [164]. But even in this study, their collagen concentration was higher than in the peptide hydrogel (low collagen density: 1mg/ml, high density: 4mg/ml; FEFEFKFK peptide hydrogel: 33μg/ml), which makes the two studies incomparable. In addition, collagen in the peptide hydrogel promoted greater IFNγ cytokine release than fibronectin, which confirms T cells costimulation effect of this protein [474]. In most scenarios, low-density fibronectin and collagen networks of inflamed tissues permit T cell migration and adhesion in the tissue areas [173,

211]. This could explain why T cells in the peptide hydrogel responded well to lower fibronectin concentrations than to excessive amounts of proteins.

On the other hand, low proliferation T cell response to the collagen functionalised hydrogel could be attributed to the hydrogel's stiffness level rather than the ECM protein itself. The stiffness level amongst functionalised hydrogels was inconsistent, resulting in some cases with a higher storage modulus of the hydrogel than unmodified gel. Previous studies (Chapter 3) demonstrated how the increased stiffness of the material could reduce T cells proliferation and expansion. Further studies need to define the true impact of high matrix protein content effect on cells in the peptide hydrogel.

One question was left unanswered in this study: whether collagen and fibronectin polarized into fibres in the peptide hydrogel. Collagen assembly into fibrils occurs after proteolytic cleavage of procollagen domains [470]. But it was also shown fibronectin can mediate their assembly by providing collagen binding domains [473]. Plasma fibronectin is a dimeric protein, which assembles into multimeric form in acute and chronic tissue inflammations [487]. Fibronectin assembly in tissues is either mediated on pre-existing fibronectin fibers, collagen or even cell surface which express fibronectin themselves [468, 470, 487]. T cells upon activation synthesise fibronectin themselves, to enhance cell-cell interaction with nearby T cells for co-stimulatory effect [467]. However, there is some indication that fibronectin assembly in hydrogel has occurred, as soluble plasma fibronectins are known for their inability to affect the cells [468, 488].

After all, further studies are needed to confirm ECM protein polarisation in the peptide hydrogel.

Following ECM protein optimisation in the peptide hydrogel, moderate level (3.6-11μg/mL) of fibronectin had the costimulatory effect on T cells due to enhanced proliferation. However, once T cells and moDC were encapsulated in the peptide hydrogel, no significant response was detected amongst cultures with or without fibronectin. Some of the studies highlighted the fibronectin importance in studying DC function, especially when cells are dealing with ECM proteins in the basement membranes and interstitial matrixes of tissues found in SLOs and peripheral tissues [489]. Garcia Nieto et al. (2010) showed increased antigen uptake by iDC in the presence of fibronectin, by forming long and broad dendrites. After antigen exposure, the DC enhanced T cell response by inducing higher IFNγ secretion and proliferation of cells, compared to the DC cultured in the absence of ECM protein [489]. Also, other research highlighted upregulated integrins (α5β1) on monocyte-derived mDC which mediated cell adherence to the fibronectin [490]. But the same research analysed skin-derived DC and noted that cells were more motile with less adhesion to the fibronectin. However, Burns et al. (2003) showed during DC maturation they form less podosomes cellular protrusions mediated by the cytoskeleton which are important for cell adhesion and motility [491]. mDC appeared more in round morphology, which made fewer contacts to the fibronectin, and mainly short protrusions were noted on cells to maintain their motility. Also, DCs in the first hours of the maturation process were highly expressing podosomes, which was suspected

within this time DCs were 'escaping' the peripheral tissues by interacting with ECM to enter the lymphoid tissues [491]. This indicates that iDC benefit more from ECM-fibronectin than mDC, as mDC needs less assistance from fibronectin since they are trying to migrate to the lymph nodes. This could explain why co-cultures of mDC and T cells were neutral to the fibronectin in the peptide hydrogel. However, further analyses are needed as the ratio between DC and T cells could be too high to notice the fibronectin effect, in the same way as with artificial APC. Moreover, by the time mDC were encapsulated with T cells they already lost some of their effectiveness as APC (i.e. reduced cytokine release, down-regulation of costimulatory molecules; Chapter 4) which could limit DC reaction to the fibronectin presence.

Another co-culture study was set up in the peptide hydrogel, but this time with CD1c+ cells, a conventional myeloid DC derived from blood. Unlike moDC, CD1c+ are naturally occurring cells and do not require a differentiation process in in vitro as moDC [477]. After antigen exposure, mature moDC release cytokines and stimulate T cells but for a limited period, as they later reach the functional 'exhaustion' [492]. CD1c+ cells are the most potent DC cells to stimulate T cell response, as upon their activation they release large amounts of IL-12 – a cytokine which primes IFNγ secreting T cells [428, 477, 492]. CD1c+ are highly considered for cancer immunotherapy than moDC, and various research have been conducted to develop DC vaccine against glioblastoma, melanoma, prostate cancers etc. [426, 477, 478, 493]. The majority of research were

completed in 2D culture settings, which lacked some of the tissue relevant features in their studies.

A peptide hydrogel was tested for its ability to replicate published 2D culture studies, which explored immunomodulating drug effect on CD1c+ and T cells' response [426]. Adhikaree et al. (2019) studied p38 inhibitor drug effect on CD1c+ cells for glioblastoma tumour [426]. The study showed promising results for cancer immunotherapy, but due to in vitro experiments, it lacked the tumour environment features (e.g. 3D dimensions, architecture, ECM) found in glioblastoma [494]. In this case, cells were analysed in fibronectin functionalised peptide hydrogels, which were reported to be deposited by glioblastoma tumour cells to support their invasion through the matrix and survival against therapies [495]. Selected fibronectin concentration in the peptide hydrogel might underrepresent the excess amount found in the tumour tissue, but its presence gave an insight on how the matrix protein could influence the cells.

T cells in the peptide hydrogel responded distinctively to the conditioned CD1c+ cells. Immature CD1c+ (iDC) induced higher proliferation of T cells than mature CD1c+, which could possibly occurred due to mDC exhaustion (Chapter 4), However, p38 inhibitor treated CD1c+ gave a robust T cell response evident by the highest proliferation and IFNγ secretion in the peptide hydrogel. p38 is part of MAPK pathway which regulates the inflammation response in CD1c+ [425, 496]. It suppresses IL-12 secretion from cells, which eventually reduces CD1c+ function and T cells response [425]. p38 inhibitor recovers CD1c+ activity,

especially after dexamethasone treatment, and enhances IL-12 secretion and co-stimulatory molecule expression for T cells [426]. The obtained results in the peptide hydrogel replicated the established 2D in vitro results, indicating the peptide hydrogels' potential use for cancer immunotherapy studies.

However, fibronectin presence in the peptide hydrogel had negative impact on the co-culture of CD1c+ and T cells. A noticeable change was found between T cells and p38 inhibitor-treated CD1c+ cells, where IFNγ proliferating T cells response was reduced. There is a lack of literature explaining fibronectin's influence on CD1c+ cells, especially on p38 inhibitor-treated cells. However, p38 inhibitor-treated CD1c+ cell response to fibronectin in the peptide hydrogel could be explained based DCs and p38 functions. After antigen exposure, iDC becomes mDC, which also simultaneously activates p38 to reduce cell antigen uptake and podosome formation by dissembling actin filaments [491, 497]. Due to change of morphology and less interaction with ECM, mDC migration is more enhanced than iDC [491]. Inhibition of p38 in mDC recovers podosome formation and antigen uptake, without affecting costimulatory molecule expression for T cells activation [497]. In addition, myeloid DC (CD1c+) are known to express integrin for fibronectin to mediate their migration and adhesion via ECM [498]. By adding all these DC characteristics and p38 activity it is assumed that p38 inhibitor-treated CD1c+ in the peptide hydrogel were ‘locked’ into one position in the hydrogel and prevented from interacting with T cells. As podosome formation is secured by p38 inhibitor, long protrusions with integrins binding to fibronectin enhanced CD1c+ adhesion, eventually retaining

cells in one location. Of course, this type of hypothesis needs to be tested in the peptide hydrogel to understand the effect of fibronectin on CD1c+ cells. However, future cancer immunotherapy studies should consider 3D cultures, especially when solid tumours have an abundant amount of ECM content [4, 211, 494].

One limitation of the peptide hydrogel has to be taken into account for the future studies is uncontrolled stiffness level due to presence of ECM proteins. This possibly resulted from various proteins interacting with FEFEFKFK peptide gel during its gelation process. Collagen type I fibril formation mainly depends on the hydrogen bonds from primary to tertiary protein structure, whereas final fibril formation relies on hydrophobic and electrostatic interaction between the adjacent molecules [499]. Fibronectin dimers are connected by disulphide bridges, but as the protein is composed mainly from negatively charged amino acids, which via electrostatic interactions define the protein folding [500]. Taking these specific protein characteristics, especially what charges, and electrostatic interactions they use to form the complex proteins, it is no question that parts of ECM components could be interacting with FEFEFKFK octapeptides in hydrogels. To some extent this could result in variable peptide hydrogels, no matter of consistently used peptide density, as uncontrolled and random proteins interaction will affect the formation of nanofibrous FEFEFKFK network.

Future studies require more experimental repeats due to variations occurring from donor-to-donor responses and various stiffness level resulted from ECM-

functionalised hydrogels. The majority of results lacked statistical significances to get a definitive conclusions on modified environment's influence on cells. In addition, some questions remained to be answered such as: ECM protein effect on T cells adhesion and migration in the peptide hydrogel. This could help to understand whether the peptide hydrogel structure allows T cell migration and whether stimulation occurred from the frequent encounter of cells or proximal distances between cells. However, the preliminary results gave a first insight into how modified peptide hydrgel influenced T cells. Nevertheless, it also gave a promising result on using peptide hydrogel as a 3D culture system for immunomodulatory therapy studies.

Chapter 6 Discussion

This research has shown FEFEFKFK peptide hydrogel's potential as a 3D culture system for immune cells. T cells in novel in vitro settings were viable, functional, and responsive to different stimuli (artificial to actual APC) demonstrating T cell characteristics normally found in 2D in vitro and in vivo studies. The biomaterial itself was inert and non-toxic to cells, without any adverse effect on immune cells' function. This study provides another step towards more advanced studies, where T cell-related questions could be answered with biocompatible material.

A key property of the peptide hydrogel is that whilst inert in its native form, it is readily modifiable. With this feature, it is possible to model different microenvironments, which could advance current in vitro studies by including the tissue-relevant properties. The mechanical properties of the peptide hydrogel can be regulated by varying peptide concentrations. The impact of increased material stiffness on T cells showed reduced proliferation and cell viability. In contrast, the lower stiffness level of the material supported T cell expansion, demonstrating T cell preference to the soft tissue-like environment. This could represent cancer-like solid tissues or healthy lymph nodes, respectively, with unique stiffness level and architecture affecting cells [2, 177, 501-503].

Peptide hydrogel had unmodified environment, which gives an opportunity to include ECM components commonly found in the specific tissue areas. In this case, the peptide hydrogel was functionalised with fibronectin and collagen type I: tissue matrix proteins commonly found to interact with cells [196, 453, 504]. The dynamic ECM environment in the peptide hydrogel influenced T cells uniquely, as preliminary results indicated excessive amounts of both proteins had an inhibitory effect on cell proliferation. However, moderate levels of fibronectin on its own delivered a costimulatory effect, showed by enhanced proliferation. Whereas collagen on its own enhanced cytokine secretion only. The current data provides an insight into how the tissue microenvironment could influence the immune cells, but more experimental repeats are needed to obtain conclusive results.

The importance of 3D culture was highlighted whilst studying the immunomodulatory effect of p38 inhibitor treated CD1c cells against T cells. The study itself gave the first indication on how the fibronectin presence could diminish the CD1c-p38 induced T cell response, which could reflect the glioblastoma tumour scenario in cancer immunotherapy [494]. Taking all these results into one scope, peptide hydrogel shows the ability of replicating 2D culture related T cell studies, and modifying cell's response with tissue specific features. However, the study itself needs to be repeated again to ensure the consistency of results, especially to confirm hydrogel's ability of supporting immunomodulatory effect on cells. But once 3D culture system is fully

established, it could be used to test novel drug/therapy efficacy and give a 'preview' to the possible scenario in in vivo like studies.

To the best of our knowledge, no other studies explored the potential of peptide hydrogel and primary T cell for 3D culture studies. Various research explored the benefits and usefulness of hydrogel systems for T cells, which were described in more details in previous chapters. Combining the conclusions from the current peptide hydrogel and other biomaterial system studies give a positive view on using 3D culture settings for T cells related studies. In this regard, such peptide hydrogel systems provide a platform in which to address complex in vivo related questions that could not be addressed by conventional culture. For example, Fruhauf et al. (2020) were able to study T cell and microglia interaction in collagen type I hydrogel recreating brain microenvironment functionalised with glycosaminoglycans [166]. Whereas Ando et al. (2019) used GelMA hydrogel with established oxygen gradient to mimic hypoxia of tumours and study its effect on CAR-T cells function [157]. These studies were able to observe T cell survival, migration, and cytotoxic effect in a tissue-like environment.

Peptide hydrogel as the material holds several advantages which makes it a great candidate to be used for 3D culture studies. Before the gelation process, the precursor hydrogel retains the liquid state which allows an easy introduction of cells and matrix proteins to modify the hydrogel. Consequently, this results in an effective mixing process which ensures the homogenous distribution of cells, nutrients and ECM components. Moreover, peptide hydrogel solidifies and

maintains its structure at biocompatible conditions of pH 7 and 37^{o}C. In addition to controlling hydrogel's stiffness, it is possible to modulate porosity, swelling (retained amount of water) and degradation, depending on the hydrogel's designated application [307]. FEFEFKFK hydrogel could achieve stiffness level from 500 Pa to 5kPa, giving a wider range to replicate tissue models. It was clearly demonstrated by Ashworth et al. (2020), where increasing stiffness level of hydrogel reduced normal breast cell viability, whereas MCF7 (invasive breast cancer cells) survived in the firmest high-density gels. Similar findings were noted in the current studies, where primary human T cells struggled to retain their viability and support expansion in the stiff hydrogels [311]. Moreover, peptide hydrogel could be modified via a simple adsorption method and retain ECM components, without additional crosslinking methods [306, 311, 312]. In agreement with current and other studies, functionalised peptide hydrogel retained their biological activity and mitigated cell's response.

Several questions regarding other T cell functions within the peptide hydrogel remain to be addressed. Future studies should investigate helper-T-cell polarisation from Th0 to Th1 etc, or Th-plasticity of effector cell under 3D culture settings. T cell phenotype is mainly influenced by cytokines secreted by the APC cells, but it also could be mediated by environmental factors. For example, poor hyaluronan acid synthesis in tissues induced Th1 polarization towards Treg phenotype [505]. Another study demonstrated how stiffness impacted activated cells [506]. T cells were encapsulated in PEG hydrogel with fibrinogen, and the stiffness level equivalent to the tumour tissues induced IFNγ expressing T cells

(i.e. Th1), whereas material representing a healthy tissue environment suppressed Th1 responses. However, to this date very few 3D culture studies explored T cell polarization/plasticity behaviour, and therefore there remains a paucity of answers on how external factors could influence cells.

The effect of peptide hydrogels on T cell migration is presently unstudied. During inflammation processes, T cells migrate through the matrix to the 'injury' site, by interacting with collagen, fibronectin and hyaluronan acid to mediate antigen-specific response [172, 196, 365, 453, 507]. Peptide hydrogel provides nanofibrous material, where its cavities could be too small for T cells to pass. As it was previously mentioned, lymph node's reticular meshwork interspaces ranges between 5-20µm wide which is enough for 2-3 T cells to pass, whereas peptide hydrogel at 10mg/ml provides ~30nm meshwork size [148, 301]. This leaves an open question whether nanofibrous architecture of hydrogel could promote or inhibit T cell migration. Furthermore, functionalised peptides with fibronectin and collagen could promote T cells migration. These two matrix proteins are already used by cells during the inflammation process, which enhances T cell migration through interstitial matrix [196, 453]. Future studies could consider the analyses with environmental confocal high-content imaging microscopy by collecting images at different time intervals and observing cell movements in the hydrogel. The method was used by Majedi et al (2020) and Mollica et al. (2021), to analyse the velocity of T cells migration in different stiffness of alginate hydrogel, or cell infiltration across endothelial barrier to pancreatic cancer region in collagen hydrogel, respectively [161, 170]. In this case thinner layer of peptide hydrogel could be created to achieve

compatible optical thickness for microscope and analyse whether resting T cells use ameboid like movement across the biomaterial, and whether activated T cells use integrins for migration [172, 186]. The method could be also adapted to analyse chemokinesis of T cells, a cell movement mediated by chemokine gradient [508].

The diffusion of small molecules and soluble proteins through the peptide hydrogel also remains to be investigated. This especially reflects on nutrient, gas molecule (i.e. oxygen) distribution across the material, and whether a specific region or entire hydrogel receives these molecules. It will indicate whether all encapsulated cells retrieve these exogenous factors, and equally maintain their survival and functional response. The experimental approach on testing molecule diffusion across the peptide hydrogel could be taken from de Haan et al. (2021) study where they used 10 kDa dextran labelled with FITC [168]. The aim was to test endothelial barrier function, formed at the edge of the collagen hydrogel in the microfluidic device. In the absence of endothelial barrier, dextran diffused across the collagen hydrogel, which emitted fluorescent colour from the whole hydrogel. Another study by Burla et al. (2020) analysed particles diffusion across the hyaluronan hydrogel by using differential dynamic microscopy and single-particle tracking analyses [509]. The study indicated how hyaluronan's pore size and crosslink in tissues affected various size particle diffusion [509]. Figueiredo et al. (2018) used oxygen and glucose sensors implanted in silatedhydroxypropylmethylcellulose (Si-HPMC) hydrogel [510]. This study detailed how glucose diffusion increased with gel pore size, whereas

oxygen diffusion was lowered by increased polymer concentration. Overall, as for 3D culture system, peptide hydrogel nutrient and molecule diffusion need to be investigated. This could be used to analyse immunomodulatory drug diffusion, chemokines gradients, and cytokines distribution as well.

Another study should analyse the location of activated and proliferating T cells in the hydrogel, and indicate whether 3D culture equally supports functional cells. There is possibility that most of T cells proliferation occurred towards the surface of the hydrogel in exposure to DCs, rather than from the entire material. Several scenarios could influence T cells location in the peptide hydrogel and they are: DC migrates towards the surface of the peptide hydrogel, effectively starting to stimulate nearby T cells; greater nutrient exposure at the surface of the material mediates better cell response, than the middle part of the hydrogel; greater nutrient exposure results in highly metabolically active cells, which increase hydrogel's structural collapse and cause greater cell-cell interactions than middle 'intact' part of the hydrogel; middle part of the hydrogel causes too much restrain on cells and their interactions. These hypotheses are illustrated in Graph 7.1 depicting various scenarios of co-culture in the peptide hydrogel. Future experiments investigating cells' locations could use light-sheet fluorescence microscopy (LSFM), which with a focal plane excites fluorophores of the specimen's thin volume, penetrates the depths of the 3D culture sample and acquire data of live cells [511-513]. Collected images at different time points could indicate how different cells behave within the hydrogel.

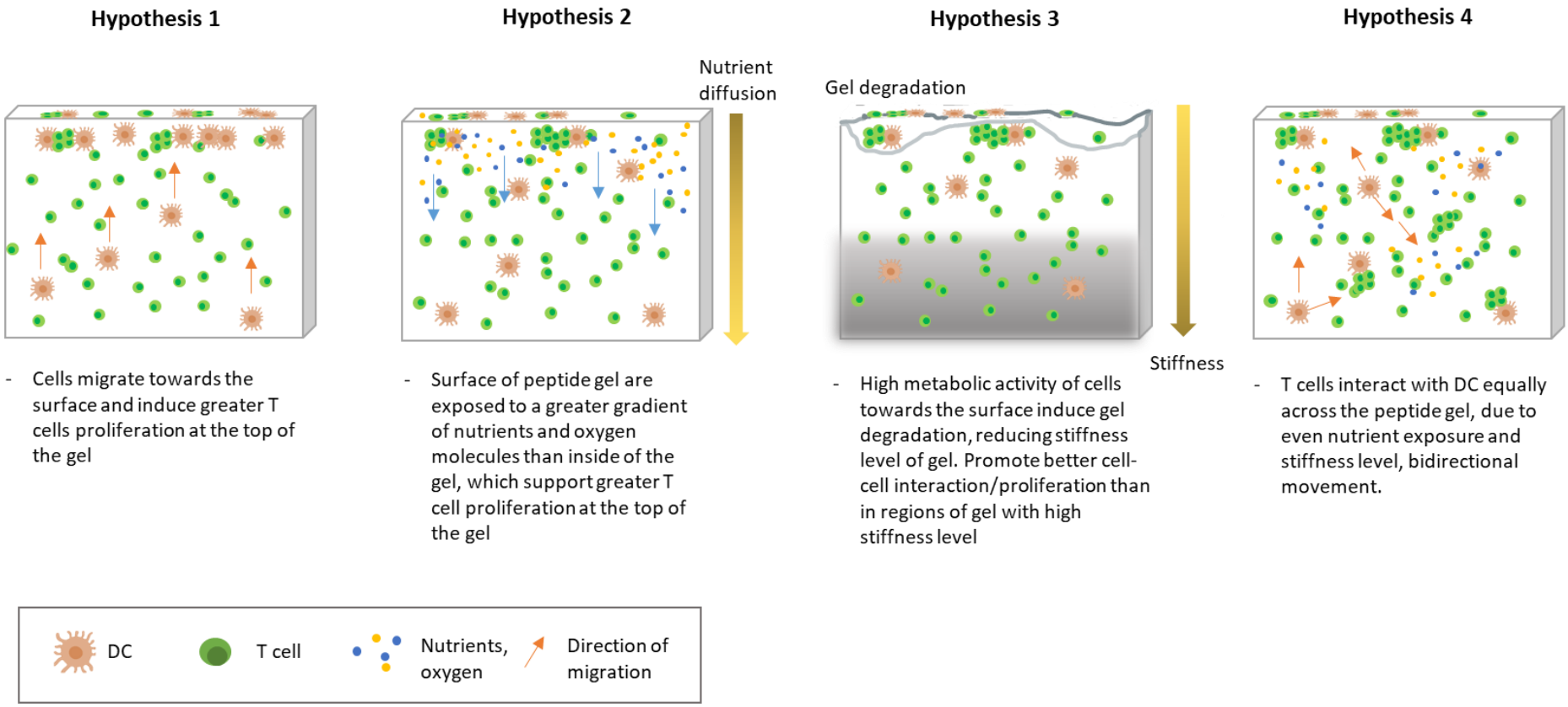

Graph 7.1. The location of T cell and DC encounter in the peptide hydrogel. Several hypotheses depict possible scenarios of how peptide hydrogel could influence T cell and DC interactions, and overall T cell activation. **Hypothesis 1**: DC migrate to a specific site of peptide hydrogel and affect T cells locally. **Hypothesis 2**: greater nutrient/oxygen diffusion at the top of the hydrogel promote better cell-cell interaction and response. **Hypothesis 3:** uneven stiffness level of the peptide hydrogel affect cell-cell interactions. **Hypothesis 4**: hydrogel support even nutrient/oxygen diffusion, retain similar stiffness level across the material and support bidirectional cell movement which overall result in all functional cells.

There are limitations associated with the biomaterial as well, and need to be addressed before actual research. First, the regulation of stiffness level, impacts the meshwork (pore) size and molecular diffusion throughout the gel [301, 307, 309]. It is reasonable to expect that varying stiffness level could impact the motility, cell-cell interactions, and nutrient access for cells. Nevertheless, restrictions of these parameters can be advantageous if the peptide hydrogel is intended to replicate tumour or fibrotic microenvironments that possess similar stiffness level [3, 213, 216, 502]. On the other hand, by modulating specific tissue area with high stiffness level and large porosity, e.g. swollen lymph nodes due to bacterial infections, bone structures or peripheral inflammation sites, the use of peptide hydrogels could be challenging [179, 514, 515]. Majedi et al (2020) used alginate hydrogel with various stiffness level but with the same pore size to analyse T cell function [161]. T cells clearly showed enhanced responses to APC in the rigid material with augmented proliferation and activation. The aim of this study was to produce replicate secondary lymphoid organs or peripheral tissues with varying stiffness level but retain similar pore sizes. Whereas with peptide hydrogel increased porosity or pore size, could weaken the hydrogel's structure towards the complete structural collapse. This leaves the future studies to decide the suitability of peptide hydrogel before actual studies

The durability or biodegradability of peptide hydrogels is another factor to be considered before studies. Due to the material's physical crosslinking, it is susceptible for degradation caused by enzymes, hydrolysis, pH change, high activity of cells and metabolic waste. This could be a challenge for long-term

culture studies, limiting cell activity under 3D culture settings. Depending on the goal of the study, degradation could be advantageous to permit cell migration, ECM deposition, drug release and even recovery of cells [146, 285, 295, 334, 476]. In contrast, if biodegradation becomes an issue for the study, it could be controlled by additional crosslinking (chemical bonding) process, which is known to reduce the biodegradation of other natural hydrogels [258, 516-518]. To this date, no crosslinking methods of FEFEFKFK peptide were studied, however other self-assembling peptide hydrogel such as FAQ(LDLK)3 have been successfully crosslinked with genipin [519]. Without genipin the hydrogel only lasted for 4 weeks, whereas in addition of the crosslinker the hydrogel degraded after 8-10 weeks. This also increased the stiffness level of the material, widening its use for other cell culture studies e.g. osteoblasts culture, which require high stiffness level. From FEFEFKFK perspective, the researcher could adjust other properties to minimise the degradation process e.g. reduce cell density, increase peptide concentration or functionalise with ECM components which promote the survival of cells i.e. fibronectin. All these factors could reduce the peptide hydrogel's degradation and prolong the studies' timeline.

One of the challenges with a 3D culture system is the limited access to the equipment or assays which are suitable for 3D culture type The majority of assays or equipment are designed for planar and suspension type cultures, without the presence of solid materials i.e. hydrogels [162]. There is an increase in equipment and assays adapted to analyse cells in greater dimensions, but their applicability is also limited by the type of biomaterials used in 3D cultures.

For example, MTT (tetrazolium salt) assay is used to assess cells' metabolic activity in hydrogels. For MTT assay, the media from the alginate hydrogel was collected for further analyses, whereas peptide and fibrin hydrogels did not produce MTT results even if they were degraded by DMSO [520, 521]. The advantage of the FEFEFKFK based hydrogel is that is modifiable, and methods could be adapted to obtain the required results. For example, in this study 3h-Thymidine and CFSE Cell Trace assays were adapted to study cells' proliferation, flow cytometry for phenotype marker expression, ELISA for secreted cytokines (with no background), and confocal microscopes for 3D imaging of cells. Nevertheless, due to 3D culture's increasing popularity and its importance in the academic fields, the methods will be more applicable for scientists to analyse cells.

Considering what has been established with the peptide hydrogels and T cells, future studies could study more 3D-tissue related questions and T cell's behaviour. The list of possible studies are:

- TME effect on T cell phenotype and function. Peptide hydrogel could provide a suppressive environment (i.e. stiffness, relevant ECM) against anti-tumour T cells, and analyse how TME affect cell's phenotype and functions.
- The efficacy of CAR-T cells or other genetically engineered T cells targeting cancer cells under TME influence. Produced anti-tumour T cells could be tested for their efficacy and effectiveness against cancer cells, that are cultured in hydrogel with defined TME features.

- Immune synapse formation of T cells and APC in the presence of healthy or tumour-related ECM components. One study showed that an increased stiffness level of the hydrogel induced larger immunological synapse formation than the soft material [161]. A similar question could be raised on whether ECM of tumour environment (i.e. increased stiffness level by added collagen) has a positive or negative impact on T cells synapse formation with APCs.

Furthermore, peptide hydrogel could be used as a 3D cell culture platform to analyse other immune cells. In this study, different T cell subtypes (CD4+ and CD8+) and monocyte or myeloid-derived DCs were tested in the peptide hydrogel, which confirmed the material's biocompatibility to host other immune cells. Future studies could consider analysing the NK cells, which are lymphocytes of the innate immune system with cytotoxic capabilities as T cells [522, 523]. NK cells have potential in cancer immunotherapy, but solid tumour environment challenges these cells' function [524-526]. The explanation relies on TME-created immunosuppressive environment due to metabolic depletion, inhibitory protein expression (e.g. PD-1, TGF-β) and presence of immunosuppressive cells (i.e. Tregs, TAMs) limiting NK anti-tumour effect [527-529]. One study used a microfluidic tumour-on-a-chip device, where MC7 cancer cells were encapsulated in collagen hydrogel [530]. NK cells migrated from the blood vessel-like structure to the tumour area and displayed exhaustion-related markers due to nutrient and oxygen depletion induced by the cancer cells [530]. FEFEFKFK peptide hydrogel could also explore the physical barrier (i.e. stiffness,

ECM) or defined ECM environment's effect, and determine the impact on NK cells. A better understanding of NK de-activation under TME settings could help to select a better therapeutic approach for solid tumours [531]. Other cells such as CAR-T cells, B cells, DCs and macrophages could be studied in the peptide hydrogel and understand how the tissue environment affects these cells.

An established 3D culture system could be also used to screen the personalised therapy and its efficacy before administering to the patient. Various hydrogels were adapted to find optimal treatment strategies for the disease [144, 250, 304, 308, 324, 331, 515, 517]. For example, hyaluronan hydrogel was used to recreate lung-invasive cancer environment and screen various drugs against patient-derived cancer cells [532]. The study showed how the currently used rapamycin (mTORC1 inhibitor) in clinics, had a small effect on lung cancer. The same study also tested various drugs in a 3D model and detected new potential drugs which suppressed the viability or invasiveness of cancer cells [532]. The same approach could be considered with peptide hydrogels for drug-screening tests.

Peptide hydrogel's purpose is not only limited to the 3D culture system and drug-screening platform but it could be also adapted for clinical use. One of the examples is the clinical implant, where self-assembling peptide hydrogel contained tumour-related antigens to induce anti-tumour response [533]. Su et al (2021) used peptide gel as a vaccine, which was composed of KWKAKAKAKWK peptides and contained tumour-related OVA antigens [533]. The gel promoted

DCs activation and enhanced CD4+ and CD8+ responses, which resulted in OVA-tumour regression in mice. Moreover, a recent study with FEFEFKFK showed its potential use for cancer immunotherapy [534]. The peptide hydrogel was used to expand CAR-T cell population to overcome 'traditional' protocol challenges, which result in poor T cells survival and effector function against solid tumours in vivo [534]. FEFEFKFK functionalised with LDV (adhesion motif) promoted better T cell expansion, and once injected into mice the gel reduced tumour growth and improved overall survival. This is the first study showing FEFEFKFK peptide hydrogel used for therapeutic purposes, which confirmed the material's biocompatibility for primary immune cells. At last, the peptide hydrogel could be used for tissue regeneration as well, where immune cells such as macrophages, could induce a healing process without scar tissue formation after inflammation [535].

In conclusion, the FEFEFKFK peptide hydrogel could enhance future in vitro studies, and nevertheless expand its horizon for studying various immune cells. Additional studies need to be conducted to confirm other T cell-related functions (i.e. migration, differentiation) and comprehend hydrogel's limitations and benefits for 3D culture studies. Nevertheless, T cell-related studies could shift from 2D culture to a more realistic 3D in vitro studies with more support given by the peptide hydrogels.

Appendix 1

Optimisation of peptide hydrogel degradation to release cells for flow cytometry analyses

Flow cytometry is an essential instrument to study immune cell function and phenotype, but it is only designed to analyse single cell or particle suspensions. For this matter, various degradation methods were explored to degrade the hydrogel effectively, without altering the cell's viability or their phenotype.

The first approach of this optimisation process was to find an effective reagent that could degrade the peptide hydrogel into smaller fragments, and pass through the flow cytometry with the lowest number of events (i.e. debris). Reagents were selected based on their ability to degrade proteins, such as: sodium dodecyl sulfate (SDS), KCl, media with acidic pH and enzyme trypsin [536-538]. 6mg/ml peptide gel was formed without cells and incubated with various reagents for 10 minutes, followed by a washing step at 300 x g for 10 minutes. After discarding the supernatant, the residue was reconstituted in media and analysed by flow cytometer for gel debris counts (events) (Figure 1). Peptide hydrogel was degraded efficiently by SDS higher than 1%. However, SDS degrades cells, and this hydrogel degradation method was applied for 3H-Thymidine assay to release DNA content. Trypsin at different concentrations (1x, 2x, 5x) and different incubation times (with 1x concentration) showed better results than KCl, in comparison to hydrogel degraded by water or PBS solutions

only. Acidic media were excluded from further studies since they could cause a negative effect on cells.

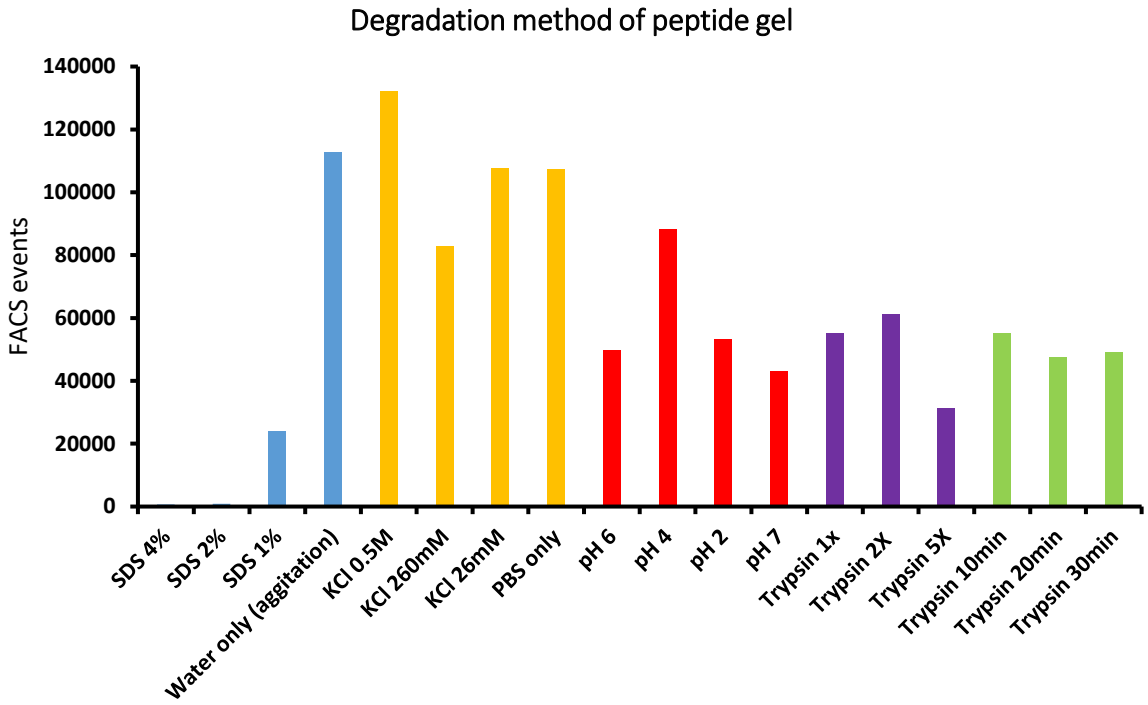

Figure 1. Gel debris (events) count by flow cytometer after peptide gel degradation. Peptide hydrogel were incubated with various reagents for 10 minutes, washed and centrifuged before flow cytometry analyses. The experiment was completed one time.

Trypsin is commonly used to detach adherent cells from the culture plates, so it was decided that this enzyme should be safe for cells. Higher concentrations of the trypsin were not tested further due to possible risks of affecting expression markers on the cells. Prolonged incubation with 1x Trypsin was tested first on T cells set up in 2D culture. Cells were incubated for the defined amount of time (minutes), washed and tested for CD4+ and CD3+ marker expression (resting T cells) and CD69+ (upregulated marker by activated T cells) (Figure 2). In comparison to control (no trypsin), prolonged incubation had a negative effect on resting T cells as the CD4+ and CD3+ markers expression was downregulated. Whereas activated T cells in exposure to Trypsin formed a second population

expressing CD69+, which was absent in the control. It was clear that Trypsin-based method is not ideal for cell release from the hydrogel, as it caused adverse effects on cells.

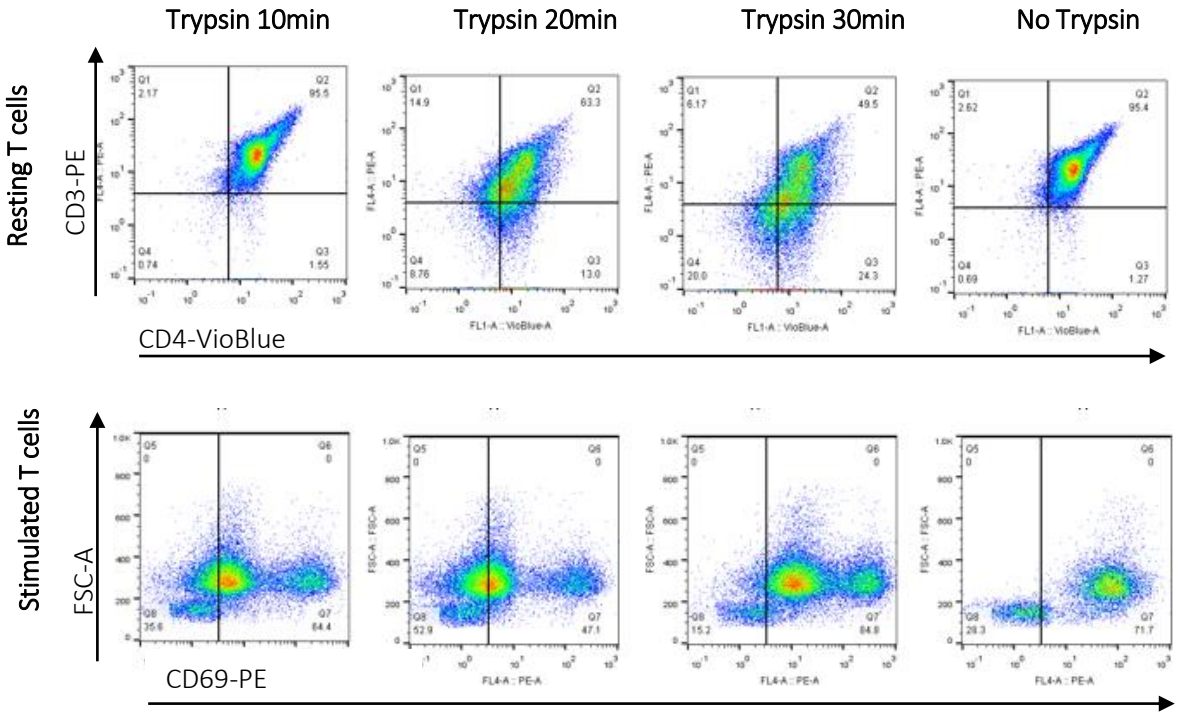

Figure 2. Prolonged incubation of Trypsin 1x effect on T cell marker expression. Cells were incubated in mediium containing 1x Trypsin concentration and incubated for the specific time (minutes). Cells were washed and stained with specific markers, to indicate trypsin effect on phenotype (CD3+CD4+ resting T cells) and dynamic markers (CD69+ for activated T cells) expression. Cells were analysed by flow cytometer. Experiment was completed one time.

Trypsin enzyme is a great candidate for degradation method due to its cleaving abilities at carboxyl group of lysine (K) region, which are also found in FEFEFKFK peptide hydrogels. In this case, Trypsin was substituted with TrypLE to degrade the hydrogels. TrypLE is a recombinant enzyme with the same cleaving target as Trypsin, however TrypLe is more 'safe' on cells that do not affect their markers expression and cell viability [539]. TrypLe (1x concentration) was tested with T cells labelled with CellTrace Violet encapsulated in the peptide hydrogel. Peptide

hydrogel was degraded by using TrypLE solution three times, including with multiple washing steps. After hydrogel degradation, the sample was also stained for CD4+ and CD3+ marker expression and compared against 2D cell culture. Cell gates from 2D culture were applied to the 3D culture, to define the regions of cells (Figure 3 (a)). After singlet exclusion, CellTrace Violet labelled T cells were excluded from the gel debris and showed CD4+ and CD3+ markers expression as 2D controls. However, the population of double positive cells appeared differently to 2D culture which could mean some of the cells are still surrounded by gel debris and interfere with marker specific antibodies (Figure 3 (b)).

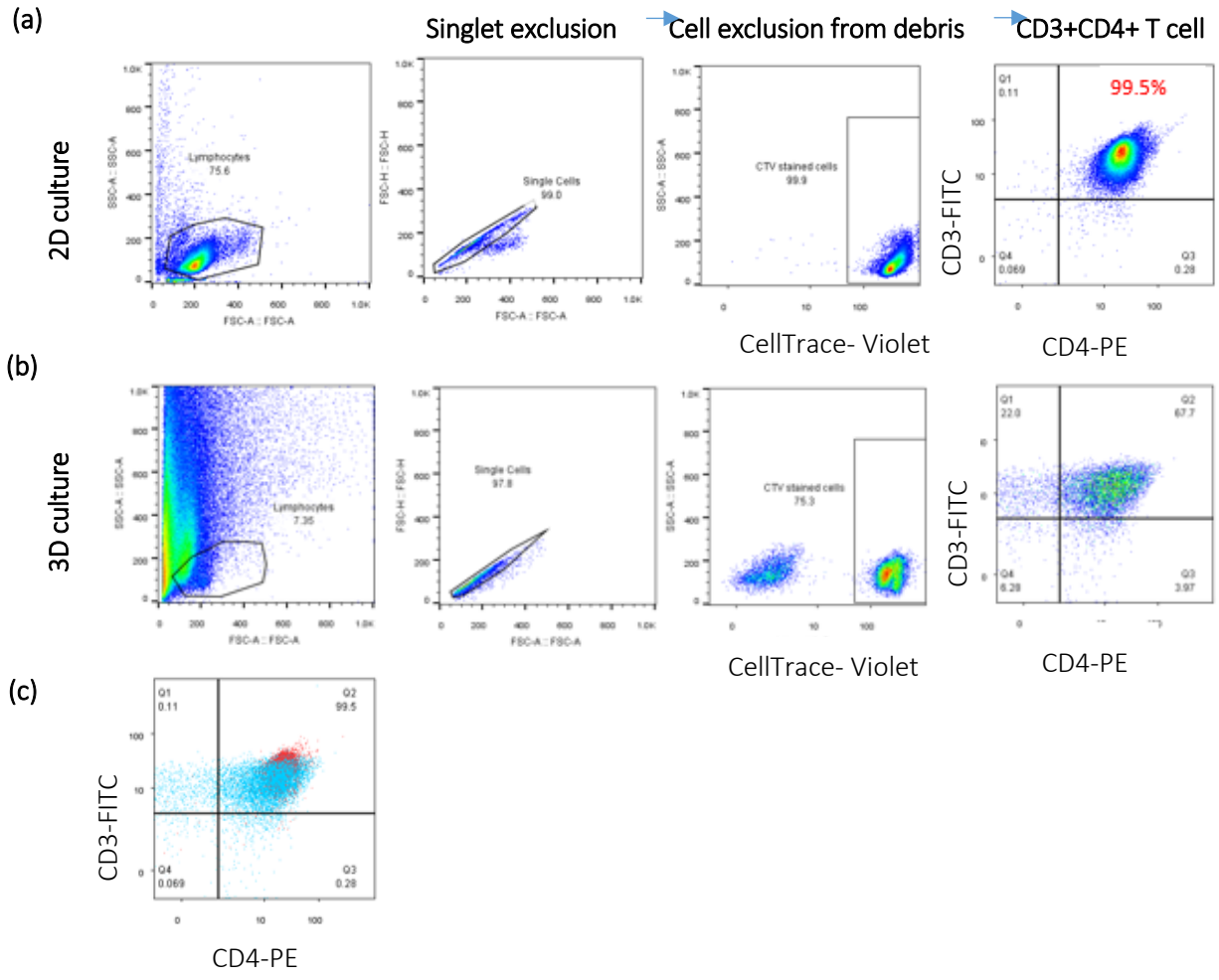

Figure 3. Releasing cells from the peptide hydrogel by TrypLE 1x solution. CellTrace Violet labelled T cells were encapsulated in the peptide hydrogel. a) 2D culture T cells were set up alongside 3D culture, and showed a double positive for CD3+ and CD4+ markers. b) Released T cells by TrypLE solution from the peptide hydrogel, were excluded from the rest of gel debris by CellTrace Violet dye. After staining, cells appeared as double positive for selected markers, but the fluorescent intensity and cell distribution didn't match the 2D culture (red colour) which was evident by overlying both population (c, backgating). Experiment completed one time.

Several adjustments for the degradation process were taken to improve removal of gel debris. It was noticed in one of the experiments that 50 Ficoll tubes improve gel debris removal during washing steps with TrypLE solution, then previously used 15 ficoll tubes (Figure 4). Also, hydrogel debris interacted with antibodies no matter their isotype, thus it was decided to include irrelevant antibodies to exclude hydrogel's fragments. In this case, isotype with selected fluorophore was used which cannot bind to cells and interact with debris only.

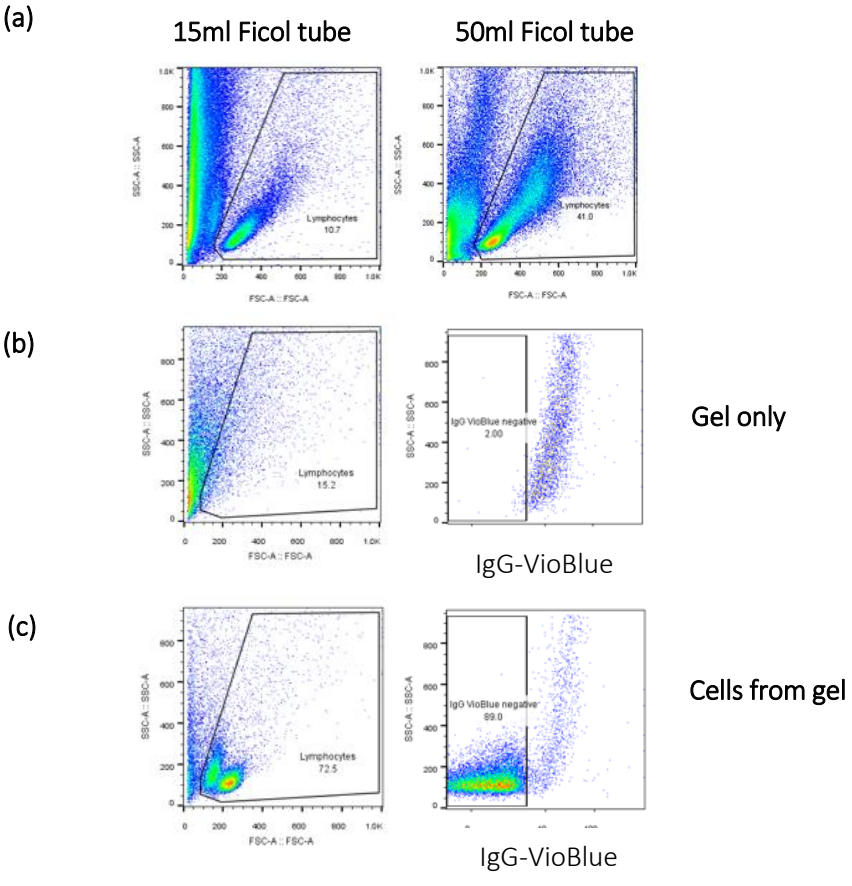

Figure 4. Change of Ficol tube during washing steps and irrelevant antibody exclude gel debris from analyses. a) Peptide gel was washed in 50ml Ficol tube, which improved gel debris removal from flow cytometry analyses. b) Peptide gel fragments were stained with IgG-VioBlue fluorophore, which appeared positive in VioBlue channel. This left a negative region where cells (c) released from peptide gel could be selected and further analysed in absence of gel fragments.

Adjusted degradation protocols were tested against resting and stimulated T cells encapsulated in the peptide hydrogel. Released cells were stained for CD3+CD4+ (phenotype markers) and CD25+ (upregulated during activation) and compared to the 2D culture. On day 3 of 3D culture, released resting T cells from the peptide hydrogel by TrypLE solution appeared CD3+ and CD4+ positive cells, but showed very low CD25+ expression which was expected from non-stimulated cells (Figure 5). Moreover, stimulated T cells released from the hydrogel retained their phenotype markers and were positive for CD25 as well. The same results were produced by 2D culture cells. Cell distribution and fluorescence intensity of each marker were comparable to the 2D culture, indicating a fully optimised degradation process of the peptide hydrogel.

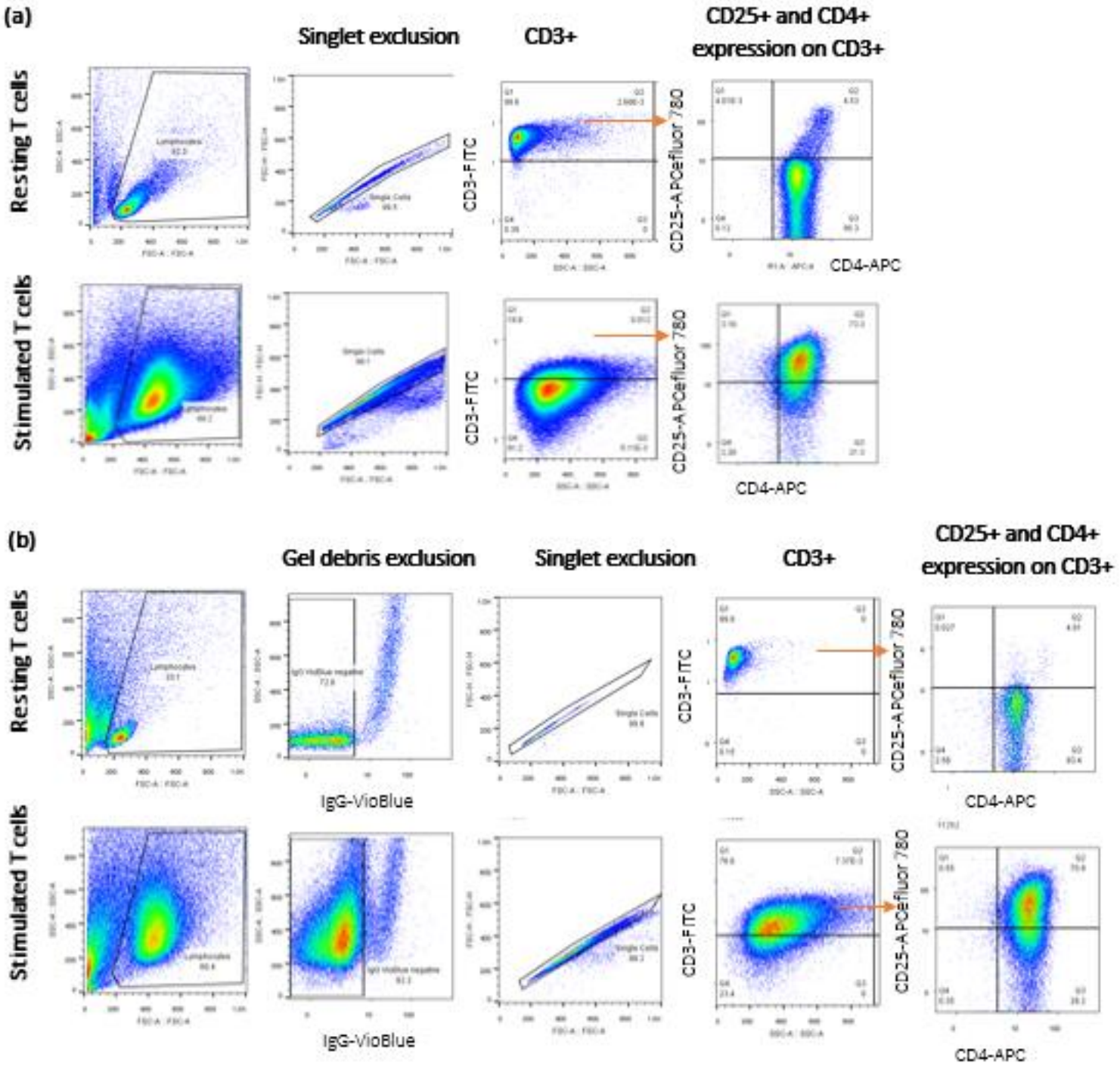

Figure 5. Comparison of T cell phenotype between 3D and 2D culture. Resting and activated T cells were encapsulated in the peptide hydrogel for 3 days and released by TrypLE solution. Same cells were also set up in 2D culture, and T cells from both cultures were stained for CD3+, CD4+ and CD25 marker expression and analysed by flow cytometry. 3D culture was stained with IgG-VioBlue for gel debris removal. a) 2D culture and b) 3D culture T cells show the same marker expressions. No peptide hydrogel fragments were interfering with flow cytometry analyses. Experiment completed one time.

References

1. Kambayashi, T. and T.M. Laufer, *Atypical MHC class II-expressing antigen-presenting cells: can anything replace a dendritic cell?* Nat Rev Immunol, 2014. **14**(11): p. 719-30.
2. Du, H., et al., *Tuning immunity through tissue mechanotransduction.* Nat Rev Immunol, 2022: p. 1-15.
3. Frantz, C., K.M. Stewart, and V.M. Weaver, *The extracellular matrix at a glance.* J Cell Sci, 2010. **123**(Pt 24): p. 4195-200.
4. Acerbi, I., et al., *Human breast cancer invasion and aggression correlates with ECM stiffening and immune cell infiltration.* Integrative Biology, 2015. **7**(10): p. 1120-1134.
5. D'Elios M.M., B.C.T., Annunziato F., *Cellular Primary Immunodeficiencies*. Rare Diseases of the Immune System. 2021: Springer Cham. XIV, 513.
6. DuPage, M. and J.A. Bluestone, *Harnessing the plasticity of CD4(+) T cells to treat immune-mediated disease.* Nat Rev Immunol, 2016. **16**(3): p. 149-63.
7. Roozendaal, R., R.E. Mebius, and G. Kraal, *The conduit system of the lymph node.* Int Immunol, 2008. **20**(12): p. 1483-7.
8. Handel, A.E., S.R. Irani, and G.A. Hollander, *The role of thymic tolerance in CNS autoimmune disease.* Nat Rev Neurol, 2018. **14**(12): p. 723-734.
9. Comabella, M., et al., *Targeting dendritic cells to treat multiple sclerosis.* Nat Rev Neurol, 2010. **6**(9): p. 499-507.
10. Woodland, D.L. and J.E. Kohlmeier, *Migration, maintenance and recall of memory T cells in peripheral tissues.* Nat Rev Immunol, 2009. **9**(3): p. 153-61.
11. Migalska, M., A. Sebastian, and J. Radwan, *Profiling of the TCRbeta repertoire in non-model species using high-throughput sequencing.* Sci Rep, 2018. **8**(1): p. 11613.
12. Girard, J.P., C. Moussion, and R. Forster, *HEVs, lymphatics and homeostatic immune cell trafficking in lymph nodes.* Nat Rev Immunol, 2012. **12**(11): p. 762-73.
13. Chaplin, D.D., *Overview of the immune response.* J Allergy Clin Immunol, 2010. **125**(2 Suppl 2): p. S3-23.
14. Corthay, A., *Does the immune system naturally protect against cancer?* Front Immunol, 2014. **5**: p. 197.
15. Marshall, J.S., et al., *An introduction to immunology and immunopathology.* Allergy Asthma Clin Immunol, 2018. **14**(Suppl 2): p. 49.
16. Iwasaki, A. and R. Medzhitov, *Control of adaptive immunity by the innate immune system.* Nat Immunol, 2015. **16**(4): p. 343-53.
17. McCusker, C., J. Upton, and R. Warrington, *Primary immunodeficiency.* Allergy Asthma Clin Immunol, 2018. **14**(Suppl 2): p. 61.
18. McLane, L.M., M.S. Abdel-Hakeem, and E.J. Wherry, *CD8 T Cell Exhaustion During Chronic Viral Infection and Cancer.* Annu Rev Immunol, 2019. **37**: p. 457-495.
19. Thommen, D.S. and T.N. Schumacher, *T Cell Dysfunction in Cancer.* Cancer Cell, 2018. **33**(4): p. 547-562.
20. Dispenza, M.C., *Classification of hypersensitivity reactions.* Allergy Asthma Proc, 2019. **40**(6): p. 470-473.
21. Pugliese, A., *Autoreactive T cells in type 1 diabetes.* J Clin Invest, 2017. **127**(8): p. 2881-2891.
22. Goodarzi, H., J. Trowbridge, and R.L. Gallo, *Innate immunity: a cutaneous perspective.* Clin Rev Allergy Immunol, 2007. **33**(1-2): p. 15-26.
23. Trompette, A. and N.D. Ubags, *Skin barrier immunology from early life to adulthood.* Mucosal Immunol, 2023. **16**(2): p. 194-207.
24. Chen, Y.E., M.A. Fischbach, and Y. Belkaid, *Skin microbiota-host interactions.* Nature, 2018. **553**(7689): p. 427-436.

25. Hunt, R.H., et al., *The stomach in health and disease.* Gut, 2015. **64**(10): p. 1650-68.
26. Netea, M.G., et al., *Immune sensing of Candida albicans requires cooperative recognition of mannans and glucans by lectin and Toll-like receptors.* J Clin Invest, 2006. **116**(6): p. 1642-50.
27. Pott, J., et al., *Age-dependent TLR3 expression of the intestinal epithelium contributes to rotavirus susceptibility.* PLoS Pathog, 2012. **8**(5): p. e1002670.
28. Zindel, J. and P. Kubes, *DAMPs, PAMPs, and LAMPs in Immunity and Sterile Inflammation.* Annu Rev Pathol, 2020. **15**: p. 493-518.
29. Jung, H.C., et al., *A distinct array of proinflammatory cytokines is expressd in human colon epithelial cells in response to bacterial invasion.* J Clin Invest, 1995. **95**(1): p. 55-65.
30. Berin, M.C., et al., *Production of MDC/CCL22 by human intestinal epithelial cells.* Am J Physiol Gastrintest Liver Physiol, 2001. **280**(6).
31. Perez-Ruiz, M., et al., *Vascular endothelial growth factor production in peritoneal macrophages of cirrhotic patients: regulation by cytokines and bacterial lipopolysaccharide.* Hepatology, 1999. **29**(4): p. 1057-63.
32. Tinsley, J.H., et al., *Activated neutrophils induce hyperpermeability and phosphorylation of adherens junction proteins in coronary venular endothelial cells.* J Biol Chem, 1999. **274**(35): p. 24930-4.
33. DiStasi, M.R. and K. Ley, *Opening the flood-gates: how neutrophil-endothelial interactions regulate permeability.* Trends Immunol, 2009. **30**(11): p. 547-56.
34. Escudero-Perez, B., et al., *Shed GP of Ebola virus triggers immune activation and increased vascular permeability.* PLoS Pathog, 2014. **10**(11): p. e1004509.
35. Sun, L., et al., *Innate-adaptive immunity interplay and redox regulation in immune response.* Redox Biol, 2020. **37**: p. 101759.
36. Thomsen, I.P., et al., *Children with invasive Staphylococcus aureus disease exhibit a potently neutralizing antibody response to the cytotoxin LukAB.* Infect Immun, 2014. **82**(3): p. 1234-42.
37. Taborda, C.A. and A. Casadevall, *CR3 (CD11b/CD18) and CR4 (CD11c/CD18) Are Involved in Complement-Independent Antibody-Mediated Phagocytosis of Cryptococcus neoformans.* Immunity, 2002. **16**: p. 791-802.
38. Duesber, U., et al., *Natural cytotoxicity and antibody-dependent cellular cytotoxicity (ADCC) is not impaired in patients suffering from chronic hepatitis C.* Journal of hepatology, 2001. **35**(5): p. 650-7.
39. Roth, K., et al., *Tracking plasma cell differentiation and survival.* Cytometry A, 2014. **85**(1): p. 15-24.
40. Nishioka, Y. and P.E. Lipsky, *The role of CD40-CD40 ligand interaction in human T cell-B cell collaboration.* The Journal of Immunology, 1994. **153**(3): p. 1027-1036.
41. Maliszewski, C.R., et al., *Recombinant CD40 ligand stimulation of murine B cell growth and differentiation: cooperative effects of cytokines.* Eur J Immunol, 1993. **23**(5): p. 1044-9.
42. Bukowski, J.F., et al., *Dengue virus-specific cross-reactive CD8+ human cytotoxic T lymphocytes.* Journal of virology, 1989. **63**(12): p. 5086-5091.
43. Jin, Y., et al., *CXCR5(+)CD8(+) T cells could induce the death of tumor cells in HBV-related hepatocellular carcinoma.* Int Immunopharmacol, 2017. **53**: p. 42-48.
44. Pennock, N.D., et al., *T cell responses: naive to memory and everything in between.* Adv Physiol Educ, 2013. **37**(4): p. 273-83.
45. Akkaya, M., K. Kwak, and S.K. Pierce, *B cell memory: building two walls of protection against pathogens.* Nat Rev Immunol, 2020. **20**(4): p. 229-238.
46. Weinberg, A. and M.J. Levin, *VZV T cell-mediated immunity.* Curr Top Microbiol Immunol, 2010. **342**: p. 341-57.
47. Freer, G. and M. Pistello, *Varicella-zoster virus infection: natural history, clinical manifestations, immunity and current and future vaccination strategies.* New Microbiologica, 2018. **41**(2): p. 95-105.

48. Gershon, A.A., S.P. Steinberg, and L. Gelb, *Clinical Reinfection with Varicella-Zoster Virus.* The Journal of infectious disease, 1984. **149**(2): p. 137-142.
49. Sherwood, E.R., et al., *Innate Immune Memory and the Host Response to Infection.* J Immunol, 2022. **208**(4): p. 785-792.
50. Broere, F., et al., *A2 T cell subsets and T cell-mediated immunity*, in *Principles of Immunopharmacology: 3rd revised and extended edition*, F.P. Nijkamp and M.J. Parnham, Editors. 2011, Birkhäuser Basel: Basel. p. 15-27.
51. Rutishauser, R.L. and S.M. Kaech, *Generating diversity: transcriptional regulation of effector and memory CD8 T-cell differentiation.* Immunol Rev, 2010. **235**(1): p. 219-33.
52. Kagi, D., et al., *Fas and Perforin Pathways as Major Mechanisms of T cell Mediated Cytotoxicity.* Science, 1994. **265**(5171): p. 528-530.
53. Sakaguchi, S., et al., *Regulatory T cells and immune tolerance.* Cell, 2008. **133**(5): p. 775-87.
54. Morel, P.A., et al., *Modeling the T cell immune response: a fascinating challenge.* J Pharmacokinet Pharmacodyn, 2014. **41**(5): p. 401-13.
55. Mahallawi, W.H., et al., *MERS-CoV infection in humans is associated with a pro-inflammatory Th1 and Th17 cytokine profile.* Cytokine, 2018. **104**: p. 8-13.
56. Zhu, J., *T Helper Cell Differentiation, Heterogeneity, and Plasticity.* Cold Spring Harb Perspect Biol, 2018. **10**(10).
57. Robinson, S.R., et al., *Predominant Th2-like bronchoalveolar T-lymphocyte population in atopic asthma.* The New Enfland Journal of Medicine, 1992. **326**(5): p. 298-304.
58. Dudakov, J.A., A.M. Hanash, and M.R. van den Brink, *Interleukin-22: immunobiology and pathology.* Annu Rev Immunol, 2015. **33**: p. 747-85.
59. Stanko, K., et al., *CD96 expression determines the inflammatory potential of IL-9-producing Th9 cells.* Proc Natl Acad Sci U S A, 2018. **115**(13): p. E2940-E2949.
60. Chen, T., et al., *Th9 Cell Differentiation and Its Dual Effects in Tumor Development.* Front Immunol, 2020. **11**: p. 1026.
61. Whiteside, T.L., *Regulatory T cell subsets in human cancer: are they regulating for or against tumor progression?* Cancer Immunol Immunother, 2014. **63**(1): p. 67-72.
62. Zhao, H., X. Liao, and Y. Kang, *Tregs: Where We Are and What Comes Next?* Front Immunol, 2017. **8**: p. 1578.
63. Gol-Ara, M., et al., *The role of different subsets of regulatory T cells in immunopathogenesis of rheumatoid arthritis.* Arthritis, 2012. **2012**: p. 805875.
64. Cazac, B.B. and J. Roes, *TGF-beta receptor controls B cell responsiveness and induction of IgA in vivo.* Immunity, 2000. **13**(4): p. 443-451.
65. Brockmann, L., et al., *IL-10 Receptor Signaling Is Essential for TR1 Cell Function In Vivo.* J Immunol, 2017. **198**(3): p. 1130-1141.
66. Hoyne, G.F., *Notch signaling in the immune system.* J Leukoc Biol, 2003. **74**(6): p. 971-81.
67. Metcalf, D., *On hematopoietic stem cell fate.* Immunity, 2007. **26**(6): p. 669-73.
68. Chen, E.L.Y., P.K. Thompson, and J.C. Zuniga-Pflucker, *RBPJ-dependent Notch signaling initiates the T cell program in a subset of thymus-seeding progenitors.* Nat Immunol, 2019. **20**(11): p. 1456-1468.
69. Sottoriva, K. and K.V. Pajcini, *Notch Signaling in the Bone Marrow Lymphopoietic Niche.* Front Immunol, 2021. **12**: p. 723055.
70. Shah, D.K. and J.C. Zuniga-Pflucker, *An overview of the intrathymic intricacies of T cell development.* J Immunol, 2014. **192**(9): p. 4017-23.
71. James, K.D., W.E. Jenkinson, and G. Anderson, *T-cell egress from the thymus: Should I stay or should I go?* J Leukoc Biol, 2018. **104**(2): p. 275-284.
72. Takaba, H. and H. Takayanagi, *The Mechanisms of T Cell Selection in the Thymus.* Trends Immunol, 2017. **38**(11): p. 805-816.
73. Owen, D.L., L.E. Sjaastad, and M.A. Farrar, *Regulatory T Cell Development in the Thymus.* J Immunol, 2019. **203**(8): p. 2031-2041.

74. van den Broek, T., J.A.M. Borghans, and F. van Wijk, *The full spectrum of human naive T cells.* Nat Rev Immunol, 2018. **18**(6): p. 363-373.
75. Nishana, M. and S.C. Raghavan, *Role of recombination activating genes in the generation of antigen receptor diversity and beyond.* Immunology, 2012. **137**(4): p. 271-81.
76. Jameson, S.C. and D. Masopust, *Understanding Subset Diversity in T Cell Memory.* Immunity, 2018. **48**(2): p. 214-226.
77. Jenkins, M.K. and J.J. Moon, *The role of naive T cell precursor frequency and recruitment in dictating immune response magnitude.* J Immunol, 2012. **188**(9): p. 4135-40.
78. Peng, Y., et al., *An immunodominant NP(105-113)-B*07:02 cytotoxic T cell response controls viral replication and is associated with less severe COVID-19 disease.* Nat Immunol, 2022. **23**(1): p. 50-61.
79. Cachot, A., et al., *Tumor-specific cytolytic CD4 T cells mediate immunity against human cancer.* Science Advances, 2021. **7**(9).
80. Penkava, F., et al., *Single-cell sequencing reveals clonal expansions of pro-inflammatory synovial CD8 T cells expressing tissue-homing receptors in psoriatic arthritis.* Nat Commun, 2020. **11**(1): p. 4767.
81. Junt, T., E. Scandella, and B. Ludewig, *Form follows function: lymphoid tissue microarchitecture in antimicrobial immune defence.* Nat Rev Immunol, 2008. **8**(10): p. 764-75.
82. Gasteiger, G., M. Ataide, and W. Kastenmuller, *Lymph node - an organ for T-cell activation and pathogen defense.* Immunol Rev, 2016. **271**(1): p. 200-20.
83. Mebius, R.E. and G. Kraal, *Structure and function of the spleen.* Nat Rev Immunol, 2005. **5**(8): p. 606-16.
84. Lewis, S.M., A. Williams, and S.C. Eisenbarth, *Structure and function of the immune system in the spleen.* Sci Immunol, 2019. **4**(33).
85. Jung, C., J.P. Hugot, and F. Barreau, *Peyer's Patches: The Immune Sensors of the Intestine.* Int J Inflam, 2010. **2010**: p. 823710.
86. Matsuno, K., et al., *A Life-Stage of Particle-laden Rat Dendritic Cells In Vivo: Their Terminal Diviison, Active Phgaocytosis, and Translocation from the Liver to the Draining Lymph.* J Exp Med, 1996. **183**(4): p. 1865-1878.
87. Blaauboer, S.M., et al., *The mucosal adjuvant cyclic di-GMP enhances antigen uptake and selectively activates pinocytosis-efficient cells in vivo.* Elife, 2015. **4**.
88. Neupane, A.S., et al., *Patrolling Alveolar Macrophages Conceal Bacteria from the Immune System to Maintain Homeostasis.* Cell, 2020. **183**(1): p. 110-125 e11.
89. Kapsenberg, M.L., *Dendritic-cell control of pathogen-driven T-cell polarization.* Nat Rev Immunol, 2003. **3**(12): p. 984-93.
90. Rock, K.L., E. Reits, and J. Neefjes, *Present Yourself! By MHC Class I and MHC Class II Molecules.* Trends Immunol, 2016. **37**(11): p. 724-737.
91. Miller, M.J., et al., *Imaging the single cell dynamics of CD4+ T cell activation by dendritic cells in lymph nodes.* J Exp Med, 2004. **200**(7): p. 847-56.
92. Adams, N.M., S. Grassmann, and J.C. Sun, *Clonal expansion of innate and adaptive lymphocytes.* Nat Rev Immunol, 2020. **20**(11): p. 694-707.
93. Nijkamp, F.P. and M.J. Parnham, *Principles of immunopharmacology / edited by Frans P. Nijkamp and Michael J. Parnham.* 2005.
94. Fahmy, T.M., et al., *Increased TCR Avidity after T cell Activation: A Mechanism for Sensing Low-Density Antigen.* Immunity, 2001. **14**: p. 135-143.
95. Schodin, B.A., T.J. Tsomides, and D.M. Kranz, *Correlation Between the Number of T cell Receptors Required for T Cell Activation and TCR-Ligand Affinity.* Immunity, 1996. **5**(2): p. 137-146.
96. Bhattacharyya, N.D. and C.G. Feng, *Regulation of T Helper Cell Fate by TCR Signal Strength.* Front Immunol, 2020. **11**: p. 624.

97. Huse, M., *The T-cell-receptor signaling network.* J Cell Sci, 2009. **122**(Pt 9): p. 1269-73.
98. Kearney, C.J., et al., *The Role of the immunological Synapse Formed by Cytotoxic Lymphocytes in Immunodeficiency and Anti-Tumor immunity.* Crit Rev Immunol, 2015. **35**(4): p. 325-47.
99. Dustin, M.L. and T.A. Springer, *T-cell receptor crosslinking transiently stimulates adhesiveness through LFA-1.* Nature, 1989. **341**: p. 619-624.
100. Chen, X., et al., *Requirement of open headpiece conformation for activation of leukocyte integrin alphaXbeta2.* Proc Natl Acad Sci U S A, 2010. **107**(33): p. 14727-32.
101. Ma, V.P.Y., et al., *The magnitude of LFA-1/ICAM-1 forxes fine-tune TCR-triggered T cell activation.* Science Advances, 2022. **8**(8).
102. Beyersdorf, N., T. Kerkau, and T. Hunig, *CD28 co-stimulation in T-cell homeostasis: a recent perspective.* Immunotargets Ther, 2015. **4**: p. 111-22.
103. Smith-Garvin, J.E., G.A. Koretzky, and M.S. Jordan, *T cell activation.* Annu Rev Immunol, 2009. **27**: p. 591-619.
104. Boise, L.H., et al., *CD28 Costimulation Can Promote T cell Survival by Enhancing the Expression of Bcl-xl.* Immunity, 1995. **3**: p. 87-98.
105. Hubo, M., et al., *Costimulatory molecules on immunogenic versus tolerogenic human dendritic cells.* Front Immunol, 2013. **4**: p. 82.
106. Schenkel, J.M., et al., *Resident memory CD8 T cells trigger protective innate and adaptive immune responses.* N Engl J Med, 2014. **346**(6205): p. 98-101.
107. Lundie, R.J., et al., *A central role for hepatic conventional dendritic cells in supporting Th2 responses during helminth infection.* Immunol Cell Biol, 2016. **94**(4): p. 400-10.
108. Magalhaes, J.G., et al., *Nod2-dependent Th2 polarization of antigen-specific immunity.* J Immunol, 2008. **181**(11): p. 7925-35.
109. Harris, N. and W.C. Gause, *To B or not to B: B cells and the Th2-type immune response to helminths.* Trends Immunol, 2011. **32**(2): p. 80-8.
110. Chen, J.H., et al., *Enhancement of CTLs induced by DCs loaded with ubiquitinated hepatitis B virus core antigen.* World J Gastroenterol, 2012. **18**(12): p. 1319-27.
111. Snell, L.M., et al., *Overcoming CD4 Th1 Cell Fate Restrictions to Sustain Antiviral CD8 T Cells and Control Persistent Virus Infection.* Cell Rep, 2016. **16**(12): p. 3286-3296.
112. Herd, K.A., et al., *Pulmonary infection of mice with human metapneumovirus induces local cytotoxic T-cell and immunoregulatory cytokine responses similar to those seen with human respiratory syncytial virus.* J Gen Virol, 2010. **91**(Pt 5): p. 1302-10.
113. Martinez-Sanchez, M.E., et al., *Role of Cytokine Combinations on CD4+ T Cell Differentiation, Partial Polarization, and Plasticity: Continuous Network Modeling Approach.* Front Physiol, 2018. **9**: p. 877.
114. Gutcher, I. and B. Becher, *APC-derived cytokines and T cell polarization in autoimmune inflammation.* J Clin Invest, 2007. **117**(5): p. 1119-27.
115. Russ, B.E., et al., *T cell immunity as a tool for studying epigenetic regulation of cellular differentiation.* Front Genet, 2013. **4**: p. 218.
116. Tay, R.E., E.K. Richardson, and H.C. Toh, *Revisiting the role of CD4(+) T cells in cancer immunotherapy-new insights into old paradigms.* Cancer Gene Ther, 2021. **28**(1-2): p. 5-17.
117. Curtsinger, J.M. and M.F. Mescher, *Inflammatory cytokines as a third signal for T cell activation.* Curr Opin Immunol, 2010. **22**(3): p. 333-40.
118. Lamichhane, R. and J.E. Ussher, *Expression and trafficking of MR1.* Immunology, 2017. **151**(3): p. 270-279.
119. Van Rhijn, I., et al., *Lipid and small-molecule display by CD1 and MR1.* Nat Rev Immunol, 2015. **15**(10): p. 643-54.
120. Howson, L.J., M. Salio, and V. Cerundolo, *MR1-Restricted Mucosal-Associated Invariant T Cells and Their Activation during Infectious Diseases.* Front Immunol, 2015. **6**: p. 303.

121. Benvenuti, F., *The Dendritic Cell Synapse: A Life Dedicated to T Cell Activation.* Front Immunol, 2016. **7**: p. 70.
122. Hasegawa, H. and T. Matsumoto, *Mechanisms of Tolerance Induction by Dendritic Cells In Vivo.* Front Immunol, 2018. **9**: p. 350.
123. Lutz, M.B. and G. Schuler, *Immature, semi-mature and fully mature dendritic cells: which signals induce tolerance or immunity?* Trends in Immunology, 2002. **23**(9): p. 445-449.
124. Saeki, H., et al., *Cutting Edge: Secondary Lymphoid-Tissue Chemokine (SLC) and CC Chemokine Receptor 7 (CCR7) Participate in the Emigration Pathway of Mature Dendritic Cells from the Skin to Regional Lymph Nodes.* The Journal of Immunology, 1999. **162**(5): p. 2472-2475.
125. Polak, D. and B. Bohle, *Neutrophils-typical atypical antigen presenting cells?* Immunol Lett, 2022. **247**: p. 52-58.
126. Steimle, V., et al., *Regulation of MHC class II expression by interferon-gamma mediated by the transactivator gene CIITA.* Science, 1994. **265**(5168): p. 106-9.
127. Boyman, O., et al., *Homeostatic proliferation and survival of naive and memory T cells.* Eur J Immunol, 2009. **39**(8): p. 2088-94.
128. Kaech, S.M., E.J. Wherry, and R. Ahmed, *Effector and memory T-cell differentiation: implications for vaccine development.* Nat Rev Immunol, 2002. **2**(4): p. 251-62.
129. Kumar, B.V., T.J. Connors, and D.L. Farber, *Human T Cell Development, Localization, and Function throughout Life.* Immunity, 2018. **48**(2): p. 202-213.
130. Mueller, S.N., et al., *Memory T cell subsets, migration patterns, and tissue residence.* Annu Rev Immunol, 2013. **31**: p. 137-61.
131. Rodda, L.B., et al., *Functional SARS-CoV-2-Specific Immune Memory Persists after Mild COVID-19.* Cell, 2021. **184**(1): p. 169-183 e17.
132. Omilusik, K.D. and A.W. Goldrath, *Remembering to remember: T cell memory maintenance and plasticity.* Curr Opin Immunol, 2019. **58**: p. 89-97.
133. Barbouti, A., et al., *In situ evidence of cellular senescence in Thymic Epithelial Cells (TECs) during human thymic involution.* Mech Ageing Dev, 2019. **177**: p. 88-90.
134. Surh, C.D. and J. Sprent, *Homeostasis of naive and memory T cells.* Immunity, 2008. **29**(6): p. 848-62.
135. Naito, T., et al., *Transcriptional control of T-cell development.* Int Immunol, 2011. **23**(11): p. 661-8.
136. Conley, J.M., M.P. Gallagher, and L.J. Berg, *T Cells and Gene Regulation: The Switching On and Turning Up of Genes after T Cell Receptor Stimulation in CD8 T Cells.* Front Immunol, 2016. **7**: p. 76.
137. Koh, C.H., et al., *CD8 T-cell subsets: heterogeneity, functions, and therapeutic potential.* Exp Mol Med, 2023. **55**(11): p. 2287-2299.
138. Bartsch, P., et al., *Th17 cell plasticity towards a T-bet-dependent Th1 phenotype is required for bacterial control in Staphylococcus aureus infection.* PLoS Pathog, 2022. **18**(4): p. e1010430.
139. Jensen, C. and Y. Teng, *Is It Time to Start Transitioning From 2D to 3D Cell Culture?* Front Mol Biosci, 2020. **7**: p. 33.
140. Hoarau-Vechot, J., et al., *Halfway between 2D and Animal Models: Are 3D Cultures the Ideal Tool to Study Cancer-Microenvironment Interactions?* Int J Mol Sci, 2018. **19**(1).
141. Sohrabi, C., et al., *Impact of the coronavirus (COVID-19) pandemic on scientific research and implications for clinical academic training - A review.* Int J Surg, 2021. **86**: p. 57-63.
142. Langhans, S.A., *Three-Dimensional in Vitro Cell Culture Models in Drug Discovery and Drug Repositioning.* Front Pharmacol, 2018. **9**: p. 6.
143. Mahendiran, B., et al., *Decellularized natural 3D cellulose scaffold derived from Borassus flabellifer (Linn.) as extracellular matrix for tissue engineering applications.* Carbohydr Polym, 2021. **272**: p. 118494.

144. Lee, J.M., et al., *Generation of uniform-sized multicellular tumor spheroids using hydrogel microwells for advanced drug screening.* Sci Rep, 2018. **8**(1): p. 17145.
145. Michalaki, E., et al., *Perpendicular alignment of lymphatic endothelial cells in response to spatial gradients in wall shear stress.* Commun Biol, 2020. **3**(1): p. 57.
146. Caliari, S.R. and J.A. Burdick, *A practical guide to hydrogels for cell culture.* Nat Methods, 2016. **13**(5): p. 405-14.
147. Verollet, C., V. Le Cabec, and I. Maridonneau-Parini, *HIV-1 Infection of T Lymphocytes and Macrophages Affects Their Migration via Nef.* Front Immunol, 2015. **6**: p. 514.
148. Kaldjian, E.P., et al., *Spatial and molecular organization of lymph node T cell cortex: a labyrinthine cavity bounded by an epithelium-like monolayer of fibroblastic reticular cells anchored to basement membrane-like extracellular matrix.* Int Immunol, 2001. **13**(10): p. 1243-53.
149. Poirot, J., et al., *Compartmentalized multicellular crosstalk in lymph nodes coordinates the generation of potent cellular and humoral immune responses.* Eur J Immunol, 2021. **51**(12): p. 3146-3160.
150. Sixt, M., et al., *The conduit system transports soluble antigens from the afferent lymph to resident dendritic cells in the T cell area of the lymph node.* Immunity, 2005. **22**(1): p. 19-29.
151. Sobocinski, G.P., et al., *Ultrastructural localization of extracellular matrix proteins of the lymph node cortex: evidence supporting the reticular network as a pathway for lymphocyte migration.* BMC Immunol, 2010. **11**: p. 42.
152. Sapudom, J., et al., *Dendritic cell immune potency on 2D and in 3D collagen matrices.* Biomater Sci, 2020. **8**(18): p. 5106-5120.
153. Kapalczynska, M., et al., *2D and 3D cell cultures - a comparison of different types of cancer cell cultures.* Arch Med Sci, 2018. **14**(4): p. 910-919.
154. Cha, B.H., et al., *Integrin-Mediated Interactions Control Macrophage Polarization in 3D Hydrogels.* Adv Healthc Mater, 2017. **6**(21).
155. Duval, K., et al., *Modeling Physiological Events in 2D vs. 3D Cell Culture.* Physiology (Bethesda), 2017. **32**(4): p. 266-277.
156. Fang, Y., et al., *Collagen scaffold microenvironments modulate cell lineage commitment for differentiation of bone marrow cells into regulatory dendritic cells.* Sci Rep, 2017. **7**: p. 42049.
157. Ando, Y., et al., *Evaluating CAR-T Cell Therapy in a Hypoxic 3D Tumor Model.* Adv Healthc Mater, 2019. **8**(5): p. e1900001.
158. Feder-Mengus, C., et al., *New dimensions in tumor immunology: what does 3D culture reveal?* Trends Mol Med, 2008. **14**(8): p. 333-40.
159. Gunzer, M., et al., *Antigen presentation in extracellular matrix: interactions of T cells with dendritic cells are dynamic, short lived, and sequential.* Immunity, 2000. **13**(3): p. 323-32.
160. Pavesi, A., et al., *A 3D microfluidic model for preclinical evaluation of TCR-engineered T cells against solid tumors.* JCI Insight, 2017. **2**(12).
161. Majedi, F.S., et al., *T-cell activation is modulated by the 3D mechanical microenvironment.* Biomaterials, 2020. **252**: p. 120058.
162. Fitzgerald, A.A., E. Li, and L.M. Weiner, *3D Culture Systems for Exploring Cancer Immunology.* Cancers (Basel), 2020. **13**(1).
163. Wallstabe, L., et al., *ROR1-CAR T cells are effective against lung and breast cancer in advanced microphysiologic 3D tumor models.* JCI Insight, 2019. **4**(18).
164. Kuczek, D.E., et al., *Collagen density regulates the activity of tumor-infiltrating T cells.* J Immunother Cancer, 2019. **7**(1): p. 68.
165. Levental, I., P.C. Georges, and P.A. Janmey, *Soft biological materials and their impact on cell function.* Soft Matter, 2007. **3**(3): p. 299-306.
166. Fruhauf, M., et al., *Construction of a 3D brain extracellular matrix model to study the interaction between microglia and T cells in co-culture.* Eur J Neurosci, 2021. **53**(12): p. 4034-4050.

167. Gao, H., et al., *3D Extracellular Matrix Regulates the Activity of T Cells and Cancer Associated Fibroblasts in Breast Cancer.* Front Oncol, 2021. **11**: p. 764204.
168. de Haan, L., et al., *A Microfluidic 3D Endothelium-on-a-Chip Model to Study Transendothelial Migration of T Cells in Health and Disease.* Int J Mol Sci, 2021. **22**(15).
169. Shin, J.U., et al., *Recapitulating T cell infiltration in 3D psoriatic skin models for patient-specific drug testing.* Sci Rep, 2020. **10**(1): p. 4123.
170. Mollica, H., et al., *A 3D pancreatic tumor model to study T cell infiltration.* Biomater Sci, 2021. **9**(22): p. 7420-7431.
171. Willard-Mack, C.L., *Normal structure, function, and histology of lymph nodes.* Toxicol Pathol, 2006. **34**(5): p. 409-24.
172. Krivacic, K.A. and A.D. Levine, *Extracellular matrix conditions T cells for adhesion to tissue interstitium.* J Immunol, 2003. **170**(10): p. 5034-44.
173. Krummel, M.F., F. Bartumeus, and A. Gerard, *T cell migration, search strategies and mechanisms.* Nat Rev Immunol, 2016. **16**(3): p. 193-201.
174. Tomura, M., et al., *Monitoring cellular movement in ivo with photoconvertible fluorescence protein "Kaede" trasngenic mice.* PNAS, 2008. **105**(31): p. 10871-10876.
175. Bousso, P., *T-cell activation by dendritic cells in the lymph node: lessons from the movies.* Nat Rev Immunol, 2008. **8**(9): p. 675-84.
176. Bao, X., et al., *Endothelial heparan sulfate controls chemokine presentation in recruitment of lymphocytes and dendritic cells to lymph nodes.* Immunity, 2010. **33**(5): p. 817-29.
177. de la Zerda, A., et al., *Review: Bioengineering strategies to probe T cell mechanobiology.* APL Bioeng, 2018. **2**(2): p. 021501.
178. Bae, S.J., et al., *Ex Vivo Shear-Wave Elastography of Axillary Lymph Nodes to Predict Nodal Metastasis in Patients with Primary Breast Cancer.* J Breast Cancer, 2018. **21**(2): p. 190-196.
179. Qin, Q., et al., *Evaluating Lymph Node Stiffness to Differentiate Bacterial Cervical Lymphadenitis and Lymph Node-First Presentation of Kawasaki Disease by Shear Wave Elastography.* J Ultrasound Med, 2021. **40**(7): p. 1371-1380.
180. Meng, K.P., et al., *Mechanosensing through YAP controls T cell activation and metabolism.* J Exp Med, 2020. **217**(8).
181. Bonnans, C., J. Chou, and Z. Werb, *Remodelling the extracellular matrix in development and disease.* Nat Rev Mol Cell Biol, 2014. **15**(12): p. 786-801.
182. Sorokin, L., *The impact of the extracellular matrix on inflammation.* Nat Rev Immunol, 2010. **10**(10): p. 712-23.
183. Stratman, A.N. and G.E. Davis, *Endothelial cell-pericyte interactions stimulate basement membrane matrix assembly: influence on vascular tube remodeling, maturation, and stabilization.* Microsc Microanal, 2012. **18**(1): p. 68-80.
184. Lu, P., et al., *Extracellular matrix degradation and remodeling in development and disease.* Cold Spring Harb Perspect Biol, 2011. **3**(12).
185. Vestweber, D., *How leukocytes cross the vascular endothelium.* Nat Rev Immunol, 2015. **15**(11): p. 692-704.
186. Wolf, K., et al., *Amoeboid shape change and contact guidance: T-lymphocyte crawling through fibrillar collagen is independent of matrix remodeling by MMPs and other proteases.* Blood, 2003. **102**(9): p. 3262-9.
187. Rocha-Perugini, V. and J.M. Gonzalez-Granado, *Nuclear envelope lamin-A as a coordinator of T cell activation.* Nucleus, 2014. **5**(5): p. 396-401.
188. Lee-Sayer, S.S., et al., *The where, when, how, and why of hyaluronan binding by immune cells.* Front Immunol, 2015. **6**: p. 150.
189. Bollyky, P.L., et al., *Cutting edge: high molecular weight hyaluronan promotes the suppressive effects of CD4+CD25+ regulatory T cells.* J Immunol, 2007. **179**(2): p. 744-7.
190. Ke, C., et al., *Immunostimulatory and antiangiogenic activities of low molecular weight hyaluronic acid.* Food Chem Toxicol, 2013. **58**: p. 401-7.

191. Simon Davis, D.A. and C.R. Parish, *Heparan sulfate: a ubiquitous glycosaminoglycan with multiple roles in immunity.* Front Immunol, 2013. **4**: p. 470.
192. Zhang, N., et al., *The role of apoptosis in the development and function of T lymphocytes.* Cell Res, 2005. **15**(10): p. 749-69.
193. Guimarães, C.F., et al., *The stiffness of living tissues and its implications for tissue engineering.* Nature Reviews Materials, 2020. **5**: p. 351-370.
194. Martinez-Vidal, L., et al., *Causal contributors to tissue stiffness and clinical relevance in urology.* Commun Biol, 2021. **4**(1): p. 1011.
195. Pfisterer, K., et al., *The Extracellular Matrix in Skin Inflammation and Infection.* Front Cell Dev Biol, 2021. **9**: p. 682414.
196. Pruitt, H.C., et al., *Collagen fiber structure guides 3D motility of cytotoxic T lymphocytes.* Matrix Biol, 2020. **85-86**: p. 147-159.
197. Burgstaller, G., et al., *The instructive extracellular matrix of the lung: basic composition and alterations in chronic lung disease.* Eur Respir J, 2017. **50**(1).
198. Lau, L.W., et al., *Pathophysiology of the brain extracellular matrix: a new target for remyelination.* Nat Rev Neurosci, 2013. **14**(10): p. 722-9.
199. Martinez-Hernandez, A. and P.S. Amenta, *The hepatic extracellular matrix. II. Ontogenesis, regeneration and cirrhosis.* Virchows Arch A Pathol Anat Histopathol, 1993. **423**(2): p. 77-84.
200. Novak, U. and A.H. Kaye, *Extracellular matrix and the brain: components and function.* J Clin Neurosci, 2000. **7**(4): p. 280-90.
201. Tran, C.N., S.K. Lundy, and D.A. Fox, *Synovial biology and T cells in rheumatoid arthritis.* Pathophysiology, 2005. **12**(3): p. 183-9.
202. Hanahan, D., *Hallmarks of Cancer: New Dimensions.* Cancer Discov, 2022. **12**(1): p. 31-46.
203. Weigelin, B., et al., *Cytotoxic T cells are able to efficiently eliminate cancer cells by additive cytotoxicity.* Nat Commun, 2021. **12**(1): p. 5217.
204. Raskov, H., et al., *Cytotoxic CD8(+) T cells in cancer and cancer immunotherapy.* Br J Cancer, 2021. **124**(2): p. 359-367.
205. Han, X., Y. Wang, and W.D. Han, *Chimeric antigen receptor modified T-cells for cancer treatment.* Chronic Dis Transl Med, 2018. **4**(4): p. 225-243.
206. Nixon, N.A., et al., *Current landscape of immunotherapy in the treatment of solid tumours, with future opportunities and challenges.* Curr Oncol, 2018. **25**(5): p. e373-e384.
207. Lorenzo-Sanz, L. and P. Munoz, *Tumor-Infiltrating Immunosuppressive Cells in Cancer-Cell Plasticity, Tumor Progression and Therapy Response.* Cancer Microenviron, 2019. **12**(2-3): p. 119-132.
208. Simsek, H. and E. Klotzsch, *The solid tumor microenvironment-Breaking the barrier for T cells: How the solid tumor microenvironment influences T cells: How the solid tumor microenvironment influences T cells.* Bioessays, 2022. **44**(6): p. e2100285.
209. Vuillefroy de Silly, R., P.Y. Dietrich, and P.R. Walker, *Hypoxia and antitumor CD8(+) T cells: An incompatible alliance?* Oncoimmunology, 2016. **5**(12): p. e1232236.
210. Hanahan, D. and R.A. Weinberg, *Hallmarks of cancer: the next generation.* Cell, 2011. **144**(5): p. 646-74.
211. Di Modugno, F., et al., *3D models in the new era of immune oncology: focus on T cells, CAF and ECM.* J Exp Clin Cancer Res, 2019. **38**(1): p. 117.
212. Northey, J.J., et al., *Stiff stroma increases breast cancer risk by inducing the oncogene ZNF217.* J Clin Invest, 2020. **130**(11): p. 5721-5737.
213. Bauer, J., et al., *Author Correction: Increased stiffness of the tumor microenvironment in colon cancer stimulates cancer associated fibroblast-mediated prometastatic activin A signaling.* Sci Rep, 2020. **10**(1): p. 7606.
214. Rice, A.J., et al., *Matrix stiffness induces epithelial-mesenchymal transition and promotes chemoresistance in pancreatic cancer cells.* Oncogenesis, 2017. **6**(7): p. e352.

215. Yang, Z., et al., *Extracellular Matrix Characterization in Gastric Cancer Helps to Predict Prognosis and Chemotherapy Response.* Front Oncol, 2021. **11**: p. 753330.
216. Zhang, J.Y., et al., *Cancer-associated fibroblasts promote oral squamous cell carcinoma progression through LOX-mediated matrix stiffness.* J Transl Med, 2021. **19**(1): p. 513.
217. Nicolas-Boluda, A., et al., *Tumor stiffening reversion through collagen crosslinking inhibition improves T cell migration and anti-PD-1 treatment.* Elife, 2021. **10**.
218. Jing, X., et al., *Role of hypoxia in cancer therapy by regulating the tumor microenvironment.* Mol Cancer, 2019. **18**(1): p. 157.
219. Sethumadhavan, S., et al., *Hypoxia and hypoxia-inducible factor (HIF) downregulate antigen-presenting MHC class I molecules limiting tumor cell recognition by T cells.* PLoS One, 2017. **12**(11): p. e0187314.
220. Scharping, N.E., et al., *Mitochondrial stress induced by continuous stimulation under hypoxia rapidly drives T cell exhaustion.* Nat Immunol, 2021. **22**(2): p. 205-215.
221. Comito, G., et al., *Cancer-associated fibroblasts and M2-polarized macrophages synergize during prostate carcinoma progression.* Oncogene, 2014. **33**(19): p. 2423-31.
222. Afik, R., et al., *Tumor macrophages are pivotal constructors of tumor collagenous matrix.* J Exp Med, 2016. **213**(11): p. 2315-2331.
223. Saleh, R. and E. Elkord, *FoxP3(+) T regulatory cells in cancer: Prognostic biomarkers and therapeutic targets.* Cancer Lett, 2020. **490**: p. 174-185.
224. Raber, P.L., et al., *Subpopulations of myeloid-derived suppressor cells impair T cell responses through independent nitric oxide-related pathways.* Int J Cancer, 2014. **134**(12): p. 2853-64.
225. Liu, Y. and X. Cao, *Immunosuppressive cells in tumor immune escape and metastasis.* J Mol Med (Berl), 2016. **94**(5): p. 509-22.
226. Wang, J.B., X. Huang, and F.R. Li, *Impaired dendritic cell functions in lung cancer: a review of recent advances and future perspectives.* Cancer Commun (Lond), 2019. **39**(1): p. 43.
227. Tran Janco, J.M., et al., *Tumor-infiltrating dendritic cells in cancer pathogenesis.* The Journal of immunology (1950), 2015. **194**(7): p. 2985-2991.
228. Guzman-Genuino, R.M. and K.R. Diener, *Regulatory B Cells in Pregnancy: Lessons from Autoimmunity, Graft Tolerance, and Cancer.* Front Immunol, 2017. **8**: p. 172.
229. Harrison, D.L., Y. Fang, and J. Huang, *T-Cell Mechanobiology: Force Sensation, Potentiation, and Translation.* Front Phys, 2019. **7**.
230. Zhu, C., et al., *Author Correction: Mechanosensing through immunoreceptors.* Nat Immunol, 2019. **20**(12): p. 1700.
231. Sun, Z., S.S. Guo, and R. Fassler, *Integrin-mediated mechanotransduction.* J Cell Biol, 2016. **215**(4): p. 445-456.
232. Rossy, J., J.M. Laufer, and D.F. Legler, *Role of Mechanotransduction and Tension in T Cell Function.* Front Immunol, 2018. **9**: p. 2638.
233. Gonzalez-Granado, J.M., et al., *Nuclear envelope lamin-A couples actin dynamics with immunological synapse architecture and T cell activation.* Sci Signal, 2014. **7**(322): p. ra37.
234. Friedl, P., K. Wolf, and J. Lammerding, *Nuclear mechanics during cell migration.* Curr Opin Cell Biol, 2011. **23**(1): p. 55-64.
235. Ritskes-Hoitinga, M., et al., *Improving Translation by Identifying Evidence for More Human-Relevant Preclinical Strategies.* Animals (Basel), 2020. **10**(7).
236. Masopust, D., C.P. Sivula, and S.C. Jameson, *Of Mice, Dirty Mice, and Men: Using Mice To Understand Human Immunology.* J Immunol, 2017. **199**(2): p. 383-388.
237. Wagar, L.E., R.M. DiFazio, and M.M. Davis, *Advanced model systems and tools for basic and translational human immunology.* Genome Med, 2018. **10**(1): p. 73.
238. Brentville, V.A., et al., *T cell repertoire to citrullinated self-peptides in healthy humans is not confined to the HLA-DR SE alleles; Targeting of citrullinated self-peptides presented by HLA-DP4 for tumour therapy.* Oncoimmunology, 2019. **8**(5): p. e1576490.

239. Mestas, J. and C.C. Hughes, *Of mice and not men: differences between mouse and human immunology.* J Immunol, 2004. **172**(5): p. 2731-8.
240. Perlman, R.L., *Mouse models of human disease: An evolutionary perspective.* Evol Med Public Health, 2016. **2016**(1): p. 170-6.
241. Estes, J.D., S.W. Wong, and J.M. Brenchley, *Nonhuman primate models of human viral infections.* Nat Rev Immunol, 2018. **18**(6): p. 390-404.
242. Guzman, E. and M. Montoya, *Contributions of Farm Animals to Immunology.* Front Vet Sci, 2018. **5**: p. 307.
243. Huebsch, N. and D.J. Mooney, *Inspiration and application in the evolution of biomaterials.* Nature, 2009. **462**(7272): p. 426-32.
244. Han, L., et al., *Targeted drug delivery to ischemic stroke via chlorotoxin-anchored, lexiscan-loaded nanoparticles.* Nanomedicine, 2016. **12**(7): p. 1833-1842.
245. Kim, J., et al., *Quantitative evaluation of cardiomyocyte contractility in a 3D microenvironment.* J Biomech, 2008. **41**(11): p. 2396-401.
246. Tavakol, D.N., et al., *Oxygen-Sensing Biomaterial Construct for Clinical Monitoring of Wound Healing.* Adv Skin Wound Care, 2020. **33**(8): p. 428-436.
247. Wong, C.W., et al., *Biomaterial substrate-derived compact cellular spheroids mimicking the behavior of pancreatic cancer and microenvironment.* Biomaterials, 2019. **213**: p. 119202.
248. Stephan, S.B., et al., *Biopolymer implants enhance the efficacy of adoptive T-cell therapy.* Nat Biotechnol, 2015. **33**(1): p. 97-101.
249. Luo, Z., et al., *A Powerful CD8(+) T-Cell Stimulating D-Tetra-Peptide Hydrogel as a Very Promising Vaccine Adjuvant.* Adv Mater, 2017. **29**(5).
250. Griffin, D.R., et al., *Activating an adaptive immune response from a hydrogel scaffold imparts regenerative wound healing.* Nat Mater, 2021. **20**(4): p. 560-569.
251. Xue, Y., et al., *Recent advances in biomaterial-boosted adoptive cell therapy.* Chem Soc Rev, 2022. **51**(5): p. 1766-1794.
252. Morotti, M., et al., *Promises and challenges of adoptive T-cell therapies for solid tumours.* Br J Cancer, 2021. **124**(11): p. 1759-1776.
253. Lin, H., et al., *Automated Expansion of Primary Human T Cells in Scalable and Cell-Friendly Hydrogel Microtubes for Adoptive Immunotherapy.* Adv Healthc Mater, 2018. **7**(15): p. e1701297.
254. Haycock, J.W., *3D cell culture: a review of current approaches and techniques.* Methods Mol Biol, 2011. **695**: p. 1-15.
255. Nikolova, M.P. and M.S. Chavali, *Recent advances in biomaterials for 3D scaffolds: A review.* Bioact Mater, 2019. **4**: p. 271-292.
256. Lv, D., et al., *Three-dimensional cell culture: A powerful tool in tumor research and drug discovery.* Oncol Lett, 2017. **14**(6): p. 6999-7010.
257. Nishinari, K. *Some Thoughts on The Definition of a Gel*. 2009. Berlin, Heidelberg: Springer Berlin Heidelberg.
258. Hu, W., et al., *Advances in crosslinking strategies of biomedical hydrogels.* Biomater Sci, 2019. **7**(3): p. 843-855.
259. Brovold, M., et al., *Naturally-Derived Biomaterials for Tissue Engineering Applications.* Adv Exp Med Biol, 2018. **1077**: p. 421-449.
260. Chuang, C.H., et al., *Comparison of covalently and physically cross-linked collagen hydrogels on mediating vascular network formation for engineering adipose tissue.* Artif Cells Nanomed Biotechnol, 2018. **46**(sup3): p. S434-S447.
261. Ma, J. and C. Huang, *Composition and Mechanism of Three-Dimensional Hydrogel System in Regulating Stem Cell Fate.* Tissue Eng Part B Rev, 2020. **26**(6): p. 498-518.
262. Xu, F., et al., *Hydrogels for Tissue Engineering: Addressing Key Design Needs Toward Clinical Translation.* Front Bioeng Biotechnol, 2022. **10**: p. 849831.

263. Monette, A., et al., *Chitosan thermogels for local expansion and delivery of tumor-specific T lymphocytes towards enhanced cancer immunotherapies.* Biomaterials, 2016. **75**: p. 237-249.
264. Perez, L.A., et al., *Hyaluronic Acid Hydrogels Crosslinked in Physiological Conditions: Synthesis and Biomedical Applications.* Biomedicines, 2021. **9**(9).
265. Zamboni, F., et al., *The potential of hyaluronic acid in immunoprotection and immunomodulation: Chemistry, processing and function.* Progress in Materials Science, 2018. **97**: p. 97-122.
266. Paepe, I.D., et al., *Novel hydrogels based on methacrylate-modified agarose.* Polymer International, 2002. **51**(10): p. 867-870.
267. Fan, Y., et al., *Alginate Enhances Memory Properties of Antitumor CD8(+) T Cells by Promoting Cellular Antioxidation.* ACS Biomater Sci Eng, 2019. **5**(9): p. 4717-4725.
268. Aisenbrey, E.A. and W.L. Murphy, *Synthetic alternatives to Matrigel.* Nat Rev Mater, 2020. **5**(7): p. 539-551.
269. Semler, E.J., C.S. Ranucci, and P.V. Moghe, *Mechanochemical manipulation of hepatocyte aggregation can selectively induce or repress liver-specific function.* Biotechnol Bioeng, 2000. **69**(4): p. 359-69.
270. Bigi, A., et al., *Stabilization of gelatin films by crosslinking with genipin.* Biomaterials, 2002. **23**(24): p. 4827-32.
271. Suraiya, A.B., et al., *Gelatin-Based 3D Microgels for In Vitro T Lineage Cell Generation.* ACS Biomater Sci Eng, 2020. **6**(4): p. 2198-2208.
272. Xing, Q., et al., *Increasing mechanical strength of gelatin hydrogels by divalent metal ion removal.* Sci Rep, 2014. **4**: p. 4706.
273. Kim, J., et al., *Characterizing natural hydrogel for reconstruction of three-dimensional lymphoid stromal network to model T-cell interactions.* J Biomed Mater Res A, 2015. **103**(8): p. 2701-10.
274. Bednarek, M., K. Borska, and P. Kubisa, *Crosslinking of Polylactide by High Energy Irradiation and Photo-Curing.* Molecules, 2020. **25**(21).
275. Kuriakose, A.E., et al., *Scaffold-based lung tumor culture on porous PLGA microparticle substrates.* PLoS One, 2019. **14**(5): p. e0217640.
276. Zhou, N., et al., *Thermo-Sensitive PLGA-PEG-PLGA Tri-Block Copolymer Hydrogel as Three-Dimensional Cell Culture Matrix for Ovarian Cancer Cells.* J Nanosci Nanotechnol, 2018. **18**(8): p. 5252-5255.
277. Perez Del Rio, E., et al., *CCL21-loaded 3D hydrogels for T cell expansion and differentiation.* Biomaterials, 2020. **259**: p. 120313.
278. Schulte, V.A., et al., *Microengineered PEG hydrogels: 3D scaffolds for guided cell growth.* Macromol Biosci, 2013. **13**(5): p. 562-72.
279. Ahumada, M., et al., *Porosity in Biomaterials: A Key Factor in the Development of Applied Materials in Biomedicine*, in *Handbook of Ecomaterials*. 2019. p. 3503-3522.
280. Loh, Q.L. and C. Choong, *Three-dimensional scaffolds for tissue engineering applications: role of porosity and pore size.* Tissue Eng Part B Rev, 2013. **19**(6): p. 485-502.
281. Murphy, C.M., et al., *Effect of collagen-glycosaminoglycan scaffold pore size on matrix mineralization and cellular behavior in different cell types.* J Biomed Mater Res A, 2016. **104**(1): p. 291-304.
282. Yin, Y., et al., *Pore size-mediated macrophage M1-to-M2 transition influences new vessel formation within the compartment of a scaffold.* Applied Materials Today, 2020. **18**.
283. Conoscenti, G., et al., *PLLA scaffolds produced by thermally induced phase separation (TIPS) allow human chondrocyte growth and extracellular matrix formation dependent on pore size.* Mater Sci Eng C Mater Biol Appl, 2017. **80**: p. 449-459.
284. Geckil, H., et al., *Engineering hydrogels as extracellular matrix mimics.* Nanomedicine (Lond), 2010. **5**(3): p. 469-84.

285. Hamilton, M., et al., *Hyaluronic Acid Hydrogel Microspheres for Slow Release Stem Cell Delivery.* ACS Biomater Sci Eng, 2021. **7**(8): p. 3754-3763.
286. Patterson, J., et al., *Hyaluronic acid hydrogels with controlled degradation properties for oriented bone regeneration.* Biomaterials, 2010. **31**(26): p. 6772-81.
287. Spicer, C.D., E.T. Pashuck, and M.M. Stevens, *Achieving Controlled Biomolecule-Biomaterial Conjugation.* Chem Rev, 2018. **118**(16): p. 7702-7743.
288. Drobota, M., S. Ursache, and M. Aflori, *Surface Functionalities of Polymers for Biomaterial Applications.* Polymers (Basel), 2022. **14**(12).
289. Custodio, C.A., et al., *Immobilization of fibronectin in chitosan substrates improves cell adhesion and proliferation.* J Tissue Eng Regen Med, 2010. **4**(4): p. 316-23.
290. Hotaling, N.A., et al., *Biomaterial Strategies for Immunomodulation.* Annu Rev Biomed Eng, 2015. **17**: p. 317-49.
291. Fishman, J.M., K. Wiles, and K.J. Wood, *The Acquired Immune System Response to Biomaterials, Including Both Naturally Occurring and Synthetic Biomaterials*, in *Host Response to Biomaterials*. 2015. p. 151-187.
292. Andorko, J.I. and C.M. Jewell, *Designing biomaterials with immunomodulatory properties for tissue engineering and regenerative medicine.* Bioeng Transl Med, 2017. **2**(2): p. 139-155.
293. Park, J. and J.E. Babensee, *Differential functional effects of biomaterials on dendritic cell maturation.* Acta Biomater, 2012. **8**(10): p. 3606-17.
294. Ding, X., et al., *Synthetic peptide hydrogels as 3D scaffolds for tissue engineering.* Adv Drug Deliv Rev, 2020. **160**: p. 78-104.
295. Dou, X.Q. and C.L. Feng, *Amino Acids and Peptide-Based Supramolecular Hydrogels for Three-Dimensional Cell Culture.* Adv Mater, 2017. **29**(16).
296. Hong, J.Y., et al., *Self-assembling peptide gels promote angiogenesis and functional recovery after spinal cord injury in rats.* J Tissue Eng, 2022. **13**: p. 20417314221086491.
297. Kopesky, P.W., et al., *Self-assembling peptide hydrogels modulate in vitro chondrogenesis of bovine bone marrow stromal cells.* Tissue Eng Part A, 2010. **16**(2): p. 465-77.
298. Gough, J.E., A. Saiani, and A.F. Miller, *Peptide hydrogels: mimicking the extracellular matrix.* Bioinspired, Biomimetic and Nanobiomaterials, 2012. **1**(1): p. 4-12.
299. Sun, L., C. Zheng, and T.J. Webster, *Self-assembled peptide nanomaterials for biomedical applications: promises and pitfalls.* Int J Nanomedicine, 2017. **12**: p. 73-86.
300. Maude, S., E. Ingham, and A. Aggeli, *Biomimetic self-assembling peptides as scaffolds for soft tissue engineering.* Nanomedicine (Lond), 2013. **8**(5): p. 823-47.
301. Saiani, A., et al., *Self-assembly and gelation properties of α-helix versus β-sheet forming peptides.* Soft Matter, 2009. **5**(1): p. 193-202.
302. De Leon Rodriguez, L.M., et al., *Structure-mechanical property correlations of hydrogel forming beta-sheet peptides.* Chem Soc Rev, 2016. **45**(17): p. 4797-824.
303. Rambaran, R.N. and L.C. Serpell, *Amyloid fibrils: abnormal protein assembly.* Prion, 2008. **2**(3): p. 112-117.
304. Carter, T., et al., *Self-Assembling Peptide Solution Accelerates Hemostasis.* Adv Wound Care (New Rochelle), 2021. **10**(4): p. 191-203.
305. Genove, E., et al., *The effect of functionalized self-assembling peptide scaffolds on human aortic endothelial cell function.* Biomaterials, 2005. **26**(16): p. 3341-51.
306. Mujeeb, A., et al., *Self-assembled octapeptide scaffolds for in vitro chondrocyte culture.* Acta Biomater, 2013. **9**(1): p. 4609-17.
307. Gao, J., et al., *Controlling Self-Assembling Peptide Hydrogel Properties through Network Topology.* Biomacromolecules, 2017. **18**(3): p. 826-834.
308. Burgess, K.A., et al., *Functionalised peptide hydrogel for the delivery of cardiac progenitor cells.* Mater Sci Eng C Mater Biol Appl, 2021. **119**: p. 111539.
309. Castillo Diaz, L.A., et al., *Human osteoblasts within soft peptide hydrogels promote mineralisation in vitro.* J Tissue Eng, 2014. **5**: p. 2041731414539344.

310. Boothroyd, S., A.F. Millerb, and A. Saiani, *From fibres to networks using self-assembling peptides.* Faraday Discuss, 2013. **166**: p. 195-207.
311. Ashworth, J.C., et al., *Peptide gels of fully-defined composition and mechanics for probing cell-cell and cell-matrix interactions in vitro.* Matrix Biol, 2020. **85-86**: p. 15-33.
312. Castillo Diaz, L.A., et al., *Osteogenic differentiation of human mesenchymal stem cells promotes mineralization within a biodegradable peptide hydrogel.* J Tissue Eng, 2016. **7**: p. 2041731416649789.
313. Strober, W., *Trypan Blue Exclusion Test of Cell Viability.* Curr Protoc Immunol, 2015. **111**: p. A3 B 1-A3 B 3.
314. Biotec, M. *CD4 MicroBeads human - lyophilized*. 2020. 1-4.
315. Biotec, M. *CD14 MicroBeads human*. 2023. 1-5.
316. Biotec, M. *CD1c (BDCA-1)+ Dendritic Cell Isolation Kit*. 2020. 1-4.
317. Inc., B.L. *Adsorption to Microspheres*. 2013. 1-5.
318. Ganesan, N., S. Ronsmans, and P. Hoet, *Methods to Assess Proliferation of Stimulated Human Lymphocytes In Vitro: A Narrative Review.* Cells, 2023. **12**(3).
319. Quah, B.J., H.S. Warren, and C.R. Parish, *Monitoring lymphocyte proliferation in vitro and in vivo with the intracellular fluorescent dye carboxyfluorescein diacetate succinimidyl ester.* Nat Protoc, 2007. **2**(9): p. 2049-56.
320. Crowley, L.C., et al., *Measuring Cell Death by Propidium Iodide Uptake and Flow Cytometry.* Cold Spring Harb Protoc, 2016. **2016**(7).
321. Christine, L. *Two Ways to Count Cells with ImageJ*. 2020. 1-4.
322. Sigma-Aldrich *PKH26 Red Fluorescent Cell Linker Kits for General Cell Membrane Labelling*. 2017. 1-4.
323. Sturm, A., et al., *Dual function of the extracellular matrix: stimulatory for cell cycle progression of naive T cells and antiapoptotic for tissue-derived memory T cells.* J Immunol, 2004. **173**(6): p. 3889-900.
324. He, T., et al., *FEK self-assembled peptide hydrogels facilitate primary hepatocytes culture and pharmacokinetics screening.* J Biomed Mater Res B Appl Biomater, 2022. **110**(9): p. 2015-2027.
325. Szkolar, L., et al., *Enzymatically triggered peptide hydrogels for 3D cell encapsulation and culture.* J Pept Sci, 2014. **20**(7): p. 578-84.
326. Li, L., et al., *3D Molecularly Functionalized Cell‐Free Biomimetic Scaffolds for Osteochondral Regeneration.* Advanced Functional Materials, 2018. **29**(6).
327. Li, X., Y. Shou, and A. Tay, *Hydrogels for Engineering the Immune System.* Advanced NanoBiomed Research, 2021. **1**(3).
328. Perez Del Rio, E., et al., *Artificial 3D Culture Systems for T Cell Expansion.* ACS Omega, 2018. **3**(5): p. 5273-5280.
329. Cui, R., et al., *Hydrogel-By-Design: Smart Delivery System for Cancer Immunotherapy.* Front Bioeng Biotechnol, 2021. **9**: p. 723490.
330. Weiden, J., et al., *Injectable Biomimetic Hydrogels as Tools for Efficient T Cell Expansion and Delivery.* Front Immunol, 2018. **9**: p. 2798.
331. Song, H., et al., *Injectable polypeptide hydrogel-based co-delivery of vaccine and immune checkpoint inhibitors improves tumor immunotherapy.* Theranostics, 2019. **9**(8): p. 2299-2314.
332. Yang, P., et al., *Engineering Dendritic-Cell-Based Vaccines and PD-1 Blockade in Self-Assembled Peptide Nanofibrous Hydrogel to Amplify Antitumor T-Cell Immunity.* Nano Lett, 2018. **18**(7): p. 4377-4385.
333. Xing, R., et al., *Self-Assembled Injectable Peptide Hydrogels Capable of Triggering Antitumor Immune Response.* Biomacromolecules, 2017. **18**(11): p. 3514-3523.
334. Lopez-Silva, T.L., et al., *Chemical functionality of multidomain peptide hydrogels governs early host immune response.* Biomaterials, 2020. **231**: p. 119667.

335. Zhang, H., et al., *Rational design of charged peptides that self-assemble into robust nanofibers as immune-functional scaffolds.* Acta Biomater, 2017. **55**: p. 183-193.
336. Gelain, F., Z. Luo, and S. Zhang, *Self-Assembling Peptide EAK16 and RADA16 Nanofiber Scaffold Hydrogel.* Chem Rev, 2020. **120**(24): p. 13434-13460.
337. Markey, A., et al., *Peptide hydrogel in vitro non-inflammatory potential.* J Pept Sci, 2017. **23**(2): p. 148-154.
338. Lardner, A., *The effects of extracellular pH on immune function.* J Leukoc Biol, 2001. **69**(4): p. 522-30.
339. Lei, K., A. Kurum, and L. Tang, *Mechanical Immunoengineering of T cells for Therapeutic Applications.* Acc Chem Res, 2020. **53**(12): p. 2777-2790.
340. Ramli, H., et al., *Basic principle and good practices of rheology for polymers for teachers and beginners.* Chemistry Teacher International : best practices in chemistry education, 2022. **4**(4): p. 307-326.
341. Miranda-Carus, M.E., et al., *Human T cells constitutively express IL-15 that promotes ex vivo T cell homeostatic proliferation through autocrine/juxtacrine loops.* J Immunol, 2005. **175**(6): p. 3656-62.
342. Ma, Q., et al., *Cell density plays a critical role in ex vivo expansion of T cells for adoptive immunotherapy.* J Biomed Biotechnol, 2010. **2010**: p. 386545.
343. Thomas, A.K., et al., *A cell-based artificial antigen-presenting cell coated with anti-CD3 and CD28 antibodies enables rapid expansion and long-term growth of CD4 T lymphocytes.* Clin Immunol, 2002. **105**(3): p. 259-72.
344. Li, Y. and R.J. Kurlander, *Comparison of anti-CD3 and anti-CD28-coated beads with soluble anti-CD3 for expanding human T cells: differing impact on CD8 T cell phenotype and responsiveness to restimulation.* J Transl Med, 2010. **8**: p. 104.
345. Eagle, H., *Buffer Combinations for Mammalian Cell Culture.* Science (American Association for the Advancement of Science), 1971. **174**(4008): p. 500-503.
346. Gramer, M.J. and T. Ogorzalek, *A semi-empirical mathematical model useful for describing the relationship between carbon dioxide, pH, lactate and base in a bicarbonate-buffered cell-culture process.* Biotechnol Appl Biochem, 2007. **47**(Pt 4): p. 197-204.
347. Chen, L. and D.B. Flies, *Molecular mechanisms of T cell co-stimulation and co-inhibition.* Nat Rev Immunol, 2013. **13**(4): p. 227-42.
348. Capasso, M., et al., *Costimulation via CD55 on human CD4+ T cells mediated by CD97.* J Immunol, 2006. **177**(2): p. 1070-7.
349. Hoofnagle, A.N. and M.H. Wener, *The fundamental flaws of immunoassays and potential solutions using tandem mass spectrometry.* J Immunol Methods, 2009. **347**(1-2): p. 3-11.
350. Singh, N., et al., *CD4(+)CD25(+) regulatory T cells resist a novel form of CD28- and Fas-dependent p53-induced T cell apoptosis.* J Immunol, 2010. **184**(1): p. 94-104.
351. Hu, Q., et al., *Resting T cells are hypersensitive to DNA damage due to defective DNA repair pathway.* Cell Death Dis, 2018. **9**(6): p. 662.
352. Felgentreff, K., et al., *Differential DNA Damage Response of Peripheral Blood Lymphocyte Populations.* Front Immunol, 2021. **12**: p. 739675.
353. Dolff, S., et al., *Urinary CD8+ T-cell counts discriminate between active and inactive lupus nephritis.* Arthritis Res Ther, 2013. **15**(1): p. R36.
354. Havran, W.L. and J.M. Jameson, *Epidermal T cells and wound healing.* J Immunol, 2010. **184**(10): p. 5423-8.
355. Previtera, M.L., *Mechanotransduction in the Immune System.* Cellular and Molecular Bioengineering, 2014. **7**(3): p. 473-481.
356. Salmon, H., et al., *Matrix architecture defines the preferential localization and migration of T cells into the stroma of human lung tumors.* J Clin Invest, 2012. **122**(3): p. 899-910.
357. McQuitty, C.E., et al., *Immunomodulatory Role of the Extracellular Matrix Within the Liver Disease Microenvironment.* Frontiers in Immunology, 2020. **11**.

358. Rye, I.H., et al., *Breast cancer metastasis: immune profiling of lymph nodes reveals exhaustion of effector T cells and immunosuppression.* Mol Oncol, 2022. **16**(1): p. 88-103.
359. Xu, S., et al., *The role of collagen in cancer: from bench to bedside.* J Transl Med, 2019. **17**(1): p. 309.
360. Restrepo, C., et al., *Both HCV Infection and Elevated Liver Stiffness Significantly Impacts on Several Parameters of T-Cells Homeostasis in HIV-Infected Patients.* J Clin Med, 2020. **9**(9).
361. Saitakis, M., et al., *Different TCR-induced T lymphocyte responses are potentiated by stiffness with variable sensitivity.* Elife, 2017. **6**.
362. O'Connor, R.S., et al., *Substrate rigidity regulates human T cell activation and proliferation.* J Immunol, 2012. **189**(3): p. 1330-9.
363. Sutavani, R.V., et al., *CD55 costimulation induces differentiation of a discrete T regulatory type 1 cell population with a stable phenotype.* J Immunol, 2013. **191**(12): p. 5895-903.
364. Zappasodi, R., et al., *In vitro assays for effector T cell functions and activity of immunomodulatory antibodies.* Methods Enzymol, 2020. **631**: p. 43-59.
365. Baaten, B.J., C.R. Li, and L.M. Bradley, *Multifaceted regulation of T cells by CD44.* Commun Integr Biol, 2010. **3**(6): p. 508-12.
366. Radvar, E. and H.S. Azevedo, *Supramolecular Peptide/Polymer Hybrid Hydrogels for Biomedical Applications.* Macromol Biosci, 2019. **19**(1): p. e1800221.
367. Tanzer, M.C., et al., *Quantitative and Dynamic Catalogs of Proteins Released during Apoptotic and Necroptotic Cell Death.* Cell Rep, 2020. **30**(4): p. 1260-1270 e5.
368. Wen, J., et al., *Lactate anions participate in T cell cytokine production and function.* Sci China Life Sci, 2021. **64**(11): p. 1895-1905.
369. Stampouloglou, E., et al., *Yap suppresses T-cell function and infiltration in the tumor microenvironment.* PLoS Biol, 2020. **18**(1): p. e3000591.
370. Gitlin, I., J.D. Carbeck, and G.M. Whitesides, *Why are proteins charged? Networks of charge-charge interactions in proteins measured by charge ladders and capillary electrophoresis.* Angew Chem Int Ed Engl, 2006. **45**(19): p. 3022-60.
371. Ling Tan, H., Y. Pei Lim, and M. Sufian So'aib, *Tracking self-assembly morphology of cationic peptide analogues using turbidimetric- potentiometric titration.* International Journal of Engineering & Technology, 2018. **7**(3).
372. Bertram, E.M., P. Lau, and T.H. Watts, *Temporal segregation of 4-1BB versus CD28-mediated costimulation: 4-1BB ligand influences T cell numbers late in the primary response and regulates the size of the T cell memory response following influenza infection.* J Immunol, 2002. **168**(8): p. 3777-85.
373. Bachmann, M.F., et al., *Distinct roles for LFA-1 and CD28 during activation of naive T cells: adhesion versus costimulation.* Immunity, 1997. **7**: p. 549-557.
374. Rozanski, C.H., et al., *Sustained antibody responses depend on CD28 function in bone marrow-resident plasma cells.* J Exp Med, 2011. **208**(7): p. 1435-46.
375. Esensten, J.H., et al., *CD28 Costimulation: From Mechanism to Therapy.* Immunity, 2016. **44**(5): p. 973-88.
376. Dho, S.H., J.C. Lim, and L.K. Kim, *Beyond the Role of CD55 as a Complement Component.* Immune Netw, 2018. **18**(1): p. e11.
377. West, E.E., M. Kolev, and C. Kemper, *Complement and the Regulation of T Cell Responses.* Annu Rev Immunol, 2018. **36**: p. 309-338.
378. Linterman, M.A., et al., *CD28 expression is required after T cell priming for helper T cell responses and protective immunity to infection.* Elife, 2014. **3**.
379. Jankovic, D., D.G. Kugler, and A. Sher, *IL-10 production by CD4+ effector T cells: a mechanism for self-regulation.* Mucosal Immunol, 2010. **3**(3): p. 239-46.
380. Badr, M., et al., *Expansion of regulatory T cells by CD28 superagonistic antibodies attenuates neurodegeneration in A53T-alpha-synuclein Parkinson's disease mice.* J Neuroinflammation, 2022. **19**(1): p. 319.

381. Alegre, M.L., K.A. Frauwirth, and C.B. Thompson, *T-cell regulation by CD28 and CTLA-4.* Nat Rev Immunol, 2001. **1**(3): p. 220-8.
382. Guasch, J., et al., *Integrin-Assisted T-Cell Activation on Nanostructured Hydrogels.* Nano Lett, 2017. **17**(10): p. 6110-6116.
383. Dong, D., et al., *Structural basis of assembly of the human T cell receptor-CD3 complex.* Nature, 2019. **573**(7775): p. 546-552.
384. Lanzavecchia, A., G. Iezzi, and A. Viola, *From TCR engagement to T cell activation: a kinetic view of T cell behavior.* Cell, 1999. **96**(1): p. 1-4.
385. Borovsky, Z., et al., *Serial triggering of T cell receptors results in incremental accumulation of signaling intermediates.* J Biol Chem, 2002. **277**(24): p. 21529-36.
386. Chapman, N.M., M.R. Boothby, and H. Chi, *Metabolic coordination of T cell quiescence and activation.* Nat Rev Immunol, 2020. **20**(1): p. 55-70.
387. Hickey, J.W., et al., *Engineering an Artificial T-Cell Stimulating Matrix for Immunotherapy.* Adv Mater, 2019. **31**(23): p. e1807359.
388. El Hentati, F.Z., et al., *Variability of CD3 membrane expression and T cell activation capacity.* Cytometry B Clin Cytom, 2010. **78**(2): p. 105-14.
389. Waldman, A.D., J.M. Fritz, and M.J. Lenardo, *A guide to cancer immunotherapy: from T cell basic science to clinical practice.* Nat Rev Immunol, 2020. **20**(11): p. 651-668.
390. Varadhachary, A.S., et al., *Differential Ability of T cell Subsets to undergo Activation-Induced Cell Death.* Proceedings of the National Academy of Sciences - PNAS, 1997. **94**(11): p. 5778-5783.
391. Wu, H., et al., *T-cells produce acidic niches in lymph nodes to suppress their own effector functions.* Nat Commun, 2020. **11**(1): p. 4113.
392. Quinn, W.J., 3rd, et al., *Lactate Limits T Cell Proliferation via the NAD(H) Redox State.* Cell Rep, 2020. **33**(11): p. 108500.
393. Davis, L.S., et al., *Fibronectin promotes proliferation of naive and memory T cells by signaling through both the VLA-4 and VLA-5 integrin molecules.* J Immunol, 1990. **145**(3): p. 785-93.
394. Campbell, J.P. and J.E. Turner, *Debunking the Myth of Exercise-Induced Immune Suppression: Redefining the Impact of Exercise on Immunological Health Across the Lifespan.* Front Immunol, 2018. **9**: p. 648.
395. Okawa, T., M. Nagai, and K. Hase, *Dietary Intervention Impacts Immune Cell Functions and Dynamics by Inducing Metabolic Rewiring.* Front Immunol, 2020. **11**: p. 623989.
396. Salam, N., et al., *T cell ageing: effects of age on development, survival & function.* Indian J Med Res, 2013. **138**(5): p. 595-608.
397. Aung, A., et al., *An Engineered Tumor-on-a-Chip Device with Breast Cancer-Immune Cell Interactions for Assessing T-cell Recruitment.* Cancer Res, 2020. **80**(2): p. 263-275.
398. Sallusto, F. and A. Lanzavecchia, *The instructive role of dendritic cells on T-cell responses.* Arthritis Res, 2002. **4 Suppl 3**(Suppl 3): p. S127-32.
399. Guermonprez, P., et al., *Antigen presentation and T cell stimulation by dendritic cells.* Annu Rev Immunol, 2002. **20**: p. 621-67.
400. Hilligan, K.L. and F. Ronchese, *Antigen presentation by dendritic cells and their instruction of CD4+ T helper cell responses.* Cell Mol Immunol, 2020. **17**(6): p. 587-599.
401. Morbe, U.M., et al., *Human gut-associated lymphoid tissues (GALT); diversity, structure, and function.* Mucosal Immunol, 2021. **14**(4): p. 793-802.
402. Eisenbarth, S.C., *Dendritic cell subsets in T cell programming: location dictates function.* Nat Rev Immunol, 2019. **19**(2): p. 89-103.
403. Wakim, L.M., et al., *Dendritic cell-induced memory T cell activation in nonlymphoid tissues.* Science, 2008. **319**(5860): p. 198-202.
404. Duraiswamy, J., et al., *Myeloid antigen-presenting cell niches sustain antitumor T cells and license PD-1 blockade via CD28 costimulation.* Cancer Cell, 2021. **39**(12): p. 1623-1642 e20.

405. Duong, E., et al., *Type I interferon activates MHC class I-dressed CD11b(+) conventional dendritic cells to promote protective anti-tumor CD8(+) T cell immunity.* Immunity, 2022. **55**(2): p. 308-323 e9.
406. Gardner, A. and B. Ruffell, *Dendritic Cells and Cancer Immunity.* Trends Immunol, 2016. **37**(12): p. 855-865.
407. Hiraoka, N., Y. Ino, and R. Yamazaki-Itoh, *Tertiary Lymphoid Organs in Cancer Tissues.* Front Immunol, 2016. **7**: p. 244.
408. Sato, Y., et al., *CD153/CD30 signaling promotes age-dependent tertiary lymphoid tissue expansion and kidney injury.* J Clin Invest, 2022. **132**(2).
409. Rodriguez, A.B., et al., *Immune mechanisms orchestrate tertiary lymphoid structures in tumors via cancer-associated fibroblasts.* Cell Rep, 2021. **36**(3): p. 109422.
410. Shipman, W.D., D.C. Dasoveanu, and T.T. Lu, *Tertiary lymphoid organs in systemic autoimmune diseases: pathogenic or protective?* F1000Res, 2017. **6**: p. 196.
411. Kuhbacher, A., et al., *Central Role for Dermal Fibroblasts in Skin Model Protection against Candida albicans.* J Infect Dis, 2017. **215**(11): p. 1742-1752.
412. Daneshmandi, S., S.P. Dibazar, and S. Fateh, *Effects of 3-dimensional culture conditions (collagen-chitosan nano-scaffolds) on maturation of dendritic cells and their capacity to interact with T-lymphocytes.* J Immunotoxicol, 2016. **13**(2): p. 235-42.
413. Stewart, D.C., et al., *Quantitative assessment of intestinal stiffness and associations with fibrosis in human inflammatory bowel disease.* PLoS One, 2018. **13**(7): p. e0200377.
414. Tourkova, I.L., et al., *Mechanisms of dendritic cell-induced T cell proliferation in the primary MLR assay.* Immunology letters, 2001. **78**(2): p. 75-82.
415. Sabins, N.C., et al., *Differential Expression of Immune Checkpoint Modulators on In Vitro Primed CD4(+) and CD8(+) T Cells.* Front Immunol, 2016. **7**: p. 221.
416. Belmant, C., et al., *Conventional and non-conventional recognition of non-peptide antigens by T lymphocytes.* Comptes Rendus de l'Académie des Sciences-Series III-Sciences de la Vie, 1999. **322**(11): p. 919-924.
417. Lopez-Relano, J., et al., *Monocyte-Derived Dendritic Cells Differentiated in the Presence of Lenalidomide Display a Semi-Mature Phenotype, Enhanced Phagocytic Capacity, and Th1 Polarization Capability.* Front Immunol, 2018. **9**: p. 1328.
418. Dumortier, H., et al., *Antigen presentation by an immature myeloid dendritic cell line does not cause CTL deletion in vivo, but generates CD8+ central memory-like T cells that can be rescued for full effector function.* J Immunol, 2005. **175**(2): p. 855-63.
419. Tasnim, H., et al., *Quantitative Measurement of Naive T Cell Association With Dendritic Cells, FRCs, and Blood Vessels in Lymph Nodes.* Front Immunol, 2018. **9**: p. 1571.
420. Battisto, J.R. and M.M. Dustoor, *Allogeneic and autologous mixed lymphocyte reactions.* Methods in Enzymology, 1987. **150**: p. 83-91.
421. Matasic, R., A.B. Dietz, and S. Vuk-Pavlovic, *Dexamethasone inhibits dendritic cell maturation by redirecting differentiation of a subset of cells.* J Leukoc Biol, 1999. **66**(6): p. 909-14.
422. Chen, M. and J. Wang, *Programmed cell death of dendritic cells in immune regulation.* Immunol Rev, 2010. **236**: p. 11-27.
423. Kushwah, R. and J. Hu, *Dendritic cell apoptosis: regulation of tolerance versus immunity.* J Immunol, 2010. **185**(2): p. 795-802.
424. Chen, M., et al., *Dendritic cell apoptosis in the maintenance of immune tolerance.* Science, 2006. **311**(5764): p. 1160-4.
425. Franks, H.A., et al., *Novel function for the p38-MK2 signaling pathway in circulating CD1c+ (BDCA-1+) myeloid dendritic cells from healthy donors and advanced cancer patients; inhibition of p38 enhances IL-12 whilst suppressing IL-10.* Int J Cancer, 2014. **134**(3): p. 575-86.

426. Adhikaree, J., et al., *Impaired circulating myeloid CD1c+ dendritic cell function in human glioblastoma is restored by p38 inhibition - implications for the next generation of DC vaccines.* Oncoimmunology, 2019. **8**(7): p. 1593803.
427. Tosh, K.W., et al., *The IL-12 Response of Primary Human Dendritic Cells and Monocytes to Toxoplasma gondii Is Stimulated by Phagocytosis of Live Parasites Rather Than Host Cell Invasion.* J Immunol, 2016. **196**(1): p. 345-56.
428. Leal Rojas, I.M., et al., *Human Blood CD1c(+) Dendritic Cells Promote Th1 and Th17 Effector Function in Memory CD4(+) T Cells.* Front Immunol, 2017. **8**: p. 971.
429. Langenkamp, A., et al., *Kinetics of dendritic cell activation: impact on priming of TH1, TH2 and nonpolarized T cells.* Nat Immunol, 2000. **1**(4): p. 311-6.
430. Keselowsky, B.G. and J.S. Lewis, *Dendritic cells in the host response to implanted materials.* Semin Immunol, 2017. **29**: p. 33-40.
431. Zhu, F.J., et al., *Role of dendritic cells in the host response to biomaterials and their signaling pathways.* Acta Biomater, 2019. **94**: p. 132-144.
432. Liu, Y., et al., *Surface hydrophobicity of microparticles modulates adjuvanticity.* J Mater Chem B, 2013. **1**(32): p. 3888-3896.
433. Tesar, B.M., et al., *The role of hyaluronan degradation products as innate alloimmune agonists.* Am J Transplant, 2006. **6**(11): p. 2622-35.
434. Chen, R., et al., *Precision-porous templated scaffolds of varying pore size drive dendritic cell activation.* Biotechnol Bioeng, 2018. **115**(4): p. 1086-1095.
435. Lin, Y.C., P.J. Lou, and T.H. Young, *Chitosan as an adjuvant-like substrate for dendritic cell culture to enhance antitumor effects.* Biomaterials, 2014. **35**(31): p. 8867-8875.
436. Mondino, A., A. Khoruts, and M.K. Jenkins, *The anatomy of T-cell activation and tolerance.* Proc Natl Acad Sci U S A, 1996. **93**(6): p. 2245-52.
437. Steponavicius-Cruz, K., V.M. Freitas, and J.A.M. Barbuto, *Dendritic Cells and T Lymphocytes Interactions in a Novel 3D System.* Procedia Engineering, 2013. **59**: p. 166-173.
438. Sathe, A., et al., *In vitro methotrexate as a practical approach to selective allodepletion.* Biol Blood Marrow Transplant, 2007. **13**(6): p. 644-54.
439. Haase, C., et al., *Immunomodulatory dendritic cells require autologous serum to circumvent nonspecific immunosuppressive activity in vivo.* Blood, 2005. **106**(13): p. 4225-33.
440. Chan, G. and D.J. Mooney, *Ca(2+) released from calcium alginate gels can promote inflammatory responses in vitro and in vivo.* Acta Biomater, 2013. **9**(12): p. 9281-91.
441. Jin, Z., et al., *Engineering the fate and function of human T-Cells via 3D bioprinting.* Biofabrication, 2021. **13**(3).
442. Trebak, M. and J.P. Kinet, *Calcium signalling in T cells.* Nat Rev Immunol, 2019. **19**(3): p. 154-169.
443. Baker, B.M. and C.S. Chen, *Deconstructing the third dimension: how 3D culture microenvironments alter cellular cues.* J Cell Sci, 2012. **125**(Pt 13): p. 3015-24.
444. Molzer, C., et al., *Activation of dendritic cells by crosslinked collagen hydrogels (artificial corneas) varies with their composition.* J Tissue Eng Regen Med, 2019. **13**(9): p. 1528-1543.
445. Lee, S.W.L., et al., *Characterizing the Role of Monocytes in T Cell Cancer Immunotherapy Using a 3D Microfluidic Model.* Front Immunol, 2018. **9**: p. 416.
446. Braham, M.V.J., et al., *Cellular immunotherapy on primary multiple myeloma expanded in a 3D bone marrow niche model.* Oncoimmunology, 2018. **7**(6): p. e1434465.
447. Cunha, C., et al., *3D culture of adult mouse neural stem cells within functionalized self-assembling peptide scaffolds.* Int J Nanomedicine, 2011. **6**: p. 943-55.
448. Boyd, D.F. and P.G. Thomas, *Towards integrating extracellular matrix and immunological pathways.* Cytokine, 2017. **98**: p. 79-86.
449. Dustin, M.L. and A.R. de Fougerolles, *Reprogramming T cells: the role of extracellular matrix in coordination of T cell activation and migration.* Curr Opin Immunol, 2001. **13**(3): p. 286-90.

450. Kim, C.H., *Crawling of effector T cells on extracellular matrix: role of integrins in interstitial migration in inflamed tissues.* Cell Mol Immunol, 2014. **11**(1): p. 1-4.
451. Shimizu, Y. and S. Shaw, *Lymphocyte interactions with extracellular matrix.* FASEB J, 1991. **5**(9): p. 2292-9.
452. Dang, N.H., et al., *Human CD4 helper T cell activation: Functional involvement of two distinct collagen receptors, 1F7 and VLA integrin family.* J. Exp. Med., 1990. **172**: p. 649-652.
453. Fernandes, N.R.J., et al., *CD4(+) T Cell Interstitial Migration Controlled by Fibronectin in the Inflamed Skin.* Front Immunol, 2020. **11**: p. 1501.
454. Theocharis, A.D., et al., *Extracellular matrix structure.* Adv Drug Deliv Rev, 2016. **97**: p. 4-27.
455. Bertoni, A., et al., *Integrins in T Cell Physiology.* Int J Mol Sci, 2018. **19**(2).
456. Damle, N.K. and A. Aruffo, *Vascular cell adhesion molecule 1 induces T cel antigen receptor-depedent activation of CD4+ T lymphocytes.* Proc Natl Acad Sci U S A, 1991. **88**: p. 6402-6407.
457. Matter, M.L. and E. Ruoslahti, *A signaling pathway from the alpha5beta1 and alpha(v)beta3 integrins that elevates bcl-2 transcription.* J Biol Chem, 2001. **276**(30): p. 27757-63.
458. Baaten, B.J., et al., *CD44 regulates survival and memory development in Th1 cells.* Immunity, 2010. **32**(1): p. 104-15.
459. Gray, A.L., et al., *Role of extracellular matrix proteoglycans in immune cell recruitment.* Int J Exp Pathol, 2022. **103**(2): p. 34-43.
460. Wrenshall, L.E. and J.L. Platt, *Regulation of T cell homeostasis by heparan sulfate-bound IL-2.* J Immunol, 1999. **163**(7): p. 3793-800.
461. Perez, V.M., J.F. Kearney, and J.J. Yeh, *The PDAC Extracellular Matrix: A Review of the ECM Protein Composition, Tumor Cell Interaction, and Therapeutic Strategies.* Front Oncol, 2021. **11**: p. 751311.
462. Sutherland, T.E., D.P. Dyer, and J.E. Allen, *The extracellular matrix and the immune system: A mutually dependent relationship.* Science, 2023. **379**(6633): p. eabp8964.
463. He, J. and L.G. Baum, *Presentation of galectin-1 by extracellular matrix triggers T cell death.* J Biol Chem, 2004. **279**(6): p. 4705-12.
464. Wan, S., et al., *Self-assembling peptide hydrogel for intervertebral disc tissue engineering.* Acta Biomater, 2016. **46**: p. 29-40.
465. McKinnon, D.D., et al., *Measuring cellular forces using bis-aliphatic hydrazone crosslinked stress-relaxing hydrogels.* Soft Matter, 2014. **10**(46): p. 9230-6.
466. Delgado, M., et al., *A Tunable Hydrogel for Encapsulation and Controlled Release of Bioactive Proteins.* Biomacromolecules, 2001. **3**: p. 262-271.
467. Wagner, C., et al., *Fibronectin synthesis by activated T lymphocytes: up-regulation of a surface-associated isoform with signalling function.* Immunology, 2000. **99**(4): p. 532-9.
468. To, W.S. and K.S. Midwood, *Plasma and cellular fibronectin: distinct and independent functions during tissue repair.* Fibrogenesis Tissue Repair, 2011. **4**: p. 21.
469. Grinnell, F., R.E. Billingham, and L. Burgess, *Distribution of fibronectin during wound healing in vivo.* J Invest Dermatol, 1981. **76**(3): p. 181-9.
470. Singh, P., C. Carraher, and J.E. Schwarzbauer, *Assembly of fibronectin extracellular matrix.* Annu Rev Cell Dev Biol, 2010. **26**: p. 397-419.
471. Guidry, C., E.J. Miller, and M. Hook, *A second fibronectin-binding region is present in collagen alpha chains.* Journal of Biological Chemistry, 1990. **265**(31): p. 19230-19236.
472. Dzamba, B.J., et al., *Fibronectin binding site in type I collagen regulates fibronectin fibril formation.* The Journal of Cell Biology, 1993. **121**(5): p. 1165-1172.
473. Velling, T., et al., *Polymerization of type I and III collagens is dependent on fibronectin and enhanced by integrins alpha 11beta 1 and alpha 2beta 1.* J Biol Chem, 2002. **277**(40): p. 37377-81.
474. Boisvert, M., et al., *Alpha2 beta1 integrin signaling augments T cell receptor-dependent production of interferon-gamma in human T cells.* Mol Immunol, 2007. **44**(15): p. 3732-40.

475. Rao, W.H., J.M. Hales, and R.D. Camp, *Potent costimulation of effector T lymphocytes by human collagen type I.* J Immunol, 2000. **165**(9): p. 4935-40.
476. Trujillo, S., et al., *Engineered 3D hydrogels with full-length fibronectin that sequester and present growth factors.* Biomaterials, 2020. **252**: p. 120104.
477. Bol, K.F., et al., *The clinical application of cancer immunotherapy based on naturally circulating dendritic cells.* J Immunother Cancer, 2019. **7**(1): p. 109.
478. Bloemendal, M., et al., *Immunological responses to adjuvant vaccination with combined CD1c(+) myeloid and plasmacytoid dendritic cells in stage III melanoma patients.* Oncoimmunology, 2022. **11**(1): p. 2015113.
479. Collin, M. and V. Bigley, *Human dendritic cell subsets: an update.* Immunology, 2018. **154**(1): p. 3-20.
480. Bougherara, H., et al., *Real-Time Imaging of Resident T Cells in Human Lung and Ovarian Carcinomas Reveals How Different Tumor Microenvironments Control T Lymphocyte Migration.* Front Immunol, 2015. **6**: p. 500.
481. Barnas, J.L., et al., *T cells and stromal fibroblasts in human tumor microenvironments represent potential therapeutic targets.* Cancer Microenviron, 2010. **3**(1): p. 29-47.
482. van Seventer, G.A., M.M. Mullen, and J.M. van Seventer, *Pyk2 is differentially regulated by beta1 integrin- and CD28-mediated co-stimulation in human CD4+ T lymphocytes.* Eur J Immunol, 1998. **28**(11): p. 3867-77.
483. Graf, B., T. Bushnell, and J. Miller, *LFA-1 mediated T cell costimulation through increased localization of TCR/class II complexes to the cSMAC and exclusion of CD45 from the immunological synpase.* J Immunol, 2007. **179**(3): p. 1616-1624.
484. Jankowska, K.I., et al., *Integrins Modulate T Cell Receptor Signaling by Constraining Actin Flow at the Immunological Synapse.* Front Immunol, 2018. **9**: p. 25.
485. Gaylo, A., et al., *T Cell Interstitial Migration: Motility Cues from the Inflamed Tissue for Micro- and Macro-Positioning.* Front Immunol, 2016. **7**: p. 428.
486. Bhattacharjee, O., et al., *Unraveling the ECM-Immune Cell Crosstalk in Skin Diseases.* Front Cell Dev Biol, 2019. **7**: p. 68.
487. Pankov, R. and K.M. Yamada, *Fibronectin at a glance.* J Cell Sci, 2002. **115**(Pt 20): p. 3861-3.
488. Gorski, A. and J.W. Kupiec-Weglinski, *Extracellular matrix proteins, regulators of T-cell functions in healthy and diseased individuals.* Clin Diagn Lab Immunol, 1995. **2**(6): p. 646-51.
489. Garcia-Nieto, S., et al., *Laminin and fibronectin treatment leads to generation of dendritic cells with superior endocytic capacity.* PLoS One, 2010. **5**(4): p. e10123.
490. Jancic, C., et al., *Interactions of dendritic cells with fibronectin and endothelial cells.* Immunology, 1998. **95**(2): p. 283-90.
491. Burns, S., et al., *Maturation of DC is associated with changes in motile characteristics and adherence.* Cell motility and the cytoskeleton, 2004. **57**(2): p. 118-132.
492. Wimmers, F., et al., *Paradigm Shift in Dendritic Cell-Based Immunotherapy: From in vitro Generated Monocyte-Derived DCs to Naturally Circulating DC Subsets.* Front Immunol, 2014. **5**: p. 165.
493. Prue, R.L., et al., *A Phase I Clinical Trial of CD1c (BDCA-1) + Dendritic Cells Pulsed With HLA-A*0201 Peptides for Immunotherapy of Metastatic Hormone Refractory Prostate Cancer.* J Immunother, 2015. **38**(2): p. 71-76.
494. Trombetta-Lima, M., et al., *Extracellular Matrix Proteome Remodeling in Human Glioblastoma and Medulloblastoma.* J Proteome Res, 2021. **20**(10): p. 4693-4707.
495. Serres, E., et al., *Fibronectin expression in glioblastomas promotes cell cohesion, collective invasion of basement membrane in vitro and orthotopic tumor growth in mice.* Oncogene, 2014. **33**(26): p. 3451-62.
496. Yang, Y., et al., *Functional roles of p38 mitogen-activated protein kinase in macrophage-mediated inflammatory responses.* Mediators Inflamm, 2014. **2014**: p. 352371.

497. West, M.A., et al., *Enhanced dendritic cell antigen capture via toll-like receptor-induced actin remodeling.* Science, 2004. **305**(5687): p. 1153-7.
498. Pribila, J.T., et al., *The alpha 1 beta 1 and alpha E beta 7 integrins define a subset of dendritic cells in peripheral lymph nodes with unique adhesive and antigen uptake properties.* J Immunol, 2004. **172**(1): p. 282-91.
499. Salvatore, L., et al., *Mimicking the Hierarchical Organization of Natural Collagen: Toward the Development of Ideal Scaffolding Material for Tissue Regeneration.* Front Bioeng Biotechnol, 2021. **9**: p. 644595.
500. Palomino-Durand, C., E. Pauthe, and A. Gand, *Fibronectin-Enriched Biomaterials, Biofunctionalization, and Proactivity: A Review.* Applied Sciences, 2021. **11**(24).
501. Deptula, P., et al., *Tissue Rheology as a Possible Complementary Procedure to Advance Histological Diagnosis of Colon Cancer.* ACS Biomater Sci Eng, 2020. **6**(10): p. 5620-5631.
502. Mieulet, V., et al., *Stiffness increases with myofibroblast content and collagen density in mesenchymal high grade serous ovarian cancer.* Sci Rep, 2021. **11**(1): p. 4219.
503. Assen, F.P., et al., *Multitier mechanics control stromal adaptations in the swelling lymph node.* Nat Immunol, 2022. **23**(8): p. 1246-1255.
504. Graf, F., et al., *The extracellular matrix proteins type I collagen, type III collagen, fibronectin, and laminin 421 stimulate migration of cancer cells.* FASEB J, 2021. **35**(7): p. e21692.
505. Kuipers, H.F., et al., *Hyaluronan synthesis is necessary for autoreactive T-cell trafficking, activation, and Th1 polarization.* Proc Natl Acad Sci U S A, 2016. **113**(5): p. 1339-44.
506. Chirivì, M., et al., *Tumor Extracellular Matrix Stiffness Promptly Modulates the Phenotype and Gene Expression of Infiltrating T Lymphocytes.* International Journal of Molecular Sciences, 2021. **22**(11).
507. Castillo, F., et al., *Levels of low-molecular-weight hyaluronan in periodontitis-treated patients and its immunostimulatory effects on CD4(+) T lymphocytes.* Clin Oral Investig, 2021. **25**(8): p. 4987-5000.
508. Loef, E.J., et al., *Live-Cell Microscopy Reveals That Human T Cells Primarily Respond Chemokinetically Within a CCL19 Gradient That Induces Chemotaxis in Dendritic Cells.* Front Immunol, 2021. **12**: p. 628090.
509. Burla, F., et al., *Particle diffusion in extracellular hydrogels.* Soft Matter, 2020. **16**(5): p. 1366-1376.
510. Figueiredo, L., et al., *Assessing glucose and oxygen diffusion in hydrogels for the rational design of 3D stem cell scaffolds in regenerative medicine.* J Tissue Eng Regen Med, 2018. **12**(5): p. 1238-1246.
511. Pampaloni, F., B.J. Chang, and E.H. Stelzer, *Light sheet-based fluorescence microscopy (LSFM) for the quantitative imaging of cells and tissues.* Cell Tissue Res, 2015. **360**(1): p. 129-41.
512. Sala, F., et al., *High-throughput 3D imaging of single cells with light-sheet fluorescence microscopy on chip.* Biomed Opt Express, 2020. **11**(8): p. 4397-4407.
513. Zhang, T., et al., *3D Visualization of Immune Cell Populations in HIV-Infected Tissues via Clearing, Immunostaining, Confocal, and Light Sheet Fluorescence Microscopy.* J Vis Exp, 2021(171).
514. Pangjantuk, A., et al., *3D culture of alginate-hyaluronic acid hydrogel supports the stemness of human mesenchymal stem cells.* Sci Rep, 2024. **14**(1): p. 4436.
515. Zhuang, Z., et al., *Control of Matrix Stiffness Using Methacrylate-Gelatin Hydrogels for a Macrophage-Mediated Inflammatory Response.* ACS Biomater Sci Eng, 2020. **6**(5): p. 3091-3102.
516. Li, R., et al., *Highly bioactive peptide-HA photo-crosslinking hydrogel for sustained promoting bone regeneration.* Chemical Engineering Journal, 2021. **415**.
517. Balion, Z., et al., *Cerebellar Cells Self-Assemble into Functional Organoids on Synthetic, Chemically Crosslinked ECM-Mimicking Peptide Hydrogels.* Biomolecules, 2020. **10**(5).

518. Hasturk, O., et al., *Enzymatically crosslinked silk and silk-gelatin hydrogels with tunable gelation kinetics, mechanical properties and bioactivity for cell culture and encapsulation.* Biomaterials, 2020. **232**: p. 119720.
519. Pugliese, R., et al., *Branched peptides integrate into self-assembled nanostructures and enhance biomechanics of peptidic hydrogels.* Acta Biomater, 2018. **66**: p. 258-271.
520. Samimi, H., et al., *Alginate-based 3D cell culture technique to evaluate the half-maximal inhibitory concentration: an in vitro model of anticancer drug study for anaplastic thyroid carcinoma.* Thyroid Res, 2021. **14**(1): p. 27.
521. Schmalz, G., et al., *Three-dimensional human cell cultures for cytotoxicity testing of dental filling materials.* Acta stomatol Croat., 2014. **48**(2): p. 99-108.
522. Paul, S. and G. Lal, *The Molecular Mechanism of Natural Killer Cells Function and Its Importance in Cancer Immunotherapy.* Front Immunol, 2017. **8**: p. 1124.
523. Bald, T., et al., *The NK cell-cancer cycle: advances and new challenges in NK cell-based immunotherapies.* Nat Immunol, 2020. **21**(8): p. 835-847.
524. White, L.G., et al., *Controlling Cell Trafficking: Addressing Failures in CAR T and NK Cell Therapy of Solid Tumours.* Cancers (Basel), 2022. **14**(4).
525. Hu, Z., *Tissue factor as a new target for CAR-NK cell immunotherapy of triple-negative breast cancer.* Sci Rep, 2020. **10**(1): p. 2815.
526. Yao, L., et al., *Cancer-associated fibroblasts impair the cytotoxic function of NK cells in gastric cancer by inducing ferroptosis via iron regulation.* Redox Biol, 2023. **67**: p. 102923.
527. Poznanski, S.M., et al., *Metabolic flexibility determines human NK cell functional fate in the tumor microenvironment.* Cell Metab, 2021. **33**(6): p. 1205-1220 e5.
528. Arianfar, E., et al., *Suppression of CD56(bright) NK cells in breast cancer patients is associated with the PD-1 and TGF-betaRII expression.* Clin Transl Oncol, 2023. **25**(3): p. 841-851.
529. La Fleur, L., et al., *Targeting MARCO and IL37R on Immunosuppressive Macrophages in Lung Cancer Blocks Regulatory T Cells and Supports Cytotoxic Lymphocyte Function.* Cancer Res, 2021. **81**(4): p. 956-967.
530. Ayuso, J.M., et al., *Microfluidic tumor-on-a-chip model to evaluate the role of tumor environmental stress on NK cell exhaustion.* Sci Adv, 2021. **7**(8).
531. Temples, M.N., et al., *Engineered Three-Dimensional Tumor Models to Study Natural Killer Cell Suppression.* ACS Biomater Sci Eng, 2020. **6**(7): p. 4179-4199.
532. Tam, R.Y., et al., *Rationally Designed 3D Hydrogels Model Invasive Lung Diseases Enabling High-Content Drug Screening.* Adv Mater, 2019. **31**(7): p. e1806214.
533. Su, Q., et al., *Supramolecular co-assembly of self-adjuvanting nanofibrious peptide hydrogel enhances cancer vaccination by activating MyD88-dependent NF-kappaB signaling pathway without inflammation.* Bioact Mater, 2021. **6**(11): p. 3924-3934.
534. Jie, J., et al., *Customized Multifunctional Peptide Hydrogel Scaffolds for CAR-T-Cell Rapid Proliferation and Solid Tumor Immunotherapy.* ACS Appl Mater Interfaces, 2022. **14**(33): p. 37514-37527.
535. Krzyszczyk, P., et al., *The Role of Macrophages in Acute and Chronic Wound Healing and Interventions to Promote Pro-wound Healing Phenotypes.* Front Physiol, 2018. **9**: p. 419.
536. Hyde, A.M., et al., *General Principles and Strategies for Salting-Out Informed by the Hofmeister Series.* Organic process research & development, 2017. **21**(9): p. 1355-1370.
537. O'Brien, E.P., B.R. Brooks, and D. Thirumalai, *Effects of pH on proteins: predictions for ensemble and single-molecule pulling experiments.* J Am Chem Soc, 2012. **134**(2): p. 979-87.
538. Simpson, R.J., *Fragmentation of protein using trypsin.* CSH Protoc, 2006. **2006**(5).
539. Tsuji, K., et al., *Effects of Different Cell-Detaching Methods on the Viability and Cell Surface Antigen Expression of Synovial Mesenchymal Stem Cells.* Cell Transplant, 2017. **26**(6): p. 1089-1102.